CHEMICAL ENGINEERING SCIENCE
GENIE CHIMIQUE

VOL. 15 1961 Nos. 3/4

Average values of catalyst properties in fluidized systems*

G. S. JOHN† and R. J. MIKOVSKY‡

Research and Development Department, Standard Oil Company (Indiana), Whiting, Indiana, U.S.A.

(*Received* 16 *May* 1960)

Abstract—The inventory of catalyst in a fluidized system may be made up of a large number of individual charges which differ in length of service. Average values of catalyst properties may be calculated if the mass and the age-dependent properties for each charge are known.

An equation can be developed that describes how the mass of each age group varies with time on stream. The mass of catalyst in each age group reflects how catalyst is added and how it is lost or withdrawn.

With this age-distribution function and information on how catalyst properties change with age, the average value of any given catalyst property can be calculated for a wide variety of operating conditions. Many concepts of fluidized-bed and slurry-phase operation can be unified by this method of analysis.

Résumé—Le catalyseur nécessaire à un système fluidisé est constitué par des charges successives qui se différencient par leur temps d'utilisation. On peut obtenir des valeurs moyennes des propriétés du catalyseur si l'on connaît pour chaque charge la masse du catalyseur et les propriétés dépendant de sa durée de service.

Une mise en équation montre comment varie avec le temps une masse de catalyseur de durée déterminée. Cette masse indique dans quelle mesure on doit ajouter du catalyseur et comment celui-ci est perdu.

La distribution en fonction du temps et la connaissance de la variation avec le temps des propriétés du catalyseur permettent de calculer la valeur moyenne des propriétés d'un catalyseur quelconque dans des conditions d'opérations très diverses. Cette méthode d'analyse permet d'unifier de nombreux concepts de milieux fluidisés.

Zusammenfassung—Der Katalysator in einem fluidierten System kann aus einer grossen Anzahl von aufeinanderfolgenden Chargen bestehen ; die Zeitdauer ihrer Verwendung ist verschieden. Durchschnittliche Werte der Eigenschaften von Katalysatoren können berechnet werden, wenn die Masse und der Verlauf der Änderung der Eigenschaften der einzelnen Katalysatoren während der Verwendungsdauer bekannt sind.

Eine mathematische Gleichung, die beschreibt wie sich die Masse in der verschiedenen Altersgruppe im Laufe der Zeit verändert, kann abgeleitet werden. In jeder Gruppe die Masse des Katalysators hässt erkennen inwiefern Katalysator ersetzt werden soll, oder wie deiser verloren ist.

Mit dieser Altersverteilung Funktion und mit der Kenntnis der Katalysatoreigenschaften die durchschnittlichen Werte von irgend einer Katalysatoreigenschaft können für sehr verschiedene Betriebsbedingungen berechnet werden. Diese analytische Methode ermoglicht auch die Vereinheitlichung der zahlreichen Fluidalstruktur Vorstellungen.

*Gordon Research Conference on Catalysis, Colby Junior College, New London, N.H., June 25, 1958 ; 134th National Meeting A.C.S., Chicago, Illinois, September 12, 1958.

†Present Address : Department of Chemical Engineering, Notre Dame University, South Bend, Indiana.

‡Present Address : Socony-Mobil Oil Co., Research Department, Paulsboro, New Jersey.

Reactor systems that handle catalysts in a fluidized bed or slurry phase have great industrial and laboratory use. In the petroleum industry, they are used for catalytic cracking, reforming, hydrogenation, desulphurization, and polymerization. Other present and possible applications [1] include the manufacture of phthalic anhydride by xylene oxidation, of ethylene oxide by ethylene oxidation, and of vinyl chloride from ethylene and hydrogen chloride.

Flow of feed and catalyst through a fluidized reactor system can be represented schematically as:

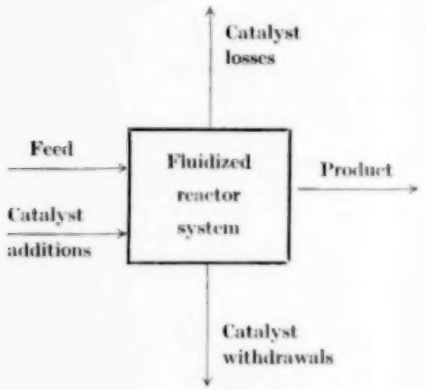

Performance is usually evaluated by determining, for example, the product yield, product quality and catalyst behaviour. Each of these may be complex functions of process variables, feed characteristics and catalyst properties.

The determination of catalyst behaviour is difficult because the catalyst changes during use. The changes depend on its ageing characteristics and how it is added to and lost from the system. Thus, calculation of the average value of a catalyst property rests upon descriptions of the ageing process and of the flow of catalyst through the unit.

The literature contains little material relating to the calculation of average values of fluidized-catalyst properties. The usual treatment deals with the steady state [2], but a significant part of the operating time is frequently under transient-state conditions. Therefore, in order to describe the behaviour of catalyst throughout an entire run a method has been developed to calculate average values of catalyst properties as a function of time-on-stream.

VOL. 15 1961

Description of Averaging Technique

The total value of a catalyst property is obtained by adding together the weighted values of the property for all catalyst groups. This total-property expression can then be developed through various stages:

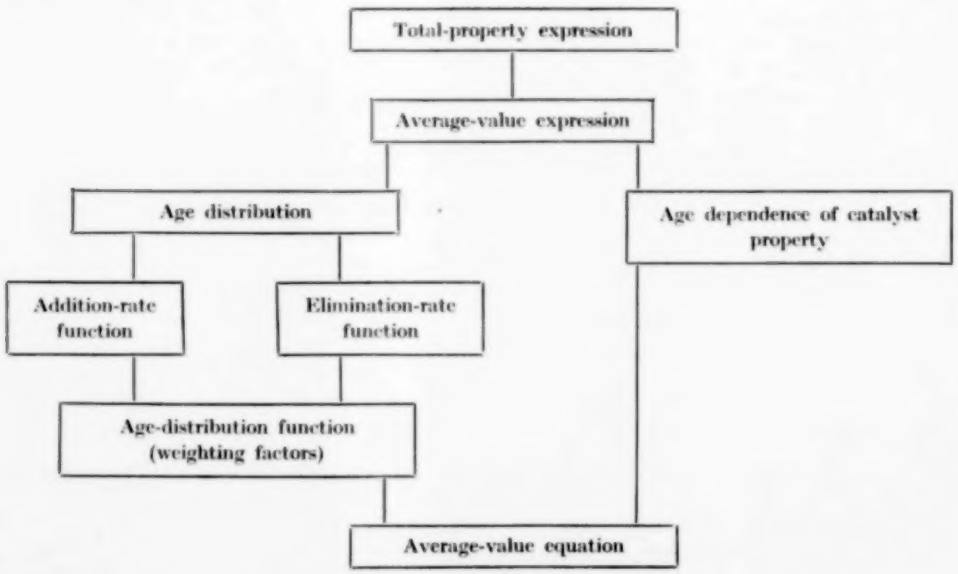

to yield an equation for the average value of a catalyst property.

An average-value expression results from dividing the total-property value by the sum of the weighting factors. For this purpose the inventory of catalyst is divided into age groups and the masses of catalyst in the age groups are used as the weighting factors. The problem then resolves itself into (a) developing an age distribution function that tells how much catalyst of a given age is in the unit, at any given time, and (b) determining the change in a catalyst property with age.

An age distribution results from the flow of catalyst to and from the system through additions and losses or withdrawals. Additions are usually known from plant records. Losses and withdrawals can be described by an elimination rate that gives the fractional rate of disappearance of any age group at any given time. A differential equation is set up that describes the rate of catalyst elimination; integration of this equation leads to an age distribution that relates the mass of any age group to its age. One of the limits of integration, however, is the initial mass of each age group when added to the system. For the age group associated with the initial charge this limit is the start-up inventory; for the age groups associated with catalyst added later it is the catalyst-addition rate.

The prediction of average values in advance of commercial operations contrasts with the analysis of past operations in that the elements of the age distribution must be generated from proposed addition or inventory schedules. A catalyst mass balance interrelates the addition rate, the elimination rate and the total inventory. This interrelationship is described by an integral equation, the solution of which gives the addition rate and thereby fixes the age distribution.

The age dependency of the catalyst property must also be described mathematically in order to be inserted into the average-value expression. The necessary data may be gained from bench-scale or pilot-plant runs wherein no additions of fresh catalyst are made. In many cases, the mathematical expression can be deduced from data obtained during the course of a commercial run.

Method for Calculating Average Property Values

The concept of an average property value can be treated mathematically to develop equations for the average values of such catalyst properties as age and relative activity.

Symbolically, the total value of a catalyst property is

$$P_{\text{total}} = \sum_i \omega_i P_i \qquad (1)$$

where ω_i is the weighting factor of the i^{th} group, which possesses the property value P_i. The average value $\bar{P}$ of the property is then defined by

$$\bar{P} \sum_i \omega_i = \sum_i \omega_i P_i \qquad (2)$$

The validity of this averaging process depends upon a proper selection of weighting factors for catalyst properties. Extensive properties – such as mass, volume or number of particles – can serve as weighting factors; intensive properties – such as relative activity, specific surface area, pore volume or density of the catalyst – as properties that can be weighted.

The inventory of catalyst in a system consists of catalyst remaining from the initial charge and that remaining from subsequent additions. By using the masses of these various charges as the weighting factors equation (2) may be rewritten:

$$\bar{P}\left[M + \sum_i m_i\right] = MP_0 + \sum_i m_i P_i \qquad (3)$$

where M is the mass remaining from the initial charge, P_0 is the value of the property for the initial charge, and m_i and P_i are the remaining mass and property values of subsequent catalyst additions, respectively. How each quantity in equation (3) changes with time must be made explicit before the transient behaviour of the system can be treated. Expressions are required for both the weighting factor and the catalyst property as functions of age. Catalyst age must therefore be defined precisely.

Catalyst added at time τ will have, at a later time, t, a residence time equal to $t - \tau$ and will have increased in age by $\beta_p (t - \tau)$ for a specific property P. The proportionality factor β_p for the property P is an ageing-severity factor that

depends on the conditions to which the catalyst is subjected in the unit. The residence time of the initial charge equals the time-on-stream, t. The age of the initial charge (and sometimes subsequent additions) presents further difficulties, because such pretreatments as steaming give it an additional age. Furthermore, the effect of the additional ageing may differ for the property to be averaged and for the property that determines catalyst attrition and which controls the mass weighting factor. The total age of the initial charge should thus be written as $\beta_p (t + t_p)$ for the property to be averaged, where t_p is the ageing caused by pretreatment. Similarly, for the attrition characteristics, the total age of the initial charge is $\beta_0 (t + t_0)$ where β_0 is the ageing-severity factor for attrition and t_0 is the ageing caused by pretreatment. Further development of the property-balance equation is simplified by assuming that the ageing-severity factor is equal to one for all properties. A more comprehensive treatment of the ageing-severity factor would require a knowledge of how this factor varies with operating conditions.

The definition of catalyst age may now be inserted into equation (3). The result is

$$P(t)\left[M(t + t_0, t) + \sum_{t-\tau} m(t - \tau, t)\right] = M(t + t_0, t)\, P(t + t_p) + \sum_{t-\tau} m(t - \tau, t)\, P(t - \tau) \qquad (4)$$

where the weighting factors are functions not only of age but also of time-on-stream. The weighting factor $M(t + t_0, t)$ is the mass of catalyst from the initial charge remaining at time t and of age $t + t_0$. Analogously, $m(t - \tau, t)$ is the mass of catalyst added at time τ that remains in the unit at time t and has the age $t - \tau$.

If catalyst is added frequently enough, the summation over $t - \tau$ in equation (4) may be replaced by an integration, leading to

$$P(t) = \frac{M(t + t_0, t)\, P(t + t_p) + \int_0^t m(t - \tau, t)\, P(t - \tau)\, d(t - \tau)}{M(t + t_0, t) + \int_0^t m(t - \tau, t)\, d(t - \tau)} \qquad (5)$$

The limits of integration are the age of the youngest added catalyst present, $t - \tau = 0$, and that of the oldest, $t - \tau = t$.

Equation (5) is the basic property-balance equation that is used to calculate the average value of catalyst properties, such as age, activity and density. The age-distribution function, composed of $M(t + t_0, t)$ and $m(t - \tau, t)$ and the properties, $P(t + t_p)$ and $P(t - \tau)$, must be known before average values can be computed.

Age-distribution function

At the beginning of a run, enough catalyst is charged to permit smooth operation; as the run progresses, more catalyst is added. Because of losses and withdrawals the mass of the initial charge decreases with time and the mass of replacement catalyst added to the unit at various times diminishes. The masses remaining at any given time will depend on how catalyst is eliminated from the system through losses and withdrawals.

Elimination rate. Losses may be expressed by a fractional loss-rate $L(t - \tau)$, which may be a function of catalyst age; withdrawals, by a fractional withdrawal rate w. Thus, the mass of an added charge of catalyst changes with residence time and age according to

$$\frac{dm(t - \tau, t)}{d(t - \tau)} = -\left[L(t - \tau) + w\right] m(t - \tau, t) \qquad (6)$$

or

$$\frac{d}{d(t - \tau)} \ln m(t - \tau, t) = -E(t - \tau).$$

In the latter

$$E(t - \tau) = L(t - \tau) + w \qquad (7)$$

is a fractional elimination rate and is analogous to a first-order rate constant but changes with catalyst age. In some cases the elimination rate may be a constant independent of catalyst age.

In fluidized beds wherein attrition and elutriation occur loss-rate data can be represented by a function of the form

$$L(t-\tau) = \frac{\sum_r s_r f_r \exp\left[-s_r(t-\tau)\right]}{\sum_r f_r \exp\left[-s_r(t-\tau)\right]} \qquad (8)$$

where the s_r's and f_r's are empirical constants and the sum of the f_r's equals one. Inserting this definition of $L(t-\tau)$ into equation (7) yields:

$$E(t-\tau) = \frac{\sum_r (s_r + w) f_r \exp\left[-(s_r + w)(t-\tau)\right]}{\sum_r f_r \exp\left[-(s_r + w)(t-\tau)\right]} \qquad (9)$$

Integration of equation (6) leads to

$$m(t-\tau, t) = m(0, \tau) \exp\left[-\int_0^{(t-\tau)} E(t-\tau)\, d(t-\tau)\right] \qquad (10)$$

where $m(0, \tau)$ is the addition rate of fresh catalyst as a function of time. Combining equations (9) and (10) gives

$$m(t-\tau, t) = m(0, \tau) \sum_r f_r \exp\left[-(s_r + w)(t-\tau)\right]. \qquad (11)$$

Expressions equivalent to equations (10) and (11) for the initial charge must consider the initial ageing, t_0, caused by steaming, calcination or other pretreatments. Under these circumstances the change in mass of the initial charge with residence time and ageing during use is

$$\frac{d}{dt} \ln M(t + t_0, t) = -E(t + t_0) \qquad (12)$$

and integration gives

$$M(t + t_0, t) = M(t_0, 0) \frac{\sum_r f_r \exp\left[-(s_r + w)(t + t_0)\right]}{\sum_r f_r \exp\left[-(s_r + w) t_0\right]}. \qquad (13)$$

In this equation the change in attritional characteristics of the initial charge is assumed the same as that of the replacement catalyst. If the initial charge differs from the replacement catalyst the empirical constants describing its loss must be distinguished from those of the replacement catalyst.

The age-distribution function of the entire catalyst inventory is given by the two functions $m(t-\tau, t)$ and $M(t + t_0, t)$, defined by equations (11) and (13). Because the start-up mass of the initial charge $M(t_0, 0)$ is a constant, the only unspecified term in the age-distribution function is the addition rate of fresh catalyst, $m(0, \tau)$, in equation (11).

Addition rate. Laboratory or plant records can usually provide the addition rate of replacement catalyst, $m(0, \tau)$, directly, and average values can be calculated immediately with equation (4) or (5). However, for purposes of predicting average values the addition rate must either be defined or be derived from a catalyst inventory balance involving losses, withdrawals and any changes in the total inventory.

The Appendix presents a derivation of the addition rate, which is found to be

$$m(0, \tau) = \frac{M(t_0, 0)}{w + s_1 f_2 + s_2 f_1} \left\{ (s_1 + w)(s_2 + w) + \frac{f_1 f_2 (s_1 - s_2)\left[s_1 \exp(-s_1 t_0) - s_2 \exp(-s_2 t_0)\right]}{f_1 \exp(-s_1 t_0) + f_2 \exp(-s_2 t_0)} \exp\left[-(w + s_1 f_2 + s_2 f_1)\tau\right] \right\}$$
$$+ \sum_j a_j \left\{ \frac{(s_1 + w)(s_2 + w)}{w + s_1 f_2 + s_2 f_1} - \frac{d_j f_1 f_2 (s_1 - s_2)^2 \exp\left[-(w + s_1 f_2 + s_2 f_1)\tau\right]}{(w + s_1 f_2 + s_2 f_1)(w + s_1 f_2 + s_2 f_1 - d_j)} \right.$$
$$\left. - \frac{(w + s_1 - d_j)(w + s_2 - d_j)}{w + s_1 f_2 + s_2 f_1 - d_j} \exp(-d_j \tau) \right\} \qquad (14)$$

under the conditions that the summation over r in equation (9) involves only two terms and that any monotonic rise or fall of the inventory could be described by

$$I(t) = M(t_0, 0) + \sum_j a_j \left[1 - \exp(-d_j t)\right] \quad (15)$$

where the a_j's and d_j's are empirical constants.

Formulating the age-distribution function

With the addition rate determined, the age-distribution function can be fully defined. The mass of catalyst from the initial charge that is of age $t + t_0$ at time t is given by equation (13).

The mass of catalyst remaining from added catalyst of age $t - \tau$ at time-on-stream t is given by

$$m(t-\tau, t) = \left\{ \frac{M(t_0, 0)}{w + s_1 f_2 + s_2 f_1} \left[(s_1 + w)(s_2 + w) + \frac{f_1 f_2 (s_1 - s_2)\left[s_1 \exp(-s_1 t_0) - s_2 \exp(-s_2 t_0)\right]}{f_1 \exp(-s_1 t_0) + f_2 \exp(-s_2 t_0)} \right. \right.$$
$$\left. \times \exp\left[-(w + s_1 f_2 + s_2 f_1)\tau\right] \right\} + \sum_j a_j \left[\frac{(s_1 + w)(s_2 + w)}{w + s_1 f_2 + s_2 f_1} \right.$$
$$\left. \left. - \frac{d_j f_1 f_2 (s_1 - s_2)^2 \exp\left[-(w + s_1 f_2 + s_2 f_1)\tau\right]}{(w + s_1 f_2 + s_2 f_1)(w + s_1 f_2 + s_2 f_1 - d_j)} - \frac{(w + s_1 - d_j)(w + s_2 - d_j)}{w + s_1 f_2 + s_2 f_1 - d_j} \exp(-d_j \tau) \right] \right)$$
$$\Sigma f_r \exp\left[-(s_r + w)(t - \tau)\right] \quad (16)$$

obtained by substituting in equation (11) the definition of $m(0, \tau)$ from equation (14).

Addition rates and age-distribution functions for specific combinations of inventory, losses and withdrawls can be obtained by specialising equations (13), (14) and (16). The simplest case occurs when the inventory is maintained at a constant value (all a_j's are zero), no withdrawals are made (w is zero) and the fractional loss-rate is a constant independent of catalyst age ($t_0 = 0$; s_1 and s_2 are equal to s; f_1 and f_2 are equal to one-half). Under these conditions, the addition rate

$$m(0, \tau) = sM(0, 0). \quad (17)$$

Thus, the addition rate is a constant fraction, s, of the start-up inventory. The age-distribution function is given by

$$M(t, t) = M(0, 0) \exp(-st) \quad (18a)$$

for the initial charge, and

$$m(t - \tau, t) = sM(0, 0) \exp\left[-s(t - \tau)\right] \quad (18b)$$

for catalyst added at time τ. If the inventory does not remain constant but changes as described by equation (15), and if the fractional loss-rate still remains constant

$$m(0, \tau) = sM(0, 0) + \sum_j a_j \left[s - (s - d_j)\exp(-d_j \tau)\right]. \quad (19)$$

Under these circumstances,

$$M(t, t) = M(0, 0) \exp(-st) \quad (20a)$$

for the initial charge, and

$$m(t - \tau, t) = \left\{ sM(0, 0) + \sum_j a_j \left[s - (s - d_j)\exp(-d_j \tau)\right] \right\} \exp\left[-s(t - \tau)\right] \quad (20b)$$

for catalyst added at time τ.

Age dependence of catalyst properties

Changes in properties with age may be observed during bench-scale or pilot-plant studies carried out without additions of catalyst. Properties so determined are denoted as the non-replacement properties of the catalyst. Frequently, reliable estimates of the change in a property with age can be made from data obtained during the initial stages of a commercial run.

The simplest age-dependent property is the catalyst age itself.

For the initial charge,

$$\text{Age} = t + t_0. \quad (21a)$$

For catalyst added at time τ,

$$\text{Age} = t - \tau. \quad (21b)$$

VOL. 15 1961

Dependence of activity upon age can be determined most conveniently by a "least-squares" treatment of activity data obtained from bench-scale or pilot-plant experiments. Equations to represent such data can take many forms; most convenient is the exponential dependence of activity upon age. Thus, the catalyst activity can be represented by

$$A_0 \exp\left[-k\,(t+t_a)\right] = A_0' \exp\left(-kt\right) \qquad (22a)$$

for the initial charge, and

$$A_0 \exp\left[-k\,(t-\tau)\right] \qquad (22b)$$

for catalyst added at time τ. A_0 is the initial activity of fresh catalyst, t_0 is the ageing due to pretreatment of the initial charge, A_0' is the activity of the initial charge at the beginning of the run and k is the exponential deactivation coefficient. The empirical constants A_0 and k are assumed to be the same for the initial charge and the added catalyst.

The age-dependence of other properties can be expressed by analogous equations and used to compute average values.

Average Property Values

All the elements of equation (5) have been formulated. The averaging technique may now be exemplified with the calculation of the average age and the average activity.

Average age

Age is one of the simplest catalyst properties that can be used to illustrate the averaging technique. On insertion of the definitions of age given in equation (21) into equation (5), the average age of the catalyst inventory for the property P is

$$\overline{(\text{Age})}_p = \frac{\left[M\,(t+t_0,\,t)\right](t+t_p) + \int_0^t \left[m\,(t-\tau,\,t)\right](t-\tau)\,d\,(t-\tau)}{M\,(t+t_0,\,t) + \int_0^t m\,(t-\tau)\,d\,(t-\tau)} \,. \qquad (23)$$

In the general case, corresponding to equations (13) and (16),

$$\begin{aligned}
\overline{(\text{Age})}_p = {} & \left\{M\,(t_0,0) + \sum_j a_j\left[1-\exp\left(-d_j\,t\right)\right]\right\}^{-1} \\
& \times \left(M\,(t_0,0)\,(t+t_p)\,\frac{\sum_{r=1}^{2} f_r \exp\left[-(s_r+w)\,(t+t_0)\right]}{\sum_{r=1}^{2} f_r \exp\left[-(s_r+w)\,t_0\right]} + \frac{(s_1+w)\,(s_2+w)}{(w+s_1f_2+s_2f_1)}\left(M\,(t_0,0)+\sum_j a_j\right)\right. \\
& \times \sum_{r=1}^{2} f_r \left\{\frac{1-\exp\left[-(s_r+w)\,t\right]}{(s_r+w)^2} - \frac{t\exp\left[-(s_r+w)\,t\right]}{(s_r+w)}\right\} + \frac{f_1f_2\,(s_1-s_2)}{w+s_1f_2+s_2f_1} \\
& \times \left[M\,(t_0,0)\,\frac{s_1\exp\left(-s_1\,t_0\right)-s_2\exp\left(-s_2\,t_0\right)}{\sum_{r=1}^{2} f_r\exp\left(-s_r\,t_0\right)} - \sum_j \frac{a_j\,d_j\,(s_1-s_2)}{w+s_1f_2+s_2f_1-d_j}\right] \\
& \times \sum_{r=1}^{2} f_r \left\{\frac{\exp\left[-(w+s_1f_2+s_2f_1)\,t\right]-\exp\left[-(s_r+w)\,t\right]}{(s_r-s_1f_2-s_2f_1)^2} - \frac{t\exp\left[-(s_r+w)\,t\right]}{s_r-s_1f_2-s_2f_1}\right\} \\
& - \sum_j \frac{a_j\,(w+s_1-d_j)\,(w+s_2-d_j)}{w+s_1f_2+s_2f_1-d_j} \\
& \left. \times \sum_{r=1}^{2} f_r \left\{\frac{\exp\left(-d_j\,t\right)-\exp\left[-(s_r+w)\,t\right]}{(s_r+w-d_j)^2} - \frac{t\exp\left[-(s_r+w)\,t\right]}{s_r+w-d_j}\right\}\right) . \qquad (24)
\end{aligned}$$

If the inventory is constant, no withdrawals are made and the fractional loss-rate is constant,

$$\overline{(\text{Age})}_p = \frac{1}{s}\left[1 - \exp(-st)\right] \tag{25}$$

If the inventory changes during the run, but the fractional loss-rate is constant.

$$\begin{aligned}\overline{(\text{Age})}_p = &\left\{M(0,0) + \sum_j a_j\left[1 - \exp(-d_j t)\right]\right\}^{-1} \\ &\times \left\{M(0,0)\, t_p \exp(-st)\right. \\ &+ \frac{M(0,0)}{s}\left[1 - \exp(-st)\right] \\ &\left. + \sum_j a_j\left[\frac{1 - \exp(-st)}{s} - \frac{\exp(-d_j t) - \exp(-st)}{s - d_j}\right]\right\}.\end{aligned} \tag{26}$$

At the steady state ($t = \infty$), both equation (25) and (26) reduce to

$$\overline{(\text{Age})}_p = \frac{1}{s} \tag{27}$$

The difference between catalyst age and residence time has been denoted by t_p which is the effective age due to pretreatment of the catalyst. The average residence time of the catalyst in a system can be computed from the average-age equation (24) by setting t_p equal to zero.

Average activity

To calculate the average activity for an inventory of catalyst equation (22) is used in equation (5) together with the age-distribution function defined by equations (13) and (16). The most general case – characterized by a changing inventory, changing loss rate and constant withdrawals – can be described by

$$\begin{aligned}\bar{A}(t) = &\left\{(M t_0, 0) + \sum_j a_j\left[1 - \exp(-d_j t)\right]\right\}^{-1} \\ &\times \left\{A_0' \exp(-kt)\, M(t_0, 0) \frac{\sum_{r=1}^{2} f_r \exp\left[-(s_r + w)(t + t_0)\right]}{\sum_{r=1}^{2} f_r \exp\left[-(s_r + w)\, t_0\right]} + \frac{A_0'(s_1 + w)(s_2 + w)}{w + s_1 f_2 + s_2 f_1}\right. \\ &\times \left[M(t_0, 0) + \sum_j a_j\right] \sum_r \frac{f_r\left(1 - \exp\left[-(k + w + s_r)t\right]\right.}{k + w + s_r} + \frac{A_0 f_1 f_2 (s_1 - s_2)}{w + s_1 f_2 + s_2 f_1} \\ &\times \left[M(t_0, 0) \frac{\sum_{r=1}^{2} s_r \exp(-s_r t_c)}{\sum_{r=1}^{2} f_r \exp(-s_r t_c)} - \sum_j \frac{a_j d_j (s_1 - s_2)}{w + s_1 f_2 + s_2 f_1 - d_j}\right] \\ &\times \sum_r f_r \frac{\exp\left[-(w + s_1 f_2 + s_2 f_1)\, t\right] - \exp\left[-(k + w + s_r)\, t\right]}{k + s_1 f_2 - s_2 f_1 + s_r} \\ &\left. - A_0 \sum_j \left(\frac{a_j (w + s_1 - d_j)(w + s_2 - d_j)}{w + s_1 f_2 + s_2 f_1 - d_j} \sum_r f_r \frac{\exp(-d_j t) - \exp\left[-(k + w + s_r)\, t\right]}{k + w + s_r - d_j}\right)\right\}.\end{aligned} \tag{28}$$

As t approaches infinity the average activity reaches a limiting value, the steady-state activity, defined by

$$\bar{A}(\infty) = \frac{A_0 (w + s_1)(w + s_2)(k + w + s_1 f_2 + s_2 f_1)}{(w + s_1 f_2 + s_2 f_1)(k + w + s_1)(k + w + s_2)}. \tag{29}$$

The complexity of these equations is greatly reduced if the inventory remains constant during the run, no withdrawals are made and the loss rate is independent of catalyst age. In this case,

$$\overline{A}(t) = A_0' \exp\left[-(k+s)\,t\right] + \frac{A_0\,s}{k+s}\left\{1 - \exp\left[-(k+s)\,t\right]\right\} \tag{30}$$

and the steady-state activity is

$$\overline{A}(\infty) = \frac{A_0\,s}{k+s} \tag{31}$$

If the inventory changes while the other conditions are maintained, the average activity is

$$\overline{A}(t) = \left\{M(0,0) + \sum_j a_j\left[1 - \exp(-d_j\,t)\right]\right\}^{-1} \times \left\{M(0,0)\,A_0' \exp\left[-(k+s)\,t\right] + \frac{A_0\,s}{k+s}\left[M(0,0) + \sum_j a_j\right] \times \left\{1 - \exp\left[-(k+s)\,t\right]\right\} + \sum_j \frac{A_0\,a_j\,(s-d_j)}{k+s-d_j}\left[\exp\left[-(k+s)\,t\right] - \exp(-d_j\,t)\right]\right\}. \tag{32}$$

The application of the averaging technique illustrated here may thus serve as a guide to calculating the average value of any intensive catalyst property.

Conclusion

An advantage of the present method of interpreting catalyst behaviour is that it can treat the transient (or non-steady) state. This advantage is especially important when (or if) such a state constitutes the greater part of a run.

The method can be used, not only for calculating and predicting average properties, but also for evaluating changes in physical properties due to ageing. For example, deactivation coefficients or attritional losses can be reliably estimated by matching the results of this type of analysis to the operational data.

Although the averaging technique has been illustrated with the calculation of average age and average activity, it can just as easily be used to calculate the average value of such properties as surface area, selectivity, pore volume and regenerability.

The analysis could be extended not only to other catalyst properties but also to other commercial operating conditions if more were known about the manner in which catalyst is lost from the unit. More research is needed on the mechanism of attrition and of catalyst losses from fluidized systems. Only then can the influence of the many operating variables on such catalyst properties as activity and selectivity be completely understood.

Appendix

Derivation of the Addition Rate

The derivation of the addition rate starts with an expression for the catalyst inventory at any given time t. This expression, in terms of the concepts used in developing equation (5), is

$$I(t) = M(t + t_0, t) + \int_0^t m(t-\tau, t)\,d(t-\tau) \tag{A1}$$

At any time, t, integration over the age $t - \tau$ is equivalent to an integration over τ; therefore, equation (A1) becomes

$$I(t) = M(t + t_0, t) + \int_0^t m(t-\tau, t)\,d\tau \tag{A2}$$

Upon substitution of the definitions of $m(t-\tau, t)$ from equation (11) and of $M(t + t_0, t)$ from equation (13), equation (A2) becomes

$$I(t) = M(t_0, 0)\,\frac{\sum_r f_r \exp\left[-(s_r + w)(t + t_0)\right]}{\sum_r f_r \exp\left[-(s_r + w)\,t_0\right]} + \int_0^t m(0,\tau) \sum_r f_r \exp\left[-(s_r + w)(t-\tau)\right] d\tau \tag{A3}$$

This equation, which implicitly defines the addition rate, $m(0, \tau)$, in terms of the inventory, losses and withdrawals, is known as Volterra's integral equation. It may be written in the general form

$$h(t) = \int_0^t m(0, \tau)\, K(t - \tau)\, d\tau \qquad \text{(A4)}$$

where

$$h(t) = I(t) - M(t_0, 0)$$

$$\frac{\sum_r f_r \exp\left[-(s_r + w)(t + t_0)\right]}{\sum_r f_r \exp\left[-(s_r + w)\, t_0\right]} \qquad \text{(A5)}$$

and

$$K(t - \tau) = \sum_r f_r \exp\left[-(s_r + w)(t - \tau)\right]. \qquad \text{(A6)}$$

Equation (A3) can be solved by several different methods. Differentiation with respect to t leads to Volterra's equation of the second kind, which can be solved by successive substitution or successive approximation. Alternatively, the methods of operational calculus can be used to obtain the solution for $m(0, \tau)$ directly from equation (A4) because it is in the form of a composition product.

Using the notation established by VAN DER POL and BREMMER*, we write the operational relations

$$U(t)\, h(t) \fallingdotseq \mathscr{H}(p), \quad U(t)\, m(0, t) \fallingdotseq \mathscr{M}(0, p),$$

$$U(t)\, K(t) \fallingdotseq \mathscr{K}(p) \qquad \text{(A7)}$$

where $U(t)$ is the unit function.

If these functions possess a common strip of convergence the solution in the p-language can be written:

$$\mathscr{M}(0, p) = p\, \frac{\mathscr{H}(p)}{\mathscr{K}(p)}. \qquad \text{(A8)}$$

If $\mathscr{M}(0, p)$ can be expanded as a sum of rational fractions the expression for $m(0, t)$ can be obtained by transposing the sum term-by-term.

To illustrate the technique, assume that the inventory $I(t)$ can be expressed as

$$I(t) = M(t_0, 0) + \sum_j a_j \left[1 - \exp(-d_j t)\right] \qquad \text{(A9)}$$

and that the summation over r only extends to $r = 2$. Thus

$$h(t) = \frac{M(t_0, 0)}{\sum_{r=1}^{2} f_r \exp\left[-(s_r + w)\, t_0\right]} \times \left\{ \sum_{r=1}^{2} f_r \exp\left[-(s_r + w) t_0\right] \left\{1 - \exp\left[-(s_r + w) t\right]\right\} \right\} + \sum a_j \left[1 - \exp(-d_j t)\right] \qquad \text{(A10)}$$

and

$$\mathscr{H}(p) = \frac{M(t_0, 0)}{\sum_{r=1}^{2} f_r \exp\left[-(s_r + w)\, t_0\right]} \times \left\{ \sum_{r=1}^{2} f_r \exp\left[-(s_r + w) t_0\right] \left(1 - \frac{p}{p + s_r + w}\right) \right\} + \sum_j a_j \left(1 - \frac{p}{p + d_j}\right). \qquad \text{(A11)}$$

From equation (A7)

$$\mathscr{K}(p) = \sum_{r=1}^{2} f_r \left(\frac{p}{p + s_r + w}\right) \qquad \text{(A12)}$$

Using in equation (A9) the definitions given in equations (A12) and (A13), we obtain

$$\mathscr{M}(0, p) = \frac{M(t_0, 0) \left\{ \sum_{r=1}^{2} f_r \exp\left[-(s_r + w)\right] \left[(s_r + w)/(p + s_r + w)\right] \right\}}{\sum_{r=1}^{2} f_r \exp\left[-(s_r + w)\, t_0\right] \sum_{r=1}^{2} \left[f_r/(p + s_r + w)\right]} + \frac{\sum_j \left[(a_j d_j)/(p + d_j)\right]}{\sum_{r=1}^{2} \left[f_r/(p + s_r + w)\right]}$$

$$= \frac{M(t_0, 0)}{f_1 \exp(-s_1 t_0) + f_2 \exp(-s_2 t_0)} \times \left\{ \frac{p\left[f_1 \exp(-s_1 t_0)(s_1 + w) + f_2 \exp(-s_2 t_0)(s_2 + w)\right] + (s_1 + w)(s_2 + w)\left[f_1 \exp(-s_1 t_0) + f_2 \exp(-s_2 t_0)\right]}{p + s_1 f_2 + s_2 f_1 + w} \right\} + \sum_j \frac{a_j d_j (p + s_1 + w)(p + s_2 + w)}{(p + d_j)(p + s_1 f_2 + s_2 f_1 + w)}. \qquad \text{(A13)}$$

Inversion and a simple transformation of the variable from t to τ leads to the addition rate, equation (14).

It is important to recognize the equivalence of the symbols $m(0, t)$ and $m(0, \tau)$; their mathematical functionalities are identical. Both t and τ represent time-on-stream; τ, however, identifies catalyst age-groups. Therefore, the expression for the addition rate $m(0, t)$, when used in the age-distribution function, must undergo a change of variable from t to τ.

*VAN DER POL and BREMMER, *Operational Calculus based on Two-sided Laplace Integral*, Cambridge University Press, London 1950.

VOL. 15 1961

Notation

A_0 = Initial activity of fresh catalyst

A_0' = Start-up activity of initial charge

$\bar{A}(t)$ = Average activity of a catalyst inventory as a function of the time-on-stream

$\bar{A}(\infty)$ = Steady-state activity

$a_1, a_2 \ldots a_j$ = empirical parameters used in an inventory equation

β_0 = Ageing-severity factor for attrition

β_p = Ageing-severity factor for the catalyst property P

$d_1, d_2, \ldots d_j$ = Empirical parameters used in an inventory equation

$E(t-\tau)$ = Fractional elimination-rate of catalyst expressed as a function of residence time (age)

$f_1, f_2, \ldots f_r$ = Empirical constants used in expressing the elimination rate

$I(t)$ = Inventory of catalyst as a function of time-on-stream

k = Exponential deactivation coefficient

$L(t-\tau)$ = Fractional loss-rate of catalyst, caused by attrition and elutriation expressed as a function of residence time (age)

m_i = mass of the i^{th} catalyst group

$M(0, 0)$, $M(t_0, 0)$ = Expressions for the start-up mass of the initial charge

$M(t+t_0, t)$ = Mass of the initial charge remaining at time t, and of age $t + t_0$.

$m(0, t)$ = Addition rate; i.e., the mass of catalyst of zero residence time at time t

$m(0, \tau)$ = Functionally identical with $m(0, t)$ but identifying the time-on-stream at which any given charge enters the system

$m(t-\tau, t)$ = Age distribution of added catalyst; i.e. the mass of catalyst of age $t - \tau$ at time-on-stream t

P = A generalized property

P_i = The value of the generalized property P for i^{th} catalyst group

P_0 = The value of a generalized property P for the initial charge

$\bar{P}(t)$ = Average value of the generalized property P as a function of the time-on-stream

$P(t+t_p)$ = The value of the generalized property P for the initial charge of age $t + t_p$

$P(t-\tau)$ = The value of the generalized property P for catalyst of age $t - \tau$

$s_1, s_2, \ldots s_r$ = Empirical constants used in expressing the attrition rate

t = Time-on-stream

t_0 = Effective age of initial charge for attrition

t_p = Effective age of the catalyst for the property P

τ = Time-on-stream, identifying time of entry of a given charge into the system

w = Fractional withdrawal rate

ω = Weighting factor used in the averaging process

References

[1] Sittig M. *Chem. Engng.* 1953 **60** 219.

[2] Andersen S. L. and Matthias R. H. *Industr. Engng. Chem.* 1954 **45** 1296.

Chemical Engineering Science, 1961, Vol. 15, pp. 172 to 175. Pergamon Press Ltd., London. Printed in Great Britain.

Calculation of the average activity of cracking catalysts*

G. S. John† and R. J. Mikovsky‡

Research and Development Department, Standard Oil Company (Indiana), Whiting, Indiana, U.S.A.

(*Received* 16 *May*, 1960)

Abstract—A mathematical technique has been used to calculate the changes of the average activity of cracking catalysts with time. Two different types of fluidized operation have been analysed. In one, a commercial unit operated at essentially constant catalyst inventory, constant catalyst loss rate and constant addition rate; in the other, the operations were characterized by a changing inventory, constant rate of attrition and no withdrawals of catalyst. The analyses show the inter-relationship of the operating variables and form a basis for predicting the future course of commercial runs.

Résumé—Utilisation d'une technique mathématique pour le calcul de la variation en fonction du temps de l'activité moyenne des catalyseurs de cracking. Deux types de fluidisation ont été étudiés. Dans l'un, une unité industrielle fonctionne avec une quantité constante de catalyseur, ce dernier étant partiellement renouvellé à débit constant. Dans l'autre on opère avec une masse variable de catalyseur, débit d'alimentation constant sans élimination de catalyseur. Cette étude permet l'établir une relation entre les différentes variables régissant le phénomène et de prévoir le mode de réalisation d'essais industriels.

Zusammenfassung—Eine mathematische Methode ist verwendet für die Darstellung der Veränderungen der durchschnittlichen Aktivität von Katalysatoren im Krackprozess als Funktion der Zeit. Zwei verschiedene Typen von fluidierten Systemen sind analysiert. In dem ersten, eine industrielle Einheit arbeitet mit konstanter Katalysatormenge, mit konstantem Verlust – und Ersetzungsanteil. In dem zweiten, die Einheit arbeitet mit variabler Katalysatormenge, mit konstantem Verbrauch des Katalysators, der nicht ersetzt und auch nicht entzogen wird. Diese Untersuchungen zeigen die innere Abhängigkeit der einzelnen Variablen und ergeben eine Grundlege für die industrielle Anwendbarkeit der Ergebnisse.

The evaluation of catalyst performance in a fluidized bed is usually made on the basis of some particular catalyst property as, for example, the average catalyst activity in the commercial catalytic cracking of petroleum fractions. The average values of such catalyst properties are continually changing during a large part of the operating time, reflecting changes in the operating conditions and catalyst additions and losses. The calculation or prediction of average values in such a transient condition is a complex problem and has received little attention [1].

A general mathematical analysis [2] permits the calculation and prediction of the average value of any catalyst property under a variety of operating conditions. Comparison of the calculated and observed average catalyst activity in commercial cracking operations has been made in two cases. The first case is that of a refinery unit operating at essentially constant inventory, constant rate of catalyst loss and constant addition rate. The second case is that of a unit characterized by a changing inventory, constant rate of catalyst attrition and no withdrawals of catalyst. The prediction of average values is made possible by the use of pilot-plant data or by successive adjustments of parameters in the analysis during the commercial run.

*Gordon Research Conference on Catalysis, Colby Junior College, New London, N.H., June 25, 1958; 134th National Meeting A.C.S., Chicago, Ill., September 12, 1958.

†Present Address: Department of Chemical Engineering, Notre Dame University, South Bend, Indiana.

‡Present Address: Socony Mobil Oil Co., Inc., Research Department, Paulsboro, New Jersey.

Constant-inventory Case

The simplest model is that of a unit operating at constant inventory, constant loss rate and constant addition rate. The average activity in such a unit as a function of the time-on-stream can be described [2] by

$$\bar{A}(t) = A_0' \exp\left[-(k+s)\,t\right] + \frac{A_0\,s}{k+s}\left\{1 - \exp\left[-(k+s)\,t\right]\right\}. \qquad (1)$$

A_0', the start-up activity of the initial charge, and s, the fractional replacement rate, can be obtained from operating records; A_0, the initial activity of the replacement catalyst, and k, the exponential deactivation coefficient, may be determined from pilot-plant activity data.

The deactivation characteristics of the catalysts used in both cases are shown in Fig. 1 where relative activity is plotted against age. The data were obtained in pilot plants running under conditions similar to those of the commercial operations but with no catalyst additions or withdrawals. These nonreplacement data are described by an exponential expression

$$A\,(\text{age}) = A_0 \exp\left[-k\,(\text{age})\right]. \qquad (2)$$

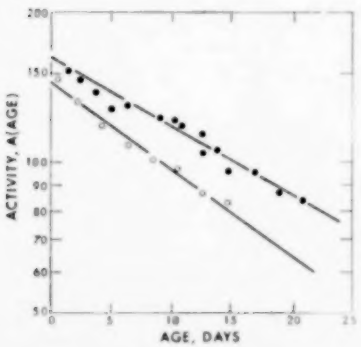

Fig. 1. Non-replacement activities of two commercial catalysts.

The line defined by the open data points, which refer to this case, fixes A_0 at 143 relative activity units and k at 0·037 day^{-1}.

The remaining data necessary to the use of equation (1) are A_0' and s. Operational records furnished the values of 70 relative activity units for A_0' and 0·0069 day^{-1} for s.

The average activity, $\bar{A}(t)$, in the commercial unit declined as time-on-stream, t, increased as shown in Fig. 2. The dashed curve is the average activity as calculated by equation (1). The

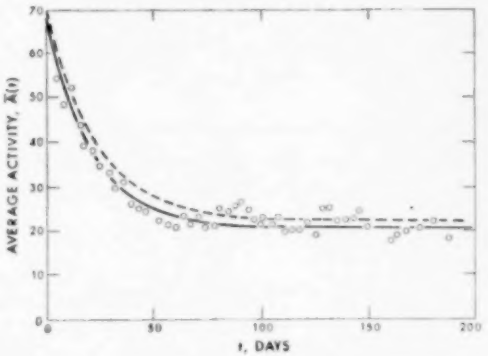

Fig. 2. Average activity for constant-inventory case.

quantities most subject to variation are the replacement rate, s, and the deactivation coefficient, k. Any improvement in agreement between the observed and and calculated values should come from knowing these quantities more accurately. The solid line shows the result of changing the fractional replacement rate, s, from 0·0069 to 0·0060; an adjustment of 13 per cent and within the limits of operating precision.

At infinite time-on-stream, equation (1) reduces to

$$\bar{A}(\infty) = \frac{A_0 s}{k+s}, \qquad (3)$$

which yields a steady-state activity of 21. This relationship, derived previously [1], accounts satisfactorily for the observed steady-state activity.

The mathematical simplicity of the analysis of this case permits the calculation of the contributions of various age groups to the inventory and to the activity. These calculations are summarized in Fig. 3, where the percentage contributions of catalyst age groups to the inventory and to the activity are given at various times-on-stream.

DAYS ON STREAM						CATALYST GROUP
0	25	50	100	150	200	
100 100	84 61	71 28	50 5	36 0	25 0	INITIAL CHARGE
	16 39	16 54	16 65	16 67	16 67	0 TO 25 DAYS OLD
		13 18	13 21	13 22	13 22	25 TO 50 DAYS OLD
			21 9	21 10	21 10	50 TO 100 DAYS OLD
				14 1	14 1	100 TO 150 DAYS OLD
					11 0	150 TO 200 DAYS OLD

Fig. 3. Contributions to inventory and activity. Upper number = per cent of inventory; lower number = per cent of activity.

The normalized catalyst inventory is described [2] by

$$\exp(-st) + \int_0^t s \exp\left[-s\,(\text{age})\right] d\,(\text{age}) = 1 \quad (4)$$

The first term denotes the fraction of the initial charge still remaining at time-on-stream, t. The integral represents the sum of the catalyst additions having ages up to time t. The integral may be partitioned to show the fractional contribution of various age groups in the unit. For example, at 200 days on stream and s equal to 0·0060 day^{-1}, equation (4) fixes the percentage contributions to the inventory shown in Fig. 3.

In order to show the fractional contributions of the catalyst groups to activity equation (1) may be rewritten as

$$\frac{A_0'}{\bar{A}(t)} \exp\left[-(k+s)\,t\right] + \frac{A_0'}{\bar{A}(t)} \int_0^t s \exp\left[-(k+s)(\text{age})\right] d\,(\text{age}) = 1 \quad (5)$$

The first term refers to the initial charge; the integral represents the fraction of the average activity due to the replacement catalyst. Again, the integral can be partitioned to distinguish the contributions of various age groups of catalyst. This calculation, in which k equalled 0·037 day^{-1} and s equalled 0·0060 day^{-1}, led to the percentage contributions to activity shown in Fig. 3.

Changing-inventory Case

The advantage of a changing-inventory model are shown by the analysis of another commercial catalytic-cracking run. The observed average activity is shown in Fig. 4 as a function of the time-on-stream. At 200 days the unit had not quite reached a steady-state condition.

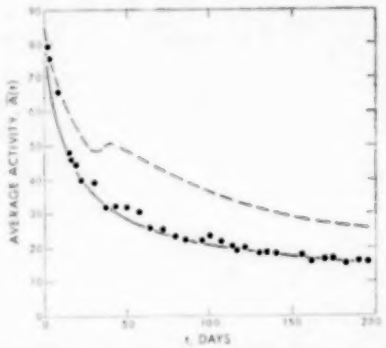

Fig. 4. Average activity for changing-inventory case.

The activity in a unit operating with changing inventory, constant attrition rate and no withdrawals is described by

$$\bar{A}(t) = \left\{M(0,0) + \sum_j a_j \left[1 - \exp(-d_j t)\right]\right\}^{-1} \times \left\{M(0,0)\,A_0' \exp\left[-(k+s)\,t\right] + \frac{A_0 s}{k+s}\left(M(0,0) + \sum_j a_j\right)\left(1 - \exp\left[-(k+s)\,t\right]\right) + \sum_j \frac{A_0\,a_j\,(s-d_j)}{k+s-d_j}\left(\exp\left[-(k+s)\,t\right] - \exp(-d_j t)\right)\right\}. \quad (6)$$

The derivation of this equation [2] assumed that any monotonic rise or fall of the catalyst inventory with time could be described by an expression of the type

$$\left(I(t) = M(0,0) + \sum_j a_j \left[1 - \exp(-d_j t)\right]\right), \quad (7)$$

where $M(0,0)$ is the start-up mass of the initial charge and the a_j's and d_j's are empirical constants. Hence, determination of the constants of equation (7) is a prerequisite to the use of equation (6).

VOL. 15 1961

The rise in catalyst inventory during the course of the run is shown in Fig. 5. The solid line is the result of fitting the data with a curve of the type given by equation (7). The constants were: $M(0, 0) = 300$ tons, $a_1 = 438$ tons, $a_2 = -168$ tons, $d_1 = 0{\cdot}0173\ \text{day}^{-1}$ and $d_2 = 0{\cdot}0446\ \text{day}^{-1}$.

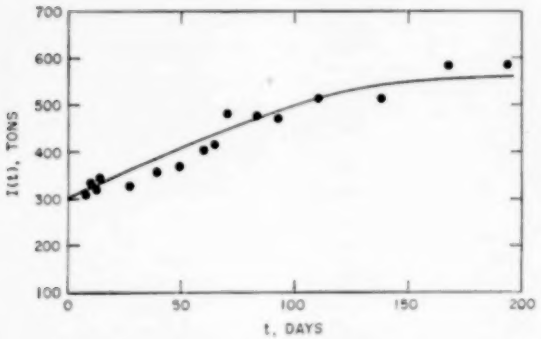

Fig. 5. Catalyst inventory for changing-inventory case.

Values for the remaining constants in equation (6) were again obtained from pilot-plant and operating data. The pilot-plant data, shown as solid points in Fig. 1, fixed A_0 at 162 relative activity units and k at $0{\cdot}0318\ \text{day}^{-1}$. From operating data A_0' and s were found to be 87·4 relative activity units and $0{\cdot}0053\ \text{day}^{-1}$, respectively.

The use of these empirical constants in equation (6) gives the average activity of the catalyst inventory represented by the dashed line in Fig. 4. The agreement with the observed values is poor, but the maximum in the curve at about 40 days on stream gives a clue to the reason. The maximum could be due to the mounting effect of the replacement catalyst as the time on stream increases. Increasing the deactivation coefficient, k, would decrease this effect and would also reduce the average activity. The best representation of the data was obtained by increasing k from $0{\cdot}0318\ \text{day}^{-1}$ to $0{\cdot}0570\ \text{day}^{-1}$. The solid line shows the excellence of the fit.

Discussion

These two commercial cases exemplify an analysis that attempts to unify the concepts regarding the operation of fluidized beds. They show that the transient state, which usually represents the greater part of a commercial run, can be followed, and that changes in it can be predicted. The agreement between the observed and calculated average values of the activity is limited by the accuracy of the non-replacement activity determination and the reliability of the knowledge of how catalyst is lost from the unit.

Analysis of the data from a unit operating at constant catalyst inventory shows that much of the inventory contributes little to the catalysis. From Fig. 3, at 100 days on stream, the initial charge represented 50 per cent of the inventory but only 5 per cent of the activity; catalyst less than 25 days old was contributing 65 per cent of the activity. Similarly, at 200 days on stream, 29 per cent of the inventory was catalyst less than 50 days old; it contributed 89 per cent of the activity. These percentages point up the importance of being able to detect old inactive catalyst and of trying to eliminate it from the unit.

The necessity of adjusting the deactivation coefficient in the changing-inventory case shows that empirical constants determined in the pilot plant should be considered as first approximations. If pilot-plant data are unavailable or inapplicable, the initial behaviour of a commercial unit can be used to estimate the value of such parameters. In general, an appreciation of the different degrees of freedom possessed by a fluidized bed should allow continuous correction of the elements of the analysis, and thereby permit prediction of average catalyst properties for the remainder of the run.

References

[1] Andersen S. L. and Matthias R. H. *Industr. Engng. Chem.* 1954 **46** 1296.
[2] John G. S. and Mikovsky R. J. *Chem. Engng. Sci.* 1961 **15** 163.

Chemical Engineering Science, 1961, Vol. 15, pp. 176 to 187. Pergamon Press Ltd., London. Printed in Great Britain.

Über das problem der optimalen Rührkesselkaskade für chemische reaktionen

F. Horn

Farbwerke Hoechst AG, vorm. Meister Lucius & Brüning, Frankfurt a.M.-Höchst

(*Received* 6 *September* 1960)

Zusammenfassung—Die Methoden der klassischen Extremalrechnung werden hier auf das Problem angewandt, die Temperaturen und Verweilzeiten in einer Rührkesselkaskade optimal zu wählen. Ein Gleichungssystem wird angegeben, dessen Lösung die gewünschten Grössen ergibt. Es werden drei Methoden zur Lösung dieses Systems diskutiert ; eine davon steht in einer engen Beziehung zu dem Verfahren der dynamischen Programmierung. Es wird untersucht, in welchen Fällen sich besondere Vereinfachungen ergeben und es werden Beziehungen angegeben, die die Rechnung bei Problemen der Klasse zwei bzw. bei linearer Kinetik erleichtern. Dies wird demonstriert an dem Reaktionssystem $A_1 \rightarrow A_2 \rightarrow A_3$, $A_2 \rightarrow A_4$. Die in anderen Arbeiten abgeleiteten Optimalbedingungen für das Reaktionsrohr werden durch einen Grenzübergang Kaskade → Rohr erhalten.

Abstract—The methods of the classical calculus using limits are applied here to the problem of choosing the optimal conditoins of temperature and duration time in a cascade stirring-boiler. A system of equations is presented, the solution of which gives the required values. Three methods for the solution of this system are discussed ; one of is them in close connexion with the dynamic programming. The possibility of special simplifications is examined and equations are presented that make easier the solution of problems of the second class and of linear kineties respectively. This is demonstrated by the reaction-system $A_1 \rightarrow A_2 \rightarrow A_3$, $A_2 \rightarrow A_4$. The optimal conditions for the reaction tube, which were discussed in other papers, are obtained here with the aid of boundary-crossing cascade → tube.

Résumé—On applique les méthodes de calcul classique utilisant les limites au problème du choix des conditions optimales de température et de durée dans le cas de réacteurs en cascade agités par ébullition. On propose un système d'équation dont les solutions donnent les valeurs recherchées. On expose trois méthodes de résolution du système ; une d'entre elles est en étroite relation avec les programmations dynamiques. On examine les possibilités de simplifications particulières et on donne les équations ce qui rend plus aisée la résolution des équations cinétiques du 1er et du 2ème ordre. On démontre ceci par le système de réactions :

$$\begin{cases} A_1 \rightarrow A_2 \rightarrow A_3 \\ A_2 \rightarrow A_4 \end{cases}$$

Les conditions optimales pour le réacteur tubulaire, qui ont été exposées dans d'autres articles, sont obtenues ici en faisant tendre une cascade de réacteurs vers le réacteur tubulaire.

Einleitung

In einigen kürzlich erschienenen Arbeiten [1, 2] wurde sehr effektvoll demonstriert, wie man mit Hilfe der dynamischen Programmierung die optimalen Betriebsbedingungen einer Rührkesselkaskade ermitteln kann. In anderen Arbeiten [3, 4, 6, 7, 8] wurde mit den Methoden der klassischen Variationsrechnung ein analoges Problem für das Reaktionsrohr untersucht. Dabei ergab es sich, dass verschiedenen Autoren unabhängig voneinander das gleiche Reaktionssystem einmal für die Kaskade [1], das anderemal für das Rohr [7] untersuchten. An diese Arbeiten soll hier angeknüpft werden.

Immer wenn man von "optimal" spricht, muss man zwei Dinge näher erklären : Erstens, welche Grösse soll ein Maximum bzw. Minimum annehmen und zweitens, welche Grössen werden variiert (d.h. sind optimal zu wählen) und welche Grössen bleiben konstant.

In früheren Arbeiten [6, 8] wurde bereits diskutiert, welche Grössen für eine Extremierung in Betracht kommen: eine sehr allgemeine Formulierung des Problems besteht in der Forderung, dass eine gegebene Funktion der Zusammensetzung des Reaktionsgemisches am Ende des Reaktors und der gesamten Verweilzeit ein Extrem annehmen soll.

Die Grössen, die hier variiert werden, sind die Temperaturen und Verweilzeiten in den einzelnen Kesseln einer Kaskade. Für eine Kaskade aus N Kesseln sind das 2N Grössen. Konstantgehalten wird die Anfangszusammensetzung des Reaktionsgemisches, die Anzahl der Kessel und – für einen Teil der Probleme – die gesamte Verweilzeit in der Kaskade.

Es sollen später die Methoden der klassischen Extremalrechnung angewandt werden, d.h., es werden differentielle Optimalbedingungen benutzt. Dagegen könnte man einwenden, dass solche Bedingungen – sofern man nur die ersten Ableitungen betrachtet – nur notwendig und nicht hinreichend sind. Wie bereits früher diskutiert [8], ist aber nicht anzunehmen, dass daraus bei Optimalproblemen, die die Temperaturführung betreffen besondere Schwierigkeiten entstehen. Ausserdem können bestimmte Ergebnisse, wie z.B. geschlossene Lösungen und andere allgemeinere Resultate (vgl. [6, 8]), ohne solche Bedingungen nicht gefunden werden. In der Tat wurden differentielle Bedingungen in vielen Fällen mit Erfolg angewendet (vgl. z.B. [3, 4]).

In den folgenden Abschnitten werden zuerst die Grundgleichungen für Rührkesselkaskaden diskutiert, dann wird das Optimalproblem näher präzisiert und anschliessend werden die Optimalbedingungen abgeleitet. Im restlichen Teil der Arbeit wird das den optimalen Reaktor bestimmende Gleichungssystem näher untersucht. Die Bezeichnungen und die Methodik schliessen sich eng an früher veröffentlichte Arbeiten [6, 7, 8] an.

Die Grundgleichungen

Da in einem Rührkessel die Durchmischung für alle Stoffe in gleicher Weise erfolgt und ebenso der Stofftransport von Kessel zu Kessel in einer Kaskade, ist die Zusammensetzung des Reaktionsgemisches an jeder Stelle einer Kaskade gegeben durch

die Anfangszusammensetzung und
die Angabe von n "Reaktionsvariablen."

Dabei soll n zunächst die Zahl der stöchiometrisch unabhängigen Reaktionen bedeuten. Diese Zahl ist im allgemeinen kleiner als die Zahl der Reaktionsteilnehmer und manchmal auch kleiner als die Zahl der tatsächlich ablaufenden Reaktionen. Z.B. enthält das Reaktionssystem

$$A_1 \rightarrow A_2 \begin{matrix} \nearrow A_3 \\ \searrow A_4 \end{matrix} \qquad (1)$$

drei stöchiometrisch unabhängige Reaktionen. Hier kann man z.B. als Reaktionsvariable die Konzentrationen der Stoffe A_1, A_2 und A_3 wählen. Bei gegebener Anfangszusammensetzung folgt die Konzentration von A_4 aus diesen drei Konzentrationen mittels einer einfachen stöchiometrischen Beziehung. Anstelle der Konzentrationen kann man auch andere Grössen als Reaktionsvariable nehmen. Allgemein sollen die Reaktionsvariablen deswegen mit x_i bezeichnet werden.

Die Reaktionsvariablen ändern sich von Kessel zu Kessel. Ihre Werte sollen im Einlauf, d.h. vor dem ersten Kessel, mit $x_i(0)$, im ersten Kessel mit $x_i(1)$ und allgemein im ν-ten Kessel mit $x_i(\nu)$ bezeichnet werden. Im letzten Kessel und im Auslauf haben die Reaktionsvariablen die Werte $x_i(N)$. Die Kesselnummer wurde in Klammer gesetzt, erstens, um sie vom Reaktionsindex gut zu unterscheiden und zweitens, um die Analogie mit dem Reaktionsrohr – hier sind die x_i Funktionen einer kontinuierlichen Variablen – besonders hervortreten zu lassen. Die Temperaturen und Verweilzeiten in den einzelnen Kesseln werden in analoger Weise mit $T(\nu)$ bzw. $\tau(\nu)$ bezeichnet.

In Abb. 1 ist eine Kaskade schematisch dargestellt. Unter jedem Kessel stehen die den Kessel charakterisierenden physikalischen Grossen. Über den Kesseln stehen die für den optimalen Entwurf wichtigen Rechengrössen λ, die später näher erläutert werden.

Bei den hier untersuchten Problemen ist die Zusammensetzung des Reaktionsgemisches am Anfang des Reaktors gegeben, d.h., es sind auch

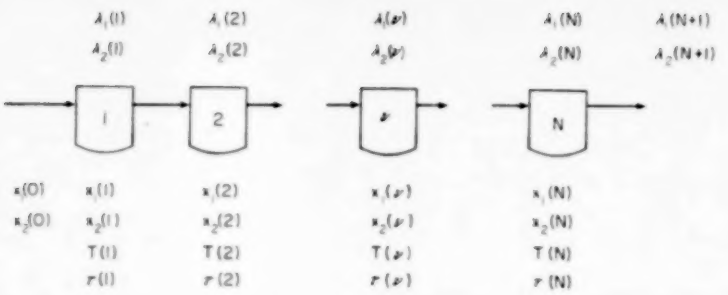

ABB. 1. Schematische Darstellung einer Kaskade mit den sie charakterisierenden physikalischen Grössen $x_1(\nu)$, $x_2(\nu)$, $T(\nu)$, $\tau(\nu)$ und den Rechengrössen $\lambda_1(\nu)$ u . $\lambda_2(\nu)$. $n = 2$.

die $x_i(0)$ gegeben. Bezeichnet man diese Werte mit a_i, dann bestehen also für die x_i die folgenden Anfangsbedingungen

$$x_i(0) = a_i, \qquad i = 1, 2, \ldots n \tag{2}$$

Es wird später gezeigt, dass auch eine Randbedingung für die λ_i besteht, hier aber für das Ende des Reaktionsapparates, d.h., für die $\lambda_i(N+1)$.

Die Stoffbilanz für den ν-ten Kessel lässt sich stets in der Form

$$x_i(\nu) - x_i(\nu-1) = \tau(\nu)\, v_i(x_i(\nu), x_2(\nu), \ldots x_n(\nu);\ T(\nu)) \tag{3}$$

schreiben. Dabei bedeuten die v_i Reaktionsgeschwindigkeiten bzw. Funktionen, die sich aus den wahren Reaktionsgeschwindigkeiten linear zusammensetzen. Z.B. gilt für das Reaktionssystem (1), wenn die x_i wieder mit den Konzentrationen c_i identifiziert werden und wenn alle Reaktionen von erster Ordnung sind und ohne Volumänderung von sich gehen

$$v_1 = -k_1 c_1,\ v_2 = k_1 c_1 - (k_2 + k_3) c_2,\ v_3 = k_3 c_2 \tag{4}$$

Man kann Gleichung (2) auch in der abgekürzten Form

$$x_i(\nu-1) = x_i(\nu) - \tau(\nu)\, v_i(\nu) \tag{5}$$

schreiben. Sind alle $T(\nu)$ und $\tau(\nu)$ gegeben, dann können die $x_i(\nu)$ für $\nu > 0$ mit Hilfe dieser Gleichungen berechnet werden. Denn setzt man in (5) $\nu = 1$, dann hat man ein System von n Gleichungen für die n unbekannten $x_i(1)$. Die unbekannten Grössen stehen in (5) alle auf der rechten Seite. Die Auflösung des Gleichungssystems liefert die $x_i(1)$. Die Reaktionsvariablen für die folgenden Kessel 2, 3, ... N erhält man, wenn man in (5) für $\nu = 2, 3, \ldots . N$ setzt und diese Gleichungssysteme sukzessive nach $x_i(2)$, x (3) u.s.w. auflöst.

DAS OPTIMALPROBLEM

Wie in früheren Arbeiten [6, 8] gezeigt wurde, erhält man eine sehr allgemeine Formulierung des Optimalproblems, wenn man fordert, dass eine Funktion M der Reaktionsvariablen am Ende des Reaktionsapparates und der gesamten Verweilzeit ein Extrem werden soll:

$$M(x_1(N), x_2(N), \ldots x_n(N);\ \tau) \to \text{Extrem} \tag{6}$$

$$\tau = \tau(1) + \tau(2) + \ldots + \tau(N) \tag{7}$$

Je nachdem ob M die Verweilzeit tatsächlich enthält oder nicht, handelt es sich um ein Ausnutzungsproblem oder um ein Umsetzgunsproblem [8]. Für ein Ausnutzungsproblem gilt also

$$\frac{\partial M}{\partial \tau} \neq 0 \tag{8}$$

und für ein Umsetzungsproblem

$$\frac{\partial M}{\partial \tau} = 0 \tag{9}$$

Eine weitere, für die praktische Berechnung wichtige Einteilung, ist die Klasseneinteilung der Probleme. Die Klassenzahl eines Problems ist gleich der Anzahl (gezählt werden hier nur die verschiedenen Indizes i) der Differenzengleichungen

der Form (3), die hinreichen, um M bei gegebenen $T(\nu)$ und $\tau(\nu)$ zu berechnen. Diese Zahl kann kleiner sein als die Zahl der stöchiometrisch unabhängigen Reaktionen. Als Beispiel diene das Reaktionssystem (1), bei dem der Stoff A_2 das erwünschte Produkt und A_3 und A_4 unerwünschte Nebenprodukte sein sollen. Ist der Rohstoff A_1 sehr teuer, dann kommt es nur darauf an, die Konzentration von A_2 am Ende des Reaktors möglichst hoch zu machen ohne Rücksicht auf die gesamte Verweilzeit im Reaktionsapparat. In diesem Fall ist also

$$M = c_2(N), \tag{10}^*$$

d.h., es handelt sich um ein Umsetzungsproblem. Zur Berechnung von M bei gegebenen $T(\nu)$ und $\tau(\nu)$ benötigt man nur die Differenzengleichungen für $i = 1$ und $i = 2$ (Vergl. Gleichung 4), denn c_3 kommt weder in v_1 und v_2 noch in M vor. D.h., das Problem ist von der Klasse 2.

Im folgenden soll unter n nicht mehr die Zahl der stöchiometrisch unabhängigen Reaktionen sondern die Klassenzahl verstanden werden.

Die Optimalbedingungen für das Umsetzungsproblem

Für das Umsetzungsproblem geht die Forderung (6) über in

$$M(x_1(N), x_2(N), \ldots, x_n(N)) \to \text{Extrem} \tag{11}$$

Dies kann als ein Extremalproblem mit den Variablen $x_i(\nu)$, $T(\nu)$ und $\tau(\nu)$ aufgefasst werden bei dem als Nebenbedingungen noch die Gleichungen (5) beachtet werden müssen. Die klassische Methode, ein solches Problem zu lösen, besteht in der Einführung von Lagrange'schen Parametern. In dem hier untersuchten Fall benötigt man $n\,N$ Parameter, je einen für jede der $n\,N$ Gleichungen (5) Bezeichnet man diese Parameter mit $\lambda_i(\nu)$, dann ist die Aufgabe (11) äquivalent mit der Aufgabe, eine Funktion F ohne Nebenbedingungen zu extremieren, wobei F gegeben ist durch

$$F = M(x_i(N)) - \sum_{\nu=1}^{N}\sum_{j=1}^{n} \lambda_j(\nu)\left[x_j(\nu) - x_j(\nu-1) - \tau(\nu)v_j(\nu)\right] \tag{12}$$

Daraus erhält man durch Differenzieren nach den verschiedenen Variablen und Nullsetzen eine Reihe von Beziehungen.

1. Differenzieren nach $x_i(\nu)$; $\nu = 1, 2, \ldots N-1$ führt zu

$$\lambda_i(\nu+1) - \lambda_i(\nu) = -\tau(\nu)\sum_{j=1}^{n}\lambda_j(\nu)\frac{\partial v_j(\nu)}{\partial x_i} \tag{13}$$

2. Differenzieren nach $x_i(N)$ führt zu

$$\frac{\partial M}{\partial x_i(N)} - \lambda_i(N) = -\tau(N)\sum_{j=1}^{n}\lambda_j(N)\frac{\partial v_j(N)}{\partial x_i} \tag{14}$$

3. Differenzieren nach $T(\nu)$ führt zu

$$\sum_{j=1}^{n}\lambda_j(\nu)\frac{\partial v_j(\nu)}{\partial T} = 0 \tag{15}$$

4. Differenzieren nach $\tau(\nu)$ führt zu

$$\sum_{j=1}^{n}\lambda_j(\nu)v_j(\nu) = 0 \tag{16}$$

Die Gleichungen (13) und (14) lassen sich zu einer Gleichung zusammenfassen, wenn man setzt

$$\lambda_i(N+1) = \frac{\partial M}{\partial x_i(N)}$$

und wenn man ausserdem den Gültigkeitsbereich der Gleichung (13) erweitert auf

$$\nu = 1, 2, \ldots N-1, N$$

Da bei den weiteren Untersuchungen immer wieder auf diese Beziehungen und auf die Beziehungen (2) und (5) verwiesen wird, sind alle diese Gleichungen noch einmal zusammengestellt und mit besonderen Beziechungen (römische Zahlen) versehen. Die Gleichungen (13) sind in der Zusammenstellung durch Einführung des Kroneckerschen δ* umgeformt.

*Versteht man unter M eine Kostenfunktion [8], dann wäre es richtig, zu setzen $M = M(c_2(N))$. Jedoch macht dies keinen Unterschied für die folgenden Rechnungen.

* $\delta_{ik} = 1$ für $i = k$; $\delta_{ik} = 0$ für $i \neq k$

$$i, j = 1, 2, \ldots . n$$

$$\nu = 1, 2 \ldots . N$$

$$x_i(0) = a_i \qquad \text{I}$$

$$x_i(\nu - 1) = x_i(\nu) - \tau(\nu)\, v_i(\nu) \qquad \text{II}$$

$$\sum_{j=1}^{n} \lambda_j(\nu) \frac{\partial v_j(\nu)}{\partial T} = 0 \qquad \text{III (a)}$$

$$\sum_{j=1}^{n} \lambda_j(\nu) v_j(\nu) = 0 \qquad \text{III (b)}$$

$$\lambda_i(\nu + 1) = \sum_{j=1}^{n} \left[\delta_{ij} - \tau(\nu) \frac{\partial v_j(\nu)}{\partial x_i} \right] \lambda_j(\nu) \qquad \text{IV}$$

$$\lambda_i(N + 1) = \frac{\partial M}{\partial x_i(N)} \qquad \text{V}$$

Wenn Temperaturgrenzen oder Grenzen für die Verweilzeit in einem Kessel gegeben sind, dann kommen zu diesen Beziehungen noch Nebenbedingungen in Ungleichungsform, die dann vorrangig vor den Gleichungen III sind. Im allgemeinen lassen sich solche Bedingungen in Verbindung mit differentiellen Optimalbedingungen nur schwer berücksichtigen. Hier ist das Problem aber deshalb einfach, weil in jeder Nebenbedingung nur eine Variable vorkommt:

$$T_{unt} \leqslant T \leqslant T_{ob}, \qquad \tau_{unt} \leqslant \tau \leqslant \tau_{ob} \qquad (17)$$

D.h. im ($2N$-dimensionalen) T, τ-Raum hat das zulässige Gebiet die Form eines Quaders. Solche Bedingungen verursachen keine besonderen Schwierigkeiten. Es soll hier aber trotzdem von der Existenz derartiger Nebenbedingungen abgesehen werden. Die Aufgabe, den optimalen Reaktionsapparat zu berechnen, ist dann identisch mit der Aufgabe, das Gleichungssystem I–V zu lösen.

Dies scheint sehr schwierig zu sein; es zeigt sich aber, dass es einfach ist, wenn man entweder Gleichung I oder die Gleichungen III oder Gleichung V unberücksichtigt lässt. Die im folgenden beschriebenen Lösungsmethoden gehen aus von dieser Tatsache. Sie bestehen alle aus einer Folge von Schritten. Bei jedem Schritt wird entweder I oder III oder V nicht berücksichtigt, aber es wird versucht, durch geeignetes Probieren bzw. systematisches Fortschreiten diese Beziehungen schliesslich doch zu erfüllen.

Das Probieren mit den Randwerten am Ende des Reaktors

Bei diesem Verfahren wird zunächst darauf verzichtet, die Gleichungen I zu erfüllen. Für die Endwerte $x_i(N)$ werden probeweise Werte angenommen. Mit diesen Werten lässt sich dann die ganze Kaskade leicht durchrechnen, insbesondere ergeben sich auch die $x_i(0)$. Die Endwerte $x_i(N)$ müssen dann solange variiert werden, bis die Gleichungen I schliesslich erfüllt sind.

Zur Vorbereitung soll zunächst gezeigt werden, dass aus $x_i(\nu)$ und $\lambda_i(\nu + 1)$ die Werte für $T(\nu)$, $\tau(\nu)$, $x_i(\nu - 1)$ und $\lambda_i(\nu)$ mittels der Gleichungen II, III und IV zwangsläufig folgen. Durch Elimination der $\lambda_j(\nu)$ aus III(a) und IV bzw. III(b) und IV erhält man nämlich die Gleichungen

$$\begin{vmatrix} \lambda_i(\nu + 1) & \delta_{ij} - \tau(\nu) \dfrac{\partial v_j(\nu)}{\partial x_i} \\ 0 & \dfrac{\partial v_j(\nu)}{\partial T} \end{vmatrix} = 0 \qquad (18a)$$

$$\begin{vmatrix} \lambda_i(\nu + 1) & \delta_{ij} - \tau(\nu) \dfrac{\partial v_j(\nu)}{\partial x_i} \\ 0 & v_j \end{vmatrix} = 0 \qquad (18b)$$

Die Determinanten in den Gleichungen (18) sind $(n + 1)$-reihig. Zur Abkürzung wurde die n-reihige quadratische Matrix in den rechten oberen Ecken durch das allgemeine Element der Koeffizientenmatrix in IV dargestellt.

Die Gleichung (18) enthalten als Unbekannte nur $T(\nu)$ (enthalten in $v(\nu)$) und $\tau(\nu)$, wenn $x_i(\nu)$ und $\lambda_i(\nu + 1)$ bekannt sind. $T(\nu)$ und $\tau(\nu)$ können somit durch Auflösung der Gleichungen (18a) und (18b) ermittelt werden.

Ein Einzelschritt des Verfahrens besteht daher aus den folgenden Zwischenschritten:

1. Nach probeweiser Annahme der $x_i(N)$ ergeben sich die $\lambda_i(N + 1)$ nach Gleichung V.

2. Aus $x_i(N)$ und $\lambda_i(N + 1)$ folgen mit Hilfe der Gleichung (18a) und (18b) die Werte $T(N)$ und $\tau(N)$.

3. Nun ist auch das Koeffizientenschema von IV für $\nu = N$ bekannt, d.h. die $\lambda_i(N)$ können durch Auflösen von IV berechnet werden.

4. Mit Hilfe von II ergeben sich jetzt auch die $x_i(N-1)$, denn die rechten Seiten der Gleichungen II sind jetzt für $\nu = N$ bekannt.

5. Die in 1.–4. beschriebene Rechnung wird von Stufe zu Stufe solange wiederholt, bis schliesslich auch die Anfangswerte $x_i(0)$ bekannt sind.

Diese Anfangswerte werden natürlich wegen der zunächst willkürlichen Annahme der $x_i(N)$ nicht mit den gegebenen Werten a_i übereinstimmen, d.h., das ganze Verfahren muss unter Variation der $x_i(N)$ solange wiederholt werden, bis diese Übereinstimmung erzielt ist, d.h. bis Gleichung I erfüllt ist.

Dieses Verfahren hängt sehr eng mit dem Verfahren der dynamischen Programmierung zusammen, das von Aris [1] zur Berechnung von optimalen Kaskaden angewandt wurde. Denn der Zusammenhang zwischen dem probeweise angenommenen Satz der $x_i(N)$ und dem daraus zwangsläufig folgenden Satz der $x_i(N-k)$ ist die Beziehung, die bei dem Verfahren von Aris als Zwischenresultat auftritt und die benutzt wird, um das Problem der Optimierung einer N-Kaskade auf das der Optimierung einer k-Kaskade zurückführen. Bei dem Auflösen der Gleichungen (18) nach T und τ wird eine optimale $(N-\nu+1)$ — Kaskade aus den Resultaten für eine optimale $(N-\nu)$ — Kaskade berechnet. Derselbe Vorgang findet sich auch bei Aris. Allerdings werden dort im allgemeinen keine differentiellen Optimalbedingungen verwendet (wie z.B. Gleichung III eine ist), d.h. auf die Berechnung der λ wird verzichtet.

Besondere Vereinfachungen bei speziellen Reaktionssystemen

Bei dem eben beschriebenen Verfahren ist ein "n-dimensionales Probieren" erforderlich um schliesslich zu bestimmten Anfangswerten zu gelangen. Das wäre nicht weiter schlimm, wenn optimale Kaskaden für viele verschiedene Anfangszusammensetzungen interessieren, denn es gibt dann keinen Grund ausgerechnet auf bestimmten Anfangsbedingungen zu bestehen. Ist diese Vereinfachung nicht gegeben, dann ist es wichtig zu wissen, in welchen Fällen die – bei grösseren n ausserordentlich mühsame – Arbeit des n-dimensionalen Probierens verringert werden kann. Bei dem Verfahren von Aris tritt an die Stelle des n-dimensionalen Probierens ein numerisches Arbeiten mit Funktionen von n Argumenten. Auch hier ist eine Reduktion der Dimensionszahl von grosser Bedeutung für die praktische Berechnung.

Eine Reduktion ist immer dann möglich, wenn eine Transformationsgruppe der x_i gefunden wird, die die Gleichungen II – V invariant lässt. Zwei Möglichkeiten sollen näher diskutiert werden:

(1) *Die Kinetik ist linear und M ist eine lineare Funktion der x_i.*

Die Kinetik soll als "linear" bezeichnet werden, wenn die v_i in der Form

$$v_i = \sum_{k=1}^{n} b_{ik} x_k \tag{19}$$

beschrieben werden können. Die Koeffizienten b_{ik} dürfen dabei nur von der Temperatur abhängen. In diesem Fall sind die Gleichungen II–V invariant gegenüber einer Multiplikation aller $x_i(\nu)$ mit einem Faktor. D.h. statt der n Variablen $x_i(N)$ braucht man jetzt nur deren $n-1$ Verhältnisse zu variieren: Die Dimensionszahl des Verfahrens hat sich von n auf $n-1$ verringert.

(2) *M ist linear in einer Variablen z.B. in $x_n(N)$ und diese Variable kommt ausserdem in keiner Geschwindigkeit vor.*

Es ist dann

$$\frac{\partial v_i(\nu)}{\partial x_n} = 0 \quad \text{für alle } i,\ \nu \tag{20}$$

und man erkennt leicht, dass die Gleichungen II–V invariant sind gegenüber Addition einer beliebigen Konstanten zu allen $x_n(\nu)$. Auch hier reduziert sich die Dimension des Problems um Eins, denn ist die Rechnung für einen Satz der $x_i(N)$ durchgeführt, dann ist sie es auch für alle Sätze, die aus diesem Satz durch Veränderung von $x_n(N)$ hervorgehen.

Bei dem Problem von Denbigh [5], das für die Rührkesselkaskade [1] und für das Reaktionsrohr [7] untersucht wurde, sind beide

Vereinfachungen gleichzeitig gegeben. Da dieses Problem von der Klasse 3 ist, reduziert sich die Dimension von 3 auf $3 - 1 - 1 = 1$. Für das Rohr reduziert sich die Dimension, wie später gezeigt wird, sogar noch weiter. Diese Möglichkeiten zur Vereinfachung wurden in den zitierten Arbeiten ausgenutzt.

Die Methode des Stärksten Anstiegs

Bei diesem Verfahren wird zunächst darauf verzichtet, die Optimalbedingungen III zu erfüllen Dafür werden alle anderen Gleichungen, insbesondere die Randbedingungen I berücksichtigt.

Zur Vorbereitung soll die Funktion M als eine Funktion der $x_i(0)$, $T(\nu)$ und $\tau(\nu)$ aufgefasst werden. Diese Grössen bestimmen nämlich (vgl. S. 180) die ganze Kaskade, und daher auch die $x_i(N)$ ind die Funktion M.

Um die Ableitungen von M nach $T(\nu)$ und $\tau(\nu)$ zu bestimmen, kann man sich der Funktion F (vgl. Gleichung 12) bedienen. Es gilt nämlich

$$\frac{\partial M}{\partial T(\nu)} = \frac{\partial F}{\partial T(\nu)}; \quad \frac{\partial M}{\partial \tau(\nu)} = \frac{\partial F}{\partial \tau(\nu)} \tag{21}$$

und daraus folgt:

$$\frac{\partial M}{\partial T(\nu)} = \tau(\nu) \sum_{j=1}^{n} \lambda_j(\nu) \frac{\partial v_j(\nu)}{\partial T} \tag{22a}$$

$$\frac{\partial M}{\partial \tau(\nu)} = \sum_{j=1}^{n} \lambda_j(\nu) v_j(\nu) \tag{22b}$$

Für die weitere Rechnung soll angenommen werden, dass ein Maximum von M angestrebt wird.*

Geht man aus von einem Satz $T(\nu)$ und $\tau(\nu)$, dann ist die "Richtung des stärksten Anstiegs" von M bekanntlich gegeben durch den Satz der Ableitungen von M nach $T(\nu)$ und $\tau(\nu)$. D.h. zu dem Satz

$$T(\nu) + \epsilon \frac{\partial M}{\partial T(\nu)}; \quad \tau(\nu) + \epsilon \frac{\partial M}{\partial \tau(\nu)} \tag{23}$$

gehört bei hinreichend kleinem positiven ϵ ein grösseres M als zu dem alten Satz, d.h. die diesem Satz entsprechende Kaskade ist besser als die alte.

Das Verfahren beginnt damit, dass man eine beliebige Kaskade mit der gewünschten Kesselzahl annimmt, d.h. man gibt die $T(\nu)$ und $\tau(\nu)$ willkürlich vor. Jeder weitere Schritt des Verfahrens besteht aus den folgenden Zwischenschritten:

1. Ausgehend von den gegebenen $x_i(0)$ berechnet man mit Hilfe der Gleichungen II alle $x_i(\nu)$ (vgl. S 180). Aus $x_i(N)$ berechnet man M und mit Hilfe von Gleichung V die $\lambda_i(N+1)$.
2. Ausgehend von $\lambda_i(N+1)$ berechnet man durch sukzessives Auflösen der Gleichungen IV alle $\lambda_i(\nu)$.
3. Man geht zu einer besseren Kaskade über mit Hilfe der Gleichungen

$$T(\nu)_{\text{neu}} = T(\nu)_{\text{alt}} + \epsilon\, \tau(\nu)_{\text{alt}} \sum_{j=1}^{n} \lambda_j(\nu) \frac{\partial v_j(\nu)}{\partial T} \tag{24a}$$

$$\tau(\nu)_{\text{neu}} = \tau(\nu)_{\text{alt}} + \epsilon \sum_{j=1}^{n} \lambda_j(\nu)\, v_j(\nu) \tag{24b}$$

ϵ muss hinreichend klein gewählt werden. Näheres über die Wahl von ϵ in [7]*.

4. Schliesslich wird die neue Kaskade als Startpunkt für eine wiederholte Rechnung 1.–4. genommen.

Man rechnet in der beschreibenen Weise solange, bis sich M bzw. die $T(\nu)$ unf $\tau(\nu)$ nicht mehr ändern. Das hier beschriebene Verfahren hat sich in der praktischen Berechnung sogar bei Variationsaufgaben bewährt, d.h. bei Aufgaben, bei denen die Zahl der Stufen unendlich gross ist (vgl. [7]).

Bestehen für die Temperaturen und die Verweilzeiten aus Gründen, die durch die Praxis gegeben sind, Beschränkungen, dann kann dies bei der Methode des stärksten Anstiegs sehr leicht berücksichtigt werden: Man benutzt die Gleichungen (24) nur, wenn die neuen Werte innerhalb der vorgegebenen Grenzen liegen. Führt die Anwendung von (24) über eine Grenze hinaus, dann nimmt man für die neuen Werte die entsprechenden Grenzwerte.

*Dies ist natürlich keine wesentliche Einschränkung; wird ein Minimum angestrebt, so hat man einfach M durch $-M$ zu ersetzen.

*In [7] ist statt ϵ das Symbol μ verwendet.

VOL. 15 1961

Das Probieren mit den Randwerten am Anfang des Reaktors

Dieses Verfahren soll nur kurz diskutiert werden, es scheint bei der Berechnung von Kaskaden gegenüber den anderen Methoden keinen besonderen Vorteil zu besitzen.

Verzichtet man zunächst darauf, die Gleichungen V zu erfüllen, dann kann man die $\lambda_i(1)$ am Anfang des Reaktors frei annehmen. Mit Hilfe der Gleichungen III kann jetzt $T(1)$ und $\tau(1)$ berechnet werden. Man muss dazu die $x_i(1)$ durch Auslösen der Gleichung II als Funktionen von $x_i(0)$, $T(1)$ und $\tau(1)$ darstellen. Setzt man die $x_i(1)$ dann in Gleichung III ein, so hat man zwei Gleichungen für $T(1)$ und $\tau(1)$, aus denen sich diese beiden Grössen berechnen lassen. Als nächstes ergeben sich die $x_i(1)$ mit Hilfe der nach $x_i(1)$ aufgelösten Gleichungen II und die $\lambda(2)$ mit Hilfe von Gleichung IV. So fortschreitend gelangt man schliesslich zu den $x_i(N)$ und $\lambda_i(N+1)$. Die Randbedingung V muss durch Probieren mit den Anfangswerten $\lambda_i(1)$ erfüllt werden. Ein Vorteil des verfahrens besteht in der Homogenität der Gleichungen in den λ: In jedem Fall ist hier deswegen nur ein $(n-1)$ – dimensionales Probieren erforderlich. Dies wirkt sich besonders bei den Ausnutzungsproblemen der Klasse 2 für das Reaktionsrohr aus (vgl. den Abschnitt über das Rohr).

Das Ausnutzungsproblem

Es soll jetzt der Fall untersucht werden, dass M von der gesamten Verweilzeit abhängt. Man geht dann zweckmässig in zwei Schritten vor (vgl. [8]):

1. Man hält die gesamte Verweilzeit fest, d.h. man betrachtet Gleichung (7) als Nebenbedingung und sucht den für diese Gesamtverweilzeit optimalen Reaktor.

2. Aus den für verschiedene Gesamtverweilzeiten berechneten "Optimalreaktoren" sucht man sich den wirtschaftlichsten aus.

Diese Aufteilung ist vor allem dann zweckmässig, wenn es sich um ein Qutputproblem (vgl. [5, 8]) handelt, d.h. wenn M von der Form

$$M = M\left(m\left(x_1(N), x_2(N), \ldots x_n(N)\right); \tau\right) \qquad (25)$$

ist. In diesem Fall kann man beim ersten Schritt die komplizierte Funktion M durch die einfachere Funktion m ersetzen (vgl. [8]), d.h. man fordert

$$m \rightarrow \text{Extrem} \qquad (26)$$

In den folgenden Gleichungen soll trotzdem – um im allgemeinen zu bleiben – immer das Symbol M verwendet werden. Führt man μ als neven Lagrange'schen Faktor ein, dann hat man zur rechten Seite von Gleichung (12) noch den Ausdruck

$$-\mu\left[\tau(1) + \tau(2) + \ldots + \tau(N) - \tau\right]$$

hinzuzufügen. Die weitere Rechnung ergibt, dass die Gleichungen I–V unverändert bleiben mit Ausnahme von Gleichung III(b). Diese Gleichung lautet jetzt

$$\sum_{j=1}^{n} \lambda_j(\nu)\, v_j(\nu) = \mu \qquad \text{III (b')}$$

Als Folge davon ändert sich auch Gleichung (18b): Anstelle der Null im linken unteren Eck der Determinante ist μ zu schreiben. Im ersten Teil der Aufgabe müssen Rechnungen mit verschieden angenommenen μ durchgeführt werden; in den Gleichungen V kann dabei M gegebenfalls durch m ersetzt werden. Als Ergebnis dieser Rechnungen erhält man Optimalreaktoren für verschiedene Gesamtverweilzeiten. Dies ist dann der Ausgangspunkt für den zweiten Schritt.

Man kann beide Schritte 1. und 2. in einem erledigen, wenn $M(x_i(N), \tau)$ analytisch gegeben ist. Dann kann man von vornherein mit dem richtigen μ rechnen. Man findet nämlich leicht mit Hilfe von (12) (M hängt jetzt von τ ab):

$$\mu = -\frac{\partial M}{\partial \tau} \qquad (27)$$

bzw.

$$\sum_{j=1}^{n} \lambda_j(\nu)\, v_j(\nu) + \frac{\partial M}{\partial \tau} = 0 \qquad (28)$$

Die früher beschriebenen Lösungsmethoden sind für das Ausnutzungsproblem geringfügig zu modifizieren. Da sich diese Modifikationen aber fast von selbst ergeben, soll hier nicht weiter darauf eingegangen werden.

Die Gleichungen für das Reaktionsrohr

Man gewinnt aus den Gleichungen I–V leicht die entsprechenden Gleichungen für das Reaktionsrohr durch einen Grenzübergang ($\tau(v) \to 0$). Auf diese Weise erhält man:

$$x_i(0) = a_i \tag{29}$$

$$\frac{dx_i}{d\tau} = v_i \tag{30}$$

$$\sum_{j=1}^{n} \lambda_j \frac{\partial v_j}{\partial T} = 0 \tag{31a}$$

$$\sum_{j=1}^{n} \lambda_j v_j = \mu \tag{31b}$$

($\mu = 0$ für das Umsetzungsproblem)

$$\frac{d\lambda_i}{d\tau} = -\sum_{j=1}^{n} \lambda_j \frac{\partial v_j}{\partial x_i} \tag{32}$$

$$\lambda_{ie} = \frac{\partial M}{\partial x_{ie}} \tag{33}$$

In diesen Gleichungen verweist der Index e auf das Ende des Reaktionsapparates. M ist aufzufassen als eine Funktion der x_{ie} und von τ_e. Die Variablen x_i und λ_i sind Funktionen von τ. Dabei bedeutet jetzt τ die Verweilzeit im Reaktionsrohr vom Anfang an gemessen. Die Gleichungen (29)–(33) wurden bereits früher mit den Methoden der Variationsrechnung abgeleitet [6, 7, 8]. Es besteht folgender bemerkenswerter Unterschied zwischen Gleichung III (b) und Gleichung (31b): Gleichung (31b), welche für das Rohr gilt, ist eine Folge der Gleichungen (30), (31a) und (32) (vgl. [7, 8]). D.h., das optimale Reaktionsrohr ist bereits durch die Gleichungen (29)–(31a), (32) und (33) bestimmt. Bei der Kaskade ist das nicht so: Gleichung III (b) ist völlig unabhängig von den übrigen Gleichungen I–V. Das ist verständlich, denn beim Rohr hat man für jedes τ nur eine Grösse, nämlich T, optimal zu wählen, während es bei der Kaskade für jedes v zwei Grössen sind, nämlich T und τ. Im letzteren Fall benötigt man daher eine unabhängige Gleichung mehr.

Es soll jetzt noch gezeigt werden, dass das Verfahren des "Probieren mit den Randwerten am Anfang des Reaktors" in etwas modifizierter Form bereits früher von verschidenen Autoren angewandt wurde, und zwar bei Ausnutzungsproblemen der Klasse 2 im Reaktionsrohr. Dort lässt sich nämlich die Optimalbedingung auf die Form

$$\frac{dT}{d\tau} = w(x_1, x_2, T) \tag{34}$$

bringen [6]. Erstmalig haben eine solche Bedingung Bilous und Amundson [3, 4] abgeleitet und für die Berechnung von optimalen Rohrreaktoren ausgenutzt. Bei der Berechnung geht man so vor, dass man T für $\tau = 0$ vorgibt und Gleichung (34) zusammen mit Gleichung (30) über τ integriert. Man sieht auf den ersten Blick eine Übereinstimmung mit dem Verfahren des "Probierens mit den Randwerten am Anfang des Reaktors": In beiden Fällen beginnt die Rechnung am Reaktoranfang und endet am Reaktorende. Darüberhinaus entspricht jeder Wahl von T eine Wahl des λ-Verhältnisses am Reaktoranfang, denn nach Gleichung (31a) ist

$$\frac{\lambda_1}{\lambda_2} = -\frac{\partial v_2/\partial T}{\partial v_1/\partial T} \tag{35}$$

Nach den Ausführungen auf S. 185 wäre hier eindimensionales Probieren erforderlich, nämlich Probieren mit $\lambda_1(0)/\lambda_2(0)$ bzw. mit $T(0)$. Wirklich probieren muss man aber beim Rohr nur, wenn man eine bestimmte Verweilzeit vorgibt. Das ist in der Regel nicht der Fall: Man wünscht nur Optimalreaktoren für verschiedene aber nicht genau festgelegte Verweilzeiten zu berechnen. Dann braucht man aber nach Vorgabe von $T(0)$ nur solange zu integrieren bis eine bestimmte Randbedingung erfüllt ist (vgl. [3, 4, 6, 8] und Gleichung 37).

Weitere Vereinfachungen bei speziellen Problemen

Zunächst soll das Problem von Denbigh [5] für das Rohr betrachtet werden. Wie früher gezeigt, reduziert sich die Dimension des Problems bei der Kaskade von 3 auf 1. Im Fall des Umsetzungsproblems gelingt beim Rohr eine weitere Reduktion. Es gilt dann nämlich für das Ende des Reaktors eine Beziehung, die die Wahl der $x_i(N)$ einschränkt: Für das Rohr hat man zu setzen

VOL. 15 1961

$$\lambda_i(N) = \lambda_i(N+1) = \lambda_{ie} \qquad (36)$$

und daraus folgt mit Hilfe von III (b) und V weiter

$$\sum_{j=1}^{n} \frac{\partial M}{\partial x_{je}} v_{je} = 0 \qquad (37)$$

Diese Beziehung erhält man auch unmittelbar aus Gleichung (31a) und (33). Dadurch reduziert sich die Dimensionalität weiter von 1 auf o. D.h., bei dem als Probierverfahren bezeichneten Verfahren ist das Probieren überflüssig geworden; man hat nur ein Anganfswertproblem für ein gewöhnliches System von Differentialgleichungen zu lösen (vgl. [7]). Bei der Kaskade ist eine Reduktion der Dimensionszahl von 1 auf 0 aus prinzipiellen Gründen unmöglich: Hier muss mindestens ein Parameter frei bleiben, der die Anzahl der Kessel in der Kaskade festlegt.

Als nächstes sollen Systeme mit linearer Kinetik betrachtet werden. Für solche Systeme findet man nach einigen Zwischenrechnungen mit Hilfe der Gleichungen II–IV die Beziehung

$$\sum_{j=1}^{n} \lambda_j(\nu) x_j(\nu) = \mu\, \tau(\nu) + C \qquad (38a)$$

Für das Umsetsungsproblem ist $\mu = 0$ und es gilt dann

$$\sum_{j=1}^{n} \lambda_j(\nu) x_j(\nu) = C \qquad (38b)$$

Eine analoge Beziehung gilt für das Reaktionsrohr (vgl. [7]). Gleichung (38) kann nützlich sein für die Elimination der Lagrange'schen Parameter (vgl. [7]) oder zu Kontrollzwecken bei der numerischen Berechnung.

Hat man ausser der linearen Kinetik noch eine isotherme Kaskade, d.h. sind alle Kesseltemperaturen gleich, dann findet man aus II, III(b), IV u. (19) (Anschreiben von III(b) für zwei aufeinanderfolgende ν und Bilden der Differenz):

$$[\tau(\nu) - \tau(\nu-1)] \sum_{i=1}^{n} \sum_{k=1}^{n} b_{ik} \lambda_i(\nu-1) v_k(\nu) = 0 \qquad (39)$$

Diese Gleichung gilt sowohl für das Umsetzungsproblem als auch für das Ausnutzungsproblem. Da die Doppelsumme im allgemeinen von Null verschieden ist, folgt als notwendige Bedingung für die optimale isotherme Kaskade:

$$\tau(\nu) = \tau(\nu-1) \quad \text{bzw.} \quad \tau(\nu) = \text{Const.} \qquad (40)$$

D.h., alle Kessel müssen bei einer solchen Kaskade gleich gross sein.

Als letzter spezieller Fall soll das Umsetzungsproblem der Klasse 2 untersucht werden. Hier lauten die Gleichungen III

$$\lambda_1(\nu) \frac{\partial v_1(\nu)}{\partial T} + \lambda_2(\nu) \frac{\partial v_2(\nu)}{\partial T} = 0 \qquad (41a)$$

$$\lambda_1(\nu) v_i(\nu) + \lambda_2(\nu) v_2(\nu) = 0 \qquad (41b)$$

Daraus kann man die λ_i leicht eliminieren. Das führt auf

$$\frac{\partial}{\partial T}\left(\frac{v_2}{v_1}\right) = 0 \quad \text{bzw.} \quad \frac{\partial}{\partial T}\left(\frac{v_1}{v_2}\right) = 0 \qquad (42)$$

Dieselben Gleichungen gelten für das Rohr (vgl. [8]). Im Gegensatz zum Rohr genügt aber die Beziehung (42) nicht, um den optimalen Reaktor vollständig zu errechnen. Sie vereinfacht aber in manchen Fällen die Aufgabe beträchtlich, so z.B. bei dem auf S. 181 diskutierten Beispiel, das das Reaktionsysstem (1) betrifft. Hier führt Gleichung (42) auf eine konzentrationsunabhängige Beziehung für die Temperatur, die als Lösung eine für alle Kessel gleiche optimale Temperatur liefert (vorausgesetzt die Aktivierungsenergie der erwünschten Reaktion liegt zwischen denen der beiden unerwünschten Reaktionen, vgl. [8]). Da also die optimale Kaskade isotherm und ausserdem die Kinetik linear ist, müssen alle Kessel gleich gross sein. Jetzt ist nur noch eine Grösse unbekannt, nämlich die Verweilzeit in einem Kessel (bzw. die gesamte Verweilzeit). Deren optimalen Wert zu ermitteln ist aber sehr einfach.

Diskussion

In den früheren Abschnitten wurden drei verschiedene Methoden zur Berechnung einer optimalen Kaskade untersucht:

(a) Das Probieren mit den Randwerten am Ende des Reaktors,

(b) Die Methode des stärksten Anstiegs und

(c) Das Probieren mit den Randwerten am Anfang des Reaktors.

Soll für eine gegebene Anfangszusammensetzung und Stufenzahl eine optimale Kaskade berechnet werden, dann liefern die drei Methoden folgende Zwischenresultate:

Methode (a): Optimale Kaskaden für andere Anfangszusammensetzungen mit Stufenzahlen zwischen 1 und N.

Methode (b): Nicht optimale Kaskaden für die richtige Anfangszusammensetzung und Stufenzahl.

Methode (c): Kaskaden für die richtige Anfangszusammensetzung, die eine nicht interessierende Optimalforderung erfüllen.

Hieraus würde folgen, dass die Methode (a) den beiden anderen Methoden überlegen ist. Doch lässt sich diese Methode nur anwenden, wenn die Dimensionzahl* genügend klein ist. Die Dimensionszahl reduziert sich für ein Problem der Klasse n auf $n - l$, wenn ein l-parametrige Transformationsgruppe der Reaktionsvariablen existiert, die die Gleichungen II–V invariant lässt. Bei dem Problem von DENBIGH [5] z.B. ist eine solche Gruppe gegeben durch

$$x_i' = c_1 x_i + c_2 c_{ni} \qquad (43)$$

$$c_{ni} = 0 \quad \text{für } i \neq n, \quad c_{ni} = 1 \quad \text{für} \quad i = n$$

c_1 und c_2 sind die beiden Parameter der Gruppe. Die Klassenzahl des Problems ist drei, daher reduziert sich die Dimensionszahl von 3 auf $3 - 2 = 1$. Die Methode (a) is hier vorteilhafter als (b) und (c). Das gleiche gilt für das Verfahren der dynamischen Programmierung, das mit (a) eng verwandt ist.

Die Methode (b) hat den Vorteil, dass man sie auch bei hochdimensionalen Problemen anwenden kann. Ausserdem zeigen hier die Zwischenresultate wie stark der bei der optimalen Kaskade erzielte Effekt sinkt, wenn man von den optimalen Bedingungen abgeht.

Die Methode (c) scheint nur in speziellen Fällen einen Vorteil zu bringen, so z.B. bei Ausnutzungsproblemen der Klasse 2. In der folgenden Tabelle sind die drei Lösungsprinzipien gegenübergestellt; es sind Veröffentlichungen angegeben, in denen diese Prinzipien für die Berechnung von speziellen Beispielen benutzt wurden.

Lösungsprinzip	*Berechnung vom Reaktorende zum Reaktoranfang*	*Schrittweise Verbesserung des ganzen Reaktors*	*Berechnung vom Reaktoranfang zum Reaktorende*
Methode	Methode (a) Dynamische Programmierung	Methode (b)	Methode (c)
Zu bevorzugen bei	nicht allzu komplizierten Problemen	sehr komplizierten Problemen	speziellen Problemen Z.B. Ausnutzungsproblemen d. Klasse 2 im Rohr
Kaskade	[1, 2]	nichts publiziert	
Rohr	[7]	[7]	[3, 4]

Das ausserordentlich elegante Verfahren der dynamischen Programmierung, das von ARIS [1] zur Berechnung von optimalen Temperaturen und Verweilzeiten in einer Kaskade angewandt wurde unterscheidet sich von der Methode (a) im wesentlichen nur dadurch, dass im allgemeinen keine differentiellen Optimalbedingungen angewandt worden. D.h. die Gleichungen III werden für die Lösung* des Problems nicht herangezogen. Damit werden auch IV und V nicht mehr benötigt. Ein solches Vorgehen hat Vor-und Nachteile und je nach dem speziellen Beispiel können die einen oder die anderen überwiegen. Es soll das aber hier nicht weiter diskutiert werden; ohne spezielle Beispiele wäre es schwierig. In einer späteren Arbeit sollen die verschiedenen Lösungsmethoden an Hand von Beispielen miteinander verglichen werden.

Man könnte auch die Methode (a) mit dem Verfahren der dynamischen Programmierung kombinieren. Etwa, indem man nicht nur die

*Hier ist unter Dimensionszahl nicht die Zahl der optimal zu wählenden Parameter zu verstehen, (vgl. S. 183).

*Natürlich erfüllt die optimale Kaskade in jeden Fall das Gleichungssystem I–V, wenn man von Nebenbedingungen der Form (17) absieht.

Tabellen (vgl. [2]) für die x_i berechnet sondern gleichzeitig mit Hilfe von IV und V solche für die λ_i. Dies würde die Rechnung an manchen Stellen vereinfachen und ausserdem mehr Information liefern, denn es gilt (wie mit Hilfe von (12) leicht abzuleiten):

$$\left(\frac{\partial M}{\partial x_i(0)}\right)_{T(\nu),\,\tau(\nu)} = \lambda_i(1) \qquad (44)$$

Ich hoffe, dass diese Arbeit eine Verbindung herstellt zwischen den neuen Methoden, die in [1, 2] angewandt wurden und den Verfahren der klassischen Variationsrechnung, die an anderer Stelle [3-8] für die Lösung von Optimalproblemen herangezogen wurden.

Bezeichnungen

A = Stoffsymbol
a_i = Anfangswert der i-ten Reaktionsvariablen
b_{ik} = Verallgemeinerte Geschwindigkeitskonstanten bei linearer Kinetik
c_i = Konzentrationen
C, C_1, C_2 = Konstanten
e_{ni} = Komponenten eines Einheitsvektors
F = Funktionssymbol
k = Geschwindigkeitskonstanten
M, m = Grössen, die extremiert werden sollen
N = Anzahl der Kessel in einer Kaskade
n = Anzahl der stöchiometrisch unabhängigen Reaktionen bzw. Klassenzahl
$T(\nu)$ = Temperatur im ν — ten Kessel
$x_i(\nu)$ = Reaktionsvariable im ν — ten Kessel
$\lambda_i(\nu), \mu$ = Lagrange'sche Parameter
$\tau(\nu)$ = Verweilzeit im ν — ten Kessel

Literatur

[1] Aris R. *Chem. Engng. Sci.* 1960 **12** 56.

[2] Aris R., Rudd D. F. und Amundson N. R. *Chem. Engng. Sci.* 1960 **12** 88.

[3] Bilous O. und Amundson N. R. *Chem. Engng. Sci.* 1956 **5** 81.

[4] Bilous O. und Amundson N. R. *Chem. Engng. Sci.* 1956 **5** 115.

[5] Denbigh K. G. *Chem. Engng. Sci.* 1958 **8** 125.

[6] Horn F. *2nd Europ. Symp. Chem. React. Engng. Amsterdam, Chem. Engng. Sci.* 1960 **15** 77.

[7] Horn F. und Troltenier U. *Chem.-Ing.-Tech.* 1960 **32** 382.

[8] Horn F. Diskussionstagung der Deutschen Bunsengesellschaft, Ludwigshafen, Oktober 1960.

Chemical Engineering Science, 1961, Vol. 15, pp. 188 to 209. Pergamon Press Ltd., London. Printed in Great Britain.

Multicomponent isotope separation in cascades*

A. DE LA GARZA, G. A. GARRETT, J. E. MURPHY
Union Carbide Nuclear Company, Division of Union Carbide Corporation,
Oak Ridge Gaseous Diffusion Plant, Oak Ridge, Tennessee, U.S.A.

(*Received* 2 *September* 1960)

Abstract—This paper presents a theoretical study of multicomponent isotope separation cascades. A theory is developed which leads to the multicomponent analogue of the two component " ideal cascade." The multicomponent analogue is a " matched abundance ratio cascade." Multicomponent analogues are derived for " value functions," " separative work," and various relationships of importance in two-component isotope separation cascade theory.

The theory is applied specifically to the derivation of a multicomponent cost formula which could be used to price uranium containing U-236. (This cost formula is derived merely as an illustration of the theory and no recognition or commitment on the part of the U.S.A.E.C. is implied).

The multicomponent matched abundance ratio cascade does not minimize total cascade flow as does the two-component ideal cascade. It is found, however, that for uranium isotope separation the total flow in the matched U-235/U-238 abundance ratio cascade exceeds the minimum by an insignificant fraction for a wide range of U-236 concentrations.

Résumé—Cet article est l'exposé d'une étude théorique de la séparation en cascade d'un mélange isotopique de plusieurs composants. La théorie conduit pour le mélange de plusieurs composants à une " cascade analogue " à la cascade idéale binaire. Cette " cascade analogue " est une cascade dans laquelle intervient le " taux d'enrichissement comparé." Cette analogie conduit pour les mélanges de plusieurs composants aux diverses relations et notions importantes déjà rencontrées dans la théorie de la cascade de séparation isotopique binaire, par exemple la notion d' énergie de séparation.

On applique plus spécialement cette théorie à l'obtention des formules d'estimation de prix dans le cas d'uranium contenant de l'U.236. (Les formules d'estimation sont heureusement présentées comme une illustration de la théorie sans qu'il y ait garantie ou reconnaissance de la part de l'U.S.A.E.C.).

Cette cascade à plusieurs composants utilisant le taux d'enrichissement comparé, diffère de la cascade binaire idéale par le fait que son débit total ne diminue pas en cours de cascade. On trouve, cependant, que pour la séparation isotopique de l'uranium le débit global, dans la cascade utilisant le taux d'enrichissement comparé U.235/U.238, dépasse le minimum d'une faible fraction pour un large étalement des concentrations en U. 236.

Zusammenfassung—Diese Abhandlung beschreibt eine theoretische Untersuchung der multikomponenten Kaskadentrennung von Isotopen aus einem Isotopengemisch. Eine Theorie ist entwickelt, die zu der multikomponenten Analogie der von zwei Bestandteilen bestehenden " idealen Kaskade " führt. Die multikomponente Analogie ist eine " passende uberflussverkältnis-Kaskade." Multikomponente Analogien sind abgeleitet für: " Wert-Funktionen," " Trennungsenergie " und verschiedene wichtige Zusammenhänge, die in der Zweikomponenten Kaskadentheorie der Isotopentrennung von Bedeutung sind.

Die theorie ist speziell angewendet auf die Ableitung einer multikomponenten Preisformel, die bie der Preisbestimmung von Uran das U-236 enthält, verwendet werden kann. (Diese Preisformel ist abgeleitet nur als eine Illustration der Theorie und keine Anerkennung oder Verpflichtung von Seiten der U.S.A.E.C. ist angedeutet).

Die multikomponente passende Überflussverhältnis-Kaskade schätzt, im Gegensatz zu der zweikomponenten idealen Kaskade, nicht den totalen Kaskadenfluss ab. Es wurde aber gefunden, dass für Uran-Isotopenseparation der totale Fluss in der passenden U-235/U-238 Überflussverhältnis-Kaskade um einen sehr kleinen Bruchteil grösser ist, als das Minimum für eine bedeutende Reihe von U-236 Konzentrationen.

*Work done under U.S.A.E.C. Contract No. W-7405-eng. 26.

Introduction

A large part of the theory of isotope separation cascades for isotopic mixtures which contain only two components involves three mutually related concepts – " separative work," the " value function " and the " ideal cascade." This is especially true when the separation process is an irreversible discrete stage process with a small stage separation factor, as is the case for the gaseous diffusion process for the separation of uranium isotopes [1, 2]. So far there have been few developments in multicomponent isotope cascade theory, and there are no multicomponent analogues to the two-component separative work, value function and ideal cascade formulae to apply to this situation. The broad objective of this paper is to extend the theory of multicomponent isotope separation in cascades. Multicomponent analogues to the two-component separative work, value function and ideal cascade formulas are presented.

This paper also has a more specific and immediate objective. When the feed to a gaseous diffusion cascade is natural uranium, it is permissible in most situations of interest to treat U-234 concentrations as being negligibly small in comparison to the U-235 and U-238 concentrations and thus regard uranium as a mixture of two isotopes. When this is done the application of cascade theory and the three concepts mentioned above lead to simplified formulae for estimating cascade design requirements such as power, barrier area and the number and sizes of individual stages. Similar considerations lead to estimates of the unit cost for the production of U-235 at any concentration. As is well known the published U.S.A.E.C. price schedule can be fitted very precisely with a cost curve based upon a unit cost of separative work [1, 3]. In certain situations where a gaseous diffusion cascade receives as feed uranium which has been discharged from a nuclear reactor, a fourth isotope, U-236, may be present in a concentration sufficiently high so that it affects appreciably the separative work requirements and hence the unit costs for the production of enriched U-235, as shown in [4]. The more specific and immediate objective of this paper then is the derivation of a multicomponent unit cost formula which may be used to price uranium containing U-236. It is to be emphasized that this multicomponent unit cost formula is here presented solely to illustrate application of the developed theory, and in no way is it implied that the U.S.A.E.C. recognizes this formula as the basis for a price schedule for uranium containing U-236.

In view of the second objective of the paper, the development of the theory and presentation of results will be done in the setting of the separation of uranium isotopes by gaseous diffusion. It is to be understood however, that the results are not limited either to these particular isotopes or separation method. The results are applicable to any separation process in which the separation factor is small and independent of composition.

Brief review of pertinent two-component Separation Theory

To fix ideas some pertinent features of two-component separation theory are first briefly reviewed. Consider for this purpose the separation of the U-235, U-238 two-component mixture (as UF^6) by the gaseous diffusion process. By way of nomenclature, a U-235 concentration (mol fraction) is denoted by x with appropriate subscripts where required to denote feed, product and waste concentrations of a cascade. The symbols for the cascade feed, product and waste rates are F, P and W. The interstage flow rate (upflow through the barrier) at stage n is denoted by L, which is understood to be a function of stage number. The stage separation factor for the U-235, U-238 separation is denoted by ψ_1.

Consider then an isolated stage, operating at a " cut " of one half, as shown in Fig. 1.

The *separative work* done by the stage is defined as $L\,\psi_1^2/4$, and is of course, independent of concentration. The *value function* is then obtained by associating with uranium at concentration x a value $\mathscr{V}(x)$, say per mol, and requiring that the net change in value effected by the stage equal the separative work of the stage. Thus, for the stage shown in Fig. 1,

$$L\,\mathscr{V}(x+\delta x) + L\,\mathscr{V}(x-\delta x) - 2L\,\mathscr{V}(x) = \tfrac{1}{4}\,L\,\psi_1^2, \qquad (1)$$

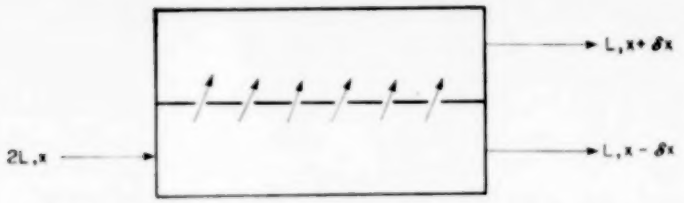

FIG 1. Schematic of stage processing a two-component mixture.
Stage increment: $2\,\delta x = \psi_1 x(1-x)$

where $\delta x = \psi_1 x(1-x)/2$. Since the concentration change δx is small, $\mathscr{V}(x+\delta x)$ and $\mathscr{V}(x-\delta x)$ are expanded about $\mathscr{V}(x)$ in a Taylor expansion, and from equation (1), one then obtains the ordinary differential equation

$$[x(1-x)]^2\, d^2\mathscr{V}/dx^2 = 1, \qquad (2)$$

which is correct to terms of order ψ_1^2. The general solution of equation (2) is

$$\mathscr{V}(x) = c_0 + c_1 x + (2x-1)\ln[x/(1-x)], \quad (3)$$

where c_0 and c_1 are arbitrary constants. Thus, the two-component value function $\mathscr{V}(x)$ has been obtained.

Application of $\mathscr{V}(x)$ to cascade theory follows immediately. Consider the cascade shown in Fig. 2.

In an *ideal cascade* for two-component separation, stages are linked together to form a cascade and feeds are introduced to the cascade so that there are no losses of separative work anywhere in the cascade. This is simply accomplished by bringing streams together at stage links and feed points only if the concentrations of the mixed streams are equal. Consequently, the separative work of the ideal cascade equals the sum of the separative work of the stages; thus:

$$\tfrac{1}{4}\sum_{\text{cascade}} L\,\psi_1^2 = \sum_{\text{cascade}}\left[L\,\mathscr{V}(x+\delta x) + L\,\mathscr{V}(x-\delta x) - 2L\,\mathscr{V}(x)\right] \qquad (4)$$

Furthermore, since an output L from one stage is an input to another, all the interstage flows cancel in the cascade summation. Hence, for the cascade of Fig. 2 – supposing the cascade to be ideal – one obtains from equation (4) the following important relation:

$$\tfrac{1}{4}\sum_{\text{cascade}} L\,\psi_1^2 = PV(x_P) + WV(x_W) - FV(x_F) \quad (5)$$

where $V(x) = (2x-1)\ln[x/(1-x)]$ (6)

In equation (5) the linear terms of the general value function $\mathscr{V}(x)$ vanish by material balance, so that henceforth for convenience in these applications the *elementary value function* $V(x)$ is used and the linear terms are added when required.

It may be seen from equation (5) that by

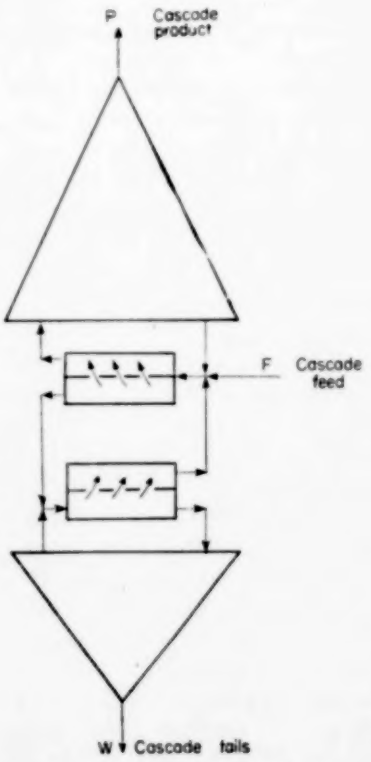

FIG. 2. Defining cascade schematic.

means of the value function the separative work of an ideal cascade may be expressed in terms of the flows and concentrations of the external cascade streams. This value function expression for the separative work of an ideal cascade leads to remarkably simple formulae for estimating cascade performance. Thus, for the cascade of Fig. 2 – supposing the cascade to be ideal –one may write the " productivity equations " below, these being the availability of separative work and the two material balances:

$$\begin{aligned} \tfrac{1}{4}\underset{\text{cascade}}{\Sigma} L\,\psi_1^2 &= PV(x_P) + WV(x_W) - FV(x_F) \\ 0 &= Px_P + Wx_W - Fx_F \\ 0 &= P + W - F \end{aligned} \qquad (7)$$

It may be seen how value function terms and material balance terms are added to the equation (7) for application to an ideal cascade with side feeds and/or side withdrawals. These productivity equations are basic, and their uses are many. As stated in [1] given an ideal cascade at specified feed and product conditions so that the cascade separative work is known, the best possible performance of the cascade at another set of conditions can by calculated from the applicable productivity equations by treating the cascade separative work as a constant property of the cascade. Such a calculation is valid provided the stages are re-arranged or the interstage flows are adjusted, if need be, so that under the changed conditions the mixing of streams of different concentrations is avoided. The following are cited in [1] as examples of cascade problems which may be solved by this means:

1. The effect of change in product rate on product concentration.
2. The effect of change in feed rate on product rate at constant product concentration.
3. The effect of incremental feeds of different concentrations on product rate.
4. The effect of withdrawing partially-enriched product on product rate.

Other examples may be cited, but the above suffice to show the usefulness of the productivity equations.

In the gaseous diffusion process the cascade operating costs are very nearly proportional to the cascade separative work. This fact quickly leads to a unit cost system for pricing uranium. Let $D(x)$ be the unit cost in dollars per kilogram of uranium whose U-235 concentration is x, and let K be the unit cost of separative work per kilogram (of uranium)*.

Then,

$$D(x) = K\left[a_0 + a_1 x + V(x)\right] \qquad (8)$$

where a_0 and a_1 are constants, is a unit cost scale which assures that the operating costs of the (ideal) cascade are accounted for by the material charges and credits; thus, for the cascade of Fig. 2:

$$\begin{aligned} \text{Cascade operating costs} &= K\left(\tfrac{1}{4}\underset{\text{cascade}}{\Sigma} L\,\psi_1^2\right) \\ &= PD(x_P) + WD(x_W) - FD(x_F) \end{aligned} \qquad (9)$$

The constants a_0 and a_1 in the unit cost expression (8) are determined so that $D(x)$ has the correct value for natural uranium and is equal to zero at a concentration x_0 called the " concentration of zero value." This concentration x_0 may be regarded as that of depleted uranium which can be used as feed at no cost in a cascade to produce a product at the natural uranium concentration x_N and at the same unit cost $D(x_N)$ as natural uranium. When the constants are thus evaluated one obtains

$$D(x) = K\left[V(x) - V(x_0) - (x - x_0)\,V'(x_0)\right] \qquad (10)$$

It has been mentioned previously that the U.S.A.E.C. price schedule can be fitted very precisely by a formula based on a unit cost for separative work; Refs. [1] and [3] should be consulted for further discussion. For the price schedule in the form [10] the constants given in [1] are:

$$\begin{aligned} K &= \$37{\cdot}286/\text{kg U} \\ D(x_N) &= D(0{\cdot}007115) = \$39{\cdot}27/\text{kg U} \\ x_0 &= 0{\cdot}0022138 \text{ weight fraction U-235} \end{aligned}$$

*Kilograms and weight fraction, rather than mols and mol fraction, are the accepted units for uranium costs. The ratio of the atomic weights of the uranium isotopes is so close to unity that the difference between mol fraction and weight fraction is negligible.

From this brief review of two-component cascade theory one can well see the relations between the concepts of separative work, value function and ideal cascade, and their possible wide application to cascade design, evaluation of cascade performance and unit cost systems. These results are particularly useful in application to gaseous diffusion plants because the ideal cascade *minimizes* the required cascade total flows, and hence leads to minimum power gaseous diffusion plants.

STATEMENT OF SPECIFIC PROBLEMS AND OUTLINE OF SOLUTION FOR A MULTICOMPONENT VALUE FUNCTION

The problems in multicomponent separation now considered are those of finding multicomponent analogues to the separative work, value function and ideal cascade which have been reviewed for two components. For convenience the problems and results are presented in the three-component setting of U-235, 236 and 238. Extension to additional isotopes will be noted where required.

First, new nomenclature is introduced as follows: U-235 and U-236 concentrations are denoted by x and y, respectively, with appropriate subscripts where required to denote the cascade feed, product and waste concentrations. The stage separation factor for the two component U-235 and U-238 separation is denoted by ψ_1, and the corresponding factor for the U-236 and U-238 separation is denoted by ψ_2. An additional symbol k is defined by

$$k = \psi_2/\psi_1 \tag{11}$$

which has the value 2/3 for the uranium problem under discussion. Other nomenclature is as before.

Consider an isolated stage at a cut of a half and handling the three-component mixture as shown in Fig. 3.

By analogy with the two component results, the *separative work* done by the stage is defined to be $L\,\psi_1^2/4$,and the three component *value function* is obtained by associating a value $\mathscr{V}(x, y)$ with material at concentrations (x, y) such that the net change in value effected by the stage equals the separative work of the stage; thus:

$$L\,\mathscr{V}(x + \delta x, y + \delta y) + L\,\mathscr{V}(x - \delta x, y - \delta y) - 2L\,\mathscr{V}(x, y) = \tfrac{1}{4} L\,\psi_1^2 \tag{12}$$

where:

$$\delta x = \tfrac{1}{2} g(x,y) = \tfrac{1}{2}\left[\psi_1 x(1 - x - y) + (\psi_1 - \psi_2) xy\right]$$

$$\delta y = \tfrac{1}{2} h(x, y) = \tfrac{1}{2}\left[\psi_2 y(1 - x - y) - (\psi_1 - \psi_2) xy\right]$$

Again carrying out the indicated Taylor expansion as with two components, one obtains the partial differential equation

$$g^2(\partial^2 \mathscr{V}/\partial x^2) + 2gh(\partial^2 \mathscr{V}/\partial x \partial y) + h^2(\partial^2 \mathscr{V}/\partial y^2) = \psi_1^2 \tag{13}$$

which is the three component analogue of the ordinary differential equation (2) for two components. There are many functions of x and y which satisfy this partial differential equation. From the possible solutions one must be chosen which has certain desirable properties discussed below.

In the situation of the uranium isotopes U-235,

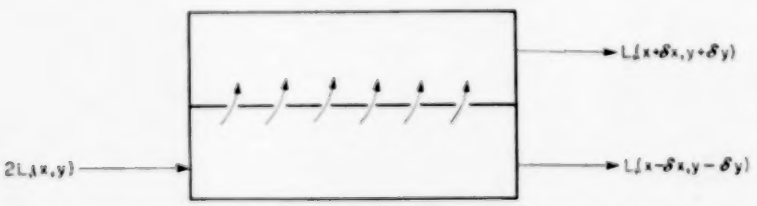

FIG. 3. Schematic of stage processing a three-component mixture.

Stage Increments:

$$2\,\delta x = g(x, y) = \psi_1 x(1 - x - y) + (\psi_1 - \psi_2) xy,$$
$$2\,\delta y = h(x, y) = \psi_2 y(1 - x - y) - (\psi_1 - \psi_2) xy.$$

236 and 238, it must be realized that not all concentration differences are effected at the expense of separative work. Thus, the addition (or depletion) of U-236 in a reactor in no way involves the expenditure of separative work, and accordingly it should be possible, for example, to feed material containing U-236 to a cascade initially free of U-236 without incurring a mixing loss in the sense of separative work losses. The three-component $\mathscr{V}(x, y)$ should then have the property that it permits the mixing of materials of some appreciably different concentrations without a loss in separative work, i.e. the value of the unmixed materials equals the value of the mix. Furthermore, this $\mathscr{V}(x, y)$ should permit the linking of stages together in a cascade and the introduction of feed materials to the cascade so that separative work is conserved everywhere in the cascade. In such a cascade, at every location where streams are brought together and mixed the value of the materials before mixing must equal the value of the resulting mix. The separative work of the cascade then equals the sum of the separative work of the stages; hence:

$$\tfrac{1}{4} \sum_{\text{cascade}} L\, \psi_1^2 = \sum_{\text{cascade}} [L\, \mathscr{V}(x + \delta x, y + \delta y) + L\, \mathscr{V}(x - \delta x, y - \delta y) - 2L\, \mathscr{V}(x, y)] \quad (14)$$

and furthermore, as in the two-component situation,

$$\tfrac{1}{4} \sum_{\text{cascade}} L\, \psi_1^2 = P\, \mathscr{V}(x_P, y_P) + W\, \mathscr{V}(x_W, y_W) - F\, \mathscr{V}(x_F, y_F) \quad (15)$$

It may be seen from equation (15) that, as in the two-component case, such a value function $\mathscr{V}(x, y)$ can then be the basis for a unit cost system for pricing three-component isotopic mixtures. Of course, such a unit cost system will be strictly applicable only to some reference cascade – in the same way that the two-component cost system is strictly applicable to the ideal cascade.

It has thus been seen that for the purpose of pricing U-235, 236 238 mixtures one requires a function $\mathscr{V}(x, y)$ which satisfies the partial differential equation (13) and furthermore has the property that it permits the mixing of some materials with appreciably different isotopic concentrations so that the value of the unmixed materials is equal to the value of the resulting mix. Given a material with concentrations (x_1, y_1), one must then be able to establish whether another material with concentrations (x_2, y_2) can be mixed with the first with value being conserved. For this purpose, consider introducing a function $M(x, y)$, called a "*match function*," with the property that if two materials have distinct concentrations (x_1, y_1) and (x_2, y_2) such that $M(x_1, y_1)$ equals $M(x_2, y_2)$, then these two materials can be mixed with value being conserved. Once the match function is known stages can be linked together to form a cascade and feeds can be introduced to the cascade so that separative work is conserved everywhere in the cascade. Such a cascade is formed by matching streams which come together, i.e. the match function for streams coming together has the same value.

For application to operations with U-235, 236 and 238 mixtures the applicable value function $\mathscr{V}(x, y)$ and associated match function $M(x, y)$ should also satisfy the boundary condition that they reduce to the usual two-component formulae when U-236 is not present, that is ,when y equals zero. Hence it is required that $\mathscr{V}(x, 0)$ equal $\mathscr{V}(x)$ in (3), and since in the absence of U-236 materials are mixed with value being conserved only when the materials have the same U-235 concentration x, it is required that $M(x, 0)$ equal x.

The above discussion on the desired properties of the value function $\mathscr{V}(x, y)$ is now summarized in concise mathematical language.

It is desired to find a value function $\mathscr{V}(x, y)$ and an associated match function $M(x, y)$ with the following properties:

1. $$g^2 (\partial^2 \mathscr{V}/dx^2) + 2gh\, (\partial^2 \mathscr{V}/\partial x \partial y) + h^2 (\partial^2 \mathscr{V}/\partial y^2) = \psi_1^2 \quad (16)$$

where:

$$g = \psi_1 x (1 - x - y) + (\psi_1 - \psi_2) xy$$
$$h = \psi_2 y (1 - x - y) - (\psi_1 - \psi_2) xy$$
$$0 \leqslant x \leqslant 1, \quad 0 \leqslant y \leqslant 1, \quad x + y \leqslant 1$$

2. $$w_1\, \mathscr{V}(x_1, y_1) + w_2\, \mathscr{V}(x_2, y_2) = (w_1 + w_2)\, \mathscr{V}(x_3, y_3) \quad (17)$$

where:

(x_1, y_1) and (x_2, y_2) are distinct and such that $M(x_1, y_1) = M(x_2, y_2)$

and

$x_3 = (w_1 x_1 + w_2 x_2)/(w_1 + w_2)$

$y_3 = (w_1 y_1 + w_2 y_2)/(w_1 + w_2)$

$w_1 \geqslant 0$, $w_2 \geqslant 0$, i.e. w_1 and w_2 are material quantities.

3. $$\mathscr{M}(x, 0) = c_0 + c_1 x + (2x - 1) \ln [x/(1 - x)] \qquad (18)$$

where c_0 and c_1 are arbitrary constants.

4. $$M(x, 0) = x \qquad (19)$$

Finding $\mathscr{M}(x, y)$ and the associated $M(x, y)$ is a formidable problem. The rigorous mathematical analysis and solution are presented in [5]. Unfortunately, the analysis there presented has resisted all attempts by the writers at simplification. Several observations, based on physical and geometrical considerations, do permit a heuristic development of the solution. Such a development follows.

Note first that equation (17) states that if *two* matched materials are mixed value is conserved. Considering that when two materials are mixed a portion of one may first be mixed with a portion of the other, and again, sub-portions may be mixed etc., until finally the two original materials are mixed, one may expect that if *any number* of matched materials are mixed, value is conserved

It may then be further concluded that the curve in the (x, y) plane described by the relation

$$M(x, y) = \text{constant} \qquad (20)$$

must be a straight line. The argument, based on Fig. 4, is as follows: As shown in Fig. 4, if $M(x, y)$ is constant on a curve not a straight line due to the above extension of (17), $\mathscr{M}(x, y)$ is a plane for concentrations (x_i, y_i) resulting from the mixing of three or more materials with distinct concentration on the curve $M(x, y) = \text{constant}$; thus:

$\mathscr{M}(x, y) = a + bx + cy$, where a, b and c are constants

But then $\mathscr{M}(x, y)$ cannot satisfy the differential equation (16). Hence the locus of (20) must be a straight line. Consider now that such lines may be described by

$$x + y B(M) = C(M) \qquad (21)$$

where $B(M)$ and $C(M)$ are functions of M only. Since (19) demands that $M(x, 0) = x$, it then follows from (21) that

$$x + y B(M) = M \qquad (22)$$

It further follows, as a consequence of (17), that over a line, such as (22), $\mathscr{M}(x, y)$ is a line, and hence

$$\mathscr{M}(x, y) = U(M, y) = \alpha(M) + y \beta(M) \qquad (23)$$

where $\alpha(M)$ and $\beta(M)$ are functions of M only. Since $\mathscr{M}(x, 0)$ is given by (18) and since from (19)

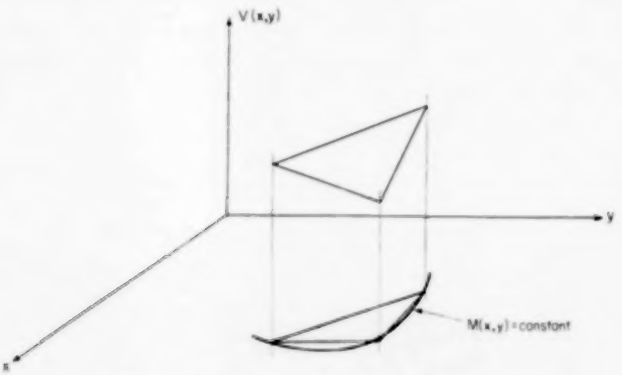

FIG. 4. $M(x, y)$ constant on a curve.

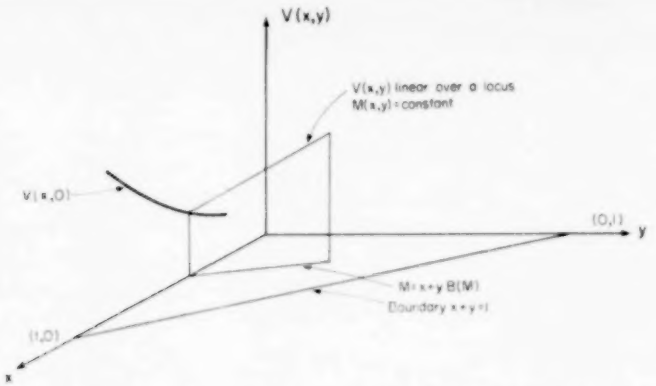

FIG. 5. Relations between $\mathscr{V}(x, y)$ and $M(x, y)$

$M(x, 0) = x$, it follows that $\alpha(M)$ in (23) is known; thus:

$$\alpha(M) = c_0 + c_1 M + (2M - 1) \ln [M/(1 - M)]$$

The picture showing these relations between $\mathscr{V}(x, y)$ and $M(x, y)$ is shown in Fig. 5.

Consider now that due to (18), which states that $\mathscr{V}(x, y)$ reduces to the usual two-component value function in the absence of *U*-236, $\mathscr{V}(x, y)$ must recognize the expenditure of separative work for the separation of U-235 and U-238. In particular, note that

$$\mathscr{V}(0) = \infty, \text{ and } \mathscr{V}(1) = \infty$$

which imply the expenditure of infinite separative work for the complete removal of U-235 or U-238 *in the absence of U*-236. One may then expect that

$$\mathscr{V}(0, y) = \infty, \quad \text{and} \quad \mathscr{V}(x, 1 - x) = \infty$$

which imply the expenditure of infinite separative work for the complete removal of U-235 or U-238 *in the prescene of U*-236. It may then be seen that $\mathscr{V}(x, y)$ should be infinite on the boundaries $x = 0$ and $x + y = 1$ in Fig. 5. Note further that again from separative work considerations $\mathscr{V}(x, y)$ should be finite for all concentration points (x, y) in the interior of the triangle formed by the three boundaries $x = 0$, $y = 0$, and $x + y = 1$. It then follows from the above considerations that lines of constant M cannot densely intersect either of the boundaries $x = 0$ and $x + y = 1$, for then $\mathscr{V}(x, y)$ over such lines would be infinite. It further follows that through every interior point (x_i, y_i), the line of constant M passing through (x_i, y_i) must intersect the boundary $y = 0$ in the interval $0 < x < 1$, for if there are interior points whose lines of constant M do not intersect the boundary $y = 0$ in this interval, then such lines must densely intersect at least one of the boundaries $x = 0$ and $x + y = 1$. In summary, lines of constant M must originate on the boundary $y = 0$ in the interval $0 < x < 1$, such lines must pass through every interior point of the triangle formed by the three boundaries and such lines cannot densely intersect the boundaries $x = 0$ and $x + y = 1$. Accordingly, either no lines of constant M may be drawn, in which case the desired $\mathscr{V}(x, y)$ does not exist, or all such lines intersect at the corner point (0, 1), in which case $\mathscr{V}(x, y)$ may be expected to have some irregularity at this one point. In the latter case,

$$M = x/(1 - y) \tag{25}$$

It remains to find out whether with the above M a value function $\mathscr{V}(x, y)$ is permitted by the partial differential equation (16). This is simply found out by using (25) to eliminate x in (16). Thus, one arrives at a partial differential equation in M and y co-ordinates in which (23) may be substituted. The only unknown in (23) is $\beta(M)$, and the differential equation in M and y co-ordinates must be solved for $\beta(M)$, provided a solution is permissible. On carrying out the necessary algebraic simplification when the substitution of (23) is made, one finds that the partial

differential equation in M and y co-ordinates reduces to an *ordinary* differential equation for $\beta(M)$, the y variable vanishing. Hence, a solution for $\beta(M)$ is permissible, and on solving for $\beta(M)$, one has found the value function $\mathscr{U}(x, y) = U(M, y)$, given by (23) with the associated match function $M(x, y)$, given by (25). The details of this part of the development are presented in the Appendix. The results are that :

for $2k = 1$

$$\mathscr{U}(x, y) = c_0 + c_1 x + c_2 y + c_3 y \ln R + \left[2x + \frac{(\ln R)}{2} y - 1\right] \ln R \qquad (26)$$

for $2k \neq 1$

$$\mathscr{U}(x, y) = c_0 + c_1 x + c_2 y + c_3 y R^{-(2k-1)} + \left(2x + \frac{2k}{2k-1} y - 1\right) \ln R \qquad (27)$$

where :

$$R = M/(1 - M) = x/(1 - x - y) \qquad (28)$$

and c_0, c_1, c_2 and c_3 are arbitrary constants.

This completes the development of the value function $\mathscr{U}(x, y)$ and its associated match function $M(x, y)$.

The Matched Abundance Ratio Cascade

It has been seen that the value function $\mathscr{U}(x, y)$ and the associated match function $M(x, y)$ developed in the previous section permit the mixing of two materials with value being conserved provided the concentrations (x_1, y_1) and (x_2, y_2) are such that $M(x_1, y_1) = M(x_2, y_2)$, i.e. the materials are matched. A cascade with the property that separative work is conserved everywhere can then be formed by matching streams wherever they come together at stage links and feed points.

The match function $M = x/(1 - y)$ and the abundance ratio $R = x/(1 - x - y)$ are related by the identity $R = M/(1 - M)$. Thus, there is no difference whether M or R is used as the match function. Since for good reasons the abundance ratio is already prevalent in isotope separation work the abundance ratio R will be used as the match function associated with the developed value function $\mathscr{U}(x, y)$. The cascade formed by matching R will be called a *matched abundance ratio cascade*, or briefly, a *matched R cascade*.

In this Section, formulae for the concentration gradients and interstage flow rates and the cascade productivity equations will be developed for the matched R cascade. The matched R cascade has very much the same role in three-component separation as the ideal cascade has in two-component separation.

(a) *Concentration gradients and interstage flows*

First, consider the concentration gradients in a three-component cascade without as yet specifying how streams are matched in the cascade. From the usual material balances and the concentration differences effected by a stage one readily obtains for stages in the enricher of the cascade in Fig. 2 the relations

$$dx/dn = g - [P(x_P - x)/L)$$
$$dy/dn = h - [P(y_P - y)/L] \qquad (29)$$

A matched abundance ratio cascade is to be considered, and hence one may expect abundance ratios rather than mol fractions to be the more convenient variables. Accordingly, introduce

$$R = x/(1 - x - y) \text{ and } S = y/(1 - x - y) \qquad (30)$$

Carrying out the necessary substitutions for the indicated transformation of variables in (29) one then obtains

$$\frac{dR}{dn} = R\,\psi_1 - \frac{P(1 + R + S)(R_P - R)}{L(1 + R_P + S_P)} \qquad (31.1)$$

$$\frac{dS}{dn} = S\,\psi_2 - \frac{P(1 + R + S)(S_P - S)}{L(1 + R_P + S_P)} \qquad (31.2)$$

These are the gradient equations in terms of abundance ratios in *any* three-component cascade*

Consider now stages in a cascade as shown in Fig. 6. Suppose the cascade in Fig. 6 to be a *matched R cascade*. Then,

$$R_{n+2} = R_n^* \qquad (32)$$

*Note how easily the total reflux gradients are obtained from these equations.

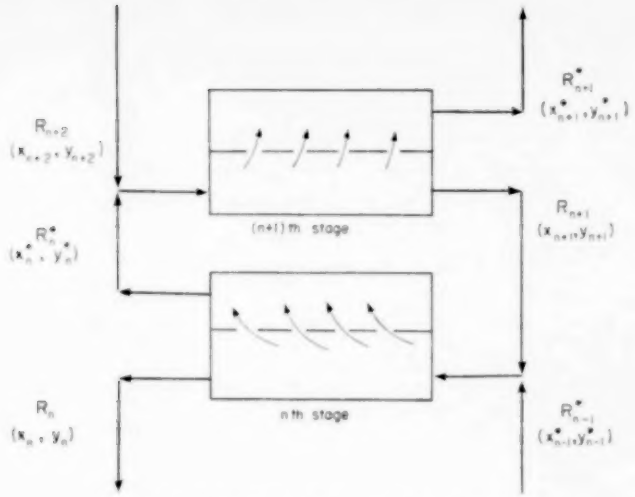

FIG. 6. Schematic of stages in a cascade.

From the concentration differences effected by the n-th stage, it follows that

$$R_n^* - R_n = \left[g\,(\partial R/\partial x) + h\,(\partial S/\partial y)\right]_n = R_n\,\psi_1$$

so that from (32) and the above, one obtains

$$R_{n+2} = R_n\,(1 + \psi_1) \tag{33}$$

In the present treatment of the stage number n as a continuous variable one has that

$$R_{n+2} - R_n = 2\,(dR/dn)$$

and hence, (33) becomes

$$dR/dn = R\,\psi_1/2 \tag{34}$$

which is the gradient equation for the R abundance ratio in a matched R cascade.

The interstage flows in the matched R cascade are now readily obtained. One substitutes (34) in (31·1), solves for L and finds that

$$L = \frac{2}{\psi_1}\,P\,\frac{1 + R + S}{1 + R_P + S_P}\cdot\frac{R_P - R}{R} \tag{35}$$

which is applicable to the enricher of the cascade shown in Fig. 2.

The relation between the R and S gradients in a matched R cascade also follows at once. Substituting (35) in (31·2) and dividing the result by (34) results in

$$dS/dR = 2k\,(S/R) - \left[(S_P - S)/(R_P - R)\right]$$

which may be reduced to

$$dS\,(R_P - R)\,R^{-2k}/dR = -\,S_P\,R^{-2k} \tag{36}$$

As in the development of the value function integration is here seen to present two cases, $2k = 1$ and $2k \neq 1$. For the case $2k \neq 1$, which is applicable to the U-235, 236 and 238 situation, one then obtains for the enricher of the cascade shown in Fig. 2,

$$\frac{S}{S_P} = -\,\frac{1}{2k - 1}\,\frac{(R_P/R)^{-(2k-1)} - 1}{(R_P/R) - 1} \tag{37}$$

At the feed point $R = R_F$, the R abundance ratio of the feed, since in the matched R cascade the R abundance ratio of the feed is matched to the cascade gradient value. The S abundance ratio S_{Fi} at the feed point is then obtained from (37) with $R = R_F$. It is to be emphasized that S_{Fi} is the cascade gradient value for the S abundance ratio at the feed point, and this value S_{Fi} is *not* necessarily equal to S_F, the S abundance ratio of the feed.

From the above examples it is clear how similar formulae may be developed for gradients and interstage flows of the stripper of the cascade in Fig. 2, as well as for more complicated cascade situations.

(*b*) *V balances and H balances*

A set of productivity equations for a matched

R cascade may be developed directly from cascade considerations; thus, the cascade separative work may be found by adding interstage flows, given by expressions such as (35), over all the cascade. Another approach, based on value function considerations, is simpler to develop, simpler to apply to more complex cascade situations and simpler to extend to additional isotopes. For this purpose, the value function either (26) or (27), is written in the form:

$$\mathscr{V}(x, y) = c_0 + c_1 x + c_2 y + c_3 H(x, y) + V(x,y) \quad (38)$$

Thus, for the case $2k \neq 1$,

$$H(x, y) = y R^{-(2k-1)} \quad (39)$$

$$V(x, y) = \left(2x + \frac{2k}{2k-1} y - 1\right) \ln R \quad (40)$$

As in the two-component situation, $V(x, y)$ is called the *elementary value function*. The new function $H(x, y)$ is called the *homogeneous function*.

For the reasons stated in the discussion leading to (15) a balance on a matched R cascade nets to the sum of the separative work of the stages; thus, for the cascade of Fig. 2 if operated as a matched R cascade one has

$$\frac{1}{4} \sum_{\text{cascade}} L \phi_1^2 = P \mathscr{V}(x_P, y_P) + W \mathscr{V}(x_W, y_W) - F \mathscr{V}(x_F, y_F)$$

More generally, for the same reasons as above, a $\mathscr{V}$ balance on some considered section of a matched R cascade leads to the sum of the separative work of the stages in the considered section. Thus, if E_j, $j = 1, 2, \ldots\ldots, J$, are the stream flows, at concentrations (x_j, y_j), cutting across the envelope defining some section of a matched R cascade

$$\frac{1}{4} \sum_{\text{Section}} L \phi_1^2 = \sum_{j=1}^{J} E_j \mathscr{V}(x_j, y_j) \quad (41)$$

where outputs are entered as positive quantities. Since c_0, c_1, c_2 and c_3 in (38) are arbitrary it follows at once from (41) that

$$\frac{1}{4} \sum_{\text{Section}} L \phi_1^2 = \sum_{j=1}^{J} E_j V(x_j, y_j), \quad \text{called a } V \text{ balance,} \quad (42)$$

and

$$0 = \sum_{j=1}^{J} E_j H(x_j, y_j), \text{ called an } H \text{ balance.} \quad (43)$$

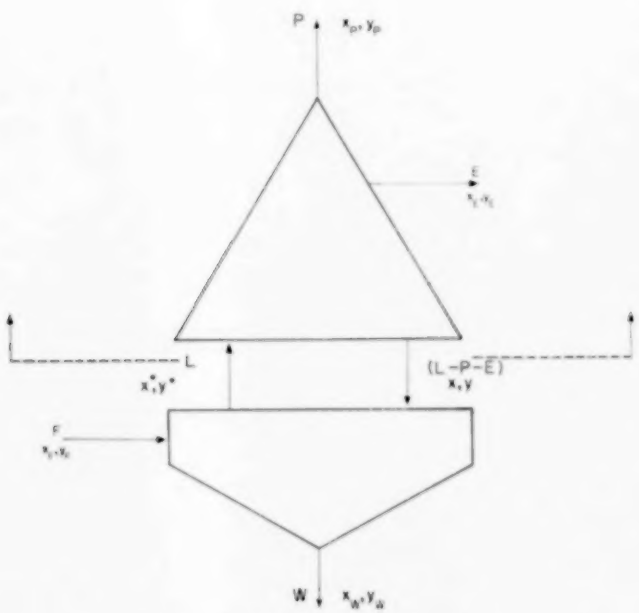

FIG. 7. Schematic of a cascade.

(One also obtains $\Sigma E_j = 0$, $\Sigma E_j x_j = 0$, and $\Sigma E_j y_j = 0$, but these are simply the three independent material balances which are true in *any* cascade).

Both V balances and H balances are of use in obtaining productivity equations. In particular, it may be noted than an H balance permits obtaining with ease the (x, y) gradient in the cascade. The use of these balances is illustrated by the following example.

Consider the cascade shown in Fig. 7.

By means of an H balance on the indicated section of the cascade in Fig. 7 an expression for the (x, y) gradient between the E withdrawal point and the F feed point will be obtained. The H balance on the section is

$$P H(x_P, y_P) + E H(x_E, y_E) + \\ + (L - P - E) H(x, y) - L H(x^*, y^*) = 0,$$

which is re-written

$$P\left[H(x_P, y_P) - H(x, y)\right] + \\ + E\left[H(x_E, y_E) - H(x, y)\right] - \\ - L\left[H(x^*, y^*) - H(x, y)\right] = 0. \qquad (44)$$

Consider now that for most isotope separations the differences $(x^* - x)$ and $(y^* - y)$ are small, so that one may write

$$H(x^*, y^*) - H(x, y) = (x^* - x)(\partial H/\partial x) + \\ + (y^* - y)(\partial H/\partial y)$$

Furthermore, by material balance,

$$L(x^* - x) = P(x_P - x) + E(x_E - x)$$
$$L(y^* - y) = P(y_P - y) + E(y_E - y)$$

Substituting the above expressions in (44) one then obtains

$$P\left[H(x_P, y_P) - H(x, y) - (x_P - x)(\partial H/\partial x) - \right. \\ \left. - (y_P - y)(\partial H/\partial y)\right] + E\left[H(x_E, y_E) - \right. \\ - H(x, y) - (x_E - x)(\partial H/\partial x) - \\ \left. - (y_E - y)(\partial H/\partial y)\right] = 0 \qquad (45)$$

which is seen to be an expression for the (x, y) gradient between the E withdrawal point and the F feed point.

From the above example it is clear how by means of H balances relations involving external flows and concentrations may be obtained for other cascade situations.

(c) *Productivity equations*

By means of V balances and H balances a set of productivity equations for any three-component cascade, operated as a matched R cascade, is quickly obtained. Thus for the cascade of Fig. 7 one immediately has the V balance, the H balance and the three material balances for the entire cascade:

$$\tfrac{1}{4}\sum_{\text{cascade}} L\,\psi_1^2 = PV(x_P, y_P) + EV(x_E, y_E) + \\ + WV(x_W, y_W) - FV(x_F, y_F)$$
$$0 = PH(x_P, y_P) + EH(x_E, y_E) + \\ + WH(x_W, y_W) - FH(x_F, y_F)$$
$$0 = Px_P + Ex_E + Wx_W - Fx_F \qquad (46)$$
$$0 = Py_P + Ey_E + Wy_W - Fy_F$$
$$0 = P + E + W - F$$

If in Fig. 7 one supposes that E is a *side feed* the above five equations suffice for the usual productivity calculations. (E is then entered as a negative quantity in the above productivity equations). Note, however, that if E is a *side withdrawal* the above five equations are not complete since both x_E and y_E cannot be specified. One may specify a desired x_E for the withdrawal but one then must take the y_E found at the point of withdrawal. The section H balance which led to (45) gives the required additional relation to complete the productivity equations in this situation. Since (x_E, y_E) are gradient concentrations (45) is evaluated at $x = x_E$ and $y = y_E$, and

$$H(x_P, y_P) - H(x_E, y_E) - (x_P - x_E)(\partial H/\partial x_E) - \\ - (y_P - y_E)(\partial H/\partial y_E) = 0 \qquad (47)$$

where

$$(\partial H/\partial x_E) = (\partial H/\partial x) \text{ at } x = x_E,\ y = y_E$$
$$(\partial H/\partial y_E) = (\partial H/\partial y) \text{ at } x = x_E,\ y = y_E$$

The five equations (46) and equation (47) complete the set of productivity equations for the cascade of Fig. 7. Other situations are similarly treated and offer no new difficulties.

Needless to say, the above three-component productivity equations have the same uses as those for two-component separation. In addition,

by means of differential analysis the three-component equations readily lead to evaluating the nuisance effects of a third component of low concentration in the separation of two major components, such as the effects of U-234 on the separation of U-235 and U-238, which can become significant at high U-235 concentrations.

Unit Cost Scale with the matched Abundance Ratio Cascade

The three-component value function $\mathscr{V}(x, y)$ which has been developed immediately leads to a unit cost scale for U-235, 236 and 238 mixtures being separated by gaseous diffusion in a matched R cascade. Let $D(x, y)$ be the unit cost in dollars per kilogram of uranium whose U-235 concentration is x and whose U-236 concentration is y. As before let K be the unit cost of separative work in $/kg. Then,

$$D(x, y) = K\left[a_0 + a_1 x + a_2 y + a_3 H(x, y) + V(x, y)\right] \quad (48)$$

where the a's are arbitrary constants, and from (39) and (40) H and V for U-235, 236 and 238 mixtures are

$$H(x, y) = y\left[x/(1 - x - y)\right]^{1/3} \quad (49)$$

$$V(x, y) = (2x + 4y - 1)\ln\left[x/(1 - x - y)\right] \quad (50)$$

For the reasons already given for the two-component cost scale used by the U.S.A.E.C. this three-component cost scale assures that the operating costs of a matched R cascade are accounted for by the material charges and credits.

There are four arbitrary constants in (48). These constants are evaluated from the following considerations:

1. The cost scale $D(x, y)$ should have a locus of zero value; thus

$$D(x_B, y_B) = 0$$

2. Uranium at concentrations (x_B, y_B) may be used as a feed to a matched R cascade to produce some product, say, at concentrations (x_T, y_T). Though this product does not accrue feed costs, it does accrue cascade separative work costs, and consequently, $D(x_T, y_T) > 0$ for concentrations (x_T, y_T) not on the locus of zero value. To assure a non-negative cost scale for the entire range of concentrations $D(x, y)$ is made a minimum on the locus of zero value; thus

$$\partial D/\partial x = 0,\ \partial D/\partial y = 0,\ \text{for } x = x_B,\ y = y_B.$$

3. In order that the resulting cost scale include the U.S.A.E.C. schedule for U-235 and 238 mixtures the locus of zero value should include x_0, the zero point of the U.S.A.E.C. price schedule; thus

$$D(x_0, 0) = 0.$$

The details of the required mathematical analysis for the evaluation of the constants are presented in Ref. [5]. Suffice it to say that in this analysis it is very convenient to consider the cost scale as a function of the abundance ratio R and the U-236 concentration y rather than a function of x and y. The resulting values of the constants are shown below:

$$a_0 = \left[(R_0 - 1) + \ln R_0\right] = -7{\cdot}1086$$

$$a_1 = -\left[\frac{(R_0 - 1)(R_0 + 1)}{R_0} + 2\ln R_0\right] = -462{\cdot}9338 \quad (51)$$

$$a_2 = -\left[(R_0 - 1) + \frac{1}{(2k - 1)^2} + \frac{2k}{2k - 1}\ln R_0\right] = 16{\cdot}4411$$

$$a_3 = \frac{1}{(2k - 1)^2} R_0^{2k-1} = 1{\cdot}738$$

where $R_0 = x_0/(1 - x_0)$. The numerical values given above are obtained with $k = 2/3$, applicable to U-235, 236 and 238 mixtures, and $x_0 = 0{\cdot}0022138$ weight fraction U-235, the zero value of the U.S.A.E.C. price schedule given in [1].

Before detailed numerical results are presented the general aspects of the resulting cost scale $D(x, y)$ are briefly reviewed. As shown in Fig. 8, the following are the more important characteristics of the cost scale:

1. The locus of zero value is the line of constant abundance ratio R_0 which passes through the two-component concentration x_0 of zero value.

2. When $y = 0$, the U.S.A.E.C. price schedule for U-235, 238 mixtures is obtained.

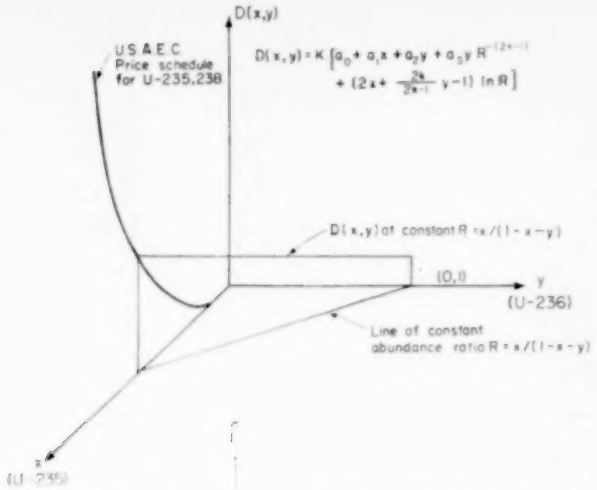

FIG. 8. The three-component unit cost scale.

3. The cost scale becomes infinite on the axis representing the U-235 and U-236 mixture, as well as that of the U-236 and U-238 mixture.

Some numerical results are now presented. Table 1 lists $D(x, y)$ so as to show the effect of U-236 on the unit cost of uranium at various U-235 concentrations of interest. The tabulated $D(x, y)$ is obtained with the constants in (48) evaluated as in (51) and a unit cost of separative work $K = 837{\cdot}286$/kg U, given in Ref. [1]. It is to be noted in Table 1 how the unit cost of uranium increases as the U-236 concentration increases at a constant U-235 concentration. The rise is small over most of the permissible U-236 range, but it may surprise one that it rises at all. The reason for the rise is that the developed cost scale accounts for cascade separative work, and as the U-236 concentration increases at fixed U-235 concentrations, it takes more separative work per kilogram of uranium for that uranium to be produced from feed material of zero value.

Some Reactor Considerations

The increase of the developed unit cost for uranium as the U-236 concentration increases at constant U-235 concentration may seem a most peculiar characteristic of the cost scale to a reactor operator. In particular, since as a rule* U-236 is produced in a reactor it might at first glance appear that by producing U-236 a reactor can *increase* the unit cost of material, and thereby conceivably generate power at no cost. Thus, some investigation of what a reactor does in relation to the developed cost scale is in order.

A reactor takes in material which contains a quantity X kg of U-235 and Z kg of U-238. The R abundance ratio of this material then is $R = X/Z$. Suppose an incremental amount δX of U-235 is burned up. At the same time an incremental amount δZ of U-238 is used. One has then that

$$(\delta R/R) = (\delta X/X) - (\delta Z/Z)$$

But since δX is proportional to $X\sigma_5$ and δZ is proportional to $Z\sigma_8$ where σ_5 and σ_8 are the appropriate cross-sections it follows that

$$(\delta R/R) = \left[1 - (\sigma_8/\sigma_5)\right](\delta X/X) \simeq 0{\cdot}99\,(\delta X/X)$$

in the thermal neutron range. Note then that a reactor always *decreases* the R abundance ratio

*A possible exception is when the U-236 concentration of the reactor charge is considerably greater than the U-235 concentration, and the U-236 production from U-235 neutron capture is less than the U-236 lost to U-237 formation.

Table 1. Unit cost scale (8 kg U) for U-235, -236, -238 mixtures

x	y*	0·00	0·02	0·04	0·06	0·08	0·10	0·12	0·14	0·16	0·18	0·20	0·30	0·40	0·50	0·60	0·70	0·80	0·90
0·90		15·335	15·302	15·302	15·428	15·479	15·557 †												
0·80		13·373	13·394	13·615	13·637	13·660	13·685	13·712	13·744	13·783	13·838	13·926†							
0·70		11·830	11·847	11·864	11·882	11·900	11·919	11·939	11·960	11·982	12·066	12·032	12·202†						
0·60		10·604	10·109	10·124	10·140	10·156	10·172	10·188	10·206	10·223	10·242	10·261	10·376	10·655†					
0·50		8565	8579	8592	8606	8420	8434	8449	8464	8479	8495	8511	8600	8717	9014†				
0·40		6642	6654	6666	6679	6691	6704	6717	6730	6743	6757	6771	6846	6935	7053	7396†			
0·30		4926	4936	4947	4958	4969	4980	4991	5003	5014	5026	5039	5103	5176	5263	5381	5710†		
0·20		3218	3227	3236	3246	3255	3264	3274	3284	3294	3304	3314	3368	3420	3498	3581	3697	4040†	
0·10		1527	1533	1540	1548	1555	1562	1570	1577	1585	1592	1600	1642	1688	1740	1801	1877	1985	2335 †
0·08		1192	1199	1205	1212	1218	1225	1232	1239	1246	1253	1260	1298	1341	1389	1445	1514	1611	1835
0·06		860·9	866·5	872·1	877·9	883·7	889·7	895·7	901·9	908·1	914·5	920·9	955·2	993·2	1036	1087	1149	1234	1398
0·04		534·4	539·0	543·7	548·5	553·4	558·3	563·4	568·5	573·8	579·1	584·5	613·5	645·9	682·9	726·6	780·5	853·5	981·7
0·03		374·6	378·6	382·7	386·8	391·0	395·3	399·7	404·2	408·7	413·4	418·1	443·5	472·2	505·3	544·5	593·2	659·4	772·7
0·02		219·5	222·6	225·9	229·1	232·5	235·9	239·4	243·0	246·7	250·5	254·3	275·0	298·8	326·6	360·0	402·1	459·9	558·0
0·01		75·46	77·36	79·30	81·30	83·36	85·47	87·63	89·89	92·21	94·59	97·03	110·6	126·7	146·1	170·5	202·3	247·7	326·6
0·009		62·44	64·16	65·93	67·75	69·63	71·56	73·56	75·62	77·74	79·93	82·20	94·73	109·7	129·0	151·0	181·4	225·0	301·4
0·008		49·80	51·42	53·09	54·83	56·61	58·45	59·85	61·70	63·62	65·61	67·66	79·09	92·89	109·9	131·5	160·2	201·9	275·4
0·007		37·93	39·26	40·64	42·06	43·53	45·05	46·63	48·26	49·96	51·71	53·54	63·70	76·24	91·80	111·8	138·7	178·2	248·7
0·006		26·76	27·86	29·01	30·20	31·44	32·73	34·06	35·45	36·90	38·41	39·97	48·84	59·86	73·79	91·97	116·8	153·8	220·8

* x — mol fraction U-235 ; y — mol fraction U-236. † At stated U-236 concentration less 0·005.

of material because of U-235 burn-up. At the same time, except for the situation already noted, U-236 is produced, so that the U-236 concentration y *increases*. Now, it may be established from the developed cost scale that

$$\partial D/\partial R > 0, \quad \text{and} \quad \partial D/\partial y < 0,$$

except on the locus of zero value. Hence, it may be seen that in the considered situation a reactor *decreases* the value of material on both counts, namely, decreasing R and increasing y. Also, in general, increases in burn-up bring about further decreases in the value of the uranium. Consequently, the fact that unit costs increase with increasing U-236 concentration at fixed U-235 concentration is not particularly advantageous to the reactor operator.

Perhaps a more natural presentation of the cost scale for the above purposes is a tabulation of the cost scale in co-ordinates of the abundance ratio R and the U-236 concentration y, as shown in Table 2. Here, it may be clearly seen that as a reactor decreases the U-235 relative to the U-238 (that is, decreases R) the unit cost drops, and as U-236 is introduced the unit cost also drops.

Some burn-up costs as determined with the developed cost scale will now be briefly reviewed. These are shown in Table 3. It is here supposed that a reactor at 50 per cent burn-up is originally charged with material at the stated charge concentrations which cover a range of U-235 concentration levels with and without U-236. The discharge concentrations are computed from the assumed burn-up of 30 per cent and from the indicated uranium isotope cross-sections in the thermal neutron range. The unit cost of burn-up in dollars per kilogram of U-235 has been computed two ways for comparison. The burn-up cost C_4 has been determined from a four-component cost scale (U-234, 235, 236 and 238) developed in the manner exemplified for three components. The other burn-up cost C_2 has been determined from the U.S.A.E.C. price schedule for U-235, 238. It is to be remembered that the four-component cost scale includes the U.S.A.E.C. schedule as a special case. The comparison between C_4 and C_2 then indicates the effects of the nuisance isotopes on some reactor economics. In particular, note how

VOL. 15 1961

*Table 2. Unit cost scale ($/kg U) for U-235, -236, -238 mixtures as a function of R and y**

R/y	0·00	0·02	0·04	0·06	0·08	0·10	0·20	0·40	0·60	0·80	0·95
10·0	15,497	15,200	14,902	14,605	14,307	14,010	12,523	9549	6574	3600	1369
5·0	14,159	13,887	13,615	13,343	13,071	12,799	11,438	8717	5996	3275	1234
2·0	11,251	11,035	10,819	10,603	10,388	10,172	9093	6935	4776	2618	999·8
1·0	8365	8206	8046	7887	7728	7568	6771	5176	3581	1986	790·4
0·5	5497	5394	5290	5187	5083	4980	4463	3429	2394	1360	584·2
0·2	2652	2604	2555	2507	2459	2410	2170	1688	1206	724·6	363·2
0·1	1374	1351	1327	1303	1279	1255	1136	898·5	660·6	422·6	244·2
0·05	658·0	647·4	636·9	626·4	615·9	605·3	552·7	447·4	342·2	236·9	158·0
0·04	509·6	501·7	493·9	486·0	478·1	470·2	430·9	352·1	273·4	194·6	135·6
0·03	360·8	355·5	350·3	345·0	339·7	334·4	308·0	255·1	202·3	149·4	109·8
0·02	213·5	210·7	207·9	205·0	202·2	199·3	185·2	156·8	128·4	100·0	78·72
·001	74·16	73·39	72·63	71·87	71·10	70·34	66·52	58·89	51·26	43·63	37·91
0·009	61·41	60·82	60·22	59·62	59·02	58·42	55·43	49·44	43·45	37·46	32·97
0·008	49·11	48·66	48·22	47·77	47·32	46·87	44·63	40·16	35·68	31·20	27·84
0·007	37·37	37·06	36·75	36·43	36·12	35·80	34·25	31·12	28·00	24·87	22·33
0·006	26·38	26·18	25·98	25·79	25·59	25·40	24·41	22·45	20·49	18·53	17·06

*R = Mol fraction U-235/Mol fraction U-238; y = mol fraction U-236

*Table 3. Examples of U-235 burn-up costs**

Charge Concentrations		Burn-up costs ($/kg U-235)	
U-235	U-236	C_2†	C_4‡
0·90	0·00	17,204	17,044
	0·05	17,204	17,072
0·80	0·00	17,148	17,018
	0·05	17,147	17,037
0·60	0·00	17,078	16,977
	0·05	17,078	16,995
0·40	0·00	17,003	16,921
	0·05	17,002	16,944
0·20	0·00	16,846	16,785
	0·05	16,844	16,826
0·10	0·00	16,585	16,540
	0·05	16,583	16,615
0·05	0·00	16,105	16,072
	0·05	16,101	16,207
0·02	0·00	14,723	14,705
	0·05	14,717	14,990
0·01	0·00	12,465	12,456
	0·05	12,457	12,931

*30 per cent burn-up assumed.

†C_2 is based on the U.S.A.E.C. price schedule for U-235, 238 mixtures.

‡C_4 is based on a four-component unit cost scale applicable to a matched-R cascade processing U-234, U-235, U-236 and U-238 mixtures.

the unit cost of burn-up increases with the presence of U-236 in the reactor charge; at least initially this rate of increase is seen to be unexpectedly small. Detailed studies on the effects of the developed cost scale on reactor economics similar to those presented in Ref. [4] are nevertheless indicated and will be the subject of another report.

Example of Permissible Cascade Operations

It has been previously stated that the developed cost scale has the property that materials having the same R abundance ratio may be mixed without incurring a mixing loss. This property permits some mixing operations of interest both in reactor and cascade operations, and an example of particular interest in cascade operations will be briefly discussed.

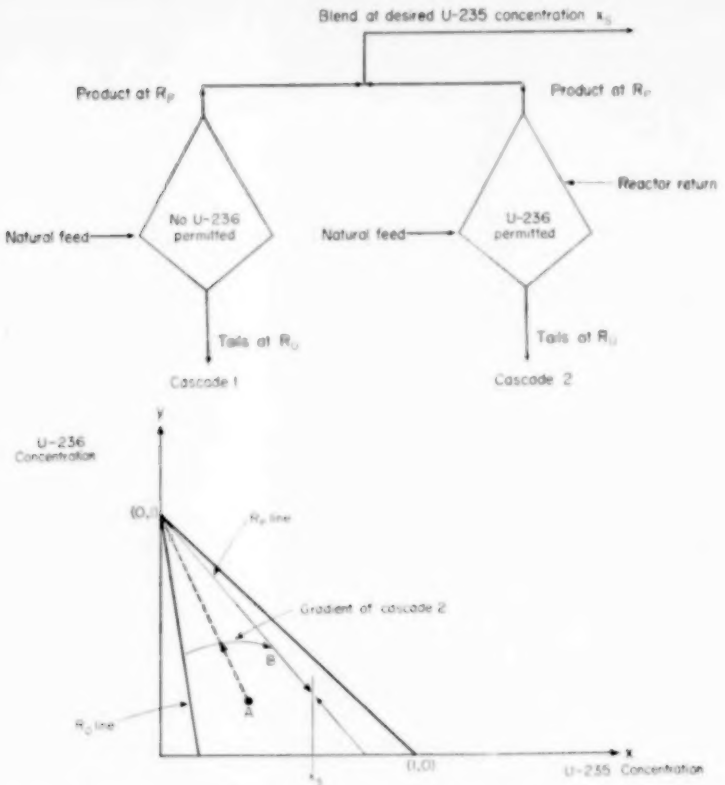

FIG. 9. Example of permissible blending operations with matched R cascades.

Consider two cascades as shown in Fig. 9. Here, Cascade 1 is kept free of U-236, and Cascade 2 receives uranium with U-236. Both cascades are matched R cascades, and both span the same R range, namely, from R_0 to R_P. (Furthermore, since both span the same R range, both have the same number of stages). The mixing operations possible are best exemplified on the (x, y) plot in Fig. 9. In the considered situation a reactor returns material at point A and requests material with a U-235 concentrations x_s. The reactor return can then be fed to Cascade 2, enriched up to point B with abundance ratio R_P, and product from Cascade 2 can be blended with product from Cascade 1 also at R_P to make a blend at the desired U-235 concentration x_s. The possibility of such blending operations is of interest particularly with mixtures containing U-234 and U-236 at relatively high U-235 concentrations. In such a situation, there is the possibility of finding oneself very short of stages if further U-235 enriching is to be done in a single cascade.

INVESTIGATION OF PROPERTIES OF THE MATCHED R CASCADE

It has been seen that the matched R cascade plays a central role in the application of the value function and unit cost scales which have been developed. It has been previously mentioned that the two-component ideal cascade has the very desirable property of being a minimum power cascade; and, of course, a similar property for the matched R cascade would also be desirable. The writers have not been able to establish such a property for the matched R cascade. Some cost properties of the matched R cascade have been established and these are discussed below.

As shown in Ref. [5] the unit cost $D(x, y)$,

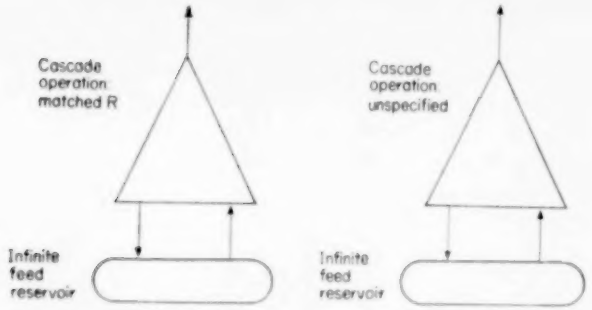

FIG. 10. Comparison of a matched R cascade operation with a minimum cost cascade operation.

developed for U-235, 236, 238 mixtures may be interpreted as the unit cost of material at concentrations (x, y) which has been produced in a matched R cascade from material of zero value with abundance ratio R_0. A pertinent question to ask is whether with some other mode of cascade operation it is possible to produce at lower cost material at the same concentrations (x, y), the feed of zero value still having abundance ratio R_0. The situation is as shown in Fig. 10.

For the situation shown in Fig. 10 it has been possible to establish a *lower bound* for min. $D(x, y)$. For the development of this lower bound reference is made to [5]; it is there shown that:

$$\text{min. } D(x, y) \geqslant (1 - y)\, D(x^*, 0) + y\, I(x, y) \quad (52)$$

where:

$$x^* = x/(1 - y)$$

$$I(x, y) = K \ln \left\{ \left[\frac{k(R - R_0) + R_0}{R_0} \right]^{1/k} \times \left[\frac{k(R - R_0) + R_0}{R} \right]^{1/(1-k)} \right\}$$

and other notation is as before. The above inequality is applicable to the situation of Fig. 10 for the case $0 < k < 1$, which includes the U-235, 236, 238 mixture with $k = 2/3$. With the lower bound given by equation (52) it is then possible to estimate how much cheaper material of specified concentrations (x, y) can be produced from material of zero value with some other mode of cascade operation than the matched R mode. Since here the feed is at zero value the difference between $D(x, y)$ and min. $D(x, y)$ is due to a difference in separative work requirements, and hence, this difference also indicates how far from minimum power a matched R gaseous diffusion cascade may be. For the purposes of these evaluations Table 4 lists the ratio $D(x, y)/\text{min. } D(x, y)$, with min. $D(x, y)$ estimated by equation (52) for concentration ranges of interest. It may be seen that the tabulated ratios indicate a very favourable comparison of the matched R cascade with some other mode of cascade operation for a large range of U-235 and U-236 concentrations. Incidentally, the fact that the matched R cascade is not a minimum power cascade implies that it is possible to mix some materials with a *gain* in value in the sense of the developed $\mathscr{V}(x, y)$. This opens some blending possibilities to both the cascade and reactor operators. Thus, for example, it may be advantageous to a reactor operator to blend two materials before returning these to the cascade and to ask the cascade operator for credit on the blend. Table 4 indicates such possibilities to be small, but nevertheless they will be considered in the previously mentioned study on the effects of the developed cost scale on reactor economics.

Another very desirable property of the two-component cascade is that considerable changes from ideality can be made without large changes from the ideal separative work requirements. Indeed, it is this stationary property which permits application of ideal cascade theory to actual non-ideal cascades. This stationary property of the ideal cascade has been established analytically [2]. It has not been possible to establish a similar property for the three-component matched R

cascade, but numerical studies do indicate that matched R cascades have a desired stability. Examples of some numerical studies are shown in Fig. 11. Here a matched x cascade has been completely determined numerically by an iterative computing scheme and the cascade separative work has been determined by summing $L\,\psi_1^2/4$ over all the stages. With the external stream flows and concentrations of the matched x cascade, a cascade value balance has been made with the developed unit cost scale so as to obtain an estimate of the cost of cascade separative work $K\,\Sigma L\,\psi_1^2/4$, whence the cascade separative work is estimated by dividing by K, the unit cost of separative work used for the cost scale. A comparison of the actual and estimated separative work is tabulated in Fig. 11 for three different cascade situations. It may be seen that the comparisons are favourable, and this would indicate that some freedom may be taken in applying the value function for matched R cascades to other modes of cascade operation in the same manner that the two-component value function for ideal cascades is applied to non-ideal cascades. Analytical investigation along these lines is nevertheless needed; results already available are presented in Ref. [5].

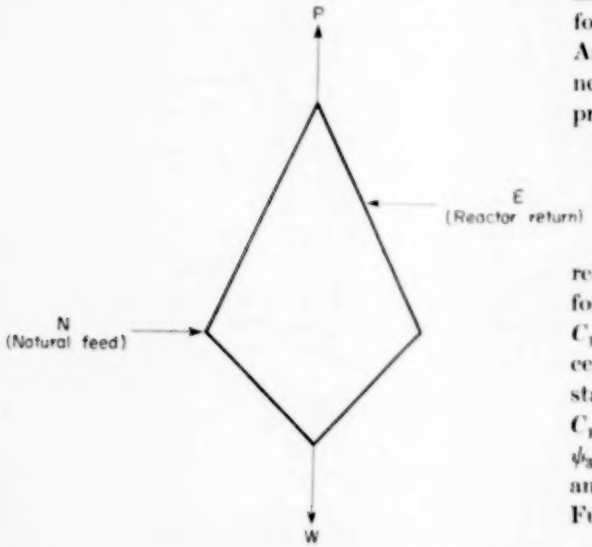

FIG. 11. Application of $D(x, y)$ for matched R cascade to a matched x cascade.

		Quantity x (U-235)	y (U-236)		Concentration
Case 1	P:	100·00	·0200	·00556	V_{c1}/V_{c2} =
2% U-235	E:	99·11	·0121	·00675	1·00014
in P	N:	159·22	·0072	·00000	
Case 2	P:	100·00	·3500	·3264	
35% U-235	E:	87·49	·2412	·3908	V_{c1}/V_{c2} =
in P	N:	2780·14	·0072	·0000	1·0080
Case 3	P:	100·00	·8000	·1536	V_{c1}/V_{c2} =
80% U-235	E:	86·35	·7427	·1811	1·0029
in P	N:	3174·37	·0072	·0000	

x_w = ·0022 for all cases.
V_{c1} = Separative work required by matched-x cascade.
V_{c2} = Separative work given by $D(x, y)$ balance on streams and stream concentrations of matched-x cascade.

Generalization to More Components

The three-component value function $\mathscr{V}(x, y)$ and the three-component matched R cascade readily generalize to more components. Consider, for example a mixture of the four components C_1, C_2, C_3, and C_4. Let x, y and z denote the concentrations of C_1, C_2 and C_3. Let ψ_1 denote the stage separation factor for the two component C_1 and C_4 separation; and similarly, let ψ_2 and ψ_3 denote the corresponding factors for the C_2 and C_4 separation and the C_3 and C_4 separation. Further, let

$$k_{2,1} = \psi_2/\psi_1,$$

$$k_{3,1} = \psi_3/\psi_1.$$

Then, a four-component value function $\mathscr{V}(x, y, z)$ applicable to the case $2k_{2,1} \neq 1$ and $2k_{3,1} \neq 1$ is

$$\mathscr{V}(x, y, z) = c_0 + c_1 x + c_2 y + c_3 z + c_4 H_{2,1}(x, y, z) + c_5 H_{3,1}(x, y, z) + V(x, y, z),$$

where the c's are arbitrary constants, and

$$H_{2,1} = y\,R^{(2k_{2,1}-1)}$$

$$H_{3,1} = z\,R^{(2k_{3,1}-1)}$$

$$V = \left(2x + \frac{2k_{2,1}}{2k_{2,1}-1}\,y + \frac{2k_{3,1}}{2k_{3,1}-1}\,z - 1\right)\ln R$$

$$R = x/(1 - x - y - z)$$

*Table 4. Comparison of $D(x, y)$ and min. $D(x, y)$**

x/y	0·00	0·02	0·04	0·08	0·10	0·12	0·14	0·16	0·18	0·20	0·30	0·40	0·50	0·60	0·70	0·80	0·90
0·90	0	0·63	0·66	0·16	0·23†												
0·80	0	0·63	0·66	0·12	0·16	0·20	0·24	0·30	0·38	0·52†							
0·60	0	0·63	0·66	0·11	0·15	0·18	0·21	0·25	0·29	0·33	0·58	1·32†					
0·40	0	0·63	0·66	0·13	0·16	0·20	0·23	0·27	0·31	0·35	0·57	0·86	1·29	2·73†			
0·20	0	0·64	0·68	0·17	0·22	0·26	0·31	0·36	0·41	0·46	0·74	1·06	1·47	2·01	2·88	6·13†	
0·10	0	0·65	0·11	0·22	0·28	0·34	0·41	0·47	0·53	0·60	0·97	1·40	1·92	2·57	3·48	4·98	10·97†
0·05	0	0·67	0·13	0·28	0·35	0·42	0·50	0·58	0·66	0·75	1·21	1·76	2·42	3·27	4·40	6·12	9·79
0·01	0	0·66	0·12	0·26	0·33	0·40	0·48	0·56	0·65	0·74	1·25	1·91	2·76	3·89	5·50	7·97	12·64
0·006	0	0·64	0·08	0·17	0·22	0·28	0·34	0·40	0·46	0·53	0·94	1·51	2·27	3·35	4·93	7·46	12·35

*The tabulated numbers are 100 $\{[D(x, y)/\min. D(x, y)] - 1\}$.
†At stated U-236 concentration y less 0·005.

The cascade associated with the above four-component value function is, of course, the matched R cascade, R now denoting $x/(1 - x - y - z)$. The two homogeneous functions, $H_{2,1}$ and $H_{3,1}$ and the elementary value function V play the same role as before.

From the above example of a four-component value function it is readily seen how other four-component value functions are obtained for different separation factor ratios, and in general, how value functions for more components are obtained.

Other Subjects

A few brief remarks will now be made on more general subjects.

Consider first the match function which has been here introduced to isotope separation in cascades. The match function played a significant role in the development of the three-component value function. The match function here prescribes how to link stages together to form a cascade and how to introduce feeds to the cascade so that separative work is conserved wherever streams are mixed. Now, most of the mixing in a cascade is done at the stage links, and the concentrations mixed at these links differ by very little in contrast to the large differences in concentration which may occur at a feed point. Hence, it makes sense to consider match functions on a purely *local* basis and ask for a match function which makes it possible to conserve separative work at the stage links to order ψ^2, which after all, is the same order of correctness of the partial differential equation defining the value function. Suffice it then to say that it is in fact possible to develop such local match functions in situations where some mixing is permissible. The development of local match functions for three-component mixtures is presented in Ref. [5].

From a more general viewpoint one can forget about an association between match functions and value functions and simply consider a match function as a recipe for linking stages together to do a certain separation job. For example, one may consider processing some mixture of isotopes in a cascade when the interest is not in enriching a particular isotope, but rather, in enhancing

some average property of the mixture, such as an average cross-section. In such a situation, there is intuitive appeal in investigating a match function which is a linear form in the concentrations of the various isotopes. From this more general viewpoint much remains to be investigated about match functions.

Finally, a word about value functions. The three-component value function here developed permits the absence of one of the components. This value function is applicable to operations with U-235, 236 and 238 mixtures which may or may not contain U-236. Suppose, however, that the isotopic mixture always includes the three components. A value function applicable to the processing of such a mixture in a cascade must then of necessity become infinite when any one of the components is absent. Furthermore, all mixing should result in a loss of separative work. A value function of particular interest in this situation is:

$$V_1(x, y) = \tfrac{1}{2}\,\phi_1^{\,2}\{\phi_1^{\,-2}(2x + y - 1) \times \ln[x/(1 - x - y)] + \phi_2^{\,-2}(x + 2y - 1) \times \ln[y/(1 - x - y)] + (\phi_1 - \phi_2)^{-2}(x - y) \times \ln(x/y)\}.$$

The function $V_1(x, y)$ is a solution of the partial differential equation given previously. It is symmetric in the concentrations and has a minimum at the point (1/3, 1/3), and these are properties analogous to those of the elementary value function for two components. The single minimum can be moved by means of the evaluation of arbitrary constants in an additive linear form in x and y to the concentrations of the natural mixture, that is, an infinite reservoir of zero value material. This function also has the property that any mixing whatsoever results in loss of value, as would be expected when all concentration changes are effected by expending separative work. The application of this function to isotope separation remains to be exploited.

In conclusion, as seen from the above remarks and others previously made there remain many unsolved problems in the theory of multicomponent isotope separation in cascades.

Appendix

Development of the Value Function, given the Match Function

Given that

$$M = x/(1 - y) \tag{A.1}$$

is the necessary match function it remains to find out whether a value function $\mathscr{V}(x, y)$ is permitted by the partial differential equation (16) in the text. This is done below.

Text equation (16) is first transformed to co-ordinates of M and y; thus:

$$\left(g^2\frac{\partial^2 M}{\partial x^2} + 2gh\frac{\partial^2 M}{\partial x\partial y} + h^2\frac{\partial^2 M}{\partial y^2}\right)\frac{\partial U}{\partial M} + \mu^2\frac{\partial^2 U}{\partial M^2} + 2\mu h\frac{\partial^2 U}{\partial M\partial y} + h^2\frac{\partial^2 U}{\partial y^2} = \phi_1^{\,2}, \tag{A.2}$$

$$\text{where } \mu = g\frac{\partial M}{\partial x} + h\frac{\partial M}{\partial y} \tag{A.3}$$

and $U(M, y)$ is given by text equation (23). From text equation (25) one finds directly that

$$\partial M/\partial x = 1/(1 - y),\ \partial M/\partial y = M(\partial M/\partial x),\ \partial^2 M/\partial x^2 = 0,$$
$$\partial^2 M/\partial y^2 = 2(\partial M/\partial x)(\partial M/\partial y),$$
$$\partial^2 M/\partial x\partial y = (\partial M/\partial x)^2 \tag{A.4}$$

Substituting from (A.4) in (A.2), one first notes that the factor of $\partial U/\partial M$ collapses to

$$2h\mu(\partial M/\partial x)$$

and hence, (A.2) may be re-written as

$$\left[2h\left(\frac{\partial M}{\partial x}\frac{\partial U}{\partial M} + \frac{\partial^2 U}{\partial M\partial y}\right) + \mu\frac{\partial^2 U}{\partial M^2}\right]\mu + h^2\frac{\partial^2 U}{\partial y^2} = \phi_1^{\,2} \tag{A.5}$$

From (A. 1, 3, 4), and the expressions for g and h it may be verified that:

$$h = \phi_1(k - M)y(1 - y)$$
$$h(\partial M/\partial x) = \phi_1(k - M)y \tag{A.6}$$
$$\mu = \phi_1 M(1 - M)$$

and from direct differentiation of text equation (22)

$$\partial U/\partial M = \alpha' + \beta' y, \qquad \partial^2 U/\partial M\partial y = \beta' \tag{A.7}$$
$$\partial^2 U/\partial M^2 = \alpha'' + \beta'' y, \qquad \partial^2 U/\partial y^2 = 0$$

and furthermore from text equation (24)

$$\alpha'' = 1/[M(1 - M)]^2 \tag{A.8}$$

One now substitutes from (A.6, 7, 8) in (A.5) and finds that

$$M(1 - M)(\alpha'' + \beta'') + 2(k - M)(\alpha' + \beta') - 1/M(1 - M) = 0 \tag{A.9}$$

the y variable vanishing, and thus, the partial differential

VOL. 15 1961

equation (A.2) *for the value function* $\mathscr{U}(x, y) = U(M, y)$ *has been reduced to an ordinary differential equation for* $\beta = \beta(M)$, *the only unknown function in the expression text equation* (23) *for the value function.* Hence, it has now been established that there is in fact a value function $\mathscr{U}(x, y)$ with an associated match function $M(x, y)$ given by (A.1); this $\mathscr{U}(x, y) = U(M, y)$ being given by text equation (23) with $\alpha = \alpha(M)$ given by text equation (24) and $\beta = B(M)$ being the solution of (A.9).

Equation (A.9) is now solved. It is easier to solve for $(\alpha + \beta)$. In carrying out the indicated integrations one finds that two cases for the integrations are necessary; namely: $2k = 1$, and $2k \neq 1$. One then obtains

for $2k = 1$:

$$\alpha + \beta = C_0 + C_1 \ln\left(\frac{M}{1-M}\right) + \tfrac{1}{2}\left[\ln\left(\frac{M}{1-M}\right)\right]^2 \quad \text{(A.10)}$$

for $2k \neq 1$:

$$\alpha + \beta = C_0 + C_1\left(\frac{M}{1-M}\right)^{(2k-1)} + \frac{1}{2k-1}\ln\left(\frac{M}{1-M}\right) \quad \text{(A.11)}$$

where C_0 and C_1 are arbitrary constants.

From equation (23) one has that

$$U(M, y) = (1 - y)\alpha + y(\alpha + \beta)$$

and hence, with text equation (24), (A.10) and (A.11) the value function may be expressed as a function $U(M, y)$ of M and y for both integration cases. To obtain $\mathscr{U}(x, y)$, one now uses (A.1) to eliminate M from $U(M, y)$ and one obtains

for $2k = 1$:

$$\mathscr{U}(x, y) = c_0 + c_1 x + c_2 y + c_3 y \ln R + \left[2x + \frac{(\ln R)}{2} y - 1\right] \ln R \quad \text{(A.12)}$$

for $2k = 1$:

$$\mathscr{U}(x, y) = c_0 + c_1 x + c_2 y + c_3 y R^{-(2k-1)} + \left(2x + \frac{2k}{2k-1} y - 1\right) \ln R \quad \text{(A.13)}$$

where $R = x/(1 - x - y)$ (A.14)

and c_0, c_1, c_2 and c_3 are arbitrary constants.

References

[1] Benedict M. and Pigford T. H. *Nuclear Chemical Engineering*, McGraw-Hill, New York 1957.

[2] Cohen K. *The Theory of Isotope Separation as applied to the Large-Scale Production of U-235.* NNES–III–1B McGraw-Hill, New York 1951.

[3] Hollister H. L. and Burington A. J. *Nucleonics* 1958 **16** 54.

[4] Garrett G. A. and Levin S. A. *2nd U.N. Int. Conf. Peaceful Uses Atomic Energy* 1958 A/CONF. 15/P/442.

[5] de la Garza A., Garrett G. A. and Murphy J. E. *Some Value Functions for Multicomponent Isotope Separation-Application to a Unit Cost Scale for Uranium-235, 236, 238 Mixtures.* K–1455. Union Carbide Nuclear Company, Oak Ridge, Tennessee July 1960.

Chemical Engineering Science, 1961, Vol. 15, pp. 210 to 219. Pergamon Press Ltd. London. Printed in Great Britain.

Interfacial resistances in the liquid extraction of inorganic nitrates

W. J. McMANAMEY

Chemical Engineering Department, University of Sydney, N.S.W.

(*Received* 8 *August* 1960)

Abstract—Studies of the extraction of divalent copper, cobalt and nickel nitrates from water by *n*-butanol at 25° C in a stirred mass transfer cell showed that the mass transfer process is influenced by an interfacial resistance due to the reaction at the water–solvent phase boundary, in addition to the water and solvent individual phase resistances. This interfacial resistance does not vary with the time of contact of the phases, and the relationships between the interfacial resistance rate constants and the nitrate concentrations at the interface are of the form predicted from the kinetics of the chemical reaction for nitrate extraction. Under the conditions in the transfer cell used the interfacial resistance was between 40 and 60 per cent of the total resistance to mass transfer.

Interfacial turbulence was observed during the transfer of all nitrates from *n*-butanol to water and, as a result the measured mass transfer rates are higher than those predicted from the water and solvent individual phase resistances. The interfacial resistances found for the extraction of cobalt and nickel nitrates by *n*-butanol from a mixture of these two nitrates in water are of the same order as the values found for the extraction of each individual nitrate.

Résumé—L'étude de l'extraction par le *n*-butanol à 25 °C des nitrates divalents du cuivre, Cobalt et Nickel en solution aqueuse, dans une cellule de transfert de masse maintenue en agitation montre l'influence de la résistance interfaciale due à la réaction dans la courbe limite solvant eau, qui s'ajoute aux résistances de chacune des phases. Cette résistance interfaciale ne varie pas avec le temps de contact des phases. Les relations entre les constantes de vitesse et les concentrations de nitrate à l'interface sont de la forme prévue par la cinétique de la réaction. Avec la cellule de transfert utilisée la résistance interfaciale varie entre 40 et 60% de la résistance totale de transfert de masse.

La turbulence à l'interface a été observée pendant le transfert des différénts nitrates du *n* butanol dans l'eau, et les vitesses de transfert de masse mesurées sont plus élevées que celles prévues à partir des résistances individuelles des phases eau et solvant. Les résistances interfaciales trouvées pour l'extraction des nitrates de Cobalt et de Nickel par le *n* butanol à partir d'un mélange de ces deux nitrates dans l'eau sont du même ordre que celles obtenues pour l'extraction de chaque nitrate pris séparément.

Zusammenfassung—Untersuchungen an Extraktionen von Zweiwertigen Kupfer-, Kobalt- und Nickelnitraten aus Wasser mit *n*-Butanol bei 25 °C in einer Rührmassen-Transferzelle haben gezeigt, dass der Massentransfer-Prozess durch den Grenzflächenwiderstand beeinflusst ist. Dieser Widerstand ist durch die Reaktion an der Wasser/Lösungs-mittel Phasengrenze verursacht, zusammen mit dem individuellen Wasser-Lösungsmittel Phasenwiderstande.

Der Grenzflächenwiderstand ändert sich nicht mit der Phasenkontaktzeit und die Zussammenhänge zwischen den Geschwindigkeitskonstanten des Grenzflächenwiderstandes und der Nitratenkonzentrationen zeigen dieselbe Form, die von der Kinetik der chemischen Reaktion von Nitratenextraktion erwartet wurden. Bei der Benützten Transferzelle der Grenzflächenwiderstand war zwischen 40 und 60% des totalen Massentransferwiderstandes.

Turbulenzen an der Grenzfläche wurden beobachtet während des Transfers von allen Nitraten zwischen *n*-butanol und Wasser, uns als ein Ergebnis die gemessenen Massentransfer-Geschwindigkeiten sind grösser, als voraussagt von den individuellen Wasser und Lösungsmittel Phasenwiderständen. Die gefundene Grenzflächenwiderstände für die Extraktion von Kobalt-und Nickelnitraten mit *n*-Butanol aus einem Gemisch von diesen Nitraten in Wasserlösung sind von derselben Wertordnung als die Werte, die bei der Extraktion von jeden einzelnen Nitraten gefunden wurden.

THE presence of an interfacial resistance to the transfer of uranyl nitrate between water and the solvents dibutyl carbitol and methyl *iso*butyl ketone was first observed by MURDOCH and PRATT [1] in a wetted-wall column. They showed that such a resistance was consistent with the reaction known to occur at the water–solvent interface between the uranyl nitrate, water and solvent molecules to form a nonionic complex, soluble in the solvent. Later SMITH *et al.* [2] found that satisfactory agreement between the experimental and predicted over-all mass transfer coefficients for the transfer of uranyl nitrate between water and methyl *iso*butyl ketones in a packed column could only be obtained by taking this interfacial resistance into account.

An extensive study of uranyl nitrate transfer between water and a number of solvents was made by LEWIS [3], using a stirred transfer cell. The experimental over-all mass transfer coefficients were compared with values predicted from individual transfer coefficients calculated by a correlation obtained previously [4]. In some cases interfacial turbulence caused the experimental mass transfer coefficients to exceed those calculated, while for other systems the observed and calculated coefficients agreed closely for a short period of time after extraction commenced, but then the observed rate of transfer diminished, apparently because of an increase in interfacial resistance with the age of the interface. This increase in interfacial resistance was independent of the uranyl nitrate concentration and all experimental variables other than the duration of the experiment.

Because liquid extraction is increasing in importance as a method of separating metals the transfer of divalent copper, cobalt and nickel nitrates between water and *n*-butanol at 25°C was studied to investigate further the mechanism of the extraction of electrolytes by organic solvents. The metals were chosen as being typical of those for which solvent extraction methods may be applicable, and *n*-butanol belongs to the class of oxygenated solvents which dissolve appreciable quantities of the nitrates. The extraction of mixtures of cobalt and nickel nitrates from water by *n*-butanol at 25 °C was also studied.

The wetted-wall column was found to be unsuitable for studying mass transfer with these systems, because the low interfacial tension and large density difference between the phases resulted in instability in the water phase film on the wall. A stirred transfer cell was, therefore, used to obtain the rates of mass transfer for the systems studied here. The results were consistent with the mechanism of mass transfer which takes into account a reaction at the water–solvent interface. The theory of this type of extraction has been presented by PRATT [1, 5] and the main points are summarized in the next section.

LIQUID EXTRACTION WITH A REACTION AT THE INTERFACE BETWEEN PHASES

The mechanism of electrolyte transfer to and from the interface is unaffected by the reaction at the interface, which is of the type

$$M^{2+} + 2NO_3^- + h\,H_2O + sS \rightarrow [M(NO_3)_2 \,.\, h\,H_2O \,.\, sS] \quad (1)$$

The electrolyte passes into the solvent phase as the solvated complex and the rate of extraction is equal to the net rate of formation of the complex.

The rate of production of the complex =

$$= k_{III}\,(C_{Wi})\,(C_{NO_3\,Wi})^2 = 4\,k_{III}\,(C_{Wi})^3 \quad (2)$$

(The concentrations of water and solvent at the interface are so much greater than the concentration of electrolyte that they can be regarded as constant).

The rate of decomposition of the complex =

$$= k_1\,C_{Si} \quad (3)$$

$$\text{Hence } j = 4\,k_{III}\,C_{Wi}^3 - k_1\,C_{Si} \quad (4)$$

$$= k_W\,(C_W - C_{Wi}) = k_S\,(C_{Si} - C_S)$$

$$= K_W\,(C_W - C_W^\bullet) = K_S\,(C_S^\bullet - C_S)$$

$$\text{Let } j = k_{RW}\,(C_{Wi} - C_{Wi}^\bullet) \quad (5)$$

$$\text{and } H_W = \frac{C_{Si} - C_S}{C_{Wi}^\bullet - C_W^\bullet} \quad (6)$$

$$\text{Then } \frac{1}{K_W} = \frac{1}{k_W} + \frac{1}{H_W\,k_S} + \frac{1}{k_{RW}} \quad (7)$$

Similarly, letting $j = k_{RS}(C^*_{Si} - C_{Si})$ (8)

$$\text{and } H_S = \frac{C^*_S - C^*_{Si}}{C_W - C_{Wi}} \quad (9)$$

$$\frac{1}{K_S} = \frac{1}{k_S} + \frac{H_S}{k_W} + \frac{1}{k_{RS}} \quad (10)$$

The last terms in equations (7) and (10) represent the resistance due to the reaction at the interface.

At equilibrium, $j = 0$. Since C^*_{Wi} is the water phase concentration in equilibrium with C_{Si} from equation (4)

$$\frac{k_I}{4k_{III}} = \frac{C^{*3}_{Wi}}{C_{Si}}$$

Combining equations (4) and (5) and substituting

$$k_{RW} = 4k_{III}(C^2_{Wi} + C^{*2}_{Wi} + C_{Wi}C^*_{Wi}) \quad (11)$$

Similarly it can be shown that $k_{RS} = k_I$ (12)

EXPERIMENTAL

(*a*) *Materials, apparatus and procedure*

The copper, cobalt and nickel nitrates were Analytical Reagent quality. Laboratory distilled water was used, and commercial pure *n*-butanol was further purified by fractional distillation. The analytical methods used and the liquid–liquid equilibrium data for the systems studied will be published elsewhere.

The stirred transfer cell and procedure used are described elsewhere [6]. Some determinations were made with a brass stirrer unit for the systems with copper and cobalt nitrates as solutes but after a few determinations with cobalt nitrate it was found that those surfaces of the unit which came into contact with the liquids had become darker in colour suggesting that some corrosion had occurred. As this might have led to contamination of the liquid–liquid interface a glass stirrer unit was then constructed, and for cobalt and nickel nitrate only the results obtained with this unit were considered in the calculation of the interfacial resistances. In all cases the stirrers were contra-rotating.

The variation in interfacial resistance with time can be investigated either by sampling each phase at several different times during each experiment, as LEWIS did [3, 4], or by making a series of determinations each with the same initial compositions of both phases and same stirrer speeds but with different durations. The latter procedure was adopted because samples of at least 5 ml were required for analysis and the removal of such volumes might possibly have disturbed the interfacial conditions. To reduce the alteration in the phase volumes during extraction both phases were partially saturated, the water phase with butanol and the butanol phase with water. The initial phase volumes were 0·4 l ; both phase volumes were measured at the end of each experiment (by calibration marks on the side of the glass transfer cell) and the densities and viscosities of all phases were also determined before and after each experiment.

In one experiment when cobalt nitrate was extracted from water by *n*-butanol both stirrers were operated at low speeds so that the Reynolds numbers in both phases were less than 500. A stagnant layer of the coloured solute formed at the interface in the butanol phase and increased in depth with time. At higher Reynolds numbers no layer formation was observed, the liquid flow during extraction being from the cell wall along the interface and up the stirrer unit, after which the liquid was mixed by the stirrer into the main body of the phase. During each extraction run the interface was carefully examined to ensure that no stagnant layers were formed.

(*b*) *Calculation of over-all mass transfer coefficients*

(i) *Single solute.* If all the resistance is assumed to be in the solvent phase, for solute transfer from water to *n*-butanol,

$$K_S = \frac{V}{A\theta}\int_{C_{S0}}^{C_S} \frac{dC_S}{C_S^* - C_S} \quad (13)$$

The equilibrium relationship between the nitrate concentrations in the water and butanol phases was found to be that the ratio C_S/C_W^n was constant for each nitrate, except at low concentrations (less than 150 g/l. in the water phase). The values of n were 1·94 for copper nitrate, 1·95 for cobalt nitrate and 1·97 for nickel nitrate, and so the relationship could be approximated by

$$C_S/C_W^2 = G \quad (14)$$

Since the phase volumes remain almost constant during extraction

$$C_{W0} + C_{S0} = C_0 = C_W + C_S$$

Hence $C_S^* = G(C_0 - C_S)^2$

$$\text{and so } K_S = \frac{V}{A\theta}\int_{C_{S0}}^{C_S} \frac{dC_S}{[G(C_0 - C_S)^2 - C_S]}$$

$$= \frac{V}{A\theta\, G(U + W)}\left[\ln\left[1 - \frac{C_S}{C_0 + U}\right] + \ln\left[1 + \frac{C_S}{C_0 - C_S - W}\right]\right] \quad (15)$$

$$\text{where } W = \frac{1}{2}\left(\frac{1}{G^2} + \frac{4C_0}{G}\right)^{0.5}$$

$$U = \frac{1}{2}\left(\frac{1}{G} + W\right)$$

VOL. 15 1961

To reduce the error caused by the use of the approximate equilibrium relationship plots were made of G against concentration from the experimental equilibrium results and the value of G corresponding to the mean concentration was used. If $C_{W0} + C_{S0}$ did not equal $C_W + C_S$ the mean of these two sums was taken as C_0 and the mean phase volume was used for V when the volume changed during extraction.

Expressions similar to equation (15) can be obtained for K_S for solute transfer from butanol to water and for K_W but, at the low concentrations either in the water or butanol phases used in these experiments, the relationship (14) did not hold and these over-all mass transfer coefficients were obtained from the expressions

$$K_S = \frac{V}{A\theta}\int_{C_S}^{C_{S0}} \frac{d\,C_S}{C_S - C^*_S} \quad \text{(transfer from butanol)} \qquad (16)$$

$$K_W = \frac{V}{A\theta}\int_{C_W}^{C_{W0}} \frac{d\,C_W}{C_W - C_W^*} \quad \text{(transfer from water)} \qquad (17)$$

$$K_W = \frac{V}{A\theta}\int_{C_{W0}}^{C_W} \frac{d\,C_W}{C_W^* - C_W} \quad \text{(transfer from butanol)} \qquad (18)$$

The integrals were determined graphically, using the experimental equilibrium values of C_S and C_W.

(ii) *Two solutes.* For the transfer of both cobalt and nickel nitrates between water and butanol it was assumed that an expression similar to equation (13) could be applied to each nitrate. Thus, for the transfer of nitrate M,

$$K_{MS} = \frac{V}{A\theta}\int_{C_{MS0}}^{C_{MS}} \frac{d\,C_{MS}}{C_{MS}^* - C_{MS}} \qquad (19)$$

In mixtures of cobalt and nickel nitrates C_{MS}^* depends not only on the concentration of the nitrate M in the water but also on the concentration of the other nitrate, the distribution relationship being

$$H_C = \frac{C_{CS}}{C_{CW}} = \alpha_C\,(C_{CW} + C_{NW})^{0\cdot95}$$

$$H_N = \frac{C_{NS}}{C_{NW}} = \alpha_N\,(C_{CW} + C_{NW})^{0\cdot97}$$

If $C_{CW} + C_{NW} = C_{TW}$, then, approximately,

$$H_C = \alpha_C\,C_{TW}$$

$$H_N = \alpha_N\,C_{TW}$$

As C_{TW} did not change greatly during extraction H_C and H_N could be taken as constant for any experiment. If the phase volumes remain constant during extraction

$$C_{MS} - C_{MS0} = C_{MW0} - C_{MW}$$

To allow for any changes in phase volumes, let

$$F\,(C_{MS} - C_{MS0}) = C_{MW0} - C_{MW}$$

Then $C_{MS}^* = \alpha_M\,(C_{MW0} + F\,C_{MS0} - F\,C_{MS}) =$

$$= \alpha_M\,(C_0 - F\,C_{MS})$$

Substituting in equation (18) and integrating

$$K_{MS} = \left(\frac{V}{A\theta}\right)\left(\frac{1}{\alpha_M\,F + 1}\right) \ln\left[\frac{\alpha_M\,C_0 - (\alpha_M\,F + 1)\,C_{MS0}}{\alpha_M\,C_0 - (\alpha_M\,F + 1)\,C_{MS}}\right] \qquad (20)$$

To reduce the errors introduced by the assumptions made in these derivations α_M was taken as the mean of the values corresponding to the initial and final C_{TW} values and V was taken as the mean phase volume. The error introduced by the assumption of constant α_M will be greatest for large changes in C_{TW}, and K_{CS} for the experiment in which the change in C_{TW} was greatest was calculated both from equation (20) and by graphical integration using the experimental equilibrium concentrations. The values found were $1{\cdot}00 \times 10^{-3}$ cm/sec and $0{\cdot}99 \times 10^{-3}$ cm/sec. No values of K_{MW} were determined as analysis of the results for the transfer of the individual nitrates had shown that the coefficient based on the solvent phase provided more information about the mechanism of mass transfer.

In all the extraction experiments with two solutes the transfer was from water to butanol as the interpretation of the results for single solute transfer in the reverse direction was unsatisfactory due to interfacial turbulence.

Results

The results obtained with copper nitrate as solute in the transfer cell with the glass stirrer unit are given in Table 1, as an example of the concentration range investigated and the Reynolds numbers used. Similar concentrations and Reynolds numbers were employed for copper nitrate in the transfer cell with the brass stirrer unit and for the other systems studied. The complete experimental results can be obtained from the author.

The error in the solute mass balance was taken as the difference between the weight of solute in initial solutions and the weight found in the final solutions and was calculated for each experiment. The maximum error did not exceed 2 g and the average error for all runs is 0·3 g which, in the phase volume of 0·4 *l*, would represent an error in solute concentration of 0·8 g/l., if all the error were in one phase composition.

Table 1. *Transfer of copper nitrate between water and* n-*butanol at* 25 °C

Expt.	*Duration* (min.)	*Phase*	*Re*	*Concentration* (g/l)			*K* (cm/sec × 10^3)		$1/k_R$ (sec/cm)
				C_0	C	C_i	Obsd.	Calc.	
Transfer from water to *n*-butanol									
G15	10	*W*	1330	698·5	682·0	610	0·53	0·80	650
		B	1230	28·5	44·1	106	1·09	1·79	360
G16	20	*W*	1320	698·5	678·5	615	0·34	0·84	1740
		B	1220	28·5	57·6	108	1·07	1·76	370
G17	45	*W*	1300	698·5	650·6	610	0·43	0·83	1120
		B	1150	28·5	83·7	117	1·04	1·76	380
G18	10	*W*	1570	503·0	496·6	467	0·35	0·61	1250
		B	1270	28·5	36·5	71	1·21	1·74	250
G19	30	*W*	1600	503·0	484·8	460	0·38	0·64	1100
		B	1240	28·5	48·6	76	1·14	1·75	310
G20	20	*W*	1490	408·7	401·3	381	0·28	0·48	1440
		B	1220	22·5	30·7	57	1·04	1·59	330
G21	45	*W*	1500	408·7	393·0	386	0·30	0·52	1340
		B	1190	22·5	39·4	57	1·06	1·54	310
G22	10	*W*	1510	310·1	308·9	303	0·17	0·38	3380
		B	1200	22·5	24·1	32	0·855	1·54	520
G23	20	*W*	1510	310·1	306·3	299	0·19	0·40	2760
		B	1200	22·5	25·9	37	0·945	1·54	410
G24	45	*W*	1490	310·1	303·1	299	0·23	0·41	1840
		B	1190	22·5	29·4	36	0·94	1·54	420
Transfer from *n*-butanol to water (interfacial turbulence observed)									
G25	10	*W*	1550	103·6	125·2		0·83		
		B	830	116·9	97·4		2·64		
G26	25	*W*	1510	103·6	143·8		0·68		
		B	870	116·9	78·2		2·59		

W = water phase, *B* = butanol phase.

The values of K_S obtained in experiments with the same Reynolds numbers and initial concentrations but different durations agree closely, but the corresponding K_W values scatter more (because any errors in measuring the concentrations have more effect on K_W), although there is no systematic variation with duration.

DETERMINATION OF THE INTERFACIAL RESISTANCE

The relationships between the interfacial resistances and the over-all mass transfer coefficients, individual mass transfer coefficients, H_W and H_S are defined by equations (7) and (10). A graphical representation of the concentrations in the bulk of the phases and at the interface for extraction

VOL. 15 1961

with an interfacial resistance was given by LEWIS [3], who also described a method of determining $1/k_{RS}$ and $1/k_{RW}$ by successive approximations. The interfacial resistances for the systems studied here were determined by a more direct procedure, which is as follows, for the transfer of a single solute from water to butanol:

$$\text{Since } j = k_W(C_W - C_{Wi}^2) = k_{RS}(C_{Si}^* - C_{Si}) = k_S(C_{Si} - C_S) = K_S(C_S^* - C_S)$$

then, as $C_S^* = G\,C_W^2$ and $C_{Si}^* = G\,C_W^2$,

$$\frac{1}{k_{RS}} = \frac{1}{K_S} - \left[\frac{G(C_W + C_{Wi})}{k_W} + \frac{1}{k_S}\right] = \frac{1}{K_S(\text{obsd.})} - \frac{1}{K_S(\text{calc.})} \qquad (21)$$

To determine k_{RS} the value of C_{Wi} is required. This is calculated from the relationship

$$C_{Wi} = C_W - j\left(\frac{1}{k_W}\right)$$

The value of C_W was the mean of the initial and final concentrations and j was the average rate during the experiment. As in the calculation of K_S the mean value of G was used.

In a similar way the following relationship for k_{RW} is obtained

$$\frac{1}{k_{RW}} = \frac{1}{K_W} - \left[\frac{1}{k_W} + \frac{1}{G(C_W^* + C_{Wi}^*)k_S}\right] = \frac{1}{K_W(\text{obsd.})} - \frac{1}{K_W(\text{calc.})} \qquad (22)$$

The k_{RW} values are less precise than those for k_{RS}, because the values of C_S and C_{Si}, from which C_W^* and C_{Wi}^* were obtained, were generally too low for the equilibrium relationship (14) to apply.

The individual mass transfer coefficients were calculated from the correlation obtained for this transfer cell (Ref. [6], equation 3). The diffusion coefficients of the nitrates in water and *n*-butanol, which were required for the calculation of the Schmidt numbers, were determined as part of this work. For diffusion in water at 25 °C the diffusion coefficients were: copper nitrate $1{\cdot}17 \times 10^{-5}$ cm²/sec; cobalt nitrate, $1{\cdot}16 \times 10^{-5}$ cm²/sec; nickel nitrate, $1{\cdot}18 \times 10^{-5}$ cm²/sec; for diffusion in *n*-butanol at 25 °C: copper nitrate, $0{\cdot}38 \times 10^{-5}$ cm²/sec; cobalt nitrate, $0{\cdot}40 \times 10^{-5}$ cm²/sec; nickel nitrate, $0{\cdot}38 \times 10^{-5}$ cm²/sec; all varying very little with concentration in the concentration range of the extraction experiments.

As a partial check on the values of $1/k_{RS}$, $1/k_{RW}$, C_{Si} and C_{Wi} the rate of mass transfer was calculated from them,

$$j = k_{RS}(C_{Si}^* - C_{Si}) = k_{RW}(C_{Wi} - C_{Wi}^*)$$

(This expression could, of course, be used to determine k_{RS} and k_{RW} but no check on the results would then be possible). Generally the rates calculated in this way did not differ by more than 15 per cent from the experimental rates. When a larger difference existed new values of C_{Wi} and C_{Si} were chose on the operating line for the experiment (this is the line *Ot* in Fig. 1 of Ref. [3]) until the agreement between the values of

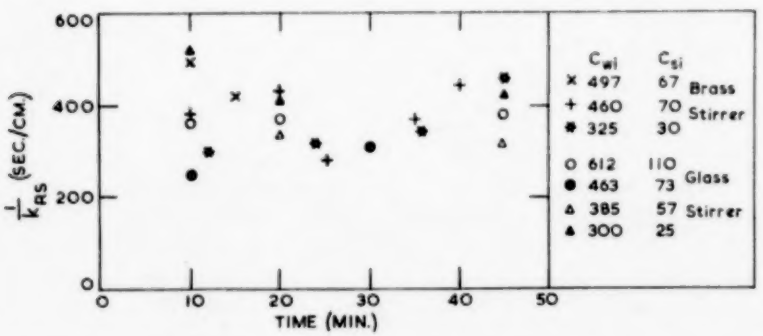

FIG. 1. $1/k_{RS}$ as a function of time and interfacial concentration for copper nitrate.

$k_W (C_W - C_{Wi})$ and $k_S (C_{Si} - C_S)$ was satisfactory; $1/k_{RS}$ and $1/k_{RW}$ were then calculated from these concentrations. It was only necessary to use this procedure in ten experiments and the changes in $1/k_{RS}$ and $1/k_{RW}$ as a result of the adjustment was never more than 10 per cent. In several cases $1/k_{RS}$ and $1/k_{RW}$ were also determined by LEWIS' procedure and the results of both methods were almost identical. The magnitude of these interfacial resistances is between 40 and 60 per cent of the total resistance ($1/K$). Values of $1/k_{RS}$ are plotted as a function of time in Figs. 1–3.

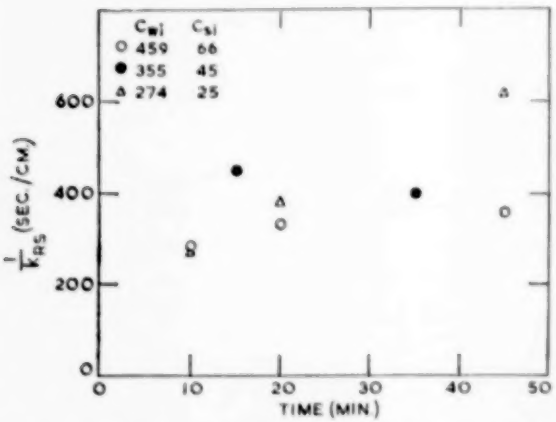

FIG. 2. $1/k_{RS}$ as a function of time and interfacial concentration for cobalt nitrate.

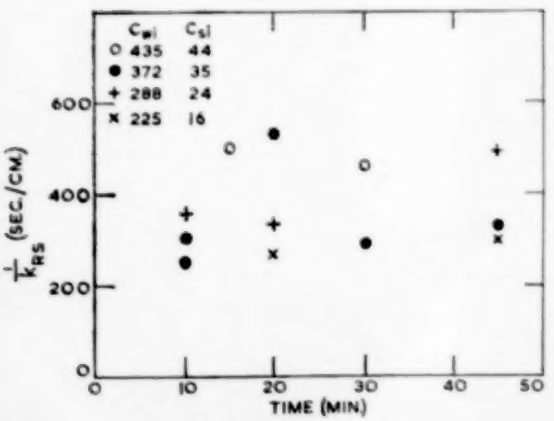

FIG. 3. $1/k_{RS}$ as a function of time and interfacial concentration for nickel nitrate.

The condition of the interface during extraction was investigated by suspending a drop of one phase containing the nitrate being extracted in the other phase and projecting the drop's image on a screen. No surface disturbance was noticed for transfer from water, but, for transfer in the reverse direction, the surface of the drop was violently agitated, due both to ripple formation and to "eruptions" of the liquid from the surface. This phenomenon of interfacial turbulence was reported by LEWIS and PRATT [7] when determining by the pendant-drop method the interfacial tension between a solvent phase containing a solute and a water phase with no solute, and LEWIS [3, 8] found that the effect of interfacial turbulence was to increase the rate of mass transfer above the values calculated from the individual mass transfer coefficients obtained from the transfer cell correlation. From consideration of a simplified mathematical model of the hydrodynamic instability at interfaces due to longitudinal variations of interfacial tension STERNLING and SCRIVEN [9] suggested that some of the factors promoting interfacial turbulence are (1) solute transfer out of the phase of higher viscosity, (2) solute transfer out of the phase in which its diffusivity is lower, (3) large differences in viscosity and solute diffusivity between the two phases and (4) steep concentration gradients near the interface. All of these factors apply for the transfer of the nitrates from *n*-butanol and the presence of interfacial turbulence lends support to their theoretical analysis.

The effect of the enhanced transfer rates caused by interfacial turbulence became apparent in the calculation of the interfacial resistances for transfer from butanol. Thus, for experiment G26 with copper nitrate as solute, $j = 20{\cdot}6 \times 10^{-3}$ g/cm² sec and $k_S = 0{\cdot}143 \times 10^{-2}$ cm/sec (calculated from Ref. [6], equation 3). Hence, $C_{Si} = C_S - j(1/k_S) = 92{\cdot}5 - 144{\cdot}1 = -51{\cdot}6$ g/l! This absurdity would not occur if k_S were higher. As the expression from which k_S was calculated was obtained from measurements on systems with negligible interfacial turbulence it is only to be expected that k_S would be larger when this turbulence occurs.

When both cobalt and nickel nitrates were

transferred from water to butanol values of $1/k_{BS}$ were obtained for each nitrate by assuming that the individual mass transfer coefficients for each nitrate were unaffected by the presence of the other nitrate and that the rate of transfer of each nitrate is given by

$$j_M = k_{MW}(C_{MW} - C_{MWi}) = k_{MRS})C_{MSi}{}^* - C_{MSi}) = k_{MS}(C_{MSi} - C_{MS})$$

In the calculation of K_{MS} it was pointed out that H_C and H_N were approximately constant and, if H_{MW} is the value of H_M corresponding to the mean total nitrate concentration in the water phase,

$$j_M\left(\frac{H_{MW}}{k_{MW}}\right) = C_{MS}{}^* - H_{MW}C_{MWi}$$

$$j_M\left(\frac{1}{k_{MRS}}\right) = C_{MSi}{}^* - C_{MSi} = H_{MWi}C_{MWi} - C_{MSi}$$

$$j_M\left(\frac{1}{k_{MS}}\right) = C_{MSi} - C_{MS}$$

Therefore $$j_M\left(\frac{H_{MW}}{k_{MW}} + \frac{1}{k_{MRS}} + \frac{1}{k_{MS}}\right) = C_{MS}{}^* - C_{MS} - (H_{MW} - H_{MWi})C_{MWi} = j_M\left(\frac{1}{K_{MS}}\right) - (H_{MW} - H_{MWi})C_{MWi}$$

and $$\frac{1}{k_{MRS}} = \frac{1}{K_{MS}} - \frac{(H_{MW} - H_{MWi})C_{MWi}}{j_M} - \frac{1}{k_{MS}} - \frac{H_{MW}}{k_{MW}} \qquad (23)$$

The Schmidt numbers for the calculation of k_{MW} and k_{MS} were obtained by dividing the kinematic viscosity of the phase by the diffusion coefficients of the nitrate in water and in butanol, as diffusion coefficient measurements showed that the value for each nitrate in the mixture was the same as in its own solution. Fig. 4 shows $1/k_{MSR}$ as a function of time.

It is unlikely that these interfacial resistances are due to surface contamination as the nitrate solutions were made from pure salts and filtered before use, and both the water and *n*-butanol were freshly distilled. Also, nitrate solutions made from at least two different batches of the nitrate were used in each set of experiments and close agreement was obtained between them.

The kinetics of the Interfacial Reaction

There is no definite trend in $1/k_{BS}$ either with time or with the interface concentrations, and this is in accord with the kinetics of the reaction assumed to occur at the interface (equation 12). The mean values for cobalt and nickel nitrates when extracted alone were 380 sec/cm and 370 sec/cm, respectively, while the corresponding values for the extraction of both together were 460 sec/cm and 310 sec/cm. Taking into account the many approximations made in obtaining both K_{MS} and $1/k_{MRS}$ for the mixture the agreement is as good as can be expected.

The values of $1/k_{BW}$ scatter considerably, but

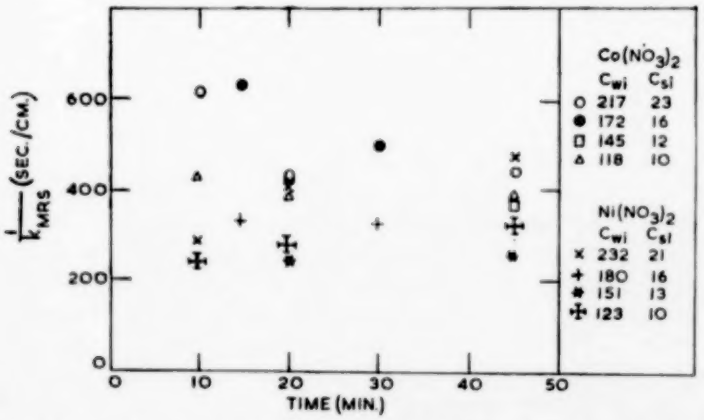

Fig. 4. $1/k_{MRS}$ as a function of time and interfacial concentration for cobalt nitrate and nickel nitrate.

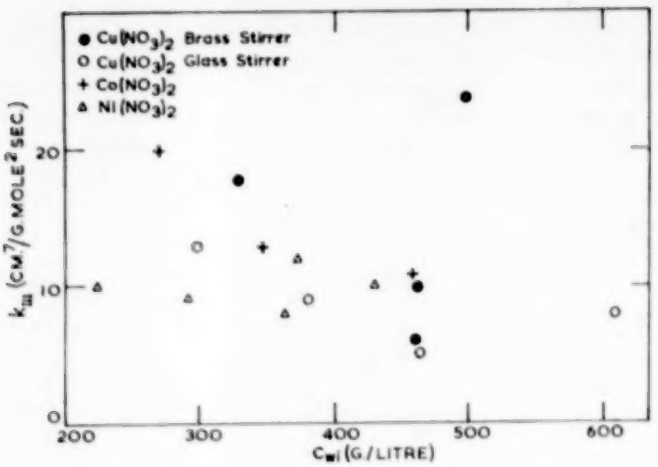

FIG. 5. k_{III} as a function of C_{WI}.

generally increase as the interface concentration decreases. Values of k_{III} were calculated by equation (11) from the mean of the values of $1/k_{RW}$ obtained at each concentration level and the plot of these against C_{WI} in Fig. 5 shows that most of the variation with concentration has been removed. The mean values of k_I and k_{III} for copper, cobalt and nickel nitrates are given in Table 2.

Table 2. Interfacial reaction rate constants for the extraction of copper, cobalt and nickel nitrates by n-butanol at 25 °C

	k_I (cm/sec × 10^3)	k_{III} (cm^7/g mole^{2}sec)
Copper nitrate	2·67	12
Cobalt nitrate	2·63	13
Nickel nitrate	2·70	10

The similarity between the rate constants for these nitrates is not unexpected, as the accompanying liquid–liquid equilibrium studies showed that the free energies of transfer of the nitrates were also similar. The only rate constants with which these can be compared are those found by MURDOCH and PRATT [1] for the extraction of uranyl nitrate by dibutyl carbitol and methyl *iso*butyl ketone. Their values of k_I lay in the range 7–47 cm/sec × 10^3 and of k_{III} in the range 370–1900 cm^7/g mole^2 sec for both solvents (their published results were $4k_{III}$, as k_{III} is defined here). The higher values of the rate constants for copper, cobalt and nickel nitrates mean that the interfacial resistances are higher for these nitrates than for uranyl nitrate.

In his studies of uranyl nitrate extraction in a stirred transfer cell LEWIS [3] found that K_S decreased with time. This decrease (which corresponds to an increase in $1/k_{RS}$) was attributed to a time lag in the build-up or breakdown of the uranyl nitrate–solvent complex. Presumably this effect does not occur in the systems studied in this work. A possible explanation is that uranyl nitrate is almost completely un-ionized in the solvents used by LEWIS – dibutyl carbitol, methyl *iso*butyl ketone and tri *n*-butyl phosphate [10, 11], while a thermodynamic study of the partition data between water and *n*-butanol for the nitrates studied here suggested that these nitrates were ionized to a significant degree in *n*-butanol [12]. The formation of an un-ionized complex from an ionized electrolyte presumably is a less simple reaction than the formation of an ionizable complex and may involve several successive reactions, all of which could affect the interfacial resistance.

Conclusions

1. The mass transfer process for the extraction of copper, cobalt and nickel nitrates from water by *n*-butanol in a stirred transfer cell is influenced by an interfacial resistance due to the reaction

$$M^{2+} + 2NO_3^- + h\,H_2O + s\,S \rightarrow [M(NO_3)_2 \,.\, h\,H_2O \,.\, s\,S] \qquad (1)$$

in addition to the water and solvent phase resistances. The interfacial resistances $1/k_{RS}$ and $1/k_{RW}$ were between 40 and 60 per cent of the total resistance. It is preferable to use K_S as the over-all mass transfer coefficient because $1/k_{RS}$ is independent of concentration.

2. The lack of variation in $1/k_{RS}$ and the variation in $1/k_{RW}$ with the nitrate concentration at the interface agree with the theoretical predictions based on the kinetics of equation (1).

3. Interfacial turbulence was observed during the transfer of all nitrates from *n*-butanol to water, and as a result, the observed mass transfer rates were higher than those predicted from the water and solvent phase resistances.

4. The values of $1/k_{RS}$ found for the extraction of cobalt and nickel nitrates from a mixture of these two nitrates in water by *n*-butanol are of the same order as the values found for the extraction of each individual nitrate.

Acknowledgements—My thanks are due to Professor T. G. Hunter for his interest in this work and to Dr. H. R. C. Pratt for his helpful comments on the Ph.D. thesis, of which this work was a part.

Notation

A = area of interfaces between phases, cm²
C = solute concentration, g/l.
C^* = solute concentration in equilibrium with the other phase, g/l.
G = constant in liquid–liquid equilibrium relationship, equation (14)
h = hydration number of nitrate in organic phase
H = distribution coefficient, defined by equations (6) and (9)
j = rate of solute transfer across unit area of the interface between phases, g moles/cm² sec
k = individual phase mass transfer coefficient, cm/sec
k_1 = first-order reaction rate constant, cm/sec
k_{III} = third-order reaction rate constant, cm⁷/g mole² sec
k_{RS} = interfacial resistance transfer coefficient based on the solvent phase, cm/sec
k_{RW} = interfacial resistance transfer coefficient based on the water phase, cm/sec
K = over-all mass transfer coefficient, cm/sec
L = length of stirrer in transfer cell, cm
M^{2+} = metal ion
N = stirrer speed, rev/sec
Re = Reynolds number = L^2N/ν
s = solvation number of nitrate in organic phase
S = solvent molecule
V = volume of phase, cm³
α = constant in liquid–liquid equilibrium relationships for cobalt and nickel nitrate mixtures
θ = duration of experiment, sec
ν = kinematic viscosity, cm²/sec

Subscripts

C = cobalt nitrate
i = condition at the interface between phases
M = metal nitrate
N = nickel nitrate
0 = initial conditions
S = solvent phase
W = water phase

References

[1] Murdoch R. and Pratt H. R. C. *Trans. Instn. Chem. Engrs.* 1953 **31** 307.
[2] Smith L. E., Thornton J. D. and Pratt H. R. C. *Trans. Instn. Chem. Engrs.* 1957 **35** 292.
[3] Lewis J. B. *Chem. Engng. Sci.* 1958 **8** 295.
[4] Lewis J. B. *Chem. Engng. Sci.* 1954 **3** 248.
[5] Pratt H. R. C. *Industr. Chem.* 1955 **31** 63.
[6] McManamey W. J. *Chem. Engng. Sci.* 1961 **15** 251.
[7] Lewis J. B. and Pratt H. R. C. *Nature, (Lond.)* 1953 **171** 1155.
[8] Lewis J. B. *Chem. Engng. Sci.* 1954 **3** 260.
[9] Sternling C. V. and Scriven L. E. *Amer. Inst. Chem. Engrs. J.* 1959 **5** 514.
[10] McKay H. A. C. and Mathieson A. R. *Trans. Faraday Soc.* 1951 **47** 428.
[11] Healy T. V. and McKay H. A. C. *Trans. Faraday Soc.* 1956 **52** 633.
[12] McManamey W. J. Ph.D. Thesis, University of Sydney 1959.

Chemical Engineering Science, 1961, Vol. 15, pp. 220 to 229. Pergamon Press Ltd., London. Printed in Great Britain.

A test of randomness for solid-solid mixtures

REUEL SHINNAR and PINHAS NAOR
Technion, Israel Institute of Technology, Haifa, Israel

(*Received* 30 *August* 1960)

Abstract—The present paper describes a new statistical criterion for testing randomness of solid–solid mixtures. The test here proposed is based on the shortest distance between particles of the component present in lower concentration.

The properties of the distribution of this characteristic are derived from the Poisson distribution. A pertinent feature of this study is that clustering is defined by a single parameter, which permits the calculation of a power function defining the sensitivity of the test.

The new test is compared with the classical x^2 test for solid–solid mixtures. The properties and shortcomings of this latter procedure for testing randomness of solid–solid mixtures are discussed.

The proposed test is especially sensitive in detecting clusters of particles. It should be important in the study of solid–solid mixing, whenever it is desirable that the mixture of the different ingredients be as intimate as physically possible.

Résumé—Cet article décrit un nouveau critère statistique pour étudier la répartition désordonnée des mélanges solide–solide, en se basant sur la plus petite distance entre deux particules adjacentes du composant présent en plus faible concentration.

Les propriétés de distribution du paramètre caractéristique sont dérivées de la distribution de Poisson. La formation d'amas est définie par un seul paramètre qui permet le calcul d'une fonction de potentiel définissant la sensibilité de l'expérience.

Ce nouvel essai est comparé à l'essai classique x^2 pour les mélanges solide–solide ; suit une dimension des propriétés et imperfections de ce dernier procédé pour l'étude de la répartition désordonnée des mêmes mélanges.

L'expérimentation proposée est spécialement sensible pour déceler les groupes de particules. Elle doit être importante dans l'étude des mélanges solide–solide toutes les fois qu'il est préférable que le mélange des différents produits soit physiquement aussi intime que possible.

Zusammenfassung—Diese Abhandlung beschreibt ein neues statistisches Kriterium für die Untersuchung der Zufälligkeitswerte von solid/soliden Gemischen. Die kürzeste Entfernung zwischen Partikeln der vorhandenen Komponenten von niedriger Konzentration bildet die Grundlage der vorgeschlagenen Untersuchungsmethode.

Die Verteilungseigenheiten dieser Charakteristik sind von der Poisson-Verteilung abgeleitet. Eine sachmässige Besonderheit dieser Ableitung ist die Einführung eines einzigen Parameters, der die Gruppenbildung definiert und dies erlaubt die Kalkulation von einer Potentialfunktion die die Empfindlichkeit der Untersuchung definiert.

Das neue Verfahren ist mit der klassischen x^2 Methode für solid-soliden Gemischen verglichen. Die Eigenkeit und Unzulänglichkeit der letzteren Methode ist besprochen.

Die vorgeschlagene Untersuchungsmethode ist besonders empfindlich für die Entdeckung von Partikelgruppen. Sie sollte eine wichtige Rolle spielen im Studium von solid/soliden Gemischen mit verschiedenen Bestandteilen, die physikalisch so intim wie nur möglich vermischt werden sollten.

1. INTRODUCTION

MIXTURES of solid materials are commonly used ; many products are sold in the form of solid–solid mixtures and often intimate blending of different materials is an essential step of a process. Extensive investigations of the solid–solid mixing process have been carried out and results have been summarized in a recent review by WEIDENBAUM [1]. It appears that one of the main difficulties in any study of the mixing process is the theoretical definition and the operational testing of randomness of particle distribution.

While in practice it is frequently necessary to

ensure that the individual particles in a mixture are distributed at random it should be emphasized that this requirement is not always essential. Thus, for instance, in powder metallurgy, pyrotechnics, solid propellants, etc. the mixture of the different ingredients should be as intimate as physically possible. On the other hand, in the mixing of pharmaceuticals for tabletting, the specifications require only that the deviations in composition of any tablet from that specified should not exceed a given value; it is hardly relevant for the intended use if the ingredients within the tablet are intimately mixed or appear in a clustered form.

Whereas in the second case it is not difficult to design statistical tests of almost any desired power to ensure compliance with specifications, criteria for complete randomness in the spatial distribution of the individual particles are much harder to define. It is the purpose of this paper to develop a procedure which in certain cases provides a sensitive criterion for testing randomness in such mixtures.

2. The Design and Interpretation of Statistical Tests Relating to Solid Mixtures

A mixture of solid particles is a very complicated system even if it consists of only two ingredients having the same particle size. Let us assume, for example, that a mixture consists of black and white spheres, and that the fraction of black spheres is p. Such a mixture may be described, for our purposes, as random, if the number of black particles in spatial samples of arbitrary form and size is binomially distributed.* If the system follows this definition, knowledge of p is sufficient to completely describe the mixture. However, if the mixture is non-random, its state is no longer described by a single parameter and a complete description may necessitate the enumeration of a very large number of parameters.

*An alternative and equivalent definition of randomness in such a case is the following: the probability of a site being occupied by a black particle is independent of the colour of its near and far neighbours; it depends only on (and is, indeed, identical with) the fraction of black particles in the total (infinite) population.

In practice, the deviations from randomness may take different forms. For example, within a solid–solid mixer there may exist large-scale concentration gradients caused by different specific gravities; in other cases, one ingredient appears in clusters which may themselves be randomly distributed in space. Furthermore, any combinations of local gradients and clustering are possible.

It is regrettable that most previous studies on statistical testing of mixtures have not pointed out that the design of a test for randomness depends on the specifications of an alternative hypothesis (or a series of alternative hypotheses) about the possible non-random character of the mixture. A short discussion of statistical testing theory seems therefore to be indicated.

The modern theory of statistical testing is based to a large extent on the work of Neyman and Pearson [2]. The interested reader may refer either to the original papers or to the excellent exposition presented in Cramer's text [3]. The underlying idea may be summarized as follows: On testing a proposed hypothesis—the so-called null hypothesis—*two kinds* of errors may be committed. The error of the first kind is the rejection of the null hypothesis when it is true; the error of the second kind is the acceptance of the null hypothesis when it is false, or in other words, the rejection of an alternative hypothesis when it is true. Specifications of the null hypothesis and the allowed magnitude of the error of the first kind—as is frequently done—is inadequate. Thus, for example, it is insufficient to classify a test of randomness as good or possibly excellent if the only information furnished in connexion with this test is that it operates on a 95 per cent or 99 per cent "certainty," the latter statement normally implying that the null hypothesis (complete randomness in our case) is accepted with a probability of 95 per cent or 99 per cent if it is true. For a test (of a null hypothesis) to be considered good, *two* things are required:

(a) that it possesses a small probability of rejecting the null hypothesis when it is true;

(b) that it possesses a large probability of rejecting the null hypothesis when it is false.

Of two tests associated with the same (small) probability of rejecting the null hypothesis when it is true we prefer the one which gives the larger probability of rejecting the null hypothesis when it is false.

In many cases it is possible to express these ideas in a more quantitative manner: As an example consider the case of tabletting mentioned before where intimate mixing is not necessarily required, but where rigorous compliance with specifications regarding the variability of the various ingredients is desired. Let us assume that we are interested in the percentage of one particular ingredient. In order to ensure the quality of the product we want to design a test which rejects batches of tablets with an excessive variability; while the possiblity of such a batch being accepted cannot be ruled out, the probability of such an event to occur should be kept very low. On the other hand, the probability of rejecting an acceptable batch has to be kept low too, otherwise the price of the product will become exorbitant. To proceed further, four numbers have to be specified. The value of the batch variance* σ_1^2 which is considered excessive and which should bring about the rejection of the batch of tablets with probability $(1 - \beta)$; the value of the batch variance σ_0^2 which is considered appropriate and which should bring about the acceptance of the batch of tablets with probability $(1 - \alpha)$. α and β can be chosen independently (except for the trivial inequality $\alpha + \beta < 1$) and they are usually of the order 1 per cent — 5 per cent; they represent the risks of arriving at incorrect conclusions. It must be pointed out that σ_1^2 must be larger than σ_0^2, since otherwise no meaningful solution may be obtained. Also clearly, σ_0^2 cannot be smaller than the "natural" variance originating from the finite number of solid particles in the tablet and the analytical errors.

A solution to the problem posed above is sought in the following terms:

(a) The number of tablets, n, to be selected from the batch and to be analysed.

(b) The computations to be performed with the n observations obtained.

(c) The numerical criterion with which the outcome of the computation is to be compared so as to arrive at a decision of acceptance or rejection of the batch.

A solution of this problem may be found in HALD's text [4]:

(a) The number of tablets to be tested equals (approximately)

$$n \simeq \tfrac{1}{2} + \tfrac{1}{2}\left(\frac{u_{1-\beta}\,\lambda + u_{1-\alpha}}{\lambda - 1}\right)^2$$

where $\lambda = \sigma_1/\sigma_0$ and $u_{1-\alpha}$, $u_{1-\beta}$ are fractiles of the unit normal distribution.*

(b) The computation required is the evaluation of the sum of squares of the n tablets tested:

$$\sum_{i=1}^{n} (x_i - \xi)^2.$$

*The batch variance, σ^2, is a measure of ingredient variability; it is defined by

$$\sigma^2 = \frac{1}{N}\sum_{i=1}^{N} (x_i - \xi)^2$$

where N is the total number of tablets in the batch, ξ is the average amount of the ingredient in a single tablet and x_i is the actual amount of this ingredient in the i-th tablet.

*The unit normal distribution is the particular Gaussian distribution which possesses zero average and unit variance. The expression describing this distribution is

$$\phi(u) = \frac{1}{\sqrt{(2\pi)}} \exp\left(-\frac{u^2}{2}\right)$$

Fractiles of the unit normal distribution are values on the u-scale corresponding to certain probabilities. The formal mathematical definition of a fractile such as $u_{1-\alpha}$ is

$$\frac{1}{\sqrt{(2\pi)}} \int_{-\infty}^{u_{1-\alpha}} \exp\left(-\frac{u^2}{2}\right) du = 1 - \alpha$$

This means that a value of u (taken at random from the distribution) falls with probability $1 - \alpha$ in the interval $(-\infty, u_{1-\alpha})$. Fractile values can be found in tables of the cumulative normal distribution function, such as those of HALD [5].

VOL. 15 1961

(c) The numerical criterion is based on the value of $\chi^2_{1-\alpha,n}$.* If $\sum_{i=1}^{n}(x_i - \xi)^2$ exceeds $\sigma_0^2\,\chi^2_{1-\alpha,n}$ (which may be shown to equal $\sigma_1^2\,\chi^2_{\beta,n}$) the batch is rejected; if $\sum_{i=1}^{n}(x_i - \xi)^2$ falls short of $\sigma_0^2\,\chi^2_{1-\alpha,n}$ the batch is accepted.

Frequently we are interested in studying the probabilities of rejection and acceptance of the batch if the true state of affairs is defined by a value σ^2 which is not necessarily identical with either σ_1^2 or σ_0^2. We may now construct a function π denoting the probability of rejecting a batch for all admissible values of σ^2. Clearly, if the argument σ^2 takes the value σ_0^2 the function π will be equal to α; for $\sigma^2 = \sigma_1^2$ we get $\pi = 1 - \beta$. Exact values of π may be found for any admissible value of the argument σ^2 and Fig. 1 depicts such a curve—the so-called *power function of the test*. Whenever hypotheses (alternative to some given null hypothesis) may be formulated in terms of a parameter (or a set of parameters) describing the character of a population the probability of making some decision—such as acceptance or rejection of a batch—can be expressed as a function of the parameter. This function is generally known as the power function of the test; it gives an account of the discriminating ability of the proposed test criterion.

In solid–solid mixtures the assumption of complete randomness of the distribution is generally taken to be the null hyopthesis. There are two major alternatives to this hypothesis:

(a) Existence of a large scale gradient of concentration.

(b) Appearance of local clusters which may be distributed at random.

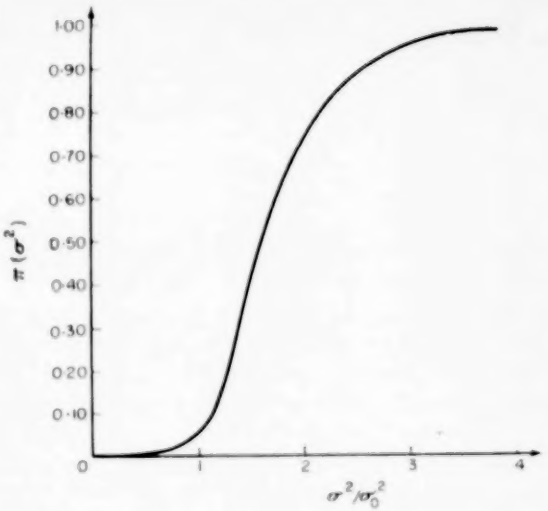

FIG. 1. Power function for a variance test ($n = 20$; $\alpha = 0{\cdot}05$).

In case (a) we expect homogeneity and randomness of particle distributions within any given single sample (small region); in case (b) there may exist local non-uniformities even within any given single sample. Obviously, both deviations from randomness may be present simultaneously. If the alternative hypothesis against which we seek to protect ourselves is a large scale gradient, the method described for the case of a batch of tablets may be successfully applied since the existence of a gradient is associated with an increase in the variance which may be calculated. If the permissible gradients can be specified in a quantitative manner a test of any desired power can be designed.

The case of clustering is much more complicated. Not only is the variance sometimes dependent on sample size but also the increase in variance due to clustering may be comparatively small and hard to detect by the above procedure. Consider,

*The family of χ^2—distributions is well known in both statistical theory and applied statistics; the expression

$$p(\chi^2) = \frac{(\chi^2)^{(f/2)-1}\exp(-\chi^2/2)}{2^{f/2}\left[(f/2)-1\right]!} \qquad \chi^2 \geqslant 0, f = 1, 2, 3, \ldots$$

describes these distributions and each member of the χ^2 family is defined by its particular value of f—the number of degrees of freedom. The fractiles of the χ^2—distribution are defined in a fashion similar to that utilized in the case of the unit normal distribution.

$$\int_0^{\chi^2_{1-\alpha}} p(\chi^2)\,d(\chi^2) = 1 - \alpha$$

The notation χ_n^2 should convey the idea that some particular value—n—has been selected for f, and $\chi^2_{1-\alpha,n}$ is the corresponding fractile. Tables of the χ^2—fractiles may be found in HALD [5].

for example, the case of a distribution of white and black particles where all black particles appear in clusters of two. Theoretically, the variance of the number of black particles in a single sample should increase by a factor of two when compared with a distribution that is completely random. However, practically the increase will be smaller since part of the clusters will be torn apart due to the process of sampling. Consistent clustering of two particles is an extreme case and in practice the problem is more complicated because clusters may arise not only in the form of aggregates of adjacent black particles but also as local regions of higher concentrations. In the latter case, the increase in the variance depends strongly on sample size and therefore the design of an appropriate test becomes very complex. It is no longer possible to specify the allowed deviations from randomness in a quantitative manner and to derive an appropriate power function. From a process engineer's point of view it is fortunate that in many practical applications specification of the allowable variance is sufficient; however, some processes require a maximum degree of randomness and clustering should be avoided as much as possible. A sensitive test for the detection of clusters in any form should therefore be highly desirable for the comparison of mixing equipment and for the study of the mixing process in general. Such a test will be developed and described in the further sections of this study.

3. A Model of Random Mixture and Some of its Statistical Properties

Consider black particles embedded in a matrix of white particles. Assume that the fraction of black particles is small—less than 5 per cent say. While we have defined a random mixture as one following the binomial distribution the approximation by a Poisson distribution is sufficiently accurate for small percentages. This is equivalent to the following description of the random mixture: the black particles are represented by points which are essentially dimensionless; these points are distributed at random in the white matrix in the sense that the position of any point (black particle) bears no influence on the probability of finding another point in its vicinity or, indeed, in any location. In other words, there is no correlation between the sites of black particles; the only factor which plays a role in the determination of distances between neighbouring black particles is their density in the white matrix. It is apparent that the problem under consideration is of three-dimensional character and mathematically there is no inherent difficulty in treating it as such. However, any experimental determination of the position of black particles relative to each other will almost always have to be carried out in two dimensions. In the following, the problem will be analysed and dealt with accordingly. It should be pointed out that there is no loss of information due to this transition from three to two dimensions.

As stated before, the desired test criterion should be especially sensitive to the existence of local clusters even if these are randomly distributed. Now if such higher local concentrations exist the particles will be less widely spaced in some regions. Preferably the test criterion should be based on a measurable variable which does not depend on sample size and form. The shortest distance between particles was chosen for this purpose and its distribution was investigated. It was found that the use of the squared shortest distance leads to simpler mathematical expressions well known to the statistician in other contexts. The important feature and advantage of this proposed method is that every single particle is considered separately and no information is lost due to any grouping process as is the case in any of the regularly adopted sampling procedures.

We shall now derive the distribution of the shortest squared distance between such random points. Select a random point and let a circle of radius r be drawn with this point as centre. According to the distribution law of Poisson the probability of this circle containing not even one additional random point is equal to $\exp(-r^2\pi\mu)$, where μ is the average number of random points in unit area. This quantity is clearly identical, by definition, with the probability of a shortest squared distance being larger than r^2. The cumulative probability distribution of r^2, $F(r^2)$, is therefore given by

$$F(r^2) = 1 - \exp(-r^2 \pi\mu) \tag{1}$$

This is the probability of a shortest squared distance being smaller than r^2; the probability density of r^2, $f(r^2)$, is found by differentiating $F(r^2)$ with respect to r^2.

$$f(r^2) = \pi\mu \exp(-r^2 \pi\mu) \tag{2}$$

This distribution—defined by (1) or by (2)—is well known in statistical theory and its main properties are easily derived. Its mean (or expected) value, $E(r^2)$, is evaluated as

$$E(r^2) \equiv \int_0^\infty r^2 f(r^2)\, d(r^2) =$$

$$= \int_0^\infty r^2 \pi\mu \exp(-r^2 \pi\mu)\, d(r^2) =$$

$$= \frac{1}{\pi\mu} \int_0^\infty r^2 \pi\mu \exp(-r^2 \pi\mu)\, d(r^2 \pi\mu) = \frac{1}{\pi\mu} \tag{3}$$

The variance of this distribution, $V(r^2)$, needs a little more elaboration

$$V(r^2) \equiv \int_0^\infty [r^2 - E(r^2)]^2 f(r^2)\, d(r^2) =$$

$$= E[(r^2)^2] - E^2(r^2) =$$

$$= \int_0^\infty r^4 \pi\mu \exp(r^2 \pi\mu)\, d(r^2) - \frac{1}{\pi^2\mu^2} =$$

$$= \frac{1}{\pi^2\mu^2} \int_0^\infty (r^2\pi\mu)^2 \exp(-r^2\pi\mu)\, d(r^2\pi\mu) -$$

$$- \frac{1}{\pi^2\mu^2} =$$

$$= \frac{2}{\pi^2\mu^2} - \frac{1}{\pi^2\mu^2} = \frac{1}{\pi^2\mu^2} \tag{4}$$

Furthermore the distribution of the squared distance may be transformed into a x^2 — distribution with two degrees of freedom. This important property of the r^2 — distribution can be derived as follows: Substitute

$$x^2 = 2 r^2 \pi\mu \tag{5}$$

The density of the transformed variable, $p(x^2)$, is evaluated by

$$p(x^2) = f(r^2) \frac{d(r^2)}{d(x^2)} = \tfrac{1}{2} \exp(-r^2 \pi\mu) =$$

$$= \tfrac{1}{2} \exp(-x^2/2) \tag{6}$$

which is the x^2 — density with 2 degrees of freedom. Now the addition theorem of the x^2 — distribution

$$x^2_{f_1} + x^2_{f_2} + \ldots x^2_{f_k} = x^2_{f_1 + f_2 + \ldots f_k}$$

leads immediately to an addition theroem concerning the distribution of the squared shortest distance between random points.

The distribution of the n independent squared shortest distances may be transformed into a x^2 — distribution with $2n$ degrees of freedom by

$$x^2_{2n} = 2 \pi\mu \sum_{i=1}^{n} r_i^2 \tag{7}$$

The additive property expressed by relation (7) serves as the basis for the test criterion proposed in this paper. If a series of independent observations of squared shortest distances is taken, added up and multiplied by $2 \pi\mu$, the result is distributed as x^2 with $2n$ degrees of freedom (if the null hypothesis of random distribution is true). If, however, the null hypothesis is false and clusters exist, $2 \pi\mu \sum_{i=1}^{n} r_i^2$ will be typically much smaller than the ordinary x^2 — variate with $2n$ degrees of freedom. Thus the following test criterion suggests itself: If $2 \pi\mu \Sigma r_i^2$ falls short of $x^2_{\alpha, 2n}$ we conclude that the distribution of the points in the plane under investigation is not random. If $2 \pi\mu \Sigma r_i^2$ exceeds $x^2_{\alpha, 2n}$ the null hypothesis of random distribution cannot be rejected.

4. The Power of the Test Criterion

In order to derive a power function of the proposed test a set of alternative hypotheses has to be defined in terms of one or more parameters describing the state of the dispersion. We recollect that we are not concerned with protection against *all* possible alternatives; we are interested only in clusters and their quantitative specification.

The degree of clustering may be defined quantitatively by the ratio ζ of the expected value of r^2 in an ideally random mixture and the

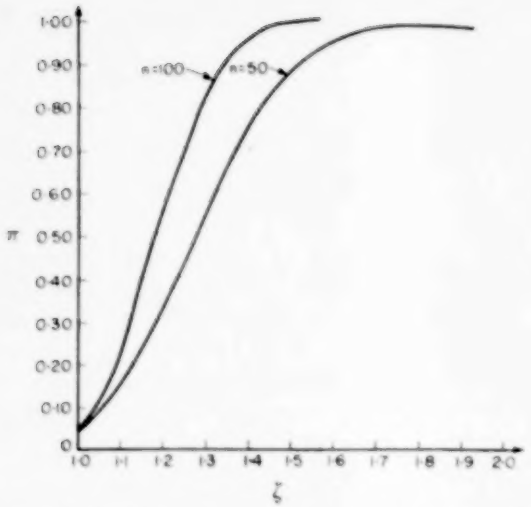

Fig. 2 (a). Power curves of the shortest distance test ($\alpha = 0{\cdot}05$).

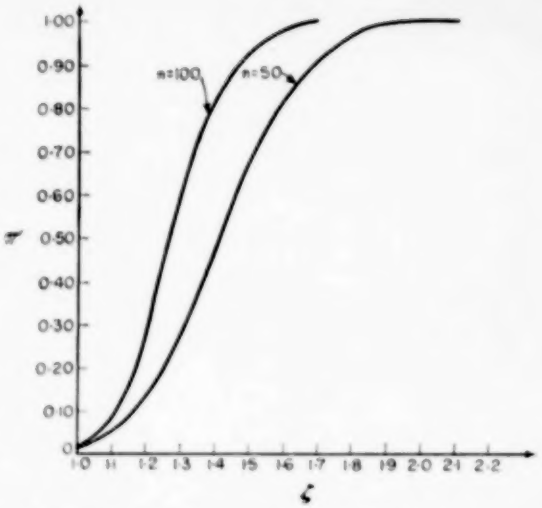

Fig. 2 (b). Power curves of the shortest distance test ($\alpha = 0{\cdot}01$).

expected value of r^2 in the actual mixture, that is, the average value of r^2 in the total real population. While any such definition must contain an element of arbitrariness it is possible to ascribe a physical interpretation to ζ: it is the reciprocal of the fractional area occupied by clusters. Obviously, ζ equals 1 for an ideal random mixture and increases if clustering prevails.* We are now in a position to present the power function $\pi(\zeta)$, i.e. the probability of rejecting the null hypothesis (random mixing) as a function of ζ, α and the number of shortest distances measured.

$$\pi(\zeta;\alpha,n) = \text{Prob}\left\{2\pi\mu\,\Sigma r_i^2 < \chi^2_{\alpha,2n};\ \text{degree of clustering} = \zeta\right\} = \text{Prob}\left\{\chi^2_{2n} < \zeta\,\chi^2_{\alpha,2n}\right\} \qquad (8)$$

Examples of power curves for different values of α and n are given in Figs. 2(a) and 2(b). These figures were obtained by utilizing χ^2 – tables wherever possible. For large values of n a normal approximation to χ^2 was used.

$$u_\pi \simeq \sqrt{\zeta}\left[\sqrt{(4n-1)} - u_{1-\alpha}\right] - \sqrt{(4n-1)} \qquad (9)$$

*Values of ζ smaller than one – mean that some order exists in the arrangement of the black particles in space; such order is extremely unlikely in the case of solid–solid mixtures.

Of course, one can also invert the procedure and choose a critical value ζ_{crit}; it is desired to reject the null hypothesis of random mixing with at least probability $(1-\beta)$ if $\zeta > \zeta_{\text{crit}}$. Manipulation of relation (9) yields

$$n = \tfrac{1}{4} + \tfrac{1}{4}\left[\frac{u_{1-\alpha}\sqrt{(\zeta_{\text{crit}})} + u_{1-\beta}}{\sqrt{(\zeta_{\text{crit}})} - 1}\right]^2 \qquad (10)$$

5. Practical Testing Procedures

Sample surfaces suitable for the proposed testing procedure may be obtained in different ways. One of them would be to take several comparatively large random samples and freeze them by letting molten wax seep into them. After cooling the mixture surface samples can be produced by slicing with a microtome. Instead of molten wax a thin-flowing monomer can be used to freeze the particles in space on polymerization. Alternatively, it is possible to use a sample thief with a transparent bottom which presents a flat surface immediately ready for investigation. Though measurements can be made directly on the sample surface enlarged under a microscope it is preferable to take photo-micrographs.

Ideally, the sample under investigation should be extremely large; the points (coloured particles) from which shortest distances are measured

should be chosen at random from the totality of points such that the probability of selecting any particular point is equal to that of selecting any other point. This method of sampling shortest distances is most satisfactory from a theoretical viewpoint and thus preferable whenever possible. However, this method necessitates a very large sample surface and considerable work if a rigorous randomizing procedure is applied.

In practice the following modification can be satisfactorily used: an area is selected from the total sample surface; the preferable form of the area is either circular or square but the rectangle obtained in a regular microphotograph is acceptable. The total number of points in the area, n, is counted and the density of points, μ, is determined. It is desirable that n exceeds 100 and if this is impossible within one sample surface, several of them can be combined and calculations pooled as if there was one large area.

The next step is to determine for every point in the area the distance to its nearest neighbour. All points inside and outside the area can serve as nearest neighbours though only points inside the area constitute origins of measurement. To avoid boundary effects brought about by cutting out the sample area from the infinite surface surrounding it a margin is left around the area selected before. The width of the margin depends on the number of points in the area and should be of the order $L\sqrt{1/n}$ where L is the length of the rectangle (or side of the sqaure or diameter of the circle). $2\pi\mu\sum_{i=1}^{n} r_i^2$ is now calculated and compared to $x^2_{\alpha,2n}$. If $2\pi\mu\sum_{i=1}^{n} r_i^2$ falls short of this number the null hypothesis of random mixing is rejected. Table 1 presents a selection of $x^2_{\alpha,2n}$ values.

Table 1. *Selected Values of* $x^2_{\alpha,2n}$

n	$x^2_{0{\cdot}01,2n}$	$x^2_{0{\cdot}05,2n}$
50	70·1	77·9
75	112·0	122·4
100	135·7	168·0
125	200·2	214·1
150	245·3	260·6
175	290·7	307·4
200	336·4	354·4

It should be pointed out that using *all* points with a given finite sample instead of selecting points at random from a very large sample introduces slight errors: the estimate of the average remains unbiased, but due to correlation the distribution of $2\pi\mu\,\Sigma r_i^2$ is not strictly x^2 with $2n$ degrees of freedom. However, if n is 50 or larger, the error due to selecting $x^2_{\alpha,2n}$ instead of the exact value, as a decision criterion, is of negligible importance.

It is advisable to perform a PEARSON's x^2—test for a good fit on the whole sample surface even before applying the shortest distance test. This is done by placing a grid on the sample surface (or surfaces) and counting the number of particles in each cell of the grid. The grid should be chosen in such a manner that the average number of points in a cell exceeds five. It is now necessary to calculate the quantity

$$\frac{\sum_{j=1}^{k}(f_j - f_{\text{ave.}})^2}{f_{\text{ave.}}}$$

where k is the number of cells in the grid, $f_{\text{ave.}}$ the average number of points in a cell and f_j the actual number of points in the j-th cell. If this quantity is larger than $x^2_{1-\alpha,k-1}$ the null hypothesis of random mixing must be rejected and it is no longer necessary to perform a shortest distance test.

While the Pearson test is much less sensitive against the appearance of clusters than the shortest distance, it is preferable if protection against *gradients* is sought. The two tests should then be combined and, as less work is involved in a Pearson test, it should precede the shortest distance test.

6. Some Illustrative Examples

The authors are currently engaged in applying the above principles and procedures to study the behaviour of some actual solid–solid systems in different mixing devices. The results will be communicated in a later publication. Two

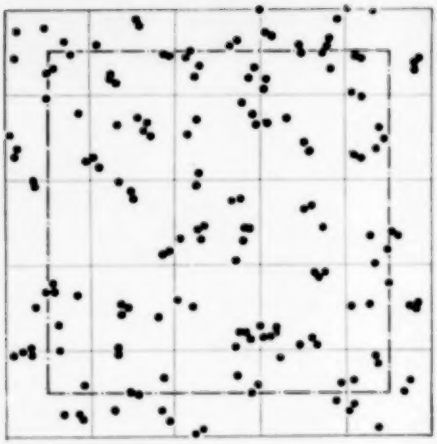

Fig. 3(a). Sample No. I

(1) Pearsons x^2 – Test: Partition into 25 squares

$$\frac{\sum_{j=1}^{25}(f_j - f_{ave.})^2}{f_{ave.}} = 22\,;\; x^2_{0.95,24} = 36.4$$

Test result *not* significant.

(2) Shortest Distance Test: Number of points in area under investigation: 106

$$2\pi\mu \sum_{i=1}^{106} r_i^2 = 99\,;\; x^2_{0.05,212} = 179$$

Test result *highly* significant:
Distribution of points not random.

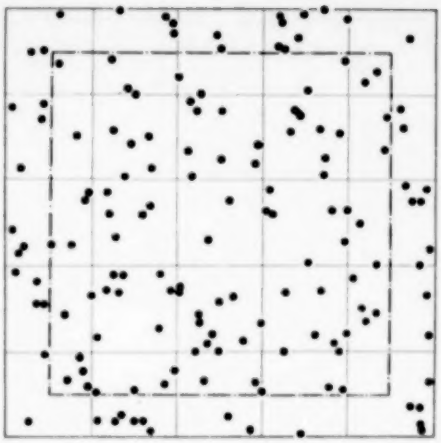

Fig. 3(b). Sample No. II

(1) Pearsons x^2 – Test: Partition into 25 squares

$$\frac{\sum_{j=1}^{25}(f_j - f_{ave.})^2}{f_{ave.}} = 21.6\,;\; x^2_{0.95,24} = 36.4$$

Test result *not* significant.

(2) Shortest Distance Test: Number of points in area under investigation: 97

$$2\pi\mu \sum_{i=1}^{97} r_i^2 = 221\,;\; x^2_{0.05,194} = 162.5$$

Test result *not* significant:
Distribution of points random.

typical examples are given in Figs. 3(a) and 3(b). Fig. 3(a) presents a sample with clustered points, whereas in Fig. 3(b) a thoroughly mixed sample of the same system is exhibited. The classical Pearson test fails completely to distinguish between these samples. On the other hand, the shortest distance test would have detected the non-randomness of Sample I (Fig. 3a) even if a significance level (error of the first type) of $\alpha = 0.0005$ had been prescribed.

7. Discussion

The test of randomness for solid–solid mixtures proposed in this paper tries to fill a gap in the existing testing procedures. The pertinent feature of this study is the quantitative definition of clustering by a single parameter ζ and, simultaneously, the derivation of a sample statistic $2\pi\mu \sum_{i=1}^{n} r_i^2$ and its distribution by which derivations from randomness ($\zeta = 1$) can be detected with any desired precision. To our knowledge, none of the parameters previously proposed for the specification of clustering permit decisions as to the existence of randomness based on statistical sampling theory.

It is only fair to point out that the proposed method is not a panacea and suffers from several drawbacks.

(i) It necessitates considerable work both in measuring the primary data and in calculating the sample statistic.

(ii) It is suitable only for mixtures in which the range in particle sizes is not excessively large.

(iii) The percentage of the "coloured" particles must be kept low—preferably less than 5 per cent though even 10 per cent may be tolerated without committing a large error.

(iv) The particles must be distinguishable by some optical method.

On the other hand the methods should be very useful in studying the process of mixing as well

VOL. 15 1961

as mixing equipment design. For any specific actual process which is not suitable to be tested by the above procedure an equivalent mixture of coloured and uncoloured particles may be synthetically prepared and its behaviour in the mixing equipment may be studied. It is very important that the simulating mixture should approach the physical properties of the actual mixture as closely as possible (average grain size, density, etc.). In most cases this can be accomplished by using the same ingredients as in the actual process.

Notation

$E(r^2)$ = mean or expected value of r^2
$F(r^2)$ = cumulative probability distribution of r^2
N = total number of tablets in batch
$V(r^2)$ = variance of r^2 – distribution
$f(r^2)$ = probability-density of r^2
$f_{ave.}$ = average number of points in cell (for Pearson test)
f_j = actual number of points in cell j
k = number of cells in grid (for Pearson test)
n = number of observations
p = fraction of black particles in mixture
r = shortest distance (distance of each particle to its nearest neighbour)
$u_{1-\alpha}, u_{1-\beta}$ = fractiles of the unit normal distribution
x_i = actual amount of ingredient i in the tablet
α, β = probabilities; risks of arriving at incorrect conclusions
ζ = ratio of expected value of r^2 in an ideal mixture to the expected value of r^2 in the real mixture
$\lambda = \sigma_1/\sigma_0$
μ = average number of points per unit area
ξ = average amount of ingredient in any tablet
σ^2 = variance
σ_0 = appropriate value of σ in batch
σ_1 = value of σ considered excessive
$x^2_{1-\alpha,n}$ = values of x^2 distribution with n degrees of freedom, which is exceeded with probability α

References

[1] Weidenbaum Sh. S. *Advances in Chemical Engineering*, Vol. 2, p. 209. Academic Press, New York 1958.

[2] Neyman J. and Pearson E. S. *Biometrika* 1928 **20A** 175.

[3] Cramer H. *Mathematical Methods of Statistics* pp. 325–336. Princeton University Press 1946.

[4] Hald A. *Statistical Theory with Engineering Applications*, p. 280. John Wiley, New York 1952.

[5] Hald A. *Statistical Tables and Formulas*. John Wiley, New York 1952.

Chemical Engineering Science, 1961, Vol. 15, pp. 230 to 242. Pergamon Press Ltd., London. Printed in Great Britain.

The sedimentation of suspensions of closely-sized spherical particles

D. R. Oliver
University of Birmingham

(*Received* 20 *October* 1960)

Abstract—The Stokes stream function for flow past a single sphere is used in order to obtain an equation relating the settling velocity of a suspension of monosize spherical particles to the volume concentration of the solid phase. The form of the equation suggests that, for dilute suspensions, there is greater dependence of settling velocity on concentration than had previously been accepted. Experimental work is described which supports this contention. It is pointed out that errors in the determination of the Stokes velocity of typical particles affect the form of the settling velocity–concentration curves; this is advanced as a possible cause for the discrepancy existing between the results of various workers. Finally, it is postulated that a form of " transient " differential settling is present during the sedimentation process which cannot be eliminated by the use of strictly equal particles.

Résumé—La fonction de Stokes pour l'écoulement près d'une seule sphère est utilisée afin d'obtenir une équation reliant la vitesse de décantation d'une suspension de particules sphériques de même dimension à la concentration volumique de la phase solide. La forme de l'équation indique que pour les suspensions diluées, la vitesse de décantation dépend considérablement de la concentration comme il avait été préalablement admis. L'expérience décrite est réalisée dans ces conditions. On montre que des erreurs dans le détermination de la vitesse de Stokes de particules typiques affecte la forme des courbes liant la vitesse de sédimentation à la concentration ; on pense que ceci est la raison de la divergence des résultats des différents expérimentateurs. Enfin, l'auteur suppose qu'i existe une forme transitoire de décantation différentielle pendant l'opération de sédimentation qui ne peut pas être éliminée même en utilisant des particules strictement identiques.

Zusammenfassung—Die Strömungsfunktion von Stokes für Strömung nake zu einer einzigen Kugel ist angewendet um eine Gleichung abzuleiten, die die Klärungsgeschwindigkeit einer Suspension von kugelförmigen Partikeln von gleicher Grösse mit der Volumenkonzentration der soliden Phase in Verbindung bringt. Die Form der Gleichung zeigt an, dass für verdünnte Suspensionen die Abhängigkeit der Klärungsgeschwindigkeit von der Konzentrationsgeschwindigkeit grösser ist, als sie bisher angenommen wurde. Fehler in der Bestimmung der Stokes-Geschwindigkeit von typischen Partikeln beeinflussen die Form der Klärungsgeschwindigkeit-Konzentration Kurven, und es ist angedeutet, dass möglicherweise dies ist die Ursache der Unstimmigkeit zwischen den Ergebnissen von verschiedenen Forschern. Endlich, es ist angenommen, dass eine Form von " vorübergehenden " Differentialklärung existiert während des Sedimentationsvorganges. Diese Differentialklärung kann mit der Hilfe von genau gleichen Partikeln nicht eliminiert werden.

Introduction

The study of sedimentation phenomena has been marked by considerable diversity of approach. Burgers [1] has suggested that the motion of a typical single particle should be influenced by both the motion and the presence of the other particles. The main effect of the motion of the other particles was to cause a " return flow " of liquid, whilst the presence of the other particles produced an effect analogous to an increase in the viscosity of the dispersing liquid. For suspensions of spherical particles Burgers obtained the equation

$$V_r = V_s / V_0 = [1 + (\lambda_1 + \lambda_2)\, c]^{-1} \qquad (1)$$

Here V_0, V_s and V_r are the Stokes velocity for a single particle in a given dispersing liquid, the settling velocity of the suspension at a solids volume concentration of c and the relative settling velocity, respectively. For random particle distributions $\lambda_1 = 15/8$ and $\lambda_2 = 5$.

Steinour [2] considered the flow spaces between

the particles and obtained an expression of the form

$$V_r = (1 - c)^2 f(c) \qquad (2)$$

the value of f being shown experimentally to be $10^{-1.82c}$. One of the factors $(1 - c)$ resulted from a consideration of the return flow effect, whilst the other arose because a typical sphere was thought of as settling in a fluid of density equal to that of the suspension rather than that of the pure liquid alone. According to BURGERS [1] increased buoyancy can result only from the motion of the settling particles – already considered – the second factor therefore appears to be repetitive.

The work of HAWKSLEY [3] also led to a relationship of the form of equation (2), the factor $(1 - c)^2$ being of similar origin. The function $f(c)$, however, representing the reciprocal of the effective relative viscosity of the suspension with respect to a single sphere, was evaluated from a theoretical equation due to VAND [4]. This allowed only for hydrodynamical interaction between particles, collisions being assumed not to occur in settling suspensions. HAWKSLEY's equation was

$$V_r = (1 - c)^2 \exp - \frac{2{\cdot}5\, c}{1 - 0{\cdot}609\, c} \qquad (3)$$

Recently obtained experimental evidence supports this equation [5].

A different approach to the problem was employed by BRINKMAN [6] who considered the forces acting on a volume element of fluid containing many particles held in stationary positions by a hypothetical external agency. The particles exerted a damping force on the flow of fluid which was assumed porportional to the mean velocity and to the viscosity of the fluid. A general expression for the flow velocity was then derived which reduced to Darcy's equation at high particle densities and could be solved (for incompressible fluids) to give the permeability of the swarm of particles. This may be modified to give the relative settling velocity as

$$V_r = 1 + \frac{3c}{4}\left\{1 - \left(\frac{8}{c} - 3\right)^{1/2}\right\} \qquad (4)$$

RICHARDSON and ZAKI [7] recognised the importance of particle distribution in governing settling velocity and assumed that since a suspension forms a sharp, constant-velocity interface the particles could be considered as moving steadily downwards in a stable configuration. The flow around two idealized particle configurations was examined theoretically and the results expressed in terms of correction factors to the Stokes resistance at different volume concentrations of solids. The two series of theoretical factors were compared with the author's experimental values given by the formula $(1 - c)^{4.65}$ [8], one series being low (16 per cent at $c = 0{\cdot}30$) and the other high (44 per cent at $c = 0{\cdot}30$). As the concentration approached zero both series of theoretical factors approached zero rather than unity, thus agreement with experimental data seems unlikely for $c < 0{\cdot}05$.

LOEFFLER and RUTH [9] considered the settling conditions obtaining when the concentration approach both zero (Stokes' law) and 0·5 (packed bed region covered by Kozeny's equation) formulating the expression

$$V_r = \left(\frac{1}{(1 - c} + \frac{5{\cdot}7\, c}{(1 - c)^3}\right)^{-1} \qquad (5)$$

The term $(1 - c)^{-1}$ was arbitrarily introduced in order that the value of V_r should approach unity as c approached zero. Satisfactory tests of the equation were carried out using suspensions of spheres for which the size variation was reduced to only 5 per cent.

Recently KYNCH [10] has advanced the simplified equation

$$V_r = (1 - c)\, \mu_r^{-1} \qquad (6)$$

where μ_r is the relative viscosity of a stable (non-settling) suspension otherwise similar to the one under observation. Experimental evidence regarding the validity of this equation is conflicting [10, 11].

THEORETICAL

Following BURGERS [1] the influence of both the motion and the presence of a mass of particles on a typical particle will be considered.

The downward motion of the particles must cause an upward flow of liquid and the velocity

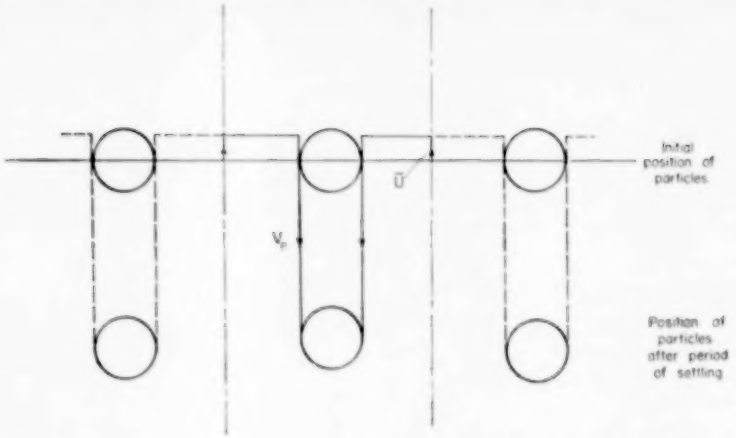

Fig. 1. Flow model based on average return flow velocity of liquid.

$\bar{U}$ of this flow averaged for the whole cross-section of the vessel must be $(1 - c)$ times the solids settling rate V_p. The particles therefore move with a velocity $\bar{U} + V_p$ relative to the liquid as a whole, as illustrated diagrammatically in Fig. 1.

However, a proportion of the liquid is always in the immediate vicinity of a sphere and is therefore being carried downwards. It follows that the liquid which rises must do so with a velocity U greater than $\bar{U}$, the extent of the difference depending in some way on the particle separation (Fig. 2).

The liquid velocity must vary from V_p (downwards) at the sphere surfaces to U (upwards) at points most distant from the spheres, and since U represents a true return flow velocity its value should have a greater influence on V_p than the value of $\bar{U}$. In addition U is not proportional to $\bar{U}$, since when the spheres are spaced further apart a greater relative quantity of liquid moves with each of the spheres. In the limiting case of a single sphere in an infinite expanse of liquid, it may be shown that the attendant liquid flowrate approaches infinity. It follows that a theory which takes into account flow of the above type will differ from existing theories primarily in the

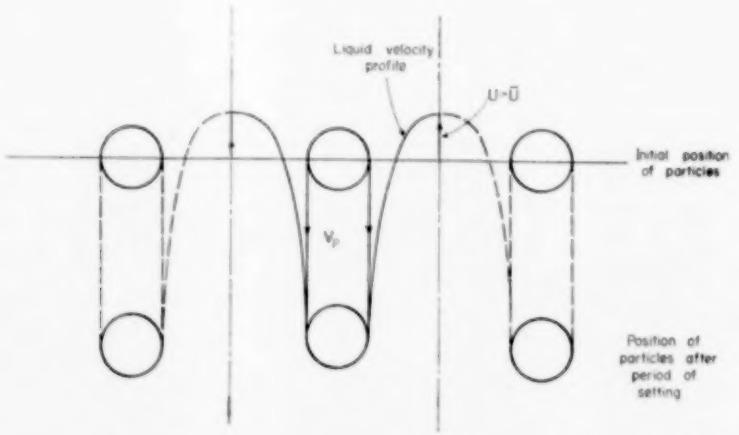

Fig. 2. Flow model based on maximum return flow velocity of liquid

region of low solids concentration. The following discussion represents a possible approach to the problem.

Consider a single sphere of radius a, falling slowly in a large expanse of liquid with a Stokes velocity V_0. The flow around the sphere will be identical to that obtained if the sphere itself were balanced in a stationary position and the liquid were rising with a velocity of V_0. Assume an imaginary cylinder of radius R to surround the sphere as shown in Fig. 3, the cylinder not influencing the flow in any way. At large distances from the sphere the axial flowrate of liquid through the cylinder will be

$$Q = \pi R^2 V_0 \tag{7}$$

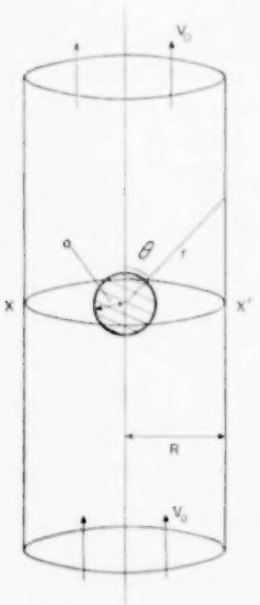

Fig. 3. Hypothetical cylinder surrounding sphere.

The stream function for Stokes flow past a single sphere is [12]

$$\psi = \tfrac{1}{2} V_0 r^2 \left(1 - \frac{3}{2}\frac{a}{r} + \frac{1}{2}\frac{a^3}{r^3}\right) \sin^2\theta \tag{8}$$

For $\theta = 90°$ this becomes

$$\psi = \tfrac{1}{2} V_0 r^2 \left(1 - \frac{3}{2}\frac{a}{r} + \frac{1}{2}\frac{a^3}{r^3}\right) \tag{9}$$

The axial volumetric flowrate through the cylinder in the plane through the centre of the sphere XX' is therefore

$$Q' = 2\pi \psi_{r=R} = \pi V_0 R^2 \left(1 - \frac{3}{2}\frac{a}{R} + \frac{1}{2}\frac{a^3}{R^3}\right) \tag{10}$$

Thus a volumetric flowrate $Q - Q'$ of liquid passes outside the cylinder in the plane XX' as a direct result of the presence of the sphere.

If now some influence is assumed to be present which effectively limits the outward bending of the streamlines and contains the flow Q within the cylinder, then the flow $Q - Q'$ must be distributed over the cross-section of the cylinder in the plane XX', causing an additional upward drift of the contents of the cylinder, including the sphere, of magnitude

$$V_A = \frac{Q - Q'}{\pi R^2} = V_0 \left(\frac{3}{2}\frac{a}{R} - \frac{1}{2}\frac{a^3}{R^3}\right) \tag{11}$$

If $a^3/R^3 \ll a/R$ this equation becomes

$$V_A = \frac{3}{2}\frac{a}{R} V_0 \tag{12}$$

The assumption will be made that the other spheres in a swarm cause a flow restriction of the above type, and that the effective "radius of action," R, of a typical sphere is directly proportional to the mean separation, d, of the sphere centres. It may be shown that the ratio a/d is proportional to the one third power of the solids concentration, c, for uniform particle distributions. Thus it follows that

$$V_A = K c^{1/3} V_0 \tag{13}$$

where K is a constant. Reverting to the case of spherical particles settling in a fluid in which their Stokes Velocity is V_0, the settling velocity, V_P, of the particles is obtained as

$$V_P = V_0 - V_A = V_0 \left(1 - \frac{3}{2}\frac{a}{R}\right) = V_0 (1 - K c^{1/3}) \tag{14}$$

This equation makes allowance for an upward flow of liquid caused by the motion of the particles and may be expected to hold for very low values of the concentration. The presence of other

particles also impedes the motion of a typical particle in the same way as if there were an increase in the viscosity of the liquid; the effective relative viscosity will be assumed to be given by the equation [13]

$$\mu_r = (1 - k\,c)^{-1} \qquad (15)$$

This effect will reduce the particle settling velocity to V_s, where

$$V_s = V_p\,(1 - k\,c) = V_0\,(1 - k\,c)\,(1 - K\,c^{1/3}) \qquad (16)$$

Thus the relative settling velocity is obtained as

$$V_r = \frac{V_s}{V_0} = (1 - k\,c)\,(1 - K\,c^{1/3}) \qquad (17)$$

The constants k and K remain to be determined by experiment; their values will be discussed later.

Experimental Difficulties

In order to test the theoretical equations it is necessary to produce large quantities of closely-sized spheres. A number of methods have been used for this purpose [5, 9, 15]; the smallest diameter variation achieved appears to be 5 per cent [9]. Size or density differences between particles allow differential settling to occur at low solids concentrations and, in addition, the Stokes velocity for a single typical particle is difficult to establish. An error in this determination affects not only the magnitude of the relative settling velocity but also the shape of the velocity–concentration curves; thus providing a likely cause for much of the discrepancy which exists between published series of experimental settling velocities (Table 1).

Sources of data are:

A. Steinour [2]; tapioca spheres, Stokes velocity by direct measurement.

B. Lewis *et al.* [14]; glass spheres (0·0040 in.), Stokes velocity from quoted friction factors.

C. Gurel [15]; glass and Kallodoe spheres, Stokes velocity from Stokes law.

D. Hanratty and Bandukwala [5]; glass spheres, Stokes velocity from Stokes' law.

E. Loeffler and Ruth [9]; glass spheres, Stokes velocity by direct measurement and also Stokes law.

The work of Loeffler and Ruth [9] showed that Stokes velocity determinations could be in error by 6 per cent even under carefully controlled conditions; settling velocity measurements on suspensions, however, can usually be carried out with greater accuracy, particularly if the concentration of solids exceeds 0·05 [16].

It is therefore desirable to plot the data without reference to the Stokes velocity, choosing the co-ordinates in such a way that a particular theory predicts a straight line relationship when using

Table 1. *Values of relative settling velocity as function of volume concentration**

Volume concentration of solids c		*Relative settling velocity* V_r				
		A	*B*	*C*	*D*	*E*
	Size Ratio:†	1·10 : 1	1·06 : 1	1·06 : 1	Not given	1·05 : 1
0		1·10	1·00	1·00	1·00	1·00
0·05		0·67	0·64	0·79	0·81	0·72
0·10		0·53	0·54	0·60	0·64	0·52
0·15		0·41	0·44	0·45	0·47	0·39
0·20		0·31	0·34	0·33	0·37	0·28
0·25		0·22	0·26	0·24	0·26	0·20
0·30		0·15	0·19	0·17	0·20	0·15
0·35		0·10	0·13	0·12	0·14	0·11

* Sources of data on p. 242.

† $\frac{\text{Dia. largest sphere}}{\text{Dia. smallest sphere}}$

VOL. 15 1961

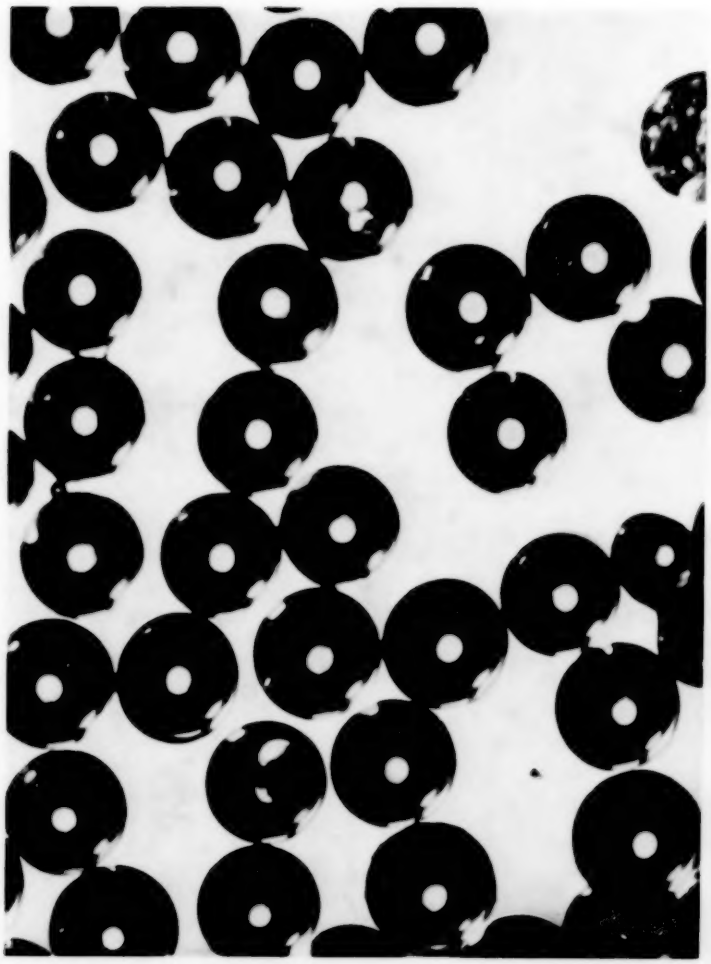

FIG. 4.

Table 2. Stokes velocities for 161 μ Kallodoc particles in three dispersing liquids

Dispersing liquid	*Number of particles timed*	*Mean time to fall 1·98 cm (sec)*	*Standard deviation* ± (sec)	*Mean velocity* (cm/sec)	*Reynolds No. (approx.)*
Water	42	7·6	0·8 (11%)	0·261 ± 0·029	0·39
20% Glycerol in water	88	21·0	1·9 (9%)	0·0943 ± 0·0085	0·074
25% Glycerol in water	200	27·9	1·9 (6·8%)	0·0710 ± 0·0062	0·044

actual settling velocities. The theory may then be judged by (a) the linearity of the experimental points, (b) the gradient of the line and (c) the closeness of the extrapolated "Stokes velocity" to the approximately-known value.

Experimental

The primary object of the present work was to obtain data in the region of low solids concentration ($c < 0{\cdot}05$), not available in the literature.

The spheres, of a methyl methacrylate polymer marketed under the trade name of "Kallodoc," were prepared by Gurel [15]. The mean diameter of the particles was 161 μ, 85 per cent having diameters within 3 per cent of this figure, whilst the mean density was 1·191 g/ml. A photomicrograph of the spheres is shown in Fig. 4.

Three dispersing liquids were used; pure water, a glycerol–water solution containing 20 per cent by volume of glycerol, and an otherwise similar solution containing 25 per cent by volume of glycerol. The respective viscosities of the solutions were approximately 1·0, 2·0 and 2·6 cp. In order to provide complete dispersion of the particles about 0·1 per cent of Dispersol O.G. was added to each of the liquids. All tests were carried out in a graduated cylinder of diameter 1·8 cm. and length 14 cm; the wall effect was negligible for the present particles [15].

Settling velocity measurements were carried out by introducing an accurately-known weight of particles into the graduated cylinder, followed by a quantity of dispersing liquid. The cylinder was then carefully mounted in a vertical position in a thermostat bath maintained at 20° ± 0·1 °C and the suspension gently agitated by the up and down motion of a disk-shaped stirrer in order to free entrapped air. A beam of light shining from behind the bath served to illuminate both air bubbles and particles. The stirring was repeated until air bubbles ceased to rise even under rapid agitation, after which the liquid level was topped up to a fixed mark on the graduated cylinder. Ten minutes were allowed for the establishment of thermal equilibrium. The suspension was then homogenized by making twenty sweeps with the stirrer, and the time taken for the solid level to fall between calibrated marks near the liquid surface recorded by means of a stopwatch. It was found possible to obtain settling velocities in this way for volume concentrations of solids as low as 0·003 (0·3 per cent). The solid level was less distinct than at higher concentrations but the usual timings were remarkably consistent, the standard deviation not exceeding ± 2 per cent of the mean value at concentrations below 0·01. The number of timings made at each concentration was reduced from 20 to 30 in the low range to below 10 at the higher concentrations, and the majority of these timings were within 2 per cent of the mean values.

The Kallodoc particles were large enough to enable Stokes velocities to be determined by direct observation or with the aid of a low-powered telescope. The stirrer was used in order to lift a few particles from the sediment to the upper part of the vessel, where a single particle uninfluenced by the immediate presence of others was selected for observation. If the particle drifted towards another particle, the wall or the stirrer during its fall the timing was rejected.

The timings showed that a very small proportion of the particles had Stokes velocities close to the mean sedimentation velocities of suspensions of concentration 0·0033 and 0·005. It could thus be argued that by observing the motion of the upper solid level during sedimentation tests, attention was being focussed on the slower-moving particles in the suspension. An experiment was therefore performed in which spheres were withdrawn from the top of the settling layer and the Stokes velocities determined immediately afterwards. These velocities did not differ appreciably from those determined for randomly-selected particles, showing that differential settling based on small differences of settling velocity was not occurring to a measureable extent.

Results

The results are summarized in Tables 2 and 3.

The figures quoted in Table 2 confirm the difficulty of obtaining accurate Stokes velocities for batches of very small particles. Nevertheless, confidence can be felt in the quoted deviations, and it is encouraging that in Table 3 no relative

Table 3. Settling velocities of suspensions of 161 μ Kallodoc in three dispersing liquids

Volume concentration of solids	Dispersing liquid					
	Water		20% Glycerol–water		25% Glycerol–water	
	V_s	V_r	V_s	V_r	V_s	V_r
0	0·261	1·000	0·0943	1·000	0·0710	1·000
0·0033			0·0815	0·864		
0·005					0·0592	0·843
0·0066			0·0761	0·808		
0·010			0·0740	0·785	0·0563	0·793
0·020			0·0688	0·729	0·0521	0·734
0·030	0·173	0·663	0·0612	0·649	0·0454	0·640
0·10	0·142	0·544	0·0492	0·522	0·0386	0·544
0·15	0·118	0·451	0·0397	0·421	0·0318	0·448
0·20	0·0803	0·308	0·0316	0·335	0·0230	0·324
0·25	0·0590	0·226	0·0234	0·248	0·0173	0·244
0·30	0·0446	0·171	0·0169	0·179	0·0122	0·172
0·35	0·0306	0·117	0·0125	0·133	0·0081	0·114

V_s = settling velocity (cm/sec) V_r = relative settling velocity

velocity differs from the mean by more than 10 per cent at any volume concentration.

The most interesting feature of the results is the marked effect of volume concentration on settling velocity in the region of low concentration, shown clearly in Fig. 5. The relationships due to Richardson and Zaki [7], Hawksley [3] and Brinkman [6] are also plotted, the latter providing the only previous theoretical data approximating to the current results at low concentrations. In general, however, the agreement between the theoretical and experimental results is poor.

The present theoretical equation may be written in the form

$$\frac{V_s}{(1 - Kc^{1/3})} = V_0(1 - kc) \qquad (18)$$

The quantity $V_s/(1 - Kc^{1/3})$ should thus be a linear function of volume concentration for each dispersing liquid. The tabulated data plotted in

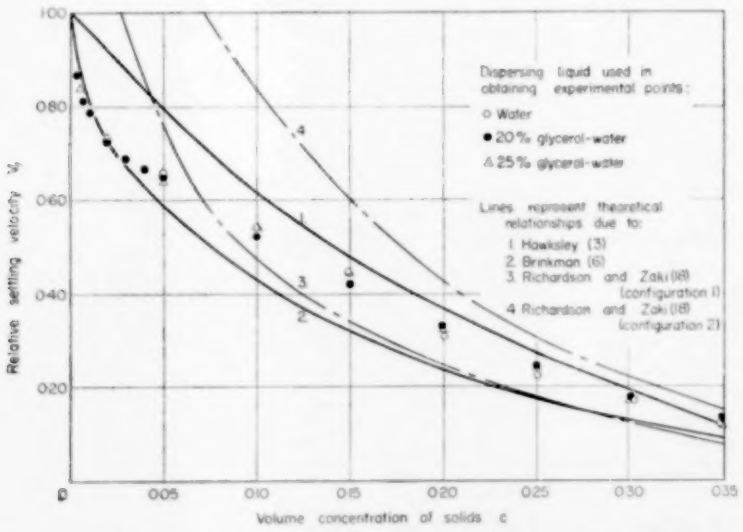

Fig. 5. Experimental values of the relative settling velocity for suspensions of 161 μ Kallodoc spheres.

VOL. 15 1961

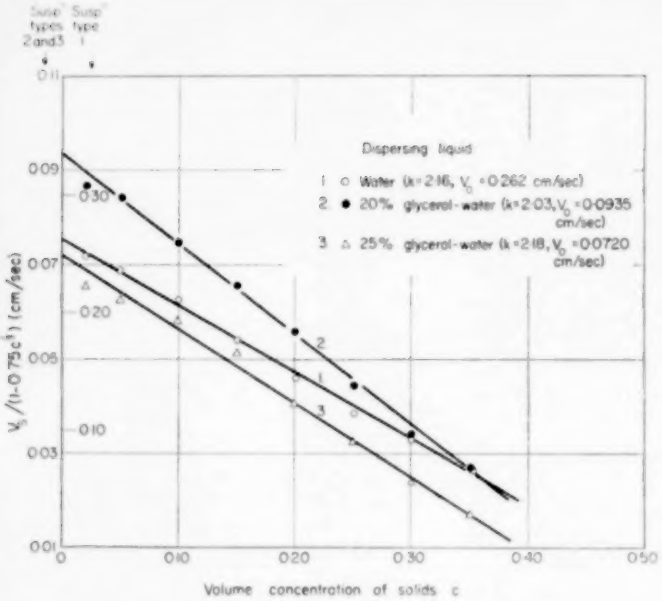

FIG. 6. Test of Equation (17) using Experimental Data for Suspensions of 161 μ Kallodoc Spheres.

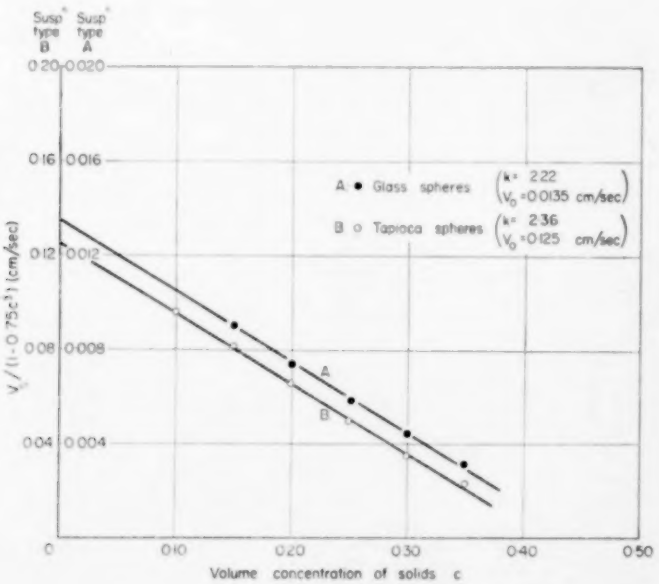

FIG. 7. Test of Equation (17) using Experimental data of STEINOUR.

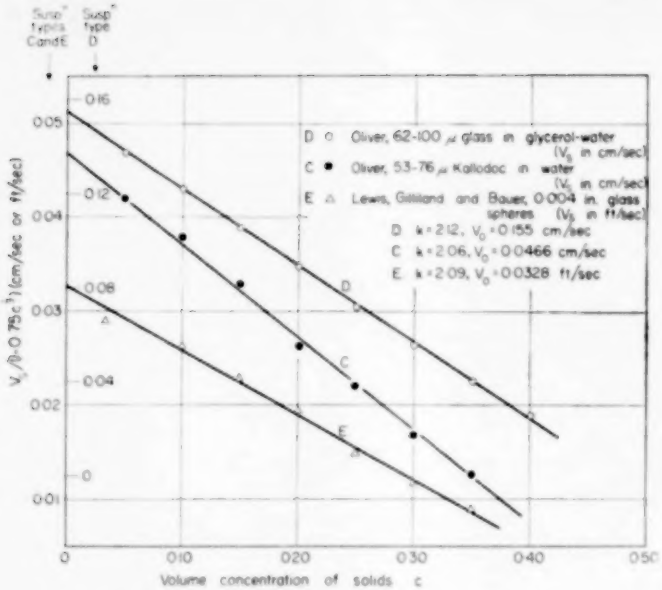

FIG. 8. Further tests of Equation (17).

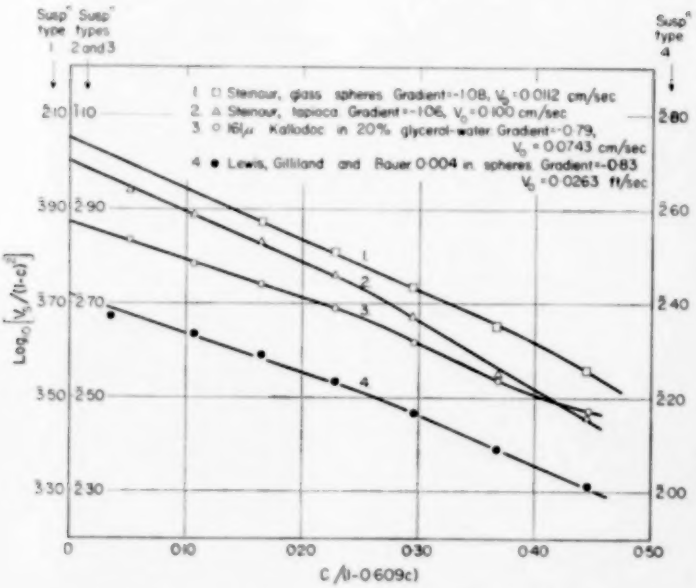

FIG. 9. Selected data plotted according to HAWKSLEY'S equation.

the above manner yielded the best straight line when a value of K equal to 0·75 was used. Fig. 6 shows the lines obtained for the three types of 161 μ Kallodoc suspensions, which on extrapolation to zero concentration give "Stokes velocities" of 0·262, 0·0935 and 0·0720 cm/sec respectively, compared with respective measured values of 0·261, 0·0943 and 0·0710 cm/sec. The corresponding values of the constant k are 2·16, 2·03 and 2·18.

Similar tests of equation (17) have been carried out using data from the literature, which is summarized in Table 4 and plotted in Figs. 7 and 8. Straight lines having gradients (k) between − 2·06 and − 2·36 were obtained. The extrapolated "Stokes velocities" have been compared with the approximate figures given in the original papers, and also with figures obtained by the extrapolation of lines plotted according to HAWKSLEY's equation [3], some of which are

Table 4. Absolute settling velocities as function of volume concentration

A *Stokes velocity, air permeability method* 0·0156 cm/sec		*B* *Stokes velocity, direct measurement* 0·119 cm/sec		*C* *Stokes velocity, calculated* 0·044 cm/sec		*D* *Stokes velocity, calculated* 0·0164 cm/sec		*E* *Stokes velocity, from quoted friction factors* 0·994 cm/sec	
c	V_s (cm/sec)	c	V_s (cm/sec)	c	V_s (cm/sec)	c	V_s (cm/sec)	c	V_s (cm/sec)
0·15	0·0054	0·074	0·0716	0·05	0·0304	0·05	0·0998	0·034	0·667
0·20	0·0041	0·078	0·0687	0·10	0·0248	0·10	0·0802	0·100	0·536
0·25	0·0031	0·106	0·0612	0·15	0·0198	0·15	0·0639	0·149	0·433
0·30	0·0021	0·110	0·0596	0·20	0·0153	0·20	0·0500	0·199	0·338
0·35	0·0015	0·215	0·0332	0·25	0·0115	0·25	0·0379	0·248	0·256
		0·268	0·0226	0·30	0·0083	0·30	0·0278	0·298	0·184
		0·273	0·0210	0·35	0·0060	0·35	0·0191	0·348	0·132
		0·309	0·0159						
		0·335	0·0120						
		0·359	0·0109						
		0·386	0·0087						

Sources of data are:
A. STEINOUR [2]; Glass spheres.
B. STEINOUR [2]; Tapioca spheres.
C. OLIVER [16]; 53–76 μ Kallodoc in water.
D. OLIVER [16]; 62–100 μ Glass spheres in glycerol–water.
E. LEWIS *et al.* [14]; 0·004 in. dia. glass particles.

Table 5. Values of Stokes velocity

Suspension type	*Stokes velocity* (cm/sec)			
	Measured	*Calculated*	*Extrapolation of plot based on equation* (17)	*Extrapolation of Hawksley plot*
A	0·0156	—	0·0135	0·0112
B	0·119	—	0·125	0·100
C	—	0·044	0·0466	0·038
D	—	0·164	0·155	0·123
E	—	0·994	1·000	0·802

Suspension types are as listed under Table 4.

shown in Fig. 9. Most of these plots gave straight lines in the lower concentration regions, and in some cases the gradients were close to the theoretical values of $-1{\cdot}09$.* The extrapolated "Stokes velocities," however, are all low, as illustrated in Table 3. This appears to confirm the indication of Fig. 5 that the Hawksley equation underestimates the effect of concentration on settling velocity in the low concentration region. Equation (17), however, yields extrapolated Stokes velocities which are in fair agreement with the approximately-known figures, an agreement which is surprising in view of the diversity of method by which these figures were obtained.

Discussion

Equation (14), in the form $V_P = V_0 (1 - 1{\cdot}5\, a/R)$, makes interesting comparison with the Ladenburg relationship [17] $V_P = V_0 (1 - 2{\cdot}4\, a/R')$ connecting the rate of fall, V_P, of a single sphere within a cylindrical vessel of radius, R', and the Stokes velocity, V_0. The equations are of similar form, but the radius R of a hypothetical cylinder in equation (14) is replaced by the vessel radius R' in the Ladenburg equation. The constant terms are different, however, which is not unreasonable in view of the fact that the liquid velocity must equal zero at $r = R$ in the Ladenburg case whereas no such restriction exists in the present analysis. In effect, the rigid cylinder inhibits the return flow of liquid, thus the velocity of the sphere is reduced to a greater extent in the former case. The main feature of the equations, however, is that they show the settling velocity to be a function of a ratio of the type a/R and not a linear function of the solids concentration c.* This is at variance with the conclusions of several workers [2, 3, 10]

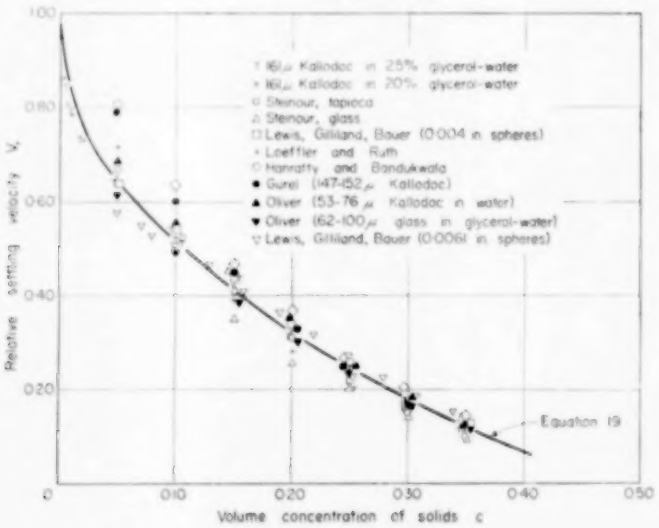

Fig. 10. Comparison of Equation (19) with existing experimental data.

The mean value of the constant k given by Figs. 6, 7 and 8 is 2·15; thus equation (17) may be written

$$V_r = \frac{V_s}{V_0} = (1 - 0{\cdot}75\, c^{1/3})(1 - 2{\cdot}15\, c) \quad (19)$$

This relationship is plotted in Fig. 10, together with the experimental data previously quoted.

*Equal to $\frac{2{\cdot}5}{\log_e 10}$ (see equation 3).

*For small values of a/R.

regarding the effects of "return flow," but provides for a much more realistic relationship between settling velocity and volume concentration for low values of the concentration.

The study of suspensions at very low solids concentrations showed the existence of a form of differential settling associated with particle distribution rather than with differences between Stokes velocities. When the suspensions were observed through a low-powered telescope, it was apparent that individual particles did not settle uniformly at the mean rate but were either accelerated by the close proximity of other particles or else held almost stationary in upward-flowing liquid. Sometimes large groups of particles formed in the suspension and moved rapidly downwards, causing visible upward motion in other parts of the vessel. Despite these local irregularities, however, the upper solid level fell uniformly at a reproducible rate.

It is clear that transient differential settling of the above type must also occur for exactly equi-sized particles; thus apart from having a fixed Stokes velocity such particles may be less helpful in sedimentation measurements than had been anticipated. The ratio between the Stokes velocity of a sphere and the settling velocity of the same sphere close to an identical sphere in an infinite medium is of the order 0·7 [18, 19] thus it seems reasonable to assume that transient differential settling should predominate over continuous differential settling (based on size difference) until a size ratio of about $(0{\cdot}7)^{-0{\cdot}5} = 1{\cdot}2$ is reached. For spheres of wider size range continuous differential settling is dominant and the solid level is difficult to follow at low concentrations. At higher concentrations, however, the behaviour may not differ greatly from that of closely-sized spheres; Fig. 8 includes information for spheres of size-ratio 1·4 and 1·6 which is in excellent agreement with results for closely sized spheres. This suggests that some of the variation of relative settling velocity with size ratio reported in the past [11, 16] might be due to the uncertain nature of the Stokes velocity for wide size-range particles.

The experimental value of 0·75 for the constant K in equation (17) also suggests non-uniformity in the particle distribution. By assuming a simple cubic distribution of particles and a "radius of action" equal to half the particle separation, a theoretical value for K of 1·85 may be obtained. In practice, therefore, the particles settle faster than is indicated by the simple theory, a possible reason for which is that a typical particle in a random distribution is nearer to its neighbour than a corresponding particle in a cubic distribution. The upward-flowing liquid is able to select channels of least resistance through which to flow; thus the particles move more freely downwards. Although this situation differs from that envisaged by the theory, a measure of agreement between theory and practice may be anticipated if the nature of the particle distribution is not concentration-dependent. The presence of cohesive forces between the particles, for instance, could readily alter the form of the settling velocity-concentration relationship. The value of the constant K therefore seems to depend on the nature of the particle distribution. Sedimentation tests show the value of the constant k to be between 2·03 and 2·36, compared with 2·50 from viscometric methods. In view of the different conditions obtaining in each case and in particular the absence of collisions during sedimentation, the agreement is quite reasonable.

Acknowledgments—The author is indebted to Dr. V. G. Jenson for his assistance in formulating the theory, and also to Professor F. H. Garner and Dr. G. F. Eveson for their invaluable help and criticism.

Notation

a = radius of typical spherical particle
c = volume concentration of solids in suspension
d = mean separation of sphere centres
k, K = constants
Q = axial volumetric flowrate of fluid through hypothetical cylinder of radius R surrounding sphere, at large distance from the sphere
Q' = axial volumetric flowrate of liquid through the same hypothetical cylinder, in the plane through the centre of the sphere
r = distance from centre of sphere
R = radius of hypothetical cylinder with vertical axis, surrounding typical sphere
R' = radius of cylindrical vessel
U = maximum upward velocity of liquid in spaces between falling particles of suspension

$\bar{U}$ = average upward velocity of liquid in settling suspension
V_A = Upward drift velocity of contents of hypothetical cylinder, when the upward flow Q–Q' is added to that already present
V_0 = Stokes velocity of typical spherical particle
V_P = settling velocity of particles allowing only for "return flow" of liquid
V_s = settling velocity of suspension
V_r = relative settling velocity of suspension, V_s/V_0
θ = angle between radius vector and direction of flow of liquid
λ_1, λ_2 = constants
μ_r = relative viscosity of suspension, i.e. $\frac{\text{viscosity of suspension}}{\text{viscosity of dispersing liquid}}$
ϕ = stream function for Stokes flow past single sphere

References

[1] Burgers, J. *Verh. Akad. Wet. Amst.* 1941 **44** 1045; 1942 **44** 1177; 1942 **45** 9.
[2] Steinour H. *Industr. Engng. Chem.* 1944 **36** 618.
[3] Hawksley P. G. W. *Some Aspects of Fluid Flow* p. 114 Edward Arnold, London 1951.
[4] Vand V. *J. Phys. Colloid. Chem.* 1948 **52** 277.
[5] Hanratty T. J. and Bandukwala *Amer. Inst. Chem. Engrs. J.* 1957 **3** 293.
[6] Brinkman H. *Research* 1949 **2** 190.
[7] Richardson J. F. and Zaki W. N. *Chem. Engng. Sci.* 1954 **3** 65.
[8] Richardson J. F. and Zaki W. N. *Trans. Inst. Chem. Engng.* 1954 **32** 35.
[9] Loeffler A. L. and Ruth B. F. *Amer. Inst. Chem. Engrs. J.* 1959 **5** 310.
[10] Kynch G. J. *Nature, (Lond.)* 1959 **184** 1311.
[11] Oliver D. R. *Nature, (Lond.)* 1960 **185** 912.
[12] Milne-Thomson L. M. *Theoretical Hydrodynamics* p. 524 Macmillan, London.
[13] Oliver D. R. and Ward S. G. *Nature, (Lond.)* 1953 **171** 396.
[14] Lewis W. K., Gilliland E. R. and Bauer W. C. *Industr. Engng. Chem.* 1949 **41** 1104.
[15] Gurel S. Ph.D. Thesis, Birmingham University 1951.
[16] Oliver D. R. Ph.D. Thesis, Birmingham University, 1954.
[17] Ladenburg R. *Ann. Phys. Lpz.* 1907 **22** 287; 1908 **23** 447.
[18] Eveson G. F., Hall E. W. and Ward S. G. *Brit. J. Appl. Phys.* 1959 **10** 43.
[19] Happel J. and Pfeffer R. *Amer. Inst. Chem. Engrs. J.* 1960 **6** 129.

VOL. 15 1961

Chemical Engineering Science, 1961, Vol. 15, pp. 243 to 250. Pergamon Press Ltd., London. Printed in Great Britain.

Interfacial resistance : diffusion into a laminar liquid-liquid jet

J. A. Quinn and P. G. Jeannin*
University of Illinois, Urbana, Illinois, U.S.A.

(*Received* 18 *July* 1960)

Abstract—Transient rates of diffusion through a liquid–liquid interface have been measured using a laminar jet. The system *iso*butanol–water at nominal contact times of 0·05 to 0·5 sec exhibits what appears to be a small interfacial resistance of approximately 80 sec/cm. Stability of the jet limits the variety of liquid pairs which can be studied. However, the method should prove useful in examining interfacial phenomena which accompany diffusion through the liquid–liquid interface.

Résumé—Les vitesses de diffusion à l'interface liquide–liquide ont été mesurées en utilisant un jet laminaire. Le système *iso*butanol-eau pour un temps de contact infime (de 0·050 à 0·5 sec) montre qu'il existe une petite résistance à l'interface d'environ 80 sec/cm. La stabilité du jet limite la variété des systèmes liquides qui peuvent être étudiés.

La méthode permet d'examiner les phénomènes d'interface qui accompagnent la diffusion.

Zusammenfassung—Die Diffusions-geschwindigkeiten durch eine Flüssigkeit/Flüssigkeit Grenzfläche wurden mit der Hilfe eines laminaren Strahles gemessen. Das System *iso*butanol/Wasser, mit einem nominalen Kontakt von 0,05–0,5 sec/cm, zeigt einen anscheinend kleinen Grenzflächenwiderstand von ungefähr 80 sec/cm. Die Stabilität des Strahles begrenzt die Mannigfaltigkeit der Flüssigkeitspaaren, die untersucht werden können. Trotzdem sollte die Methode in Untersuchungen von Grenzflächen-Erscheinungen die die Diffusion durch die Flüssigkeit/Flüssigäeit Grenzfläche begleiten, sehr nützlich angewendet werden.

Introduction

In calculations of interphase mass transfer it is usually assumed that chemical equilibrium exists at the interface and therefore the interface itself offers no resistance to the transfer. This assumption is purely a matter of convenience since a net transfer through the interface implies a non-equilibrium state. In several recent studies a variety of techniques have been used to measure the departure from equilibrium or an interfacial resistance. In particular, studies on the gas–liquid interface [1–3] indicate that equilibrium is very closely attained at a freshly-formed liquid surface within 0·001 sec and therefore any interfacial resistance in these systems is vanishingly small. However, at the liquid–liquid interface resistances of the order of 10^3 to 10^6 sec/cm have been reported [4, 5].

In the experiments of Lewis [6] and those of Blokker [4], several liquid systems were investigated with mechanical stirring in each phase. Values of the interfacial resistance were calculated from measured over-all mass transfer coefficients coupled with individual coefficients estimated from a semi-empirical equation proposed by Lewis. Blokker notes that deviations of as much as ± 50 per cent from the calculated coefficients can occur. The experiments with stirring are somewhat limited in that the flow field is not accurately defined and also interfacial resistances less than about 10^3 sec/cm cannot be detected.

Sinfelt and Drickamer [5] and Tung and Drickamer [7] measured resistances in aqueous and non-aqueous liquid pairs using radioactive tracers in a static diffusion cell. These measurements were quite precise ; however, the smallest detectable resistance was of the same order as in the stirring experiments. Also, in the one system studied by both Blokker and Drickamer, phenol–sulphuric acid–water, the former reports no surface resistance whereas the latter found

*Present address : 13 Avenue Lulli, Sceaux, Seine, France.

a resistance of 4×10^5 sec/cm. The difference in the results, as noted by BLOKKER, is probably due to the absence of interfacial turbulence in the tracer experiments.

The object of this present work was to develop a consistent technique for measuring interfacial resistances down to very low values, with the flow field and interface sharply defined.

Laminar jet

The laminar liquid jet has been used for studying transient rates of gas absorption [2, 3] and, more recently, in measuring surface ageing at liquid–liquid interfaces [8]. The jet has several distinct advantages for mass transfer studies in that the surface area can be accurately measured, small contact times can be achieved and the velocity distribution in the jet can be analysed. The diffusion calculations for a liquid–gas jet have been presented by SCRIVEN and PIGFORD [9] and the velocity distribution in a laminar liquid–liquid jet has been established by GARNER *et al.* [8].

The major experimental difficulty in using the liquid–liquid jet for diffusion measurements is the separation of the jet, intact, from the outer fluid. The jet receiver described below operated satisfactorily with no entrainment of the outer fluid or leakage of the jet.

EXPERIMENTAL

A diagram of the jet apparatus is shown in Fig. 1. Distilled, de-aerated water was used as the jet fluid and the jet chamber contained water-saturated *iso*butanol. The tubing throughout was glass except for some flexible joints of Tygon.

Precautions were taken to avoid any possible source of interface contamination. The *iso*-butanol was distilled in an all-glass apparatus and the only substances which it came in contact with were glass and the brass nozzle and receiver in the jet chamber. Also, the excellent reproducibility of the measured diffusion rates over a period of several months further supports the absence of any inadvertent contamination.

The jet flow rate was controlled by two stainless steel needle valves placed in series at the exit of the constant head tank. The flow rate was checked at frequent intervals during the course of a run by collecting the effluent from the receiver over a timed interval. The jet length and profile were measured with a cathetometer fitted with a travelling microscope.

The jet chamber was a 10 cm length of 7·62 cm inside diameter Pyrex pipe clamped between two brass flanges. The chamber itself was mounted on a sturdy, weighted platform which rested on a thick rubber mat. The chamber was sealed to the

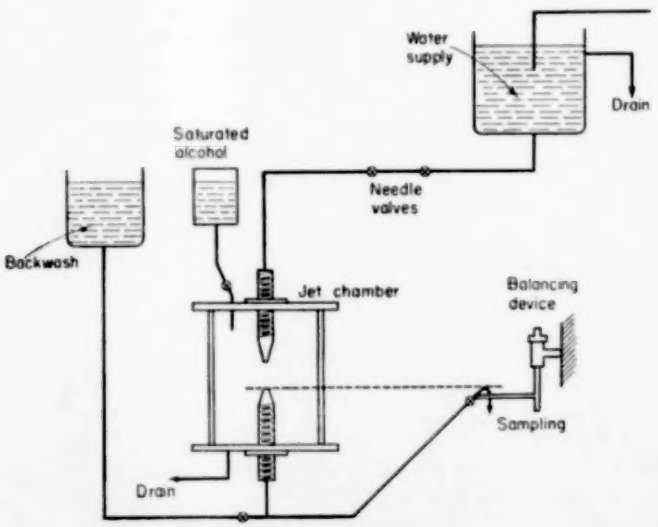

FIG. 1. Sketch of apparatus.

flanges with Neoprene gaskets; however, the *iso*butanol did not contact the gaskets because at all times there was a layer of water at the bottom of the chamber.

The brass nozzle and receiver, shown in Fig. 2, were screwed into the flanges such that the distance between them could be varied over a length of 6 cm. Both nozzle and receiver were tapered to a knife edge in order to minimize disturbance of the outer fluid. Experiments with dye injected into the chamber fluid indicated regular, laminar flow patterns with very little disturbance generated at the receiver. Several different receiver designs were tried and satisfactory operation was finally achieved by countersinking the entry of the receiver as shown in Fig. 2. In operation the jet expanded slightly at the receiver with the edge of the jet at the lip of the tapered portion. The jet was precisely balanced at the receiver by adjusting the level and the flow rate at the overflow valve (see Fig. 3. Note, the horizontal dimension is distorted by the refraction of the chamber liquid).

In starting a run, to prevent chamber fluid from entering the receiver until the jet was balanced, the overflow line was closed and water was forced up through the receiver. Then as flow through the nozzle commenced the back flow through the receiver was gradually diminished and the overflow valve opened until the jet was exactly balanced. During operation the *iso*-butanol layer extended from below the tapered portion of the receiver to the threaded part of the nozzle.

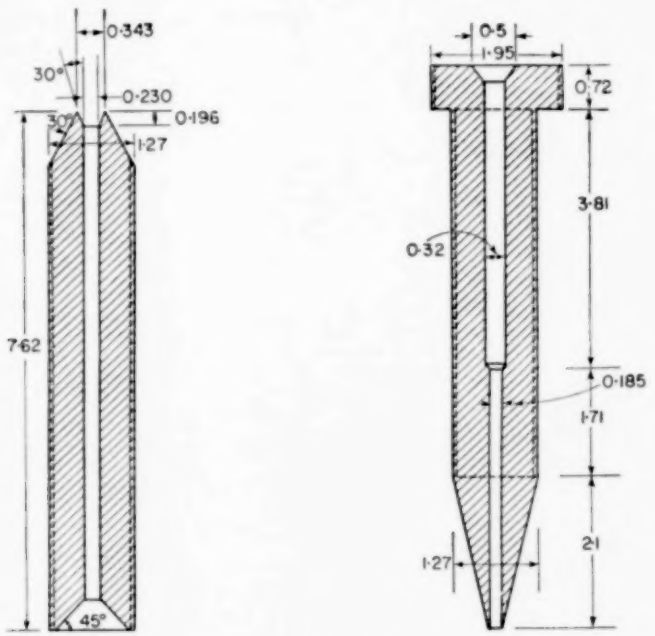

Fig. 2. Brass nozzle and receiver.

A light was focussed on the exit of the receiver and any leakage of chamber fluid could be detected rapidly. If the balanced was destroyed by jarring or vibration the discharge line was immediately flushed by forcing water back through the receiver. At most flow rates operation was quite stable and steady conditions could be maintained for a period of several hours.

The runs were made at a temperature of 25 ± 2°C. Samples of the jet were collected at the overflow valve and were analysed with a Zeiss interferometer having a cell length of 4 cm.

Concentrations ranged from 5 to 50 $\times$ 10^{-6} g moles *iso*butanol/cm^3 and in this interval the precision of the analysis was approximately 0·3 $\times$ 10^{-6} moles/cm^3.

Physical properties at 25°C

The distribution coefficient was taken as

$$m = 0{\cdot}115 \frac{\text{moles } iso\text{butanol/cm}^3 \text{ water phase}}{\text{moles } iso\text{butanol/cm}^3 \text{ alcohol phase}}$$

with a saturation solubility of 1·20 $\times$ 10^{-3} g moles *iso*butanol/cm^3 water in the water phase [10]. A viscosity of 3·27 c.p. was used for the saturated alcohol phase [10] and 0·894 c.p. for the jet. Values for the diffusivity of *n*-butanol in dilute solutions reported by Lyons and Sandquist [11] extrapolate smoothly to the results listed by Griffith [10] for *iso*butanol near saturation concentration. The variation of diffusivity with concentration is approximately linear with a value of 9·7 $\times$ 10^{-6} cm^2/sec at zero concentration and 6·3 $\times$ 10^{-6} at saturation.

Diffusion Calculations

A vertical liquid jet is subject to gravity and to surface forces such that its diameter decreases as it flows downwards, indicating a two-dimensional flow within the jet. In diffusion calculations for the jet, the flow in the immediate vicinity of the surface is of primary concern since the depth of penetration of absorbed molecules is extremely small. Absorption into a laminar jet with negligible drag at the surface has been thoroughly treated by Scriven and Pigford [9] and the analysis presented here is an approximate extension of these calculations to a liquid–liquid jet.

Neglecting axial diffusion, the steady state transport of the absorbed component is governed by the equation

$$u \frac{\partial C}{\partial x} + v \frac{\partial C}{\partial y} = D \frac{\partial^2 C}{\partial y^2} \qquad (1)$$

Assuming u to be essentially independent of y over a depth which is large compared to the penetration depth, u may be replaced by the interface velocity, u_s, and v by its equivalent from the continuity equation [9]. Equation (1) therefore becomes

$$u_s \frac{\partial C}{\partial x} - y \frac{du_s}{dx} \frac{\partial C}{\partial y} = D \frac{\partial^2 C}{\partial y^2} \qquad (2)$$

For the diffusing molecules the jet is effectively semi-infinite and therefore the following boundary conditions obtain:

$$C(o, y) = C(x, \infty) = Co \qquad (3)$$

$$C(x, o) = C^* \qquad (4)$$

where the origin of the co-ordinates is taken in the jet surface at the nozzle.

This set of equations has been solved by Scriven and Pigford [9], and the resulting rate of mass transfer into the jet is:

$$N(x) = (C^* - Co) \Big/ \sqrt{\frac{D}{\pi Z}} \qquad (5)$$

with

$$Z = \int_0^x \frac{Us\, dx}{Us^2} \qquad (6)$$

If the jet velocity were constant and equal to $4Q/\pi d_0^2$ the rate would be given by

$$N_i(x) = 2 \frac{(C^* - Co)}{\pi d_0} \sqrt{\frac{DQ}{x}} \qquad (7)$$

For a finite interfacial mass transfer coefficient, ks, equation (4) is replaced by

$$-D \frac{\partial C}{\partial y}\bigg|_{y=0} = ks\,[C^* - C(x, o)] \qquad (8)$$

The corresponding rate of mass transfer into a constant velocity jet becomes

$$N_i(x) = k_s (C^* - C_0) \exp\left[k_s^2 \left(\frac{\pi d_0^2 x}{4QD}\right)\right] \operatorname{erfc}\left[k_s \left(\frac{\pi d_0^2 x}{4QD}\right)^{1/2}\right] \qquad (9)$$

For each case the total rate of mass transfer into a jet of length L is given by:

$$\phi = \int_0^L \pi d(x)\, N(x)\, dx \qquad (10)$$

The interface velocity for a laminar liquid–liquid jet under conditions similar to this work has been studied theoretically and experimentally by Garner *et al.* [8] in connexion with their

VOL. 15 1961

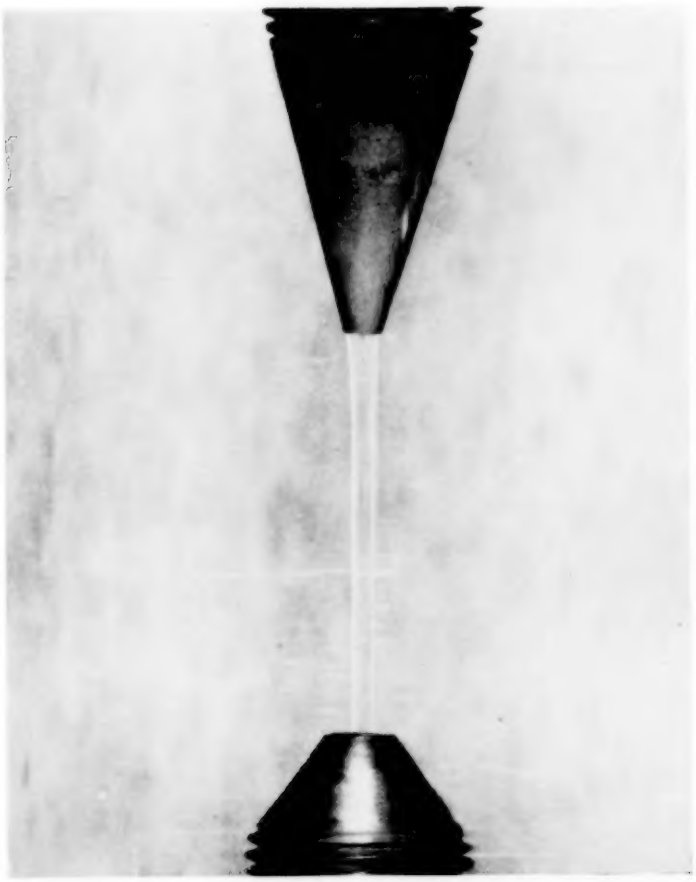

FIG. 3. Laminar jet.

recent experiments on surface ageing. Theoretically, they obtained the steady state velocity distribution for an infinitely long, cylindrical jet (of constant diameter) moving in an outer fluid which is bounded by a cylindrical container. They then considered each horizontal lamina of the contracting jet as being part of a cylindrical jet and calculated the velocity distribution, which was parabolic, at each point of the jet from the measured jet profile. Their equation for the interface velocity may be expressed as

$$u_s = \beta \bar{u} \tag{11}$$

$$\text{with } \beta = \frac{4\mu_2}{\gamma \mu_1 + 4\mu_2} \tag{12}$$

$$\text{and } \gamma = \frac{R^4 - 4R^2 + 3 + 4 \ln R}{R^4 \ln R - R^4 + 2R^2 - \ln R - 1} \tag{13}$$

where R represents the ratio of chamber to jet diameter. Velocity distributions were determined experimentally [8] by a photographic technique and excellent agreement was obtained with the theoretical results except at points within 1 mm from the tip of the nozzle.

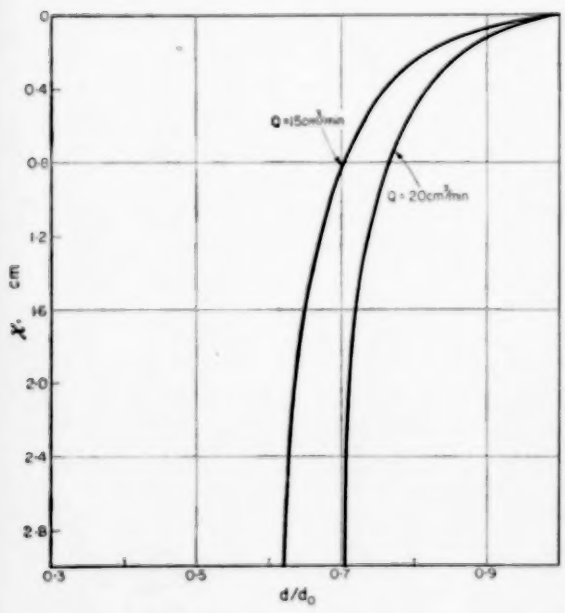

Fig. 4. Measured jet profiles. $d_0 = 0{\cdot}185$ cm.

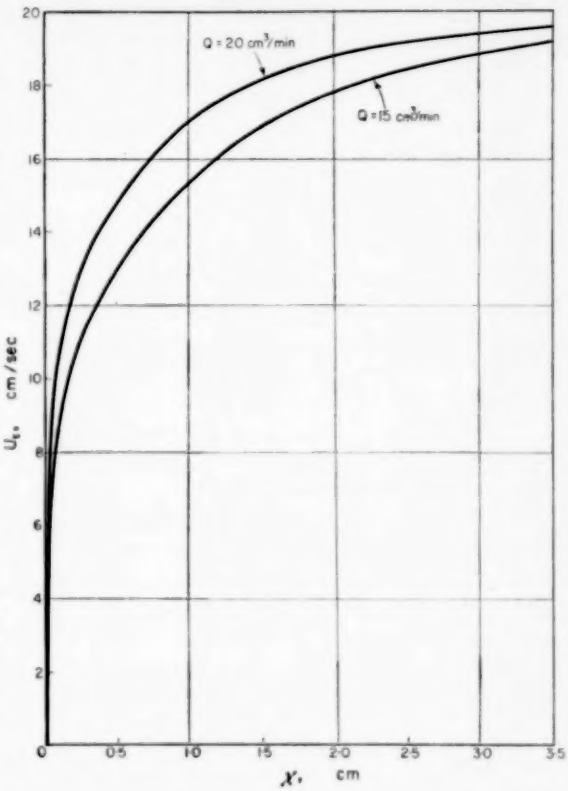

Fig. 5. Calculated interfacial velocities vs. jet length.

Results

Experiments were carried out at two flow rates, 15 and 20 cm³/min, over jet lengths of 0·5 to 5 cm. These combinations of flow rates and jet lengths represented the approximate range of stable operation for the jet. The measured jet profiles are shown in Fig. 4 and the corresponding calculated interface velocities have been plotted in Fig. 5. Equation (11) was used to calculate u_s for all points on the jet up to 1 mm from the nozzle; over the remaining interval u_s was extrapolated parabolically to zero velocity at the nozzle. The ratio of interface to average velocity, β, was practically constant over the entire jet length, having extreme values of 0·73 and 0·78. The constancy of β resulted from the large ratio of chamber to jet diameter.

The measured diffusion rates are shown in Fig. 6 along with the predicted rates for interfacial

equilibrium and for an interfacial mass transfer coefficient of 0·012 cm/sec. The dashed line of Fig. 6 represents the mass transfer rate predicted for a constant velocity jet ($Q = 20$) using equation (7). For simplicity, the interfacial resistance curves were calculated from equation (9), i.e., for constant velocity jet. Each of the experimental points represents the average of at least three-different runs, in some cases as many as ten, with several jet samples taken during each run. The standard deviation of the points was less than 5 per cent except at the minimum and maximum lengths where it was 6–8 per cent. The agreement of the experimental points with the rates predicted for a finite transfer coefficient indicate a definitely measurable departure from equilibrium at the interface.

In the experiments of LEWIS [6] and BLOKKER [4] no interfacial resistance was detected for the *iso*butanol–water system. The present results do not contradict their findings since the interfacial resistance observed here, 80 sec/cm, is an order of magnitude smaller than the minimum resistance that could be detected in the stirring experiments.

In the calculated rates the diffusivity of *iso*butanol in water was taken as $7{\cdot}4 \times 10^{-6}$ cm²/sec. This value was selected on the basis of a numerical solution to the diffusion equation with concentration dependent diffusivity listed by CRANK [12]. Actually, the calculations are not particularly sensitive to the diffusivity since it enters only as the square root and the error introduced by using a constant, average value is small [13].

The length of the jet was taken as the vertical distance from the nozzle to the tip of the receiver. No correction was made for the interfacial area created by the expansion of the jet at the receiver. The only jet length at which this additional area could have an appreciable effect on the absorption rate would be at the shortest length, 0·5 cm. Assuming that the skin of the jet expanded to the lip of the receiver, the additional area would increase the diffusion rate by an amount equivalent to lengthening the 0·5 cm jet approximately 10 per cent. It did not appear that the skin of the jet expanded, but rather that the jet entered the receiver intact and that the water in the countersunk portion of the receiver was relatively stagnant. The points at 0·5 cm, Fig. 6, are slightly higher than the predicted curve and this may be due to an end effect at the receiver.

In the calculations it is assumed that the liquid in the chamber, the alcohol phase, is saturated. Therefore, the transfer is unidirectional and the diffusional resistance occurs at the interface and in the jet phase. In the actual experiment there is some uncertainty as to the disposal of the water originally present in the chamber phase. Two possibilities exist: water from the chamber phase diffuses along with the alcohol into the jet, or, less likely, the alcohol phase adjacent to the interface becomes supersaturated. If supersaturation occurs, the water would eventually diffuse into the water layer at the bottom of the chamber. Experiments were carried out in which pure alcohol was placed in the chamber and only a few cm³ of water leaked into the chamber during the initial balancing of the jet. The results were the same as those with saturated alcohol in the chamber, indicating that sufficient water had diffused from the jet to saturate the interface or that if the interface were slightly unsaturated it had no measurable effect on the rate of diffusion.

Surface-active agents

A series of runs was made at a jet length of 2 cm and a flow rate of 20 cm³/min with a surface-active agent added to the *iso*butanol-water system. The surface-active agent used was polyoxyethylene sorbitan monolaurate, marketed by the Atlas Powder Company under the trade name Tween 20.

A concentration of 1 cm³ surface-active agent/l. of jet phase was used and the alcohol placed in the chamber was previously saturated with the jet phase. Within the precision of the analysis no difference was detected between the runs with and without the surface-active agent*. SINFELT and DRICKAMER [5] also report that the addition

*Further studies on systems in which surface-active agents show a pronounced effect are currently being carried out with the liquid–liquid jet. These results will be published in the future.

of Tween 20 had no effect in the systems which they investigated.

The present results may be explained if, as suggested by BOYE-CHRISTENSEN and TERJESEN [14], the action of surface-active agents on interphase mass transfer is of a hydrodynamic nature. water in *iso*butanol jet is not affected by the presence of surface-active agents the flow pattern remains constant.

An alternate explanation is that the contact times in the jet experiments were too small to exhibit a surface effect. The calculated surface

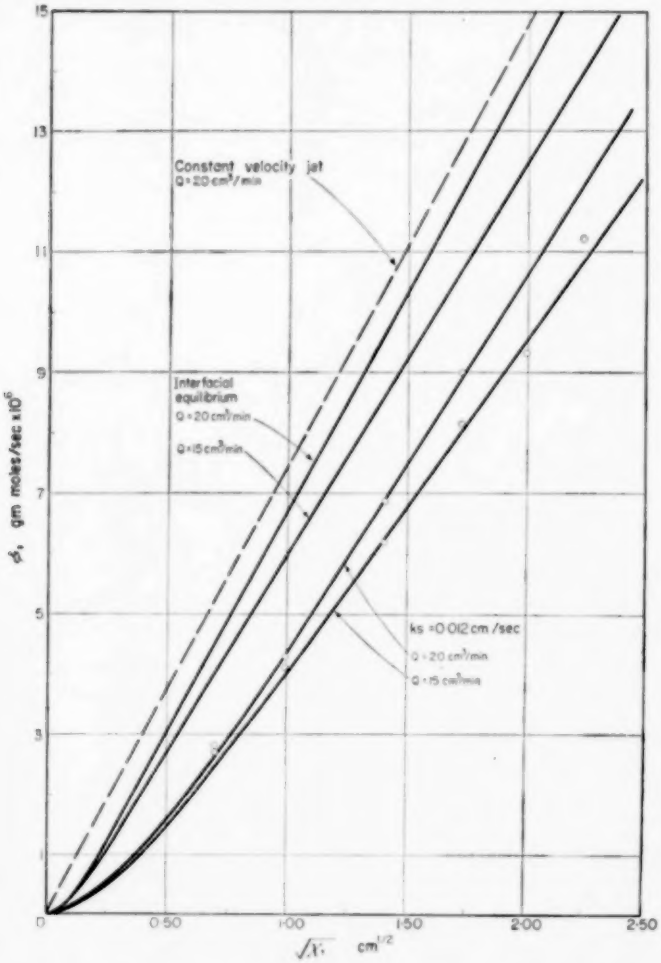

FIG. 6. Rate of mass transfer vs. square root of jet length. Diffusion of *iso*butanol into water jet at 25°C.

The interfacial tension of the *iso*butanol–water system is very small, approximately 2 dyn/cm, and therefore adding a surface-active agent can not greatly alter the tension. In the present experiments the flow pattern in the jet is determined by the jet profile and since the profile of a age of the 2 cm jet was about 1·5 sec. With the complex agent used here it is highly probable that there was not time for sufficient surface-active molecules to diffuse into the interface to alter the interfacial properties. This explanation is supported by absorption work [1] where

stationary liquids containing surface-active agents have been shown to exhibit an interfacial resistance.

Acknowledgment—Acknowledgment is made to the donors of the Petroleum Research Fund, administered by the American Chemical Society, for partial support of this research. A fellowship received by P. G. JEANNIN from the Direction Générale des Affaires Culturelles et Techniques is also gratefully acknowledged.

NOTATION

C = solute concentration in aqueous phase, g mole/cm^3
C^* = equilibrium concentration in aqueous phase, g moles/cm^3
C_0 = initial concentration in aqueous phase, g moles/cm^3
d = jet diameter, cm
d_0 = nozzle diameter, cm
D = diffusivity in aqueous phase, cm^2/sec
k_s = interfacial mass transfer coefficient, cm/sec
m = distribution coefficient
N = local mass transfer rate, g moles/cm^2 sec
N_i = mass transfer rate for constant velocity jet, g moles/cm^2 sec
R = ratio of chamber to jet diameter
Q = jet flow rate, cm^3/min
u = axial velocity component, cm/sec
$\bar{u}$ = mean jet velocity, cm/sec
u_s = interfacial velocity, cm/sec
v = radial velocity component, cm/sec
x = axial co-ordinate, cm
y = radial co-ordinate, cm
Z = defined by equation (6), sec
β = ratio of interfacial to mean jet velocity
μ_1 = chamber phase viscosity, g/cm sec
μ_2 = jet viscosity, g/cm sec
ϕ = total mass transfer rate, g moles/sec

REFERENCES

[1] HARVEY E. A. and SMITH W. *Chem. Engng. Sci.* 1959 **10** 274.
[2] RAIMONDI P. and TOOR H. L. *Amer. Inst. Chem. Engrs. J.* 1959 **5** 86.
[3] SCRIVEN L. E. and PIGFORD R. L. *Amer. Inst. Chem. Engrs. J.* 1958 **4** 439.
[4] BLOKKER P. C. *Proc. 2nd Int. Congr. Surf. Activity* Vol. 1, p. 503, Academic Press, New York, 1957
[5] SINFELT J. H. and DRICKAMER H. G. *J. Chem. Phys.* 1955 **23** 1095.
[6] LEWIS J. B. *Chem. Engng. Sci.* 1954 **3** 248.
[7] TUNG L. H. and DRICKAMER H. G. *J. Chem. Phys.* 1952 **20** 10.
[8] GARNER, F. H. MINA P. and JENSON V. G. *Trans. Faraday Soc.* 1959 **55** 1627.
[9] SCRIVEN L. E. and PIGFORD R. L. *Amer. Inst. Chem. Engrs. J.* 1959 **5** 397.
[10] GRIFFITH R. M. Ph.D. Thesis in Chemical Engineering University of Wisconsin, Madison 1958.
[11] LYONS M. S. and SANDQUIST C. L. *J. Amer. Chem. Soc.* 1953 **75** 3896.
[12] CRANK J. *The Mathematics of Diffusion* p. 150 Oxford University Press, London 1956.
[13] JEANNIN P. G., M.S. Thesis University of Illinois, Urbana 1960.
[14] BOYE-CHRISTENSEN G. and TERJESEN S. G. *Chem. Engng. Sci.* 1959 **9** 238.

Chemical Engineering Science, 1961, Vol. 15, pp. 251 to 254. Pergamon Press Ltd., London. Printed in Great Britain.

Molecular diffusion and liquid–liquid mass transfer in stirred transfer cells

W. J. McMANAMEY

Chemical Engineering Department, University of Sydney, New South Wales, Australia

(*First received* 8 *August* 1960; *in revised form* 26 *October* 1960)

Abstract—Two stirred transfer cells were used for studying the rate of mass transfer across an interface between two liquid phases, in order to investigate the influence of molecular diffusion on the mass transfer. The systems ethyl acetate–water and *n*-butanol–water at 25 °C provided a wide range of diffusion values. The relationship between mass transfer coefficients and the variables was obtained by dimensional analysis. The comparison of observed and calculated results shows that the difference is not significant. A new turbulent transfer hypothesis is suggested. The concept of additivity of film resistances seems to be valid for the transfer of the solutes studied between water and *iso*-butanol.

Résumé—On utilise deux cellules de transfert agitées pour déterminer la vitesse d'échange massique à travers l'interface de 2 phases liquides, en vue d'étudier l'influence de la diffusion moléculaire sur le transfert de masse. Les systèmes acétate d'éthyle – eau et *n*-buthanol – eau à 25 °C fournissent un large faisceau de valeurs numériques concernant la diffusion. La relation entre les coefficients de transfert de masse et les variables est obtenue à partir de l'analyse dimentionnelle. La comparaison des résultats observés et calculés montre que la différence est insignifiante. On propose une nouvelle hypothèse pour les échanges en milieu turbulent. Le concept d'additivité des résistances de film semple être valable pour le transfert des solutés étudiés entre l'eau et l'*iso*-buthanol.

Zusammenfassung—Rührtransferzellen waren benutzt bei den Untersuchungen Massentransfer – Geschwindigkeit über eine Grenzfläche zwischen zwei Flüssigkeitphasen um den Einfluss der molekularen Diffusion auf den Massentransfer zu studieren. Ethylazetat – Wasser und *n*-Butanol – Wasser um 25 °C lieferten eine grosse Anzahl von Diffusionswerten. Der Zusammenhang Zwischen Massentransfer-Koeffizienten und Variablen war mit der Hilfe von Dimensionsanalyse erhalten. Der Vergleich zwischen den beobachteten und kalkulierten Werten zeigt keine wesentliche Abweichung. Eine neue Turbulenztransfer Hypothese ist vorgeschlagen. Der Begriff der Addierbarkeit von Filmwiderständen scheint gültig zu sein für den Massentransfer zwischen Wasser und *iso*-Butanol.

THE stirred transfer cell [1, 2] is a convenient apparatus for studying the rate of mass transfer across an interface of known area between two liquid phases. However there is a lack of agreement about the influence of molecular diffusion on the mass transfer process in this apparatus. LEWIS [1] obtained a correlation for the individual phase mass transfer coefficients (determined by the method of COLBURN and WELSH [3]) which did not include the molecular diffusion coefficient (D) and suggested that the mass transfer process is entirely controlled by eddy diffusion, while GORDON and SHERWOOD [2] concluded from a study of the transfer of a number of solutes between water and *iso*-butanol that the mass transfer coefficients depended on $D^{0.5}$, as the penetration theory predicts.

An interpretation satisfying both sets of results is presented here. Also, individual mass transfer coefficients were determined by the COLBURN–WELSH technique in a transfer cell which was, in some respects, a compromise between the types of LEWIS and GORDON and SHERWOOD, having a contra-rotating stirrer (similar to LEWIS') but but not a baffle round the wall at the liquid–liquid interface. Two stirrer units were used, one made entirely from brass and the other having all parts of the unit in contact with the liquids made from glass. The systems studied were ethyl acetate – water and *n*-butanol – water at

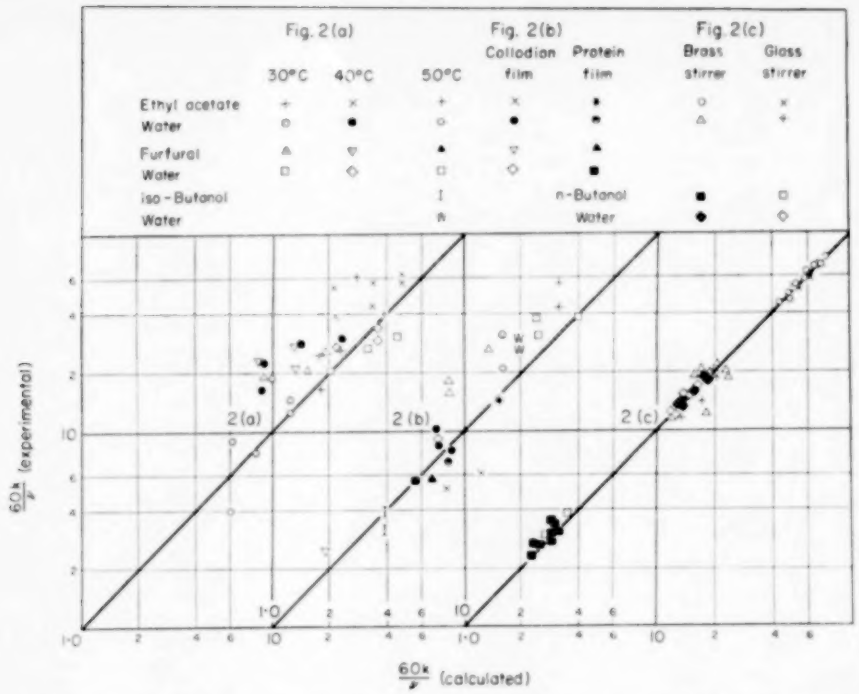

FIG. 1. Comparison of LEWIS' results at 20°C with values calculated from equation (2).

25°C, as these provide a wide range of diffusion coefficient values and Schmidt numbers. Details of the experimental procedure and results are available on request to the author.

Because of the lack of knowledge of the hydrodynamic conditions at liquid–liquid interfaces the relationship between the mass transfer coefficients and the variables which affect them was obtained by dimensional analysis. Examination of LEWIS' results showed that $60k_1$ was proportional to $(Re_1)^{0.9}$ for constant values of Re_2/Re_1 and that a linear relationship existed between $60k_1/(Re_1)^{0.9}$ and Re_2/Re_1. So, including k_1 in a dimensionless mass transfer group,

$$\frac{60k_1d}{\nu_1} = \left(\frac{\alpha_1 d}{\nu_1}\right)(Re_1)^{0.9}\left(1 + \beta_1\frac{Re_2}{Re_1}\right) \qquad (1)$$

The values of β_1 agreed closely with η_2/η_1 and α_1/ν_1 was proportional to $(Sc_1)^{-0.3}$, except for the furfural phase in the furfural – water system (which also did not fit LEWIS' original correlation). The deviation of the furfural phase results from these correlations could be caused by differences in either the method of purification or length of storage between the samples used for determining the equilibrium solubilities and mass transfer rates as HENTY [4] found these factors affected the solubility relationships in systems containing furfural. The final correlation was

$$\frac{60k_1\delta}{\nu_1} = 0.0384\,(Sc_1)^{-0.3}\,(Re_1)^{0.9}\left(1 + \frac{\eta_2 Re_2}{\eta_1 Re_1}\right) \qquad (2)$$

(d, the characteristic dimension, which appears on both sides of equation (1) has been discarded, and the numerical constant has the unit cm^{-1}). Values of $60k_1/\nu_1$ calculated from this expression are compared with LEWIS' results in Figs. 1 and 2. The correlation coefficients (which provide a numerical estimation of the goodness of fit of a line) for the calculated values with the experimental results are 0·910 for equation (2) and 0·863 for LEWIS' correlation. Mass transfer coefficients determined by LEWIS with rigid films of protein or collodion at the liquid–liquid interface were correlated by omitting from equation (2) the group $(\eta_2 Re_2/\eta_1 Re_1)$, which

represents the turbulence "transferred" from the other phase, and Fig. 2 (b) shows good agreement between the experimental and calculated values.

The correlation for the results obtained in this work was

$$\frac{60\,k_1}{v_1} = \alpha\,(\mathrm{Sc}_1)^{-0.37}\,(\mathrm{Re}_1)^{0.9}\left(1 + \frac{\eta_2\,\mathrm{Re}_2}{\eta_1\,\mathrm{Re}_1}\right) \qquad (3)$$

where α is 0·102 cm^{-1} and 0·0861 cm^{-1} for the brass and glass stirrer units, respectively (Fig. 2 (c)). The Schmidt number exponents for both these transfer cells are lower than the values predicted by the theories which assume stagnant or laminar flow conditions in the boundary layer during mass transfer, thus suggesting that turbulent conditions exist in the boundary layer. The lower numerical value of the Schmidt number exponent for LEWIS' transfer cell is in accord with this hypothesis, as the baffle round its wall prevents the phases coming into contact in this region where their turbulence at the interface would not be as great as it is further away from the wall; in consequence, the region of mass transfer in LEWIS' transfer cell is more turbulent than in the other. In the range of stirring speeds studied there seemed to be no variation in the Schmidt number exponent; however, in a subsequent investigation into the liquid–liquid mass transfer of some coloured metal nitrates, stationary layers formed at the interface at Reynolds numbers below 500 in both phases and a very much reduced mass transfer rate was then found.

For the transfer of a solute between water and *iso*-butanol, if k_1 is proportional to D_1^n when the physical properties and stirring speeds of the phases are unchanged, then [2],

$$\frac{1}{K_W}\left(\frac{D_{SW}}{D_{IW}}\right)^n = \frac{1}{k_{IW}} + \frac{1}{mk_{WI}}\left(\frac{D_{SW}\,D_{WI}}{D_{IW}\,D_{SI}}\right)^n \qquad (4)$$

GORDON and SHERWOOD assumed that n was 0·5, but the correlation obtained in this work, using a similar cell, suggests an exponent of 0·37. To decide which of these provides the better representation of the experimental results the intercepts and slopes of the best straight lines relating $(1/K_W)$ $(D_{SW}/D_{IW})^{0.5}$ and $(1/K_W)$ $(D_{SW}/D_{IW})^{0.37}$ with $1/m$ were determined by the least squares method and the correlation coefficients of these lines found. From these intercepts and slopes the values of k_{IW} and k_{WI} given in Table 1 were calculated*. The experimental results given in this Table were determined by GORDON and SHERWOOD from measurements of the rates of mutual saturation of water and *iso*-butanol. Both values of n gave the same correlation coefficient (0·9992). The statistical "t-test" was applied to the differences between the calculated k's and also the difference between each calculated k and the experimental results; in no case was the difference significant at the 1 per cent probability level. The high correlation coefficients show that the concept of the additivity of film resistances, on which equation (4) is based,

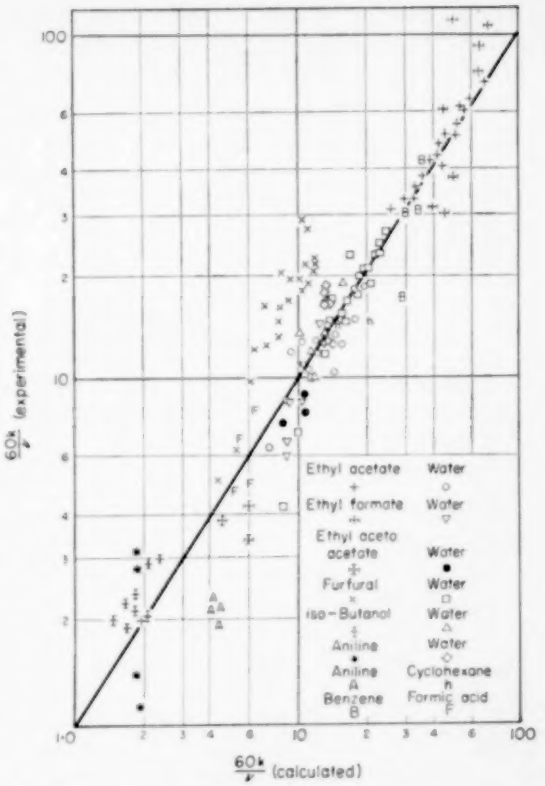

FIG. 2. Comparison of observed and calculated results.

*k_{IW} was calculated from the experimental K_W values for $1/m$ less than 2.

is valid (for the transfer of the solutes studied between water and *iso*-butanol) and the lack of significant difference between the calculated k values indicates that the experimental results are also satisfactorily correlated by $n = 0.37$.

Table 1. *Measured and calculated* k_{IW} *and* k_{WI} *values for the transfer of solutes between water and* iso-*butanol*

Source	k_{IW} (cm/hr)	k_{WI} (cm/hr)
Calculated, $n = 0.5$	8·9	5·7
Calculated, $n = 0.37$	9·1	5·6
Experimental	8·4	5·9

The turbulent transfer hypothesis suggested above is similar to that proposed by KISHINEVSKY and PAMFILOV [5] for the liquid phase in gas–liquid mass transfer, and to PRATT's "free surface diffusion theory" [6], the main difference from the latter being the retention of the molecular diffusion coefficient. A possible justification for this is that the mixing of the material in a turbulent eddy with the main body of the phase is ultimately a molecular process. Quantitatively, the transfer cell correlations suggest that the diffusion coefficient's exponent lies in the range 0·3–0·4 for mass transfer between turbulent liquid phases. The effect of eddy diffusion will be less significant in liquid phases with a very low degree of turbulence. Examples are the continuous phase for mass transfer with drops, where GARNER *et al.* [7] found the diffusion coefficient's exponent was 0·58, and the core liquid in wetted-wall columns, for which a correlation containing $(D)^{0.67}$ was developed by MURDOCH and PRATT [8].

Note added in proof: MAYER (Ph.D. Thesis, University of Cambridge, 1959) has correlated LEWIS' results with a maximum deviation of 40% by the expression

$$\frac{k_1 d}{D_1} = \beta (Sc_1)^{5/6} (Re_1 Re_2)^{0.5}$$

where β is a function of η_2/η_1. In this expression the viscosity of the second phase does not cancel out, which is an objectionable feature of equations (2) and (3). On the other hand correlation of the results of GORDON and SHERWOOD seems to require a higher exponent on D than 1/6.

Acknowledgments—The author wishes to thank Professor T. G. HUNTER for his advice and encouragement, and Dr. H. R. C. PRATT for his helpful comments on the Ph.D. thesis, of which this work was a part.

NOTATION

D	= molecular diffusion coefficient	cm²/sec
d	= characteristic dimension	cm
k	= individual mass transfer coefficient	cm/sec or cm/hr
K	= over-all mass transfer coefficient	cm/sec or cm/hr
L	= length of stirrer	cm
m	= distribution coefficient	
Re	= Reynolds number	$L^2 s/\nu$
Sc	= Schmidt number	ν/D
s	= stirring speed in transfer cell	rev/sec
α, β	= constants	
η	= dynamic viscosity	g/sec cm
ν	= kinematic viscosity	cm²/sec

subscripts

IW	= *iso*-butanol in water phase
SW	= solute in water phase
WI	= water in *iso*-butanol phase
SI	= solute in *iso*-butanol phase
1	= phase under consideration
2	= other phase

REFERENCES

[1] LEWIS J. B. A.E.R.E. CE/R 1118, Harwell 1954; *Chem. Engng. Sci.* 1955 **3** 248.
[2] GORDON K. F. and SHERWOOD T. K. *Chem. Engng. Progr.* 1954 **50** Symposium Series No. 10, p. 15.
[3] COLBURN A. P. and WELSH D. G. *Trans. Amer. Inst. Chem. Engrs.* 1942 **38** 179.
[4] HENTY C. J. Ph.D. Thesis, University of Sydney 1955.
[5] KISHINEVSKY M. K. and PAMFILOV A. V. *Zh. prikl. khim.* 1949 **22** 1173; KISHINEVSKY M. K. *Ibid.* 1954 **27** 382.
[6] PRATT H. R. C. *Industr. Chem.* 1955 **31** 63.
[7] GARNER F. H., FOORD A. and TAYEBAN M. *J. Appl. Chem.* 1959 **9** 315.
[8] MURDOCH R. and PRATT H. R. C. *Trans. Instn. Chem. Engrs.* 1953 **31** 307.

Chemical Engineering Science, 1961, Vol. 15, pp. 255 to 259. Pergamon Press Ltd., London. Printed in Great Britain.

Chromatography of substances undergoing slow reversible chemical reactions

A. KLINKENBERG

Bataafse Internationale Petroleum Maatschappij (Royal Dutch/Shell Group) The Hague, Netherlands

(*Received* 20 *October* 1960; *in revised form* 26 *November* 1960)

Abstract—A theory is presented for band-widening in chromatography due to a slow reversible first/first order reaction of a constituent.

Résumé—Théorie sur l'étalement des plages chromatographiques dû à une réaction réversible lente d'ordre 1 pour un constituant.

Zusammenfassung—Es wird eine Theorie angegeben für die Bandverbreiterung bei der Chromatografie, die durch eine reversible Reaktion (jeweils 1. Ordnung) eines Konstituenten verursacht wird.

INTRODUCTION

AT THE recent Symposium on Gas Chromatography (Edinburgh, June 1960) PHILLIPS and OWENS [1] presented data on the separation of a mixture of Cl_2, HF and ClF_3, the column being equivalent to 60–90 and 140–170 plates for HF and for ClF_3 as against about 8000–11,000 plates for Cl_2.

In the discussion, KLINKENBERG [2] suggested that this might be due to slowness of association of HF and ClF_3, the column trying to separate HF from say H_2F_2 which then re-react. A similar mechanism would have to apply to ClF_3.

In the following such a mechanism will be further examined for the case of a reversible isomerization, i.e. a first/first order reaction $A \rightleftarrows B$, occurring in the stationary phase.

Both the A and the B molecules will have a chromatographic transport rate, which is dependent in the usual manner on the volumes of the two phases and the distribution coefficient* while there is a first/first order exchange mechanism between these two groups.

The situation is similar to that of the behaviour of a single constituent with a finite transfer rate between the phases. Here the two groups are the molecules of such a constituent in either phase, while the mass-transfer coefficient as it is usually defined describes a first/first order exchange mechanism between the phases.

It will be shown in the following that the two cases can in fact be reduced to the same mathematics.

Thus, the rôles of chemical exchange between species and physical exchange between phases are analogous.

If there is no exchange at all, two sharp bands will be produced; if there is complete exchange one single sharp intermediate band will result. Increasing the rate of exchange will in either case cause the two sharp bands to tail towards each other and to fuse into one broad band which then further contracts into a single sharp one.

In the later phases of the present treatment use will be made of approximations valid for large numbers of stages i.e. only the last part of the above sequence is studied ("band widening due to a finite rate of exchange or chemical reaction").

DERIVATION OF EQUATION FOR BAND WIDTH

The following assumptions will be made:

Components A and B, when considered separately move according to the very simplest laws of ideal and linear chromatography, i.e.

Axial diffusion and eddy diffusion are absent.

* The study will be made in the language of extraction or absorption. It should not be difficult to translate this into adsorption afterwards if so desired.

Establishment of phase equilibrium is instantaneous.
Distribution ratios are constant.

The following notation will be used:
Subscripts I and II for moving and stationary phase.
Subscripts A and B for components (A is moving more quickly than B).
Fractions by volume of either phase F_I and F_{II}.
Linear velocity of moving phase v.
Linear co-ordinate x (counted in direction of v).
Time t.
Concentrations C_{IA}, C_{IB}, C_{IIA}, C_{IIB}.
Distribution coefficients K_A and K_B with moving phase in numerator so that:

$$C_{IA} = K_A C_{IIA} \tag{1}$$

$$C_{IB} = K_B C_{IIB} \tag{2}$$

(with $K_A > K_B$)

Rate constants of first-order chemical reaction in the stationary phase k_A (from A to B) and k_B (from B to A).

It is of course possible to use one rate constant together with the equilibrium constant, when in equations such as (22) the rates drop out altogether; with the present notation the equations have better symmetry.

The chromatographic balance equations now read:

$$vF_I \frac{\partial C_{IA}}{\partial x} + F_I \frac{\partial C_{IA}}{\partial t} + F_{II} \frac{\partial C_{IIA}}{\partial t} =$$

$$= (k_B C_{IIB} - k_A C_{IIA}) F_{II} =$$

$$= -\left(vF_I \frac{\partial C_{IB}}{\partial x} + F_I \frac{\partial C_{IB}}{\partial t} + F_{II} \frac{\partial C_{IIB}}{\partial t}\right) \tag{3}$$

or, by making use of (1) and (2) and introducing the "apparent" or "equivalent" fractions by volume:

$$F_i = F_I + \frac{F_{II}}{K_i} \tag{4}$$

$$vF_I \frac{\partial C_{IA}}{\partial x} + F_A \frac{\partial C_{IA}}{\partial t} = \frac{k_B F_{II}}{K_B} C_{IB} - \frac{k_A F_{II}}{K_A} C_{IA} =$$

$$- \left(vF_I \frac{\partial C_{IB}}{\partial x} + F_B \frac{\partial C_{IB}}{\partial t}\right) \tag{5}$$

In the usual theory for finite transfer rates (ANZELIUS [3], NUSSELT [4] and SCHUMANN [5]) the corresponding equations have 5 terms instead of 6, one convection term being missing. This number is reduced to 4, and the equations are reduced to dimensionless form, by introducing dimensionless co-ordinates known as Y (proportional to x) and Z (a linear combination of t and x).

The ANZELIUS–NUSSELT–SCHUMANN work deals with heat transfer. For corresponding formulae for mass transfer see e.g. KLINKENBERG [6].

For the same purpose two such linear combinations are introduced in the present case.

To this end (5) is transformed with the new variables

$$Y = px + qt \tag{6}$$

$$Z = rx + st \tag{7}$$

The four coefficients are so determined that two differential terms of equations (5) vanish, whereas the coefficients of the other two become equal to those of the 3rd and 4th terms.

This gives

$$\frac{k_A}{K_A}\left(\frac{\partial C_{IA}}{\partial Y}\right)_Z =$$

$$\frac{k_B}{K_B} C_{IB} - \frac{k_A}{K_A} C_{IA} = -\frac{k_B}{K_B}\left(\frac{\partial C_{IB}}{\partial Z}\right)_Y \tag{8}$$

with

$$Y = \frac{k_A K_B}{K_A - K_B}\left[\frac{xF_B}{vF_I} - t\right] \tag{9}$$

$$Z = \frac{k_B K_A}{K_A - K_B}\left[-\frac{xF_A}{vF_I} + t\right] \tag{10}$$

Elimination of C_{IB} from equations (8) gives

$$\frac{\partial^2 C_{IA}}{\partial Y \partial Z} + \left(\frac{\partial C_{IA}}{\partial Y}\right)_Z + \left(\frac{\partial C_{IA}}{\partial Z}\right)_Y = 0 \tag{11}$$

Equations (8) and (11) are familiar forms from the theory by ANZELIUS, SCHUMANN and NUSSELT.

The boundary conditions require special consideration. For an initially empty column being fed with a mixture at constant concentration, these read

$t = 0$	$x \geqslant 0$	$C_{IIA} = C_{IIB} = 0$
$x = 0$	$t \geqslant 0$	C_{IA} and C_{IB} are constant, ratio dependent on nature of feed.

However, after the transformation the boundaries must be redefined.

It is seen that $Y = 0$ and $Z = 0$ represent the movement of components B and A in the absence of chemical reaction (see Fig. 1), either component moving as a sharp band according to:

$$Y = 0 \qquad x = \frac{vF_I}{F_B}t = \frac{vF_I}{F_I + F_{II}/K_B}t \tag{12}$$

$$Z = 0 \qquad x = \frac{vF_I}{F_A}t \tag{13}$$

In the presence of chemical reaction according to the basic assumptions nothing can move more slowly than B or more quickly than A.

Accordingly $Y = 0$ and $Z = 0$ may serve instead of $t = 0$ and $x = 0$, the regions cut off in Fig. 1 being regions of constant (initial and final) concentration where and when the column is inoperative.

The analogous step is made in the ANZELIUS–SCHUMANN–NUSSELT derivation for one boundary only.

The ANZELIUS–SCHUMANN–NUSSELT solution is therefore applicable provided Y and Z are correctly transposed.

For large values of Y and Z this solution for a unit step function at the entrance can be expressed in terms of an error integral (" Walter's solution " [7]), see KLINKENBERG [8], it equals

$$\tfrac{1}{2}\left[1 + \operatorname{erf}(\sqrt{Z} - \sqrt{Y})\right]. \tag{14}$$

Consequently the effect of a peak in the inlet will then be a Gaussian curve in the effluent, which varies as

$$\exp\left[-(\sqrt{Z} - \sqrt{Y})^2\right] \tag{15}$$

Our problem will now be to find the relative peak width in the effluent, for instance expressed as the ratio of the standard deviation σ_t in t to the mean μ_t of t. This ratio is the inverse of the square root of the number of ideal stages n in the column (see e.g. KLINKENBERG and SJENITZER [9], Table 3).

$$\left(\frac{\sigma_t}{\mu_t}\right)^2 = \frac{1}{n} \tag{16}$$

This number is now of course being determined by chemical reaction instead of by the customary mechanisms.

When the solute leaves the column, i.e. at

$$x = l \tag{17a}$$

$$t = \mu_t \tag{17b}$$

in view of (15) the effect of increasing the time by

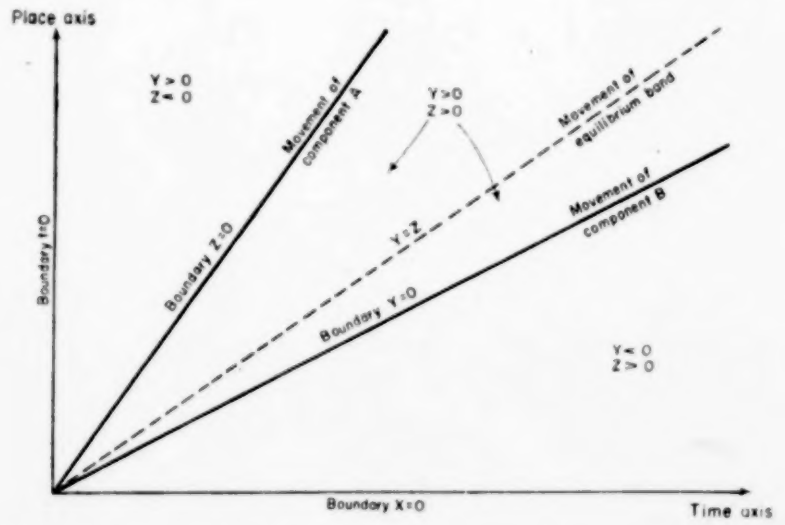

FIG. 1. Chromatography of a mixture of reversibly reacting constituents A and B.

$$\Delta l = \sigma_l \tag{18}$$

must be to change $(\sqrt{Z} - \sqrt{Y})$ by an amount

$$\Delta(\sqrt{Z} - \sqrt{Y}) = \tfrac{1}{2}\sqrt{2} \tag{19}$$

For a column equivalent to a great many stages, during the passage of a band Z remains approximately equal to Y, when

$$\frac{1}{\sigma_l\sqrt{2}} = \frac{\Delta(\sqrt{Z} - \sqrt{Y})}{\Delta l} = \left[\frac{\partial(\sqrt{Z} - \sqrt{Y})}{\partial l}\right]_{l,\,u_l} = \frac{1}{2Y_{l,\,u_l}^{1/2}}\left(\frac{\partial Z}{\partial l} - \frac{\partial Y}{\partial l}\right)_{l,\,u_l} \tag{20}$$

In view of $Y_{l,\,u_l} = Z_{l,\,u_l}$ (21)

we may find the relations between μ_l and $Y_{l,\,u_l}$ with l from (9), (10), (17a), (17b), whence

$$\mu_l = \frac{l}{vF_{\mathrm{I}}}\,\frac{k_{\mathrm{A}}K_{\mathrm{B}}F_{\mathrm{B}} + k_{\mathrm{B}}K_{\mathrm{A}}F_{\mathrm{A}}}{k_{\mathrm{A}}K_{\mathrm{B}} + k_{\mathrm{B}}K_{\mathrm{A}}} \tag{22}$$

$$Y_{l,\,u_l} = \frac{l}{vF_{\mathrm{I}}}\,\frac{k_{\mathrm{A}}k_{\mathrm{B}}F_{\mathrm{II}}}{k_{\mathrm{A}}K_{\mathrm{B}} + k_{\mathrm{B}}K_{\mathrm{A}}} \tag{23}$$

Equation (22) determines the average velocity of the reacting mixture. This could also have been derived from (12) and (13) by averaging for the components A and B with the weight ratio corresponding to chemical equilibrium and phase equilibrium, viz. the ratio

$$k_{\mathrm{B}}(F_{\mathrm{II}} + K_{\mathrm{A}}F_{\mathrm{I}}) : k_{\mathrm{A}}(F_{\mathrm{II}} + K_{\mathrm{B}}F_{\mathrm{I}})$$

or

$$k_{\mathrm{B}}K_{\mathrm{A}}F_{\mathrm{A}} : k_{\mathrm{A}}K_{\mathrm{B}}F_{\mathrm{B}} \tag{24}$$

Finally, using (9) and (10) to find the differentials occurring in (20) and substituting (22) and (23):

$$\frac{\sigma_l}{\mu_l} = \frac{K_{\mathrm{A}} - K_{\mathrm{B}}}{k_{\mathrm{A}}K_{\mathrm{B}}F_{\mathrm{B}} + k_{\mathrm{B}}K_{\mathrm{A}}F_{\mathrm{A}}}\sqrt{\left(\frac{2vF_{\mathrm{I}}}{l}\cdot\frac{k_{\mathrm{A}}K_{\mathrm{B}}}{k_{\mathrm{A}}K_{\mathrm{B}} + k_{\mathrm{B}}K_{\mathrm{A}}}\right)} \tag{25}$$

Discussion

The expression (25) found for the relative width of the band is symmetrical in A and B and it has the required property of vanishing for each of the following conditions:

$K_{\mathrm{A}} = K_{\mathrm{B}}$; $v = 0$; $l = \infty$; $k_{\mathrm{A}}/k_{\mathrm{B}} = 0$ and $k_{\mathrm{A}}/k_{\mathrm{B}} = \infty$.

As has been pointed out by KLINKENBERG and SJENITZER [9], the use of

$$\frac{\sigma}{\mu}$$

the characterize the distribution has several advantages:

1. There is a simple relation (16) with the number of stages.
2. The ratio σ/μ is independent of the units used (times, volumes of effluent etc.).
3. Values of σ^2/μ^2 derived for various simultaneous but independent mechanisms may be added together. In view of (16), the height l/n corresponding to an ideal stage is also an additive quantity.

This means that other band-widening mechanisms, such as diffusion, eddy diffusion and finite mass transfer rates may be considered independently (see e.g. KLINKENBERG and SJENITZER [9]) and the results combined. In this way we may remove some of the restrictions introduced at the start of the present article.

The restriction to first/first order reaction mechanisms, it is feared, is very real. Chromatographic processes involving a second reaction order have been discussed by THOMAS [10,11] but this treatment applied to cases where the total solute content of the stationary phase – this being an ion exchanger – had a fixed value. It cannot be used for simple reactions such as $A \rightleftarrows 2B$.

The limitation to linear isotherms is also an essential restriction in the present treatment.

Application

A possible application of the above theory might be the chromatography of H_2 (light hydrogen only). MOORE and WARD [12] have chromatographed hydrogen (with helium as a carrier gas) over alumina at 77° K. This produced sharp bands of ortho and para hydrogen. However, in the presence of a catalyst (some ferric oxide on the alumina) a single sharp band of

equilibrium hydrogen was produced (MOORE and WARD [13]). This would correspond in our Fig. 1 to:

$Y = 0$; $Z = 0$ (for sharp ortho and para peaks)

$Y = Z$, with σ/μ = very small (for sharp equilibrium peak)

The reaction mechanism can be presumed to be of first/first order and since the bands are reasonably symmetrical the requirement of linearity is also satisfied.

Under such conditions for a given column all quantities in the right-hand side of equation (25) except k_A and k_B are derivable from the positions of the two separate peaks, whereas the position of the equilibrium peak in view of (22) defines k_A/k_B, the ratio of the rate constants.

Hence the value of σ_t/μ_t should yield information about the reaction rate. If σ_t/μ_t does not tend to zero upon increasing the amount of catalyst, in view of the additivity principle mentioned earlier, the square of the limiting value should be subtracted from the square of the observed value before one proceeds with the further calculations.

It should be possible to follow the entire transition between the pair of peaks and the single peak by the use of the ANZELIUS–SCHUMANN–NUSSELT equations for low Y and Z (no longer large with respect to unity) but it was felt that no such effort should be devoted to the numerical evaluation of hypothetical cases, where the composition of the hydrogen feed enters as an essential additional variable (see discussion after equation 11).

NOTATION

C = concentration
F = fraction by volume
F_i = apparent fraction by volume, equation (4)
k_A, k_B = rate constants
K_A, K_B = distribution coefficients
l = length of column
n = number of ideal stages
t = time
v = linear velocity
x = length co-ordinate
Y and Z = dimensionless co-ordinates
μ_t = mean of elution time
σ_t = standard deviation of elution time

Subscripts

I and II = moving and stationary phase
A and B = faster and slower moving solute
i = any solute
l = at end of column
μ_t = at maximum of elution peak

REFERENCES

[1] PHILLIPS T. R. and OWENS D. R. Gas chromatography 1960 [Proceedings of Third Symposium organized by the Society for Analytical Chemistry and the Gas Chromatography Discussion Group of the Instutite of Petroleum, held at Edinburgh 8–10 June 1960], edited by SCOTT, R. P. W., London, Butterworths, 1960, see page 314.
[2] KLINKENBERG A. *ibid.*, page 386.
[3] ANZELIUS A. *Z. Math. Mech.* 1926 **6** 291.
[4] NUSSELT W. *Techn. Mech. Thermodynam.* 1930 **1** 417.
[5] SCHUMANN T. E. W. *J. Franklin Inst.* 1929 **208** 405.
[6] KLINKENBERG A. *Industr. Engng. Chem.* 1948 **40** 1992.
[7] WALTER J. E. *J. Chem. Phys.* 1945 **13** 332.
[8] KLINKENBERG A. *Industr. Engng. Chem.* 1954 **46** 2285.
[9] KLINKENBERG A. and SJENITZER F. *Chem. Engng. Sci.* 1956 **5** 258.
[10] THOMAS H. C. *J. Amer. Chem. Soc.* 1944 **66** 1664.
[11] THOMAS H. C. *Ann. N.Y. Acad. Sci.* 1948 **49** 161.
[12] MOORE W. R. and WARD H. R. *J. Amer. Chem. Soc.* 1958 **80** 2909.
[13] MOORE W. R. and WARD H. R. *J. Phys. Chem.* 1960 **64** 832.

Chemical Engineering Science, 1961, Vol. 15, pp. 260 to 269. Pergamon Press Ltd., London. Printed in Great Britain.

The flow of granular solids through orifices

W. A. Beverloo, H. A. Leniger and J. van de Velde
Technological Laboratory, Agricultural University, Wageningen, Netherlands.

(*Received* 3 *August* 1960)

Abstract—The authors have compared the results of their own investigations on the flow of granular solids (a.o. a number of seeds) with results published by others. The flow of all the seeds tested through the circular orifices used in the experiments, is represented by the equation

$$W = 35\,\rho_B \sqrt{g}\,(D_0 - 1{\cdot}4\,d)^{2{\cdot}5}\ (\mathrm{g/min})$$

Résumé—Les auteurs comparent les résultats de leurs propres recherches concernant l'écoulement de matériaux granulaires (e.a. un nombre de semences) aux résultats publiés par d'autres auteurs. Le courant de toutes les semences examinées par les auteurs à travers les orifices circulaires employées dans la recherche est décrit au moyen de la formule :

$$W = 35\,\rho_B \sqrt{g}\,(D_0 - 1{\cdot}4\,d)^{2{\cdot}5}\ (\mathrm{g/min})$$

Zusammenfassung—Die Verfasser vergleichen die Ergebnisse eigener Versuche über das Ausströmen von Schüttgut (u.a. einige Samen) mit einer Anzahl von anderer Seite veröffentlichten Befunden. Der Durchfluss aller von den Verfassern untersuchten Samen durch kreisförmige Öffnungen konnte durch die Gleichung :

$$W = 35\,\rho_B \sqrt{g}\,(D_0 - 1{\cdot}4\,d)^{2{\cdot}5}\ (\mathrm{g/min})$$

erfasst werden.

1. Introduction

Recently Fowler and Glastonbury [1] published in this journal results of investigations on the flow of granular solids through orifices. In our laboratory also observations have been made on this subject, as part of a more comprehensive study on the flow of solids in general. It seems desirable to record our results in this article in order to compare them with those of other workers and to supplement their findings. Fowler and Glastonbury [1] have published a comprehensive review of available literature on the subject, so that we will give only a survey of equations inferred by various other investigators. For comparison, the equations have been converted into the same system of units. Symbols and units are explained at the end of the paper. Newton *et al.* [2] found

$$W = 213\,D_0^{2{\cdot}96}\,H^{0{\cdot}04}\ \mathrm{g/min}$$

Franklin and Johanson [3] published for the flow from cylinders with flat bottoms, provided with orifices, the following equation :

$$W = \frac{1847\,\rho_s\,D_0^{2{\cdot}93}}{(6{\cdot}288\,\mu + 23{\cdot}16)(0{\cdot}394d + 1{\cdot}889) - 44{\cdot}90}\ \mathrm{g/min}$$

Brown and Richards [4] also studied the influence of the shape of the orifice in the flat bottom of a cylinder. As a general equation they found for a material with $\rho_s = 2{\cdot}5\ \mathrm{g/cm^3}$

$$W = 4870\,A\,D_h^{0{\cdot}5}\,\psi\ \mathrm{g/min}$$

and for circular orifices

$$W = 3730\,D_0^{2{\cdot}5}\,\psi\ \mathrm{g/min}$$

Finally Fowler and Glastonbury [1] found the equation

$$W = 14{\cdot}16\,\rho_B\,A\,\sqrt{2g\,D_h}\left[\frac{D_h}{d_s}\right]^{0{\cdot}185}\ \mathrm{g/min}$$

We will return on these results further in this article.

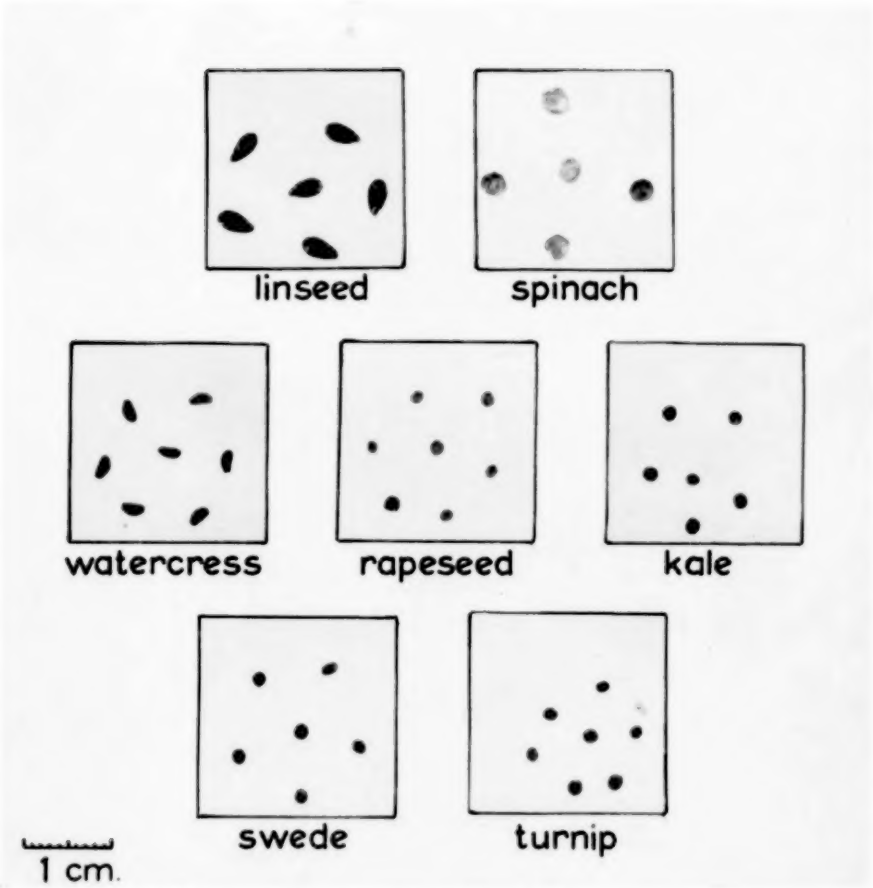

FIG. 1. View of the materials used in the tests.

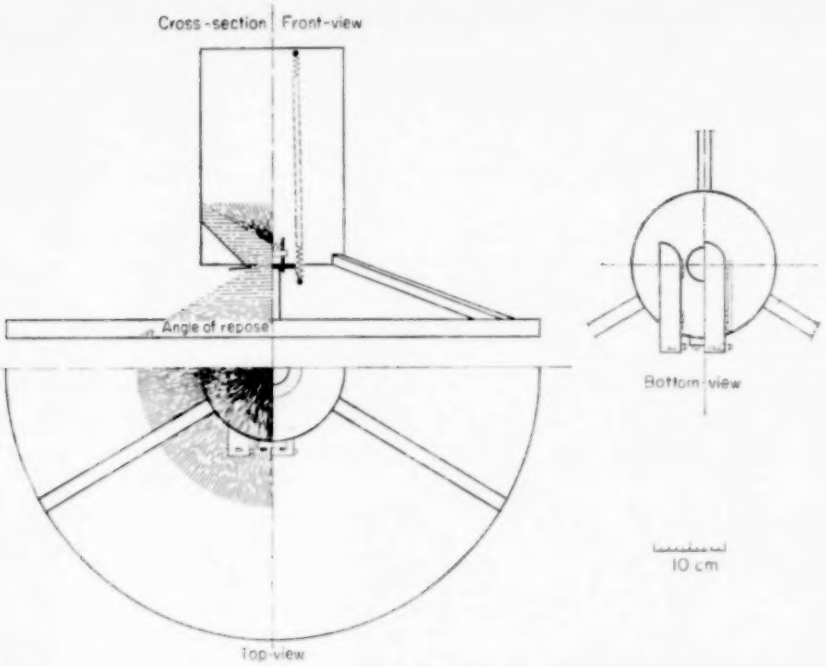

FIG. 2. Sketch of apparatus used for the determination of the angle of repose.

2. EXPERIMENTAL PROCEDURE AND MATERIALS

2.1 *Apparatus and Materials*

For an investigation of the flow of various materials use was made of three copper cylinders of 30 cm height and with internal diameters of respectively 5, 10 and 15 cm. In the flat bottoms of these cylinders were round openings which could be closed by means of valves. In these openings fitted copper disks with orifices differing in size and shape. In the cylinder with $D = 5{\cdot}0$ cm circular orifices with diameters of 0·20, 0·50, 0·75, 1·00, 1·25 and 1·50 cm could be fitted; in the cylinder with $D = 10{\cdot}0$ cm circular orifices with diameters of 0·50, 0·75, 1·00, 1·25, 1·50, 2·00, 2·50 and 3·00 cm. The largest cylinder ($D = 15{\cdot}0$ cm) could be provided with circular, square, rectangular and triangular orifices of dimensions as mentioned in Table 1.

The materials used in preliminary tests were sand-fractions and various seeds, viz. linseed, spinach (Juliana), watercress, rapeseed, kale, swede and turnip. Fig. 1 gives an impression of the shape and size of the seeds. As we could not predict exactly which properties of the materials influence their flow, we determined a number of characteristic properties, viz. the bulk density of packing, the true specific density, the void fraction (calculated from $100\,[(\rho_s - \rho_B)/\rho_s]$ per cent), the angle of repose, the number of particles per gramme and the particle size distributions of the seeds (by

Table 1
Details of orifices used in flow experiments

Circular orifices		*Square orifices* edge : a		*Rectangular orifices* side : a, 2a		*Triangular orifices* side : a, a, a,	
D_0 (cm)	A (cm²)	a (cm)	A (cm²)	a (cm)	A (cm²)	a (cm)	A (cm²)
0·26	0·056	0·22	0·049	0·16	0·055	0·38	0·064
0·50	0·20	0·49	0·24	0·35	0·24	0·74	0·24
1·03	0·84	0·89	0·80	0·63	0·80	1·46	0·92
1·50	1·76	1·35	1·84	0·99	1·96	2·06	1·84
2·03	3·24	1·77	3·16	1·25	3·16	2·79	3·36
2·50	4·96	2·22	4·96	1·58	5·00	3·52	5·36
3·02	7·20	2·65	7·04	1·90	7·28	4·02	7·00

screening with a perforated plate with circular openings and movement in a horizontal plane), from which the average screen size was calculated graphically. For the coarser materials the determination of the average screen size is less accurate than for the finer ones. For the determination of these properties current techniques were used. It should be mentioned only that the determination of the angle of repose at first presented many difficulties. The best results ultimately were obtained with the apparatus pictured in Fig. 2.

As we expected that also the shape of the particles influences the flow through orifices an attempt was made to express that shape into a "shape-factor." For this purpose the specific surface of the various materials was calculated from measurements of the resistance to the viscous flow of air through the materials according to Carman–Kozeny. Assuming that the particles were spherical, their "spherical diameter," d_s, was calculated from the specific surface and the void fraction. We defined the shape factor λ as the ratio of the average screen size of the particles to their "spherical diameter," i.e.

$$\lambda = \frac{d_s}{d} \quad (\lambda \leqslant 1)$$

The properties determined of the materials are presented in Table 2.

Table 2. Physical properties of the materials used in the flow experiments

Materials	*True density* ρ_s (g/cm³)	*Bulk density* ρ_B (g/cm³)	*Void fraction* (%)	*Average screen size d* (cm)	*Spherical diameter* d_s (cm)	*Shape factor* λ	*Angle of of repose* ϕ_s (degrees)	*Number of particles per* 10 g *N*
Sand	2·62	1·50	42·7	0·045	0·038	0·85	31·7	—
Linseed	1·16	0·69	40·5	0·25	0·12	0·48	30·9	1780
Spinach	1·19	0·57	52·1	0·30	0·16	0·54	31·3	1160
Watercress	1·22	0·71	42·6	0·16	0·11	0·71	30·4	3740
Rapeseed	1·12	0·67	40·2	0·17	0·15	0·91	28·1	4520
Kale	1·13	0·70	38·0	0·18	0·15	0·82	25·7	3250
Swede	1·09	0·66	39·4	0·18	0·14	0·75	25·6	3350
Turnip	1·12	0·68	39·3	0·17	0·13	0·79	25·8	4290

Table 3. Repeatability of the measurements

Material	*Orifice*	*Observed* (sec)	(g)	*W* (g/min)	*Average W* (g/min)	*Deviation* (%)
Sand 0·021 –0·030 cm	circular $D_0 = 0{\cdot}26$ cm	240·2 240·0 239·6	112 111 111	28·0 27·8 27·7	27·8 ± 0·2	± 0·7
Watercress	square A = 7·04 cm²	17·8 16·8 16·8	2768 2620 2639	9330 9357 9425	9370 ± 50	± 0·5
Spinach	circular $D_0 = 2{\cdot}5$ cm	37·0 38·3 37·0	2327 2436 2329	3773 3816 3777	3790 ± 25	± 0·7
Linseed	circular $D_0 = 2{\cdot}0$ cm	61·2 60·7 60·4	2469 2452 2402	2421 2424 2386	2410 ± 25	± 1·0

The flow-rates W in g/min were determined three times by catching material during a definite time, after the flow had become stationary, and weighing the quantity caught. The examples given in Table 3 may be demonstrative for the repeatability of the results.

2.2 *Experimental results*

From Table 4 it appears that the head, within the range investigated (H = 10–30 cm), has no influence on the flow-rate. Also the diameter of the cylinder does not have an influence on the flow-rate; this can be seen from Table 5.

Tests with sand fractions showed (Fig. 3) that the particle size has only a slight influence on the flow, which influence decreases as D_0/d increases. When D_0/d amounts to about 20 or more the influence is negligible. The results mentioned

Table 4. Influence of head of packing

Material	D (cm)	D_0 (cm)	*Mass flow-rate* W (g/min)		
			H = 30 cm	H = 20 cm	H = 10 cm
Sand	5·0	0·25	34·7	34·3	34·8
0·0093–0·021 cm	5·0	0·50	243	252	245
	10·0	0·50	248	250	249
	10·0	1·00	1544	1548	1548
Sand	5·0	0·25	28·0	27·8	27·7
0·021–0·030 cm	5·0	0·50	217	220	218
	10·0	0·50	226	227	226
	10·0	0·75	646	647	650
	10·0	1·00	1497	1509	1524
	15·0	0·25	24·5	24·4	24·3
	15·0	0·50	233	233	233
	15·0	0·75	665	664	664
	15·0	1·00	1514	1515	1512
Sand	15·0	0·25	19·0	19·7	19·3
0·030–0·059 cm	15·0	0·50	203	204	203

Table 5. Influence of container diameter

Diameter of circular orifice D_0 (cm)	*Mass flow-rate* W g/min					
	Sand Container diameter			*Rapeseed Container diameter*		
	D = 5 cm	D = 10 cm	D = 15 cm	D = 5 cm	D = 10 cm	D = 15 cm
0·25	27·8	—	24·4	—	—	—
0·50	218	226	233	—	—	—
0·75	662	648	664	159	150	150
1·00	1492	1510	1508	399	403	405
1·25	2620	2622	2693	764	755	779
1·50	4323	4414	4260	1317	1376	1317
2·00	—	9072	9238	—	3082	3166
2·50	—	16580	16419	—	5844	5849
3·00	—	—	—	—	9721	9822

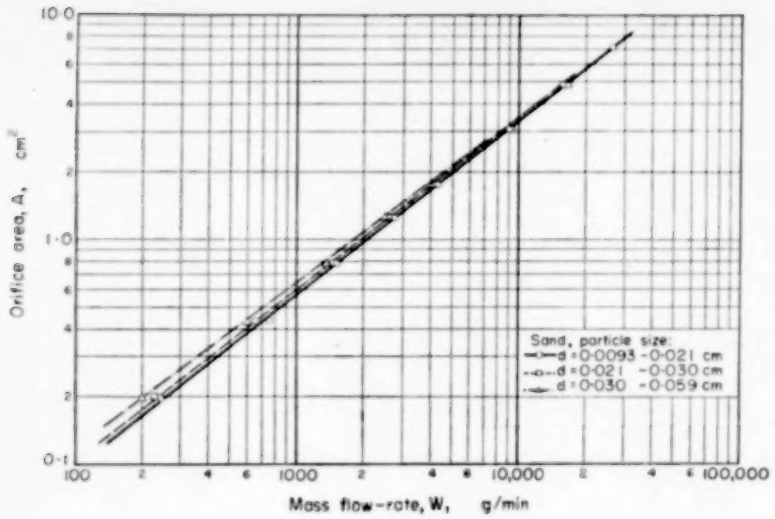

Fig. 3. Influence of orifice area on flow-rate of sand fractions.

above, are in agreement with those of earlier workers.

A large number of observations were made on the influence of the shape of the orifice. This influence was analogous with all materials investigated. Suffice therefore to give two examples, viz. of rapeseed and watercress (Figs. 4 and 5). It can be seen that with orifices of the same area the flow decreases in the order circle, square, rectangle and triangle. For mutual comparison of the materials circular orifices with diameters of at least six times the particle size were applied.

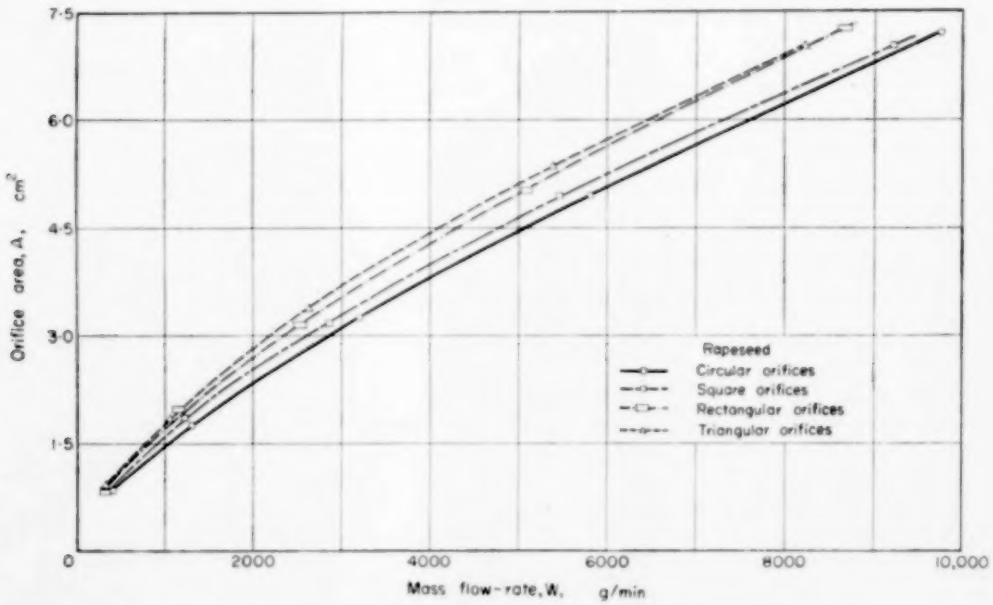

Fig. 4. Influence of orifice area on flow-rate of rapeseed.

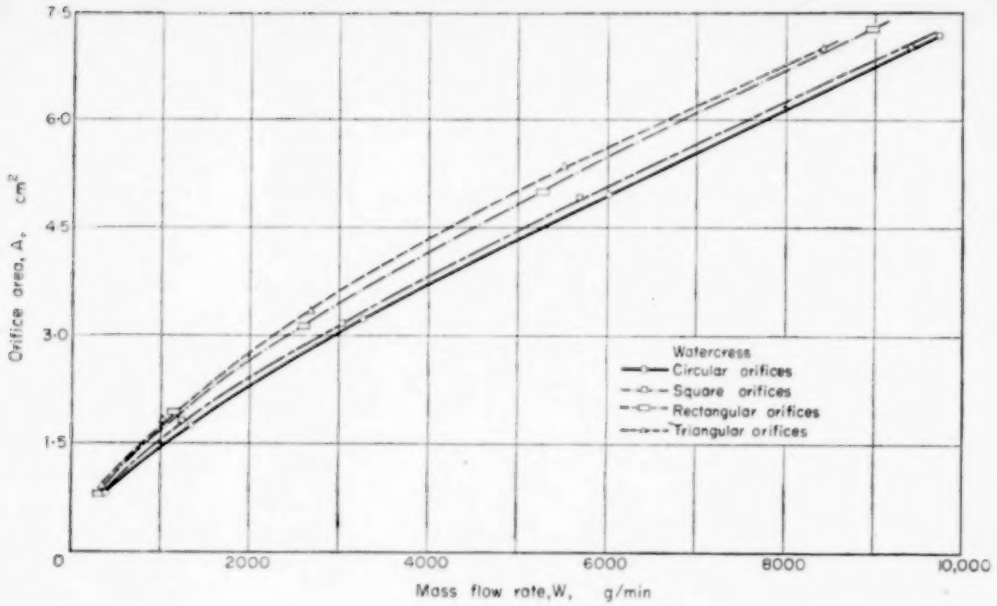

Fig. 5. Influence of orifice area on flow-rate of watercress.

The results of many observations have been presented in Fig. 6.

3. Discussion

In agreement with earlier investigations we found that W plotted double logarithmically as a function of the area of the circular orifice A gives straight lines (Fig. 6). The same holds true for non-circular orifices.

A dimensional analysis suggests that W should

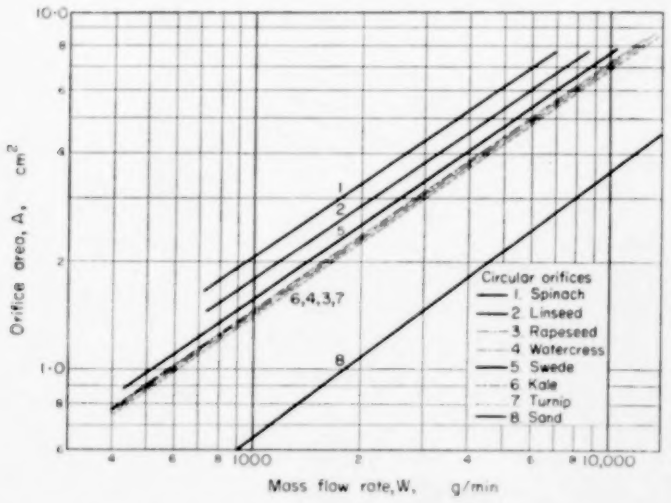

Fig. 6. Influence of orifice area on flow-rate of various materials.

be proportional to $\rho_B \sqrt{g}\, D_0^{2.5}$. However, from Fig. 6 we find exponents of D_0 greater than 2·5, particularly with larger d's, viz.:

sand	$W \div D_0^{2.77}$	rapeseed	$W \div D_0^{2.87}$
linseed	$W \div D_0^{3.09}$	kale	$W \div D_0^{2.85}$
spinach	$W \div D_0^{2.95}$	swede	$W \div D_0^{2.96}$
watercress	$W \div D_0^{2.90}$	turnip	$W \div D_0^{2.87}$

This might be explained by assuming that along the margin of the orifice a zone is useless or less fit for use for the flow. The size of that zone is proportional to d, so that the equation $W \div \rho_B \sqrt{g}\,(D_0 - k\,d)^{2.5}$ may be valid. In this equation k is a dimensionless constant.

By plotting D_0 against $W^{0.4}$ we found the following values for k:

sand	$k = 2{\cdot}9$	rapeseed	$k = 1{\cdot}4$
linseed	$k = 1{\cdot}5$	kale	$k = 1{\cdot}4$
spinach	$k = 1{\cdot}4$	swede	$k = 1{\cdot}5$
watercress	$k = 1{\cdot}3$	turnip	$k = 1{\cdot}4$

For all the seed samples examined we can therefore assume for k an average value of 1·4. The variations in k are probably related to the surface properties, but no correlation with the angle of repose could be established.

When we now introduce the factor ρ_B and $\sqrt{g}$ the following equations result:

sand	$W = 38{\cdot}8\ \rho_B \sqrt{g}\,(D_0 - 2{\cdot}9d)^{2.5}$
linseed	$W = 33{\cdot}2\ \rho_B \sqrt{g}\,(D_0 - 1{\cdot}4d)^{2.5}$
spinach	$W = 35{\cdot}7\ \rho_B \sqrt{g}\,(D_0 - 1{\cdot}4d)^{2.5}$
watercress	$W = 38{\cdot}5\ \rho_B \sqrt{g}\,(D_0 - 1{\cdot}4d)^{2.5}$
rapeseed	$W = 35{\cdot}1\ \rho_B \sqrt{g}\,(D_0 - 1{\cdot}4d)^{2.5}$
kale	$W = 36{\cdot}3\ \rho_B \sqrt{g}\,(D_0 - 1{\cdot}4d)^{2.5}$
swede	$W = 33{\cdot}2\ \rho_B \sqrt{g}\,(D_0 - 1{\cdot}4d)^{2.5}$
turnip	$W = 34{\cdot}1\ \rho_B \sqrt{g}\,(D_0 - 1{\cdot}4d)^{2.5}$

This shows that the coefficients in these equations are sufficiently constant to use for all the seed samples and for circular orifices the general formula

$$W = 35\ \rho_B \sqrt{g}\,(D_0 - 1{\cdot}4d)^{2.5}$$

At first it seems remarkable that in the above equation the shape-factor does not appear at all. However, the influence of the shape finds expression more or less in the values of both ρ_B and d, so that in our opinion it is admissable to drop the shape-factor.

Calculations with this equation show for all the seeds within the scope of our investigations deviations of about 5 per cent. If we compare the coefficient in the general formula with the coefficients in the formulae given for the various materials separately it seems that the maximum deviation is 10 per cent. It should be considered, however, that the formulae given for the various materials do not describe the observations precisely, either, so the mutual deviation between the formulae is greater than the deviation between the general formula and the observations.

Using the effective hydraulic diameter D_h' so that $D_h' = D_h - 1{\cdot}4d$ and the effective orifice area A', calculated from D_h', we find for the flow of rapeseed through orifices of various shapes the following equations:

circle	$W = 45{\cdot}0\ \rho_B A' \sqrt{g\, D_h'}$
square	$W = 46{\cdot}6\ \rho_B A' \sqrt{g\, D_h'}$
rectangle (1 : 2)	$W = 44{\cdot}4\ \rho_B A' \sqrt{g\, D_h'}$
triangle (1 : 1 : 1)	$W = 45{\cdot}7\ \rho_B A' \sqrt{g\, D_h'}$

It follows that the equation

$$W = 45\ \rho_B A' \sqrt{g\, D_h'}$$

may be applied for orifices of various shapes.

The slight influence of the particle size on the flow found for sand fractions (Fig. 3) is in agreement with the introduction of $(D_0 - k\,d)$ instead of D_0.

We cannot offer an explanation for the value of k for sand, which is somewhat different from 1·4; however, this value could not be calculated very accurately.

After having derived the general formula for seeds, mentioned above, we checked this formula with some other materials. For this purpose we used:

wheat	($d = 0{\cdot}5$ cm, $\rho_B = 0{\cdot}80$ g/cm^3)
crystallized sugar	($d = 0{\cdot}09$ cm, $\rho_B = 0{\cdot}83$ g/cm^3)
polystyrene globules	($d = 0{\cdot}10$ cm, $\rho_B = 0{\cdot}63$ g/cm^3)
green peas	($d = 0{\cdot}70$ cm, $\rho_B = 0{\cdot}84$ g/cm^3)
soybeans	($d = 0{\cdot}66$ cm, $\rho_B = 0{\cdot}75$ g/cm^3)
lupin	($d = 0{\cdot}65$ cm, $\rho_B = 0{\cdot}70$ g/cm^3)

VOL. 15 1961

From these data we calculated W with the equation

$$W = 35\,\rho_B\,\sqrt{g}\,(D_0 - 1{\cdot}4\,d)^{2{\cdot}5}$$

The following Table (6) shows the calculated and observed figures.

$$W = 35\,\rho_B\,\sqrt{g}\,(D_0 - 1{\cdot}4\,d)^{2{\cdot}5}$$

$$(\text{or } W = 45\,\rho_B\,A'\,\sqrt{g\,D_h'})$$

with that inferred by other workers it proves that our equation agrees best with the one according to FOWLER and GLASTONBURY [1], except for the

Table 6. Comparison between calculated and observed rate of flow for various granular materials

D_0 (cm)	*Wheat*		*Sugar*		*Polystyrene*		*Green peas*		*Soybeans*		*Lupin*	
	W_{calc}	W_{obs}	W_{calc}	W_{obs}	W_{calc}	W_{obs}	W_{calc}	W_{obs}	W_{calc}	W_{obs}	W_{calc}	W_{obs}
0·75	—	—	281	293	—	—	—	—	—	—	—	—
1·03	—	—	719	697	—	—	—	—	—	—	—	—
1·50	—	—	2010	2080	—	—	—	—	—	—	—	—
2·03	1790	1800	4610	4760	3400	3230	—	—	—	—	—	—
2·51	3820	3830	8050	8415	5980	5860	—	—	—	—	—	—
3·02	7210	6781	—	—	9830	9700	—	—	—	—	—	—
4·0	—	—	—	—	—	—	12590	14340	13540	13690	14220	12920
5·0	—	—	—	—	—	—	26180	29440	27060	27650	28370	26020
6·0	—	—	—	—	—	—	44890	51430	47000	47840	48520	44950

The differences between the experimental and the predicted flow rates in Table 6 amount to 5 per cent (average) and 12·5 per cent (maximum). From this we conclude that our formula can be used to make "calculated estimations" for the majority of materials with a bulk density ρ_B of about 0·7. If in any case the flow rate is to be known exactly, experiments will have to be made.

If we compare our equation

exponent. However, since the graphic representations cross each other in the field investigated (Fig. 7) the deviations within this field are not very great. In FOWLER's equation the influence of a useless zone along the margin of the orifice is expressed by multiplication with the dimensionless group $(D_h/d_s)^{0{\cdot}185}$ and in our equation by the term $1{\cdot}4\,d$, subtracted from D_h.

Attention is drawn to a discrepancy between

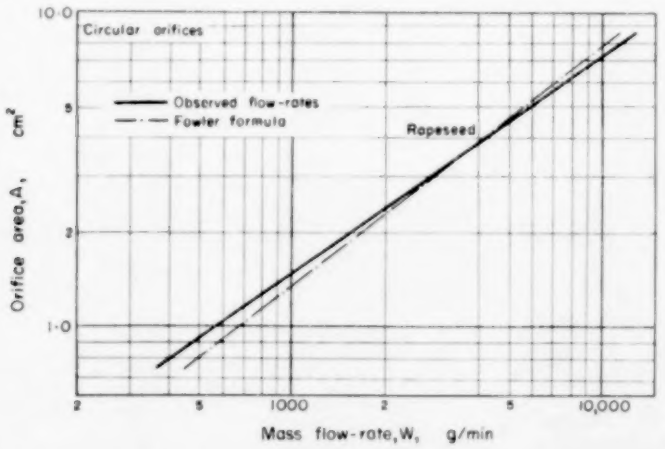

FIG. 7. Comparison of observed flow-rate of rapeseed with FOWLER's formula.

our shape factors λ (smaller than unity) and those according to Fowler and Glastonbury [1] (above unity). In a following paper Fowler and Chodziesner [5], however, use shape factors smaller than unity! All papers give the same definition of λ. For the formulae proposed above, however the discrepancy is immaterial as they do not contain λ.

Newton, *et al.* [2] have given an empirical formula for catalyst and found an exponent for D_0 of 2·96, which corresponds to the slope of the lines in our Fig. 6, e.g. for swede $W = 548\ \rho_B D_0^{2.96}$. Newton *et al.* found a very slight influence of the height, but this has not been confirmed, neither by us (Table 4) nor by others. Nor has an influence been found of the internal diameter of the container (Table 5).

According to Franklin and Johanson [3] the exponent of D_0 should be 2·93. The correction for the particle diameter is incorporated in the denominator of their formula.

Brown and Richards' [4] correlation for sand with a specific gravity of 2·5 reads $W = 3730\ D_0^{2.5}\ \psi$ g/min (circular orifices). In the range of variables considered their reduced velocity ψ can be written

$$\psi = 0{\cdot}044 \left(\frac{D_0}{d}\right)^{0.60}$$

Consequently the flow rates measured are proportional to $D_0^{3.1}$, a particle diameter correction again being incorporated in the denominator.

Addenda

After the completion and revision of the present paper two recent articles came to our attention.

Brown and Richards [6] found that the local flow density is a function of the distance as measured from the edge of the effective aperture, this function being independent of the form of the aperture (circle or slot). This fact has been used implicitely in our correlations; we used a slightly different definition of the effective aperture.

Brown and Richards' [6] equation for the local flow density may be integrated over a circular area to give the total mass flow. If an average $\psi = 1{\cdot}00$ is used and the average ratio ρ_B/ρ_s is taken as 0·58 (as for our seeds), this formula for mass flow becomes.

$$W = 31{\cdot}7\ \rho_B \sqrt{g}\,(D - kd)^{2.5}\ \text{g/min}\ *$$

which is some 10 per cent below our formula.

Luk'yanov *et al.* [7] gave a formula for the volumetric flow of spherical catalyst particles through a circular orifice. They corrected in a slightly different way for the inaccessible area at the edge of the aperture, their formula being

$$V = 5730\ \sqrt{R}\,(R^2 - 1{\cdot}9dR + 1{\cdot}66\,d^2)\ \text{cm}^3/\text{min}.$$

The numerical values according to this formula are about 7 per cent below ours.

*It should be noted that the symbol k in Brown and Richards' paper has the same meaning as kd in our formulae.

Acknowledgment—Thanks are due to Sluis en Groot's N. V. Koninklijke Zaadteelt en -Handel, Enkhuizen, Netherlands, for the seeds they placed at our disposal.

Furthermore we wish to express our gratitude to Ir. A. Harmens, who made valuable suggestions as to the method of correlation of our experimental data.

Notation

A = area of orifice	cm²
D = container diameter	cm
D_h = hydraulic diameter = 4 × A/perimeter of orifice	cm
D_0 = diameter of circular orifice	cm
d = average screen size of particles	cm
d_s = spherical diameter of particles	cm
g = gravitational constant	cm/sec²
H = head of packing above orifice	cm
k = an empirical coefficient	
λ = shape factor of particles $\lambda = d_s/d$	
N = number of particles/10 g	
ρ_B = bulk density of packing	g/cm³
ρ_s = true density of solid	g/cm³
μ = tangent to internal kinetic angle ϕ_i	
ϕ_s = angle of repose	
ψ = reduced velocity	
V = volume discharged/unit time	cm³/min
W = weight discharged/unit time	g/min

VOL. 15 1961

References

[1] Fowler R. T. and Glastonbury J. R. *Chem. Engng. Sci.* 1959 **10** 150.

[2] Newton R. H., Dunham G. S. and Simpson T. P. *Trans. Amer. Instn. Chem. Engrs.* 1945 **41** 215.

[3] Franklin F. C. and Johanson L. N. *Chem. Engng. Sci.* 1955 **4** 119.

[4] Brown R. L. and Richards J. C. *Trans. Instn. Chem. Engrs.* 1959 **37** 108.

[5] Fowler R. T. and Chodziesner W. B. *Chem. Engng. Sci.* 1959 **10** 157.

[6] Brown R. L. and Richards J. C. *Trans. Instn. Chem. Engrs.* 1960 **38** 243.

[7] Luk'yanov P. I., Gusev I. V. and Nikitina N. I. *Khim. Tekh. Top. Mas.* 1960 **5** 45.

Chemical Engineering Science, 1961, Vol. 15, pp. 270 to 275. Pergamon Press Ltd., London. Printed in Great Britain.

Latent heat of vaporization of *cyclo*hexane

W. Kozicki and B. H. Sage

Chemical Engineering Laboratory, California Institute of Technology, Pasadena, California, U.S.A.

(*Received* 18 *August* 1960)

Abstract—Experimental data concerning the latent heat of vaporization of *cyclo*hexane are not available over a wide range of temperatures. Because information concerning the enthalpy change upon vaporization has many industrial applications, experimental investigation was desirable. Direct calorimetric measurements of the latent heat of vaporization of *cyclo*hexane are reported for temperatures between 100° and 310°F. The experimental data were obtained under substantially isobaric–isothermal conditions. The results are presented in graphical and tabular form with values based upon volumetric data and limited measurements near room temperature.

Résumé—Les données expérimentales concernant la chaleur latente de vapourisation du cyclohexane ne sont pas utilisables dans un grand intervalle de témperatures. Une recherche expérimentale paraît s'imposer du fait que les données concernant la variation d'enthalpie au delà de la vaporisation sont utilisées dans l'industrie. Des mesures calorimétriques directes de la chaleur latente de vaporisation du cyclohexane ont été faites pour des températures comprises entre 100° et 310 °F. L'expérimentation a été conduite dans des conditions essentiellement isobares et isothermes. Les résultats sont donnés sous forme de tableaux et de graphiques ; les valeurs sont établies à partir des données volumétriques et les mesures sont effectuées à la température ambiante.

Zusammenfassung—Experimentelle Daten über die latente Verdampfungswärme von Cyclohexan stehen für einen grossen Temperaturbereich nicht zur Verfügung. Eine experimentelle Untersuchung schien wünschenswert, da die Enthalpieänderung bei der Verdampfung bei vielen industriellen Anwdenungen benötigt wird. Direkte kalorische Messungen der latenten Verdampfungswärme von Cyclohexan werden für Temperaturen zwischen 100 und 300 °F mitgeteilt. Die Daten wurden unter isobaren–isothermen Bedingungen erhalten. Die Ergebnisse werden in graphischer Form und in Tabellen angegeben, wobei die Werte auf volumetrischen Daten und einigen Messungen nahe der Raumtemperatur beruhen.

Measurements of the latent heat of vaporization of *cyclo*hexane have for the most part been limited to measurements near ambient temperature. Geist and Cannon [1] and Moore *et al.* [2] made sufficient measurements to establish the enthalpy change upon vaporization of *cyclo*hexane at atmospheric pressure. The critical temperature and pressure were reported by Meissner and Redding [3] and were based in part upon experimental information for substances of similar chemical nature. Vapour pressures were reported by Rossini *et al.* [4], Willingham *et al.* [5], Nagornov and Rotinjanz [6], Scatchard *et al.* [7], Aston *et al.* [8], Kay and Albert [9] and Young [10]. More recently, Reamer [11] evaluated the effect of pressure and temperature upon the molal volume of the liquid phase and measured the vapour pressure at temperatures between 100° and 460°F. Limited thermal decomposition was encountered at temperatures above 340°F.

Experimental Methods

The approach to the calorimetric measurements in this investigation was similar to that followed by Osborne *et al.* [12, 13]. The apparatus has been described in detail [14, 15]. In principle, it involves an isochoric vessel within which a heterogeneous mixture of *cyclo*hexane was confined. The calorimeter was located within an adiabatic vacuum jacket and provided with an agitator and electrical heater. Electrical energy was added to the nearly adiabatic, isochoric vessel and the quantity of *cyclo*hexane withdrawn as a gas was determined by gravimetric methods. An orifice, operating at sonic

velocity, maintained a steady rate of discharge under isobaric conditions in the calorimeter. Minor adjustments in the rate of addition of electrical energy were made so as to maintain nearly isobaric-isothermal evaporation. The total quantity of *cyclo*hexane leaving the calorimeter in a given period was determined by weighing bomb techniques [16].

A detailed thermodynamic analysis of the above-described, nearly isobaric–isothermal process is available [17]. There seems no need at this time to consider further the details of the corrections for the minor perturbations from isobaric–isothermal conditions and the means used to take into account the lack of local equilibrium at the gas–liquid interface. Under idealized conditions the latent heat of vaporization may be related to the electrical energy added and the change in weight of a heterogeneous system by the following expression:

$$l = (H_g - H_l) = \frac{Q_{1,2}}{m_1 - m_2}\frac{V_g - V_l}{V_g} = \frac{\dot{Q}}{\dot{m}}\frac{V_g - V_l}{V_g} \quad (1)$$

If the deviations from isobaric–isothermal conditions are taken into account, there is obtained a relatively complicated expression involving several line integrals describing the actual evaporative process [14, 17]. It should be remembered that equation (1) represents only the idealized behaviour and not the actual expression employed in evaluating the latent heat of vaporization from the experimental data. However, the magnitude of the corrections applied for deviations from the idealized behaviour were not greater than 0·2 per cent. For the most part these deviations were associated with the difference between temperatures of the liquid and gas phases during the evaporation process.

In addition, corrections were made for the energy added as a result of agitation and of thermal transfers between the calorimeter and the jacket [14]. The estimated uncertainty in each of the variables measured is set forth in Table 1. The uncertainties are expressed in terms of per cent of the measured latent heat of vaporization of *cyclo*hexane at the temperature in question.

Table 1. *Estimated uncertainties of measurement*

Quantity	*Probable uncertainty* (%)
Energy added electrically	0·05
Energy added by agitation	0·2
Energy exchange between calorimeter and jacket	0·006
Change in temperature of liquid	0·08
Weight of material withdrawn	0·02
Volumetric correction factor, $(V_g - V_l)/V_g$	0·04

As indicated in equation (1) there exists a primary volumetric correction relating the weight of *cyclo*hexane withdrawn from the calorimeter to that evaporated in the calorimeter. The magnitude of the volumetric correction factor, $(V_g - V_l)/V_g$, varies from 0·999 at 100°F to 0·974 at 310°F, as shown in a part of Table 2. The values of the specific volume of the liquid phase were taken from the work of Reamer [11].

No direct measurements of the specific volume of the dew-point gas appeared to be available. However, the volume of the dew-point gas is related to the latent heat of vaporization, the thermodynamic temperature, the slope of the vapour-pressure curve and the specific volume at bubble point by

$$V_g = \left[\frac{l}{T\,(dP'/dT)}\right] + V_l \quad (2)$$

The iterative solution of equations (1) and (2) yielded values of the latent heat of vaporization and the specific volume at dew point. The specific volumes at dew point obtained in this fashion were in good agreement with values estimated by the methods suggested by Pitzer [18].

As is shown in Table 1, it is not believed that uncertainties in the molal volume of the dew-point gas or of the bubble-point liquid introduced an uncertainty greater than 0·04 per cent in the volumetric correction factor, and hence in the latent heat of vaporization. This small uncertainty results from the fact that, over the range of temperatures covered in this investigation,

the volumetric correction factor did not deviate by more than 3 per cent from unity.

The internal energy change upon vaporization may be readily calculated from the latent heat of vaporization by application of the expression

$$E_g - E_l = H_g - H_l - P(V_g - V_l) \qquad (3)$$

It should be recognized that uncertainties in the specific volume of the dew-point gas or the bubble-point liquid do not materially influence the accuracy with which the change in internal energy may be evaluated from the application of equations (1) and (3). For example, an uncertainty of 1 per cent in the specific volume of the dew-point gas results in an over-all error in the evaluation of the internal energy change upon vaporization of 0·11 per cent at a temperature of 310°F. A smaller influence is encountered at the lower temperatures.

MATERIALS

The *cyclo*hexane involved in this investigation was obtained as research grade from the Phillips Petroleum Company and was reported to contain not more than 0·0006 mole fraction of impurities. The air-free sample showed an index of refraction of 1·42353 relative to the *D*-lines of sodium at 77°F, which compares favourably with a value of 1·42354 reported by ROSSINI *et al.* [4] for an air-saturated sample at the same temperature. The specific weight of the sample at 77°F was 48·3099 lb/ft³ as compared to 48·3113 lb/ft³ reported by ROSSINI *et al.* [4] for an air-saturated sample at the same temperature. The freezing point of the *cyclo*hexane was reported to be 43·07°F. On the basis of this information it is believed that the sample employed did not contain more than 0·0002 mole fraction of materials other than *cyclo*hexane. The presence of small quantities of impurities does not influence the calorimetric measurements of the latent heat of vaporization to the extent that impurities influence some other types of thermodynamic measurements.

EXPERIMENTAL RESULTS

The results of the experimental measurements upon *cyclo*hexane are shown in Table 2. For each

Table 2. Experimental results for cyclohexane

Identification	Temperature (°F)	Energy added electrically (B.th.u.)	Energy added by agitator (B.th.u.)	Energy added by conduction and radiation (B.th.u.)	Weight of material withdrawn (lb)	Superheat of liquid (°F)	Specific volume dew point (ft³/lb)	Specific volume bubble point (ft³/lb)	Volumetric correction factor	Latent heat of vaporization (B.th.u.)
273	100·00	1·6907	0·0748	0·0019	0·010745	0·16	21·55	0·02109	0·99902	164·36
261	130·00	1·8832	0·0463	0·0000	0·012016	0·20	11·85	0·02147	0·99819	159·97
262	130·00	3·9617	0·0846	0·0000	0·025262	0·20	11·85	0·02147	0·99819	159·98
272	130·00	4·1218	0·0882	0·0000	0·026244	0·20	11·85	0·02147	0·99819	160·22
291	160·00	3·9629	0·1090	0·0021	0·026148	0·21	6·995	0·02200	0·99685	155·38
289*	190·00	2·4077	0·0813	−0·0023	0·016550	0·15	4·369	0·02252	0·99485	149·34
275	220·00	3·1524	0·0660	0·0014	0·022017	0·21	2·854	0·02311	0·99190	145·15
292	220·00	3·4658	0·0782	0·0030	0·024271	0·20	2·854	0·02311	0·99190	145·04
290	250·00	2·8309	0·0431	0·0022	0·020409	0·26	1·931	0·02376	0·98771	139·28
263	280·00	5·3099	0·0584	−0·0092	0·039359	0·31	1·345	0·02442	0·98185	133·84
294	310·05	1·8129	0·0592	0·0066	0·014450	0·09	0·9559	0·02523	0·97361	126·82

*The period of time associated with obtaining these calorimetric measurements was nearly twice that required for the other measurements.

set of experimental conditions the energy added electrically by the agitator and by conduction or radiation has been indicated, along with the weight of material withdrawn and the superheat of the liquid. Included also are the specific volumes at bubble point, the volumetric correction factor and the calculated values of the latent heat of vaporization and of the specific volume at dew point. The larger correction for the energy added by conduction and radiation at the higher temperatures is evident.

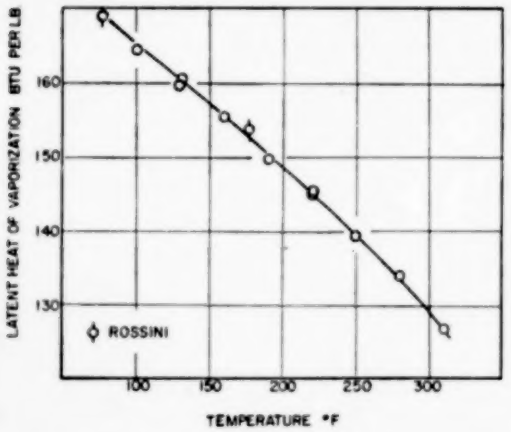

FIG. 1. Effect of temperature on latent heat of vaporization for *cyclo*hexane.

The values of the latent heat of vaporization recorded in Table 2 are depicted graphically in Fig. 1. Critically chosen values reported by ROSSINI *et al.* [4] at two temperatures have been included. The standard error of estimate of the experimental points from a smooth curve is 0·35 B.Th.U/lb. Residual methods were employed in smoothing the values of the latent heat of vaporization. For present purposes the residual latent heat of vaporization was evaluated from

$$1 = l + 0{\cdot}18t - 181 \qquad (4)$$

There is shown by the curve in Fig. 2 the residual latent heat of vaporization as established from the current experimental data. In locating this curve, the experimental measurements at 190°F, indentified in Table 2 as number 289, were not considered. These measurements at 190°F involved nearly twice the time as the other calorimetric measurements and therefore probably involve larger uncertainty. The agreement of the current measurements with the data of ROSSINI *et al.* [4] is satisfactory at the lower temperatures but the deviation at 177°F is approximately 1·3 B.Th.U/lb. Utilizing these residual techniques smoothed values of the latent heat of vaporization of *cyclo*hexane were evaluated

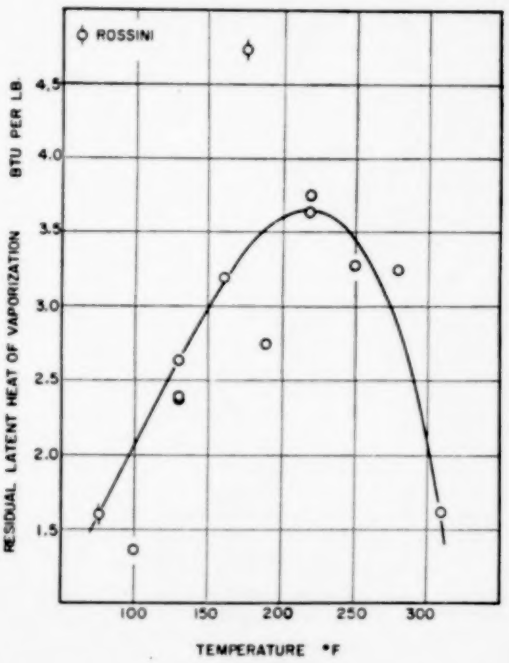

FIG. 2. Residual latent heat of vaporization for *cyclo*hexane.

for even values of temperature and are reported in Table 3. In addition, values in the change in internal energy upon vaporization and the specific volumes at dew point and at bubble point have been included. The uncertainty of the specific volumes at dew point is difficult to evaluate since the accuracy of the vapour pressure data [6–11, 19] has not been established. It is believed that the values of the latent heat of vaporization recorded in Table 3 affect the actual behaviour of *cyclo*hexane with an uncertainty of not more than 0·2 per cent.

Table 3. Critically chosen values for latent heat of vaporization

Temperature (°F)	*Internal energy change upon vaporization* (B.Th.u/lb)	*Latent heat of vaporization* (B.Th.u/lb)	*Specific volume* (ft^3/lb)	
			Dew point	*Bubble point*
100	152·10	165·05	21·55	0·02109
110	150·30	163·45	17·49	0·02121
120	148·48	161·84	14·31	0·02134
130	146·67	160·22	11·85	0·02147
140	144·88	158·61	9·893	0·02165
150	143·08	156·99	8·283	0·02180
160	141·29	155·37	6·995	0·02200
170	139·47	153·71	5·941	0·02216
180	137·64	152·03	5·085	0·02234
190	135·79	150·32	4·369	0·02252
200	133·92	148·58	3·769	0·02271
210	131·04	146·82	3·305	0·02291
220	130·15	145·04	2·854	0·02311
230	128·22	143·20	2·515	0·02333
240	126·30	141·35	2·197	0·02355
250	124·34	139·46	1·931	0·02377
260	122·38	137·54	1·710	0·02397
270	120·38	135·56	1·522	0·02418
280	117·32	133·50	1·345	0·02442
290	116·20	131·36	1·195	0·02466
300	114·00	129·13	1·066	0·02494
310	111·69	126·77	0·9559	0·02523

Acknowledgment—The experimental work reported here was made possible through the continuing support of the Standard Oil Company of California. The calorimetric equipment was made available through the courtesy of the Jet Propulsion Laboratory of the California Institute of Technology and its original construction was sponsored jointly by Project MX121 of the Air Materiel Command and by the Ordnance Department. Virginia Berry contributed to the calculation of experimental results and B. Lawson Miller assisted in the preparation of the manuscript.

Nomenclature

d = differential operator	
E = internal energy	B.Th.u/lb
H = enthalpy	B.Th.u/lb
l = latent heat of vaporization	B.Th.u/lb
$\mathfrak{l}$ = residual latent heat of vaporization	B.Th.u/lb
m = weight of material	lb
$\dot{m}$ = weight rate of flow	lb/sec
P = pressure	lb/in^2
P' = vapour pressure	lb/in^2
Q = heat	B.Th.u
$\dot{Q}$ = thermal flux	B.Th.u./sec
T = thermodynamic temperature	°R
t = temperature	°F
V = specific volume	ft^3/lb

Subscripts

g = gas phase
l = liquid phase
1 = initial condition
2 = final condition

References

[1] Geist J. M. and Cannon M. R. *Industr. Engng. Chem.* (Anal. Ed.), 1946 **18** 611.
[2] Moore G. E., Renquist M. L. and Parks G. S. *J. Amer. Chem. Soc.* 1940 **62** 1505.
[3] Meissner H. P. and Redding E. M. *Industr. Engng. Chem.* 1942 **34** 521.
[4] Rossini F. D. Pitzer K. S., Arnett, R. L., Braun, R. M. and Pimentel, G. C. *Selected Values of Physical and Thermodynamic Properties of Hydrocarbons and Related Compounds.* Carnegie Press, Pittsburgh, Pa. 1953.
[5] Willingham C. B., Taylor W. J., Pignocco J. M. and Rossini F. D. *J. Research. Nat. Bur. Stand.* 1945 **35** 219.

[6] NAGORNOV R. and ROTINJANZ L. *Ann. Inst. Anal. Phys. Chim.* 1924 **2** 371.
[7] SCATCHARD G., WOOD S. E. and MOCHEL J. M. *J. Amer. Chem. Soc.* 1939 **61** 3206.
[8] ASTON J. G., SZASZ G. J. and FINK H. L. *J. Amer. Chem. Soc.* 1943 **65** 1135.
[9] KAY W. B. and ALBERT R. E. *Industr. Engng. Chem.* 1956 **48** 422.
[10] YOUNG S. *Sci. Proc. Roy. Dublin Soc.* 1910 **12** 374.
[11] REAMER H. H. and SAGE B. H. *Chem. Engng. Data Ser.* 1957 **2** 9.
[12] OSBORNE N. S., STIMSON H. F. and FIOCK E. F. *Bur. Stand. J. Res.* 1930 **5** 411.
[13] OSBORNE N. S., STIMSON H. F. and GINNINGS D. C. *J. Res. Nat. Bur. Stand.* 1939 **23** 197.
[14] MCKAY R. A. and SAGE B. H. *J. Chem. Engng. Data* 1960 **5** 21.
[15] SAGE B. H. and HOUGH E. W. *Analyt. Chem.* 1950 **22** 1304.
[16] SAGE B. H. and LACEY W. N. *Trans. Amer. Inst. Min. (Metall.) Engrs.* 1940 **136** 136.
[17] MCKAY R. A., SAGE B. H. *Amer. Docum. Inst., Washington*, D.C., Document No. 6072, 1959.
[18] PITZER K. S., LIPPMAN D. C., CURL R. F., HUGGINS C. M. and PETERSEN D. E. *J. Amer. Chem. Soc.* 1955 **77** 3433.
[19] *International Critical Tables*, Vol. III, p. 244. McGRAW-HILL, New York 1928.

Chemical Engineering Science, 1961, Vol. 15, pp. 276 to 297. Pergamon Press Ltd., London. Printed in Great Britain.

Pressure drop in ideal fluidization

K. E. Bertil Andersson
Division of Chemical Technology, Royal Institute of Technology, Stockholm 70

(*Received* 14 *July* 1960; *in revised form* 24 *December* 1960)

Abstract—A pressure drop equation is presented for ideally fluidized beds consisting of spheres of uniform size. The equation differs from the Ergun equation inasmuch as it includes a tortuosity factor, q, a cross-section factor, z, both of which are void fraction dependent, and an inertial drag coefficient, c_i, dependent only on particle Reynolds number. The equation is written

$$\frac{\Delta P}{L} = 36\, z q^2 \frac{(1-\epsilon)^2}{\epsilon^3}\frac{\mu U}{{d_p}^2} + 6\, c_i\, q^3 \frac{1-\epsilon}{\epsilon^3}\frac{\rho U^2}{d_p}.$$

It is found that

$$q = 1{\cdot}71\left(\frac{1-\epsilon}{\epsilon}\right)^{0{\cdot}15} \quad \text{for } 0{\cdot}45 \leqslant \epsilon \leqslant 0{\cdot}94,$$

$$q \approx \epsilon^{-2} \quad \text{for } 0{\cdot}92 \leqslant \epsilon \leqslant 1$$

and

$$c_i = \tfrac{1}{6}\left(C_D - \frac{24}{\mathrm{Re}_p}\right).$$

The relationship for the cross-section factor is obtained preferably from the Vand-Hawksley relation, equation (9), or from the equivalent expression $U/U_\infty = \epsilon^{4{\cdot}59}$. About 600 experiments were performed to investigate the equation in the range: $0{\cdot}003 \leqslant \mathrm{Re}_p \leqslant 2000$ and $0{\cdot}45 \leqslant \epsilon \leqslant 0{\cdot}95$. The equation is solved explicitly for $U/U_\infty = f(\epsilon, \mathrm{Re}_p)$, equation (27), and the result is presented in a nomogram.

The author has introduced a consistent Reynolds number which includes the tortuosity factor and the cross-section factor, and the criterion for the possibility of obtaining complete similarity is discussed.

Résumé—On propose une équation de perte de charge pour les lits fluidisés idéalement constitués de sphères de diamètre uniforme. Cette équation diffère de l'équation d'Ergun en ce sens qu'elle tient compte d'un " facteur de tortuosité," q, d'un " facteur de section de passage," z, dépendant tous deux de la fraction de vide, et d'un " coefficient de frottement," c_i, dépendant uniquement du nombre de Reynolds. L'équation s'écrit :

$$\frac{\Delta P}{L} = 36\, z q^2 \frac{(1-\epsilon)^2}{\epsilon^2}\frac{\mu U}{{d_p}^2} + 6\, c_i\, q^3 \frac{1-\epsilon}{\epsilon^3}\rho U^2 \frac{}{d_p}$$

On montre que :

$$q = 1{,}71\left(\frac{1-\epsilon}{\epsilon}\right)^{0{,}15} \quad \text{pour } 0{,}45 < \epsilon < 0{,}94$$

$$q \approx \epsilon^{-2} \quad \text{pour } 0{,}92 \leqslant \epsilon < 1$$

et

$$c_1 = \tfrac{1}{6}\left(C_D - \frac{24}{\mathrm{Re}_p}\right)$$

La relation donnant le " facteur de section d epassage " s'obtient de préférence à partir de la relation de Vand-Hawksley, équation (9), ou à partir de l'expression équivalente $U/U_\infty = \epsilon^{4{,}59}$. Environ 600 expériences ont été réalisées pou rdéfinir l'équation dans le domaine : $0{,}003 \leqslant \mathrm{Re}_p \leqslant 2000$ et $0{,}45 \leqslant \epsilon \leqslant 0{,}95$ L'équation est explicitement résolue pour $U/U_\infty = f(\mathrm{Re}_p)$ équation (27), et le résultat est présenté sous forme d'abaque.

L'auteur introduit un nombre de Reynolds particulier qui tient compte des facteurs de tortuosité et de section de passage, et il discute les possibilités d'obtenir une similitude complète.

Pressure drop in ideal fluidization

Zusammenfassung—Eine Druckabfallgleichung für ideal-fluidiertes Medium, bestehend aus uniformen Kugeln, ist abgeleitet. Die erhaltene Gleichung unterscheidet sich von der Ergun'sche Gleichung insofern, als sie enthält einen Gewundenheitsfaktor, q, einen Querschnittsfaktor, z, und einen Trägheitshemmung Koeffizient, c_i, der nur von der Reynolds'schen Zahl abhängig ist. Die Gleichung ist angegeben:

$$\frac{\Delta P}{L} = 36\, z q^2 \frac{(1-\epsilon)^2}{\epsilon^3}\frac{\mu U}{{d_p}^2} + 6\, c_i q^2 \frac{1-\epsilon}{\epsilon^3}\frac{\rho U^2}{d_p}.$$

Es ist gefunden, dass

$$q = 1{,}71\left(\frac{1-\epsilon}{\epsilon}\right)^{0{,}15} \quad \text{für } 0{,}45 < \epsilon < 0{,}94,$$

$$q \approx \epsilon^{-2} \quad \text{für } 0{,}92 < \epsilon < 1$$

und

$$c_i = \tfrac{1}{6}\left(C_D - \frac{24}{Re_p}\right).$$

Die Beziehung zu dem Durchschnittsfaktor ist vorzugsweise von der Beziehung von Vand-Hawksley, Gleichung (g) oder von der äquivalenten Gleichung $U/U_\infty = \epsilon^{4.59}$ zu erhalten, es wurden ungefahr 600 Experimente ausgeführt um die Gleichung in den Bereichen: $0{\cdot}003 < \mathrm{Re}_p < 2000$ und $0{\cdot}45 < \epsilon < 0{\cdot}95$ untersuchen zu können. Die Gleichung ist ausdrücklich für $U/U_\infty = f(\epsilon, \mathrm{Re}_p)$ Gleichung (27), gelöst und die Ergebnisse sind in einem Nomogramm dargestellt.

Der Autor führt eine konstante Reynolds'sche Zahl ein, die sowohl den Gewundenheitsfaktor als den Querschnittsfaktor einschliesst, und bespricht das Kriterium für die Möglichkeit eine vollständige Ähnlichkeit erhalten zu können.

Introduction

During the past decade great efforts have been made to obtain knowledge of the dynamics of fluidized beds. To this end some investigations have aimed at the solution of the relationship between void fraction and fluid velocity in ideal (particulate) fluidization. Such ideal conditions exist in fluidized systems with a low ratio of solid density to fluid density. Liquid fluidized beds can thus usually be considered to be ideal.

A simple solution to this problem is given by Zaki [1] who proposes a correlation of the type

$$\frac{U}{U_\infty} = \epsilon^p \qquad (1)$$

where U = superficial velocity
U_∞ = terminal velocity of free falling particle
ϵ = void fraction
and p = functions of particle Reynolds number $\mathrm{Re}_p = \dfrac{d_p U_\infty}{\nu}$.

This type of correlation is quite acceptable for low particle Reynolds numbers, but its consistency fails for systems of greater particle Reynolds numbers as will be shown later.

The solution to the problem, presented here, is based on the Ergun pressure drop equation for packed beds [2]. The present author has shown earlier that this equation can be extended to ideally fluidized beds by including the tortuosity factor q and the cross-section factor z, both of which are functions of void fraction [3].

The Ergun equation can be written in the form

$$\frac{\Delta P}{L} = 4{\cdot}17\frac{\mu U}{m^2\epsilon} + 0{\cdot}292\frac{\rho U^2}{m\epsilon^2} \qquad (2)$$

where ΔP = pressure drop
L = bed height
μ = viscosity
ρ = fluid density
and $m = \epsilon/S$ = Blake's hydraulic radius [4]
where S = wetted surface per unit bed volume.

This equation is thus based on a model of parallel-connected straight channels of length L and hydraulic radius m. The fluid velocity in such a model is the Dupuit velocity U/ϵ, i.e. the

velocity component parallel to the main direction of flow in the bed. However, the flow path in packed and fluidized beds is tortuous and thus both the bed height and the Dupuit velocity have to be multiplied by a tortuosity factor $q = L_e/L$ in order that they may represent consistently the equivalent channel length L_e and the average fluid velocity $u = qU/\epsilon$. Thus the proportionality factor of the viscous term of equation (2) includes the tortuosity factor raised to the second power. Also it includes a factor z which depends only on the shape of the cross-section of the channel (perpendicular to the flow direction). Consequently the Kozeny factor may be written zq^2. This problem has been discussed several times in the past and the reader is referred to textbooks for further details [5, 6].

Upon introducing the tortuosity factor into both the viscous term and the inertia term we increase the demand for its absolute independence of the hydrodynamic state of flow, i.e. the tortuosity factor must be a function only of the geometry of the bed. Under this assumption equation (2) is transformed into

$$\frac{\Delta P}{L} = zq^2 \frac{\mu U}{m^2 \epsilon} + c_i q^3 \frac{\rho U^2}{m \epsilon^2} \qquad (3)$$

The tortuosity factor was empirically found to be a function of the ratio of the solid phase radius to the hydraulic radius, where the solid phase radius is given by means of the definition $m_s = (1 - \epsilon)/S$ in analogy with the definition of the hydraulic radius. The expression found for q was

$$q \propto \left(\frac{1 - \epsilon}{\epsilon}\right)^n$$

where $n \approx 1.6$. It was further proposed that the modified Kozeny factor is determined by

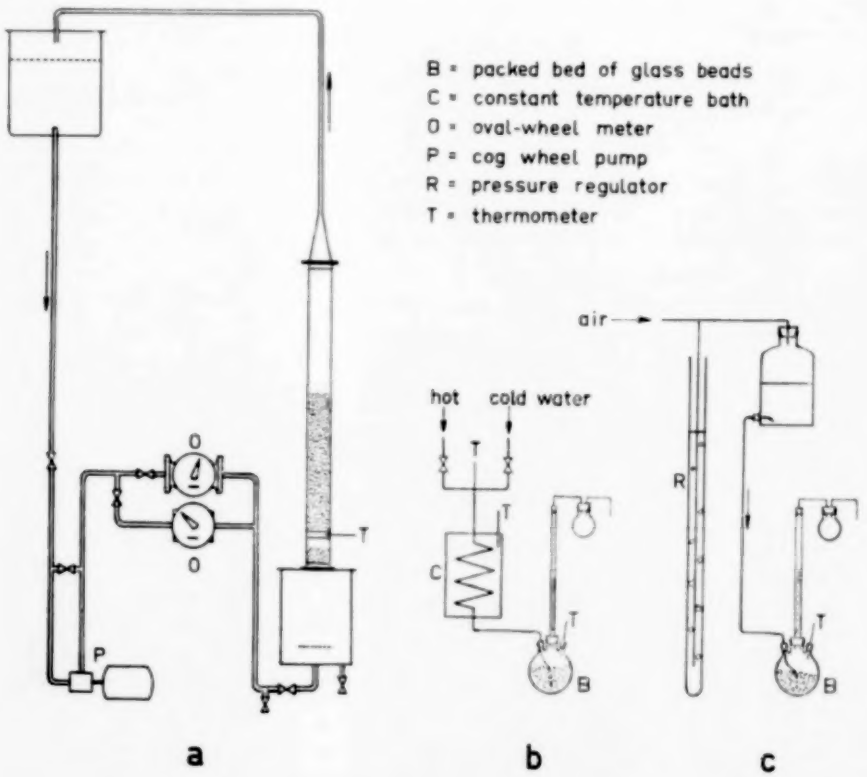

FIG. 1. (a) Large-scale equipment for circulation of oil. (b) Small-scale equipment for water fluidization. (c) Small-scale equipment for glycerol–water and oil fluidization.

$$zq^2 = \frac{1}{2}\left(\frac{1-\epsilon}{\epsilon}\right)^{-1} + \frac{5}{2}\left(\frac{1-\epsilon}{\epsilon}\right)^{2n} \qquad (4)$$

This investigation [3] was based on previously published data for comparatively limited ranges of Reynolds number, and the proportionality factor c_i was found to be approximately constant. Among other things the experimental investigation presented here will show that this is not the case.

Experimental

Apparatus

The equipment used in the present study was designed to give data over the whole Reynolds number range of interest. Thus the apparatus was designed with a view to using water, water–glycerol mixtures and lubricant oil as fluids. The large-scale equipment had columns with inner diameters of 12·0, 8·4 and 6·0 cm, while the small-scale equipment (placed in a thermostated room) had columns with inner diameters of 1·69 and 1·02 cm. In the large-scale equipment water experiments and oil experiments were performed with entrance sections consisting of packed beds and fluidized beds (respectively) containing 5 mm glass beads, whereas in the small-scale equipment the entrance sections consisted of 5 cm empty columns.

In all the water experiments the fluid was taken directly from the mains and the velocity was found either by weighing (large-scale) or by measuring the volume (small-scale). The velocity of the lubricant oil was measured by Bopp and Reuther oval-wheel meters (large-scale) or by weighing (small-scale), whereas the velocity of the glycerol–water mixtures was found by volumetric measurement (small-scale). Fig. 1 shows the different apparatus used.

Fluid and particle properties

The viscosity of the oil was determined using a Höppler Rheo-viscometer. The glycerol–water mixtures were prepared from analytical grade glycerol and distilled water and the viscosity was determined by density measurements [7]. Table 1 gives the physical properties of the fluids.

Table 1. Physical properties of the fluids

Fluid	*Temperature* (° C)	*Viscosity* (P)	*Density* (g/cm³)	*Concentration* (wt.-% glycerol)
Lubricant oil	20	6·66	0·888	
	25	4·56	0·885	
	30	3·19	0·882	
Glycerol–water	20	0·1543	1·166	64·92
	20	0·0797	1·139	54·94
	20	0·0474	1·112	45·10
	20	0·0301	1·085	34·76
Water	4–50			

The particles used in the experiments were approximately spherical, their diameter being determined by means of a large number of micrometer measurements of maximum and minimum diameter of each type of particle. The average maximum and minimum diameters were calculated in accordance with the hydraulic radius definition [4, 8].

$$\frac{1}{d_p} = \sum \frac{x_i}{d_{p_i}} \qquad (5)$$

where x_i is the weight fraction with a diameter d_{p_i}. The arithmetic mean of the average maximum and minimum diameters was used in the calculations. Table 2 gives the physical properties of the particles.

The introduction of this arithmetic mean of maximum and minimum particle diameters affords an opportunity to study the deviation from the true solid phase radius

Table 2. Physical properties of the particles

Type of particle		*Maximum diameter* (mm)	*Minimum diameter* (mm)	*Average diameter* (mm)	$\frac{d_{p,\max.}}{d_{p,\min.}}$	*Density* (g/cm³)
Glass beads	A	5·692 ± 0·150	5·295 ± 0·075	5·49	1·075	2·458
	B	3·158 ± 0·090	2·863 ± 0·126	3·011	1·103	2·527
	C	3·285 ± 0·112	2·693 ± 0·156	2·989	1·220	2·528
	D	1·186 ± 0·115	1·086 ± 0·100	1·136	1·092	2·950
Cadmiated steel balls	E	3·165 ± 0·021	3·104 ± 0·032	3·135	1·020	7·790
Lead shot	F	1·608 ± 0·065	1·553 ± 0·065	1·580	1·035	11·15
	G	1·158 ± 0·058	1·082 ± 0·051	1·120	1·070	11·07

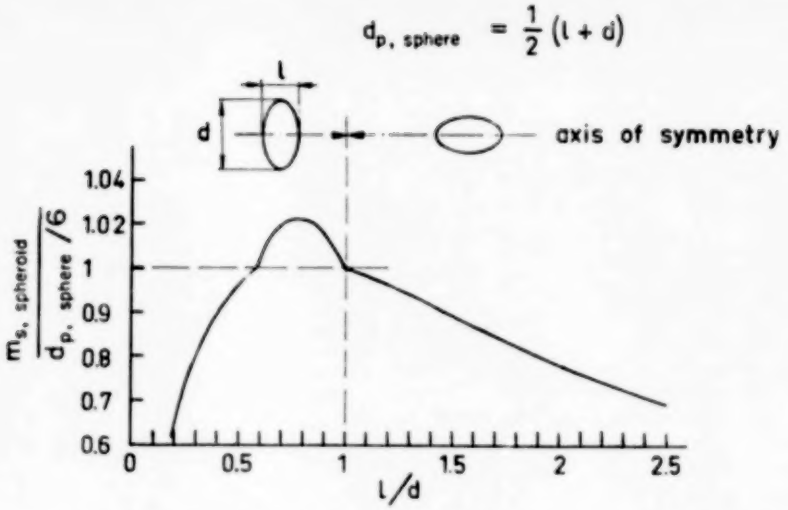

FIG. 2. The shape factor which results if the spheroid is approximated by means of a sphere with a diameter equal to the arithmetic mean of the maximum and minimum axes.

VOL. 15 1961

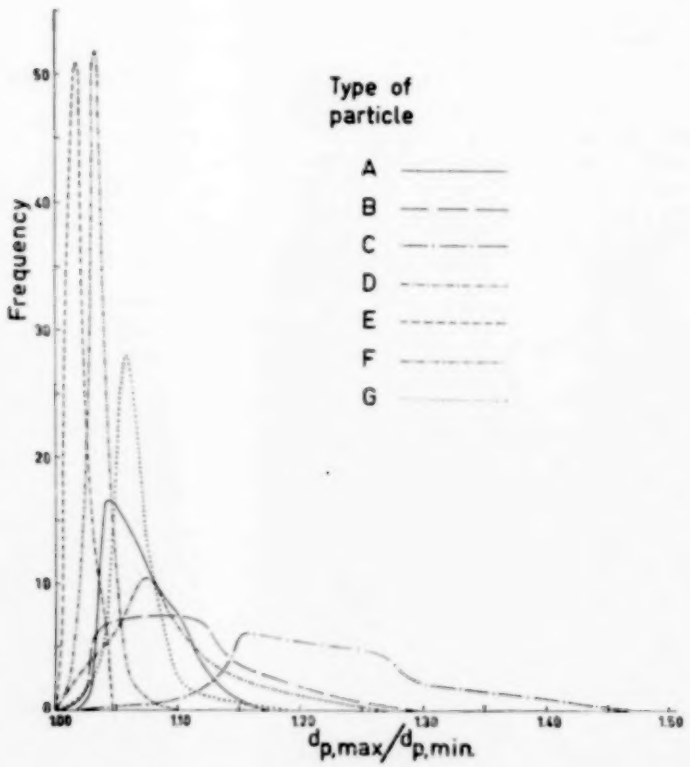

FIG. 3. Distribution of deviation from spherical shape.

(and thus from the hydraulic radius) for certain particle shapes, e.g. rotation symmetrical spheroids. The error for this case, expressed as a correction factor, is shown in Fig. 2 as a function of the axis ratio l/d. This correction factor is thus a type of shape factor, which is not equivalent to the Wadell shape factor [9] as it is not prescribed here that the spheroid and the sphere have the same volume. The volume of the sphere is instead determined by the condition that its diameter follows the relation: $d_p = (\frac{1}{3}l + d)$. Only the particles B and C with l/d equal to 0·907 and 0·820 respectively could be approximated to such spheroids whereas no special shape could be attributed to the other particles. The error was in any case low enough to be neglected.

The distribution of the deviation of the particles from a spherical shape is shown in Fig. 3 for each kind of particle; the surface under each smoothed histogram is unity.

Procedure

The experiments were performed in a conventional way. The amount of particles in each bed was selected so that the ratio $L_0/d_p\,(= L\,[1-\epsilon]/d_p)$ had one of the values 12·5, 25, 50 or 100. Equilibrium bed height was reached very quickly but was not measured until a few minutes later. At high void fractions the lubricating oil gave a somewhat diffuse upper bed level because of the sensitivity of the viscous term to even a small spread in the particle size.* The fluid temperature was measured to within 0·1 °C and thus the viscosity could be determined to within 1 per cent.

The pressure drop was measured in the water fluidization experiments using the large-scale equipment and no significant deviation was found from the static pressure drop formula

$$\frac{\Delta P}{L} = g\,(\rho_s - \rho)\,(1 - \epsilon) \qquad (6)$$

which has been used in all calculations.

Fluidization characteristics

The fluidization in the present study must be characterized as particulate, i.e. neither bubble formation (including slugging) nor channeling was observed. Thus, due to the small bed dimensions, lead shot fluidized in water showed only very small divergencies from ideal conditions. Is larger beds of the same system inhomogeneities have been reported previously [10].

Steel balls fluidized in oil ($0{\cdot}3 \leqslant \mathrm{Re}_p \leqslant 0{\cdot}8$) showed an interesting phenomenon of chain formation. These chains, each consisting of about three to seven particles, moved, broke down and reformed in an irregular manner. The phenomenon was not noticeable in oil fluidization of small lead shot ($\mathrm{Re}_p = 0{\cdot}066$). It has recently been extensively studied by Happel and Pfeffer using two spherical particles [11].

Results and Discussion

The pressure drop equation

The calculations in this investigation are analogous to those in the author's earlier paper. Thus, substituting in equation (3)

$$m = \epsilon d_p/6\,(1 - \epsilon)$$

and rearranging, we study here the function

$$zq^2 = \frac{(\Delta P/L) - 6\,c_i q^3\,[(1-\epsilon)/\epsilon^3]\,(\rho U^2/d_p)}{36\,[(1-\epsilon)^2/\epsilon^3]\,(\mu U/d_p^2)} \qquad (7)$$

in the region of mainly viscous losses, and the function

$$c_i q^3 = \frac{(\Delta P/L) - 36\,zq^2\,[(1-\epsilon)^2/\epsilon^3]\,(\mu U/d_p^2)}{6\,[(1-\epsilon)/\epsilon^3]\,(\rho U^2/d_p)} \qquad (8)$$

for systems with higher particle Reynolds numbers.

The pressure drop equation does not take into account the errors due to the wall effect and flow entrance conditions. Therefore, in calculating $c_i q^3$ from equation (8) we must know the correct value of zq^2 (and vice versa in equation 7). Thus $c_i q^3$ and zq^2 have been experimentally determined under the same geometrical conditions [L_0/d_p and d_l/d_p (and d_p)], i.e. for example oil experiments with a certain bed in a certain column have been used to determine zq^2 from equation (7) and this value has been used in the study of $c_i q^3$ when the same bed in the same column is fluidized in water or water–glycerol mixtures.

Another factor to take into consideration in the

*It is very difficult to give any limits within which the bed height was determined, since these limits are unknown functions of different factors, e.g. the distribution of particle size, the Reynolds number, the void fraction and the wall effect. The *result* of wrong bed height determination is, however, discussed later.

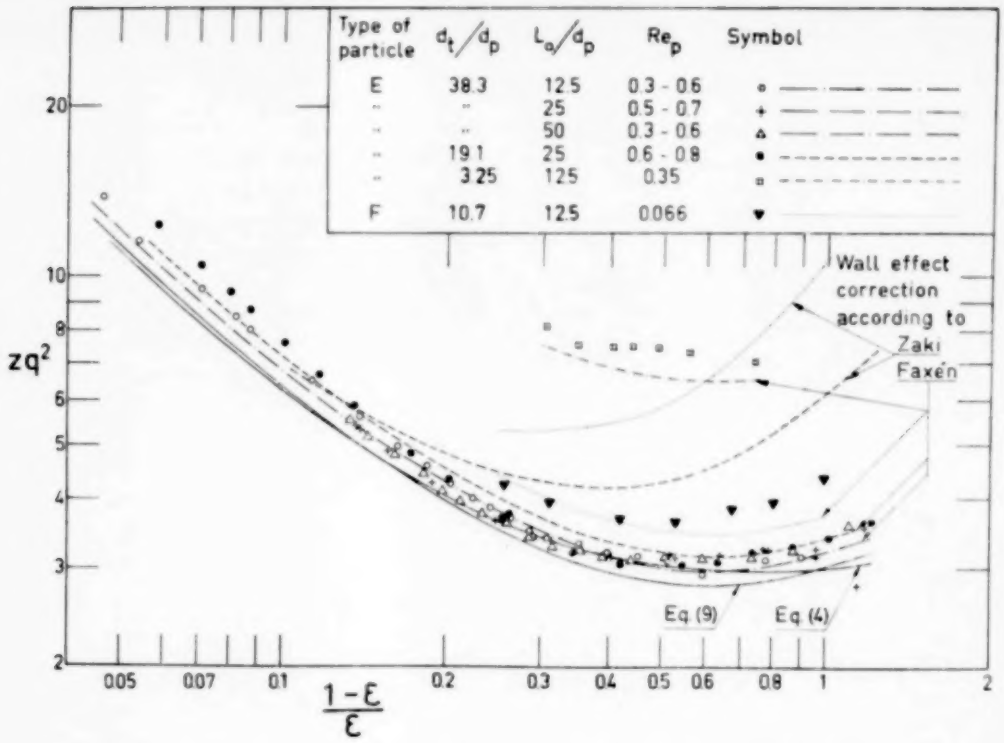

Fig. 4 (a). Some typical data for the fluidization of steel balls and lead shot in oil.

calculations is the fact that $c_i q^3$ varies considerably with particle Reynolds number. The value of $c_i q^3$ was experimentally determined for the range $5 < Re_p < 2000$ and the oil data corresponded to the range $0{\cdot}003 < Re_p < 0{\cdot}8$. Therefore, the relationship found for $c_i q^3$ had to be extrapolated when evaluating zq^2 from equation (7). This extrapolation will be shown later.

The values of $c_i q^3$ are *a priori* incorrect and this results in slightly incorrect values of zq^2 when they are applied to equation (7). However, a recalculation of $c_i q^3$ from equation (8) based on the new zq^2 increases the accuracy considerably. This interdependence between $c_i q^3$ and zq^2 results in a very rapid convergence when such successive approximations are applied to equations (7) and (8). All data shown in Figs. 4–6 have been calculated to their final values.

The results for some systems with low particle Reynolds number are shown in Figs. 4 (a) and (b), where the modified Kozeny factor is plotted vs. $m_z/m = (1-\epsilon)/\epsilon$. In Fig. 4 (a) equations (4) and (9) are also illustrated, the latter of these is derived from the Vand Hawksley relation [12, 13]:

$$zq^2 = \tfrac{1}{2}\,\frac{\epsilon}{1-\epsilon}\exp\left[\frac{2{\cdot}5\,(1-\epsilon)}{1-(39/64)\,(1-\epsilon)}\right] \qquad (9)$$

Using an exponent of 4·59 in equation (1) we get a zq^2-dependence on void fraction conforming with equation (9a):

$$zq^2 = \tfrac{1}{2}\,(1-\epsilon)^{-1}\,\epsilon^{-1{\cdot}59} \qquad (9a)$$

This equation gives values of zq^2 within 1 per cent of those derived from equation (9). Denoting the exponential term in equation (9) by y, it is thus found that $y \approx \epsilon^{-2{\cdot}59}$.

The divergence of experimental data from equation (9) is mainly due to the wall effect. Assuming that the wall effect is independent of void fraction, the Faxén correction factor for a single sphere in the centre of a tube can be used, thus the

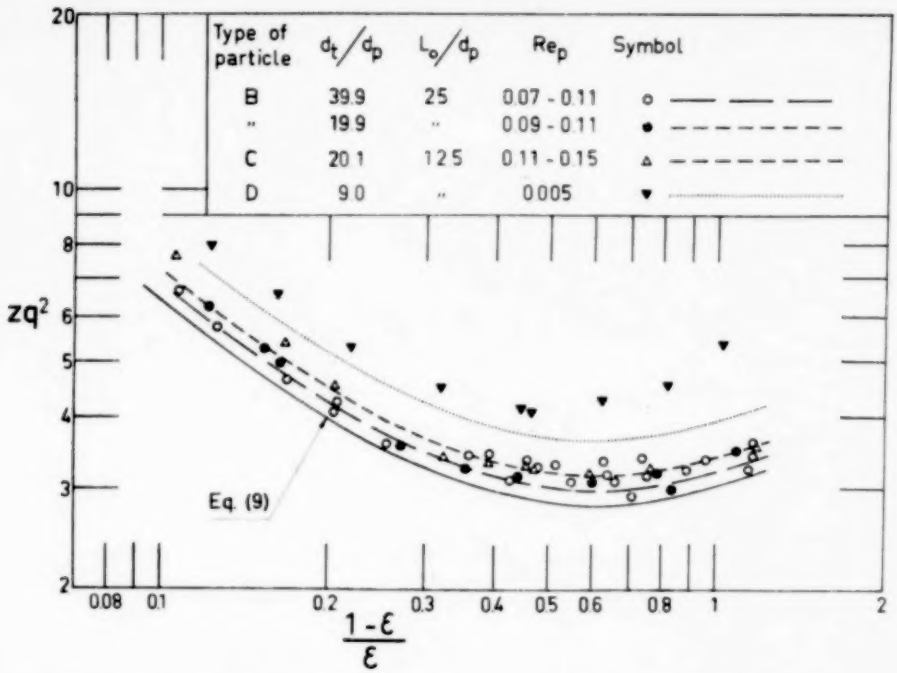

FIG. 4 (b). Some typical data for the fluidization of glass beads in oil, and a plot of equation (9) and this equation corrected according to FAXÉN.

right-hand side of equation (9) is divided by $[1 - 2{\cdot}104\, d_p/d_t + 2{\cdot}09\,(d_p/d_t)^3 - \ldots]$, [14]. These lines of corrected zq^2 are drawn in Figs. 4 (a) and (b). Obviously the assumption is somewhat crude, but this wall effect correction factor indubitably results in a better fit of data than the correction factor proposed by ZAKI, $\epsilon^{19{\cdot}5\, d_p/d_t}$, cf Fig. 4 (a). Furthermore, due to the Faxén factor, it is strongly indicated that equation (9) is more consistent than equation (4).

Turning our interest to fluidized beds with mainly inertia pressure drop losses, we find that $c_f q^3$ is a simple function of m_s/m since the data in a logarithmic plot fall on straight lines with very high significance levels (Figs. 5a and b). This fact, based on experiments in the large-scale equipment, constitutes the basis of the present work.

Furthermore, the parameter L_0/d_p has a negligible effect in ideal fluidization at both high and low Reynolds numbers, as is shown by Figs. 4 (a), 5 (a) and (b). Figs. 4 (b) and 5(b) also show that the effect of non-spherical particle shape is very small in the region of non-sphericity studied here, since the results with particle type C deviate very little from those with particle type B.

Figs. 5 (a) and (b) indicate a strong $c_f q^3$-dependence on particle Reynolds number. Therefore the investigation was extended to include also the " transition region ". This was done in the small-scale equipment using water and glycerol–water solutions as fluids. Some characteristic results are shown in Fig. 6 and the complete results are given in Table 3. In Fig. 6 are drawn the regression lines for each series (dashed lines) according to the equation

$$c_f q^3 = c' \left(\frac{1-\epsilon}{\epsilon}\right)^{3n} \qquad (10)$$

Table 3 gives c' and $3n$ as well as the confidence limits of the regression lines represented by the correlation coefficient and the degrees of freedom.

A statistical test on the data in Table 3 and Figs. 5 (a) and (b) shows that the exponent $3n$ is

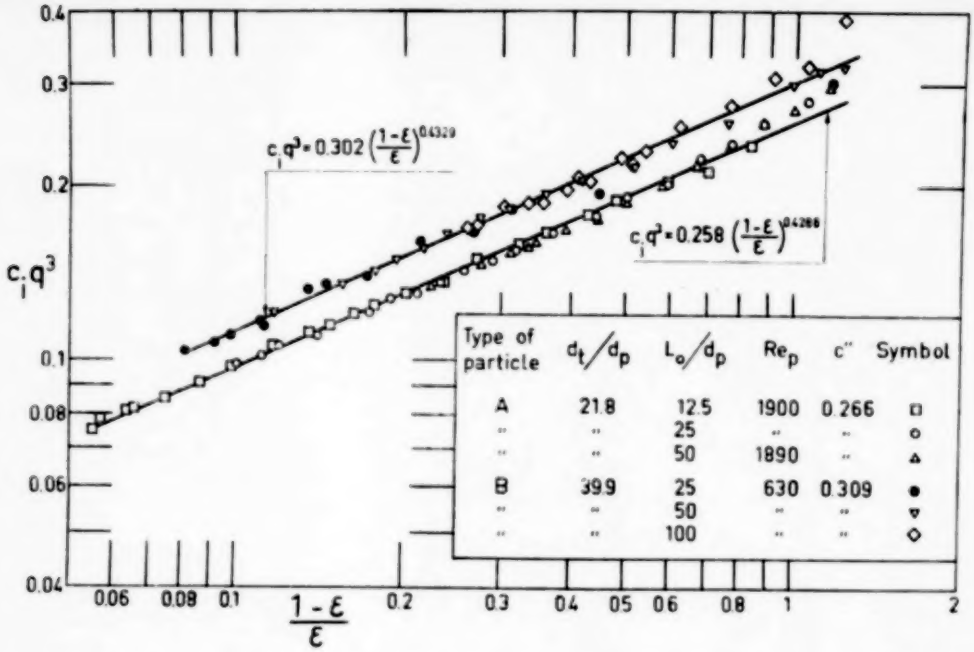

FIG. 5 (a). The factor $c_i q^3$ vs. m_s/m for fluidization of glass beads in water in a 12 cm column.

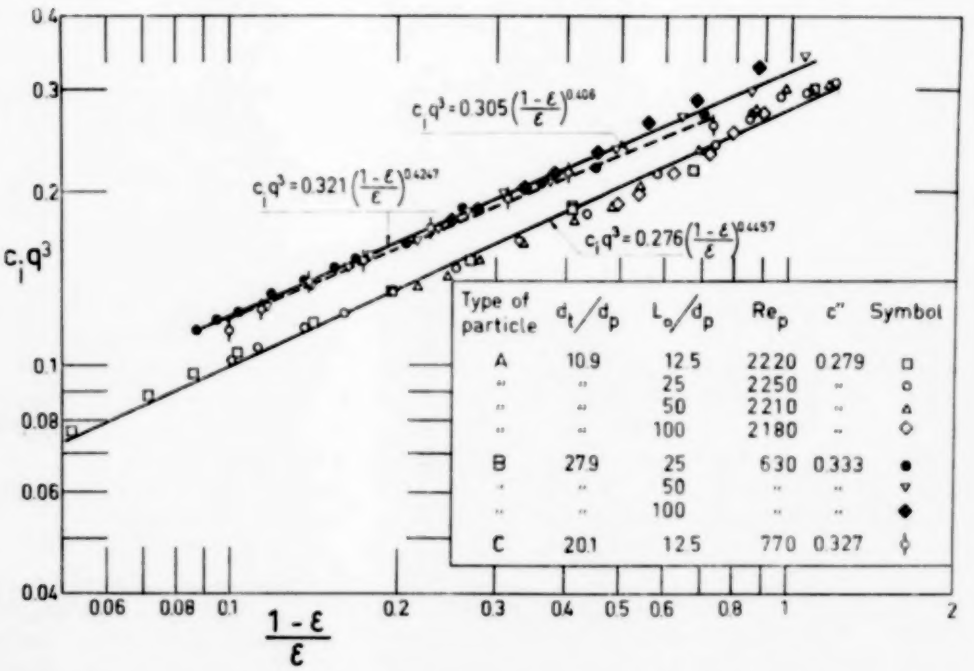

FIG. 5 (b). The factor $c_i q^3$ vs. m_s/m for fluidization of glass beads in water in 8·4 and 6 cm columns.

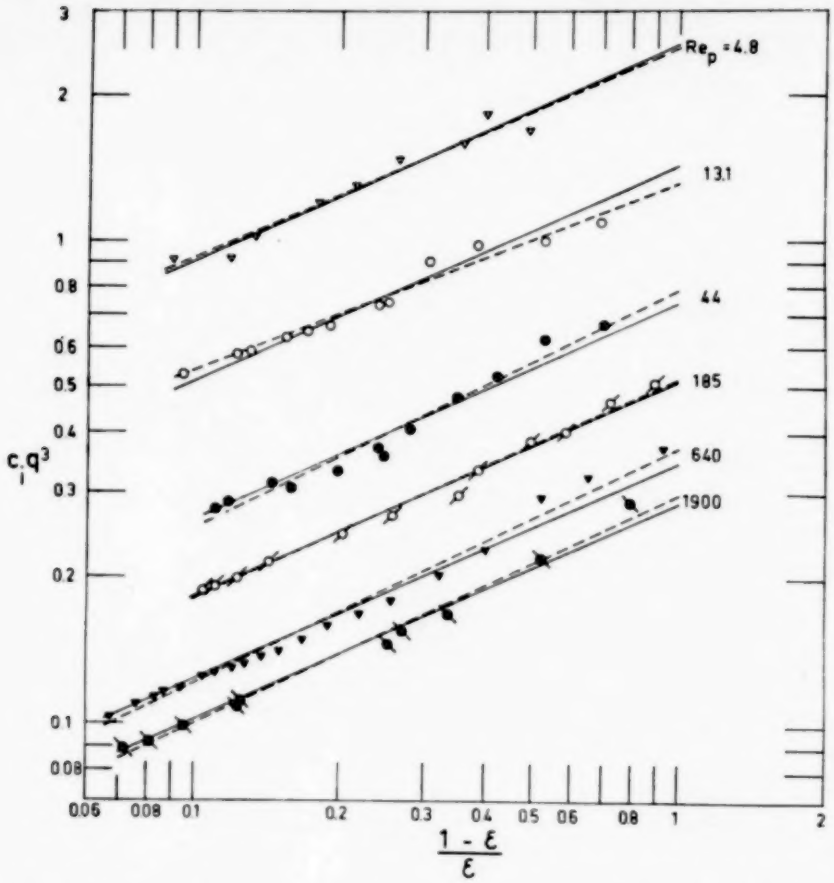

FIG. 6. Some typical results for small-scale equipment experiments. Open and filled symbols represent glass beads and lead shot respectively. Regression lines are dashed, best lines of slope 0·45 are unbroken.

independent of the particle Reynolds number in the range $5 < \mathrm{Re}_p < 2000$. The assumption of the same void fraction dependence of the tortuosity factor in the inertia and viscous terms is thus a reasonable one.

The arithmetic mean of the exponent is 0·452. A t-test shows that the assumption of a true value of 0·45 cannot be rejected ($t = 0{\cdot}199$, $f = 22$). Thus we study here the function

$$c_i q^3 = c'' \left(\frac{1 - \epsilon}{\epsilon} \right)^{0{\cdot}45} \qquad (11)$$

Corresponding lines are drawn in Fig. 6 and the factor c'' is tabulated in Table 3.

The assumption that the wall effect is independent of void fraction also at higher Reynolds numbers justifies the multiplication of c'' by the empirical factor presented by MUNROE [15], $[1 - (d_p/d_t)^{3/2}]^2$. Values of c'' thus corrected are shown in Fig. 7 as a function of particle Reynolds number. The great variation of c'' is quite analogous to the conditions for a single sphere, as is shown by the upper curve of Fig. 7 which is derived from SCHLICHTING's textbook [16]. Here the ordinate is the inertial drag coefficient C_I, which is a measure of the deviation from Stokes' law described by the relation

$$C_D = \frac{24}{\mathrm{Re}_p} + C_I \qquad (12)$$

Table 3. Results of small-scale experiments

Fluids: water and water–glycerol solutions. $L_0/d_p = 12{\cdot}5$.

Type of particle	d_t (cm)	Re_p	c'	$3n$	*Degrees of freedom*	*Correlation coefficient*	c°
D	1·69	4·80	2·519	0·436	7	0·645	2·572
D	1·69	13·1	1·324	0·393	10	0·616	1·441
D	1·69	28·2	1·168	0·546	10	0·725	1·040
D	1·69	54	0·935	0·523	9	0·713	0·846
D	1·69	127	0·631	0·479	13	0·686	0·605
D	1·69	185	0·520	0·458	10	0·673	0·515
D	1·69	265	0·429	0·414	11	0·638	0·452
D	1·69	490	0·365	0·428	13	0·652	0·377
D	1·02	356	0·355	0·360	10	0·598	0·405
G	1·69	17·1	1·155	0·491	8	0·659	1·095
G	1·69	44	0·796	0·498	10	0·695	0·744
G	1·69	90	0·634	0·528	5	0·724	0·588
G	1·69	165	0·396	0·351	9	0·558	0·444
G	1·02	360	0·394	0·429	14	0·652	0·407
G	1·02	670	0·337	0·432	15	0·652	0·346
F	1·69	640	0·374	0·491	18	0·696	0·348
F	1·69	1080	0·350	0·532	10	0·725	0·317
F	1·69	1900	0·298	0·475	8	0·685	0·286

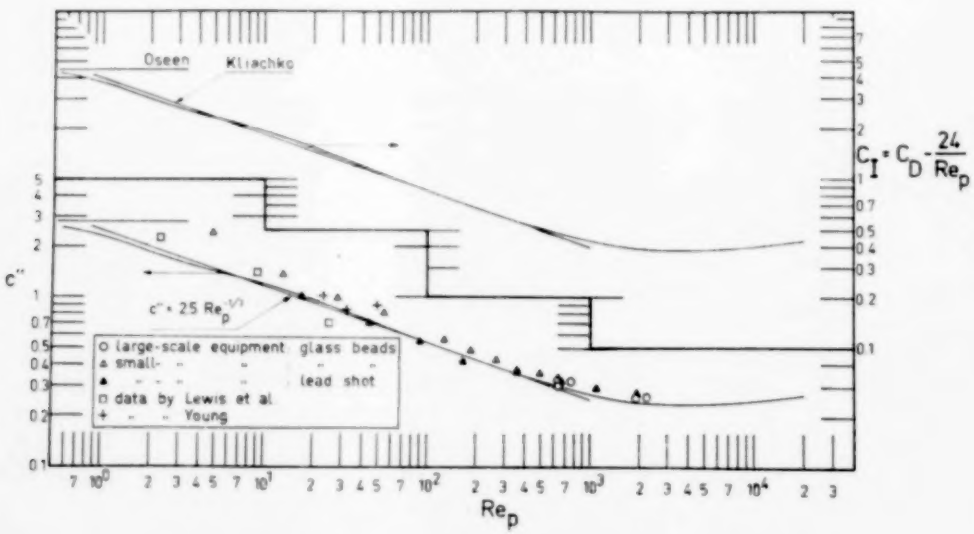

Fig. 7. The factor c° vs. particle Reynolds number (lower curve) and corresponding relationship for a single sphere (upper curve).

VOL. 15 1961

where C_D is the well-known standard drag coefficient. In the "transition region" C_I may be approximated by the relation proposed by KLIACHKO [17]:

$$C_I = 4\,\mathrm{Re}_p^{-1/3} \tag{13}$$

For lower particle Reynolds number $C_I = 4{\cdot}5$ according to the Oseen solution [18].

A vertical displacement of the upper curve obviously results in a curve coincident with that for c''. When the ordinate is changed so that the curves are coincident for the system with the lowest wall effect ($\mathrm{Re}_p = 630$, Fig. 5a) it is found that

$$c'' = \tfrac{5}{8}\,C_I \tag{14}$$

It is now possible to write equation (3) in its complete form:

$$\frac{\Delta P}{L} = 36\,z q^2 \frac{(1-\epsilon)^2}{\epsilon^3}\frac{\mu U}{{d_p}^2} + \\ + \frac{15}{4}\,C_I \frac{1-\epsilon}{\epsilon^3}\left(\frac{1-\epsilon}{\epsilon}\right)^{0.45}\frac{\rho U^2}{d_p} \tag{15}$$

where zq^2 is given by equation (9) or equation (9a).

Although the basic assumption of a pressure drop equation of second order in fluid velocity has not been directly verified, several reasons favour it. Thus, upon this assumption the tortuosity factor was shown to be a geometrical factor and was furthermore shown to be a simple function of the ratio of the solid phase radius to the mean hydraulic radius.

The generalized friction factor curve

Upon substituting $\Delta P/L$ in equation (15) according to equation (6) the viscous term is found to converge to Stokes' law, when $\epsilon \to 1$, but the inertia term makes no contribution to the pressure drop in this limit due to the fact that the tortuosity factor according to equation (11) goes to zero instead of unity. Studying this problem in detail we transform equation (3) (or 15) to a relationship between the friction factor and Reynolds number. The over-all force balance between the pressure drop and the forces F acting on the particles, composed of both shear stresses and normal stresses, is given by equation (16):

$$F = \frac{\Delta P}{L_e}\,m \tag{16}$$

Substituting in equation (3) ΔP from equation (16) and U by means of $u = qU/\epsilon$, we get, after rearrangement, the friction factor f

$$f = \frac{F}{\rho u^2} = \frac{z\mu}{mu\rho} + c_i \tag{17}$$

At $\epsilon = 1$ the friction factor $f = C_D/8$ in accordance with the definition of the standard drag coefficient. Hence the inertial coefficient c_i is defined by the simple relation

$$c_i = C_I/8 \tag{18}$$

Equation (11) is thus transformed into equation (19):

$$q^3 = \frac{8\,c''}{C_I}\left(\frac{1-\epsilon}{\epsilon}\right)^{0.45} \tag{19}$$

which according to the empirical equation (14) gives the final expression for the tortuosity factor:

$$q = 1{\cdot}71\left(\frac{1-\epsilon}{\epsilon}\right)^{0.15} \tag{20}$$

Consequently the absolute value of the tortuosity factor is independent of the particle Reynolds number which constitutes the final proof of this factor's geometric character.

From equation (9) we then get the cross-section factor

$$z = 0{\cdot}171\,y\left(\frac{1-\epsilon}{\epsilon}\right)^{-1.30} \tag{21}$$

According to equation (20) the value of the tortuosity factor equals unity at $\epsilon = 0{\cdot}973$. Hence the consistency of equation (20) ceases at some void fraction level between 0·973 and $\sim 0{\cdot}95$ where the equation still consistently represents the data and the tortuosity factor goes to unity as the void fraction approaches unity.

Equations (20) and (21) are illustrated in Fig. 8 together with interesting analytical solutions for certain analogous problems. Recently SPARROW and LOEFFLER [19] presented solutions for longitudinal, fully developed laminar flow between cylinders arranged in triangular and

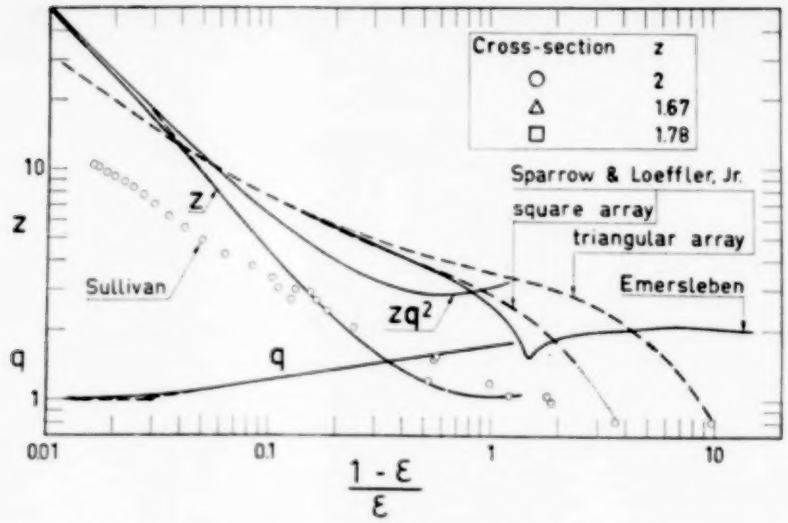

Fig. 8. The tortuosity factor and cross-section factor in ideal fluidization together with cross-section factors for other geometrical shapes.

square arrays. These results have been transformed here into values for the cross-section factor using the hydraulic radius as the characteristic dimension. The Fig. also shows the well-known Emersleben solution for longitudinal laminar flow between rods in a square array [20] which closely follows the square-array solution of Sparrow and Loeffler for $\epsilon > 0{\cdot}6$. This is expected since the rods have an approximately circular cross-section in this region but change their shape for lower void fractions in accordance with the complex zeta-function used by Emersleben. Fig. 8 also gives Sullivan's experimental data [21] for laminar flow along parallel-oriented filaments of goat's wool, blond hair, Chinese hair, glass wool, copper wire and segments of drill rod. His data are much lower than those predicted from theory except for the case of flow along cylinders in contact with each other.

Fig. 8 shows two striking features near the boundary of the packed bed. Firstly, the value of the tortuosity factor is here about 1·80 which is fairly high compared with the values of 1·40–1·45 obtained by diffusion and electrical conductivity measurements in packed beds of equally-sized spheres [5]. However, the existence of any closer analogy between the mechanisms of electrical and fluid flow has been questioned earlier [22, 23]. Secondly, the cross-section factor is about unity which is low compared with the figure of 1·67 corresponding to that for an equilaterally triangular cross-section.

However, it is known that the factor zq^2 increases about 60 per cent during the change from an ideally fluidized bed to a fixed bed [3]. This phenomenon can hardly be assigned to the tortuosity factor for the following reasons: the geometry (ϵ) changes very little in this transition region and, according to the above, an increase in the tortuosity factor would result in a still larger difference between this and published values. Accordingly, a packed bed of equally-sized spheres has about the same cross section factor as a channel whose cross-section is an equilateral triangle, whereas the corresponding factor for ideally fluidized beds in the low void fraction region is of approximately the same magnitude as that for cylindrical rods in contact.

The value of zq^2 also depends on the definition of the hydraulic radius. For an assemblage of spherical particles Reboux deduced a hydraulic radius on the basis of the classical definition, i.e. the ratio of the flow cross-section area to the wetted perimeter [8]; this radius exceeds the

Blake radius by a factor $4/\pi$. If this radius be accepted the value of the cross-section factor found here is increased by the factor $4/\pi$ whereas the tortuosity factor remains unaffected. However, the forces acting upon a particle would in this case act upon the hypothetical surface $\pi^2 d_p^2/4$ of each sphere. Accordingly the Blake hydraulic radius is superior to that of Reboux.

Different forms of Reynolds number have been used previously, such as d_pU/ν, $d_pU/\epsilon\nu$ and $mU/\epsilon\nu \propto d_pU/\nu(1-\epsilon)$, the last of which is in closest connexion to the Reynolds number to be introduced here, since it is based on the mean hydraulic radius and the Dupuit velocity. However, as the Reynolds number is proportional to the ratio of inertia losses to viscous losses it must be given the form

$$\mathrm{Re} = \frac{mu\rho}{z\mu} \tag{22}$$

$$= \frac{1}{3}\frac{d_p U\rho}{\mu}\frac{q^3}{\epsilon y} \tag{22a}$$

$$= \frac{5}{3}\frac{d_p U}{\mu}\frac{\rho}{y\epsilon}\left(\frac{1-\epsilon}{\epsilon}\right)^{0.45} \tag{22b}$$

where equation (22b) is valid only for $\epsilon \gtrsim 0.95$. Equation (22a) shows that

$$\lim_{\epsilon\to 1} \mathrm{Re} = \tfrac{1}{3}\,\mathrm{Re}_p$$

Accordingly, the characteristic length automatically changes from hydraulic radius to particle diameter in this limit of unit void fraction.

The inclusion of the cross-section factor in the Reynolds number also gives a single standard friction factor curve for each constant value of the particle Reynolds number:*

$$f = \frac{1}{\mathrm{Re}} + \frac{C_I}{8} \tag{17a}$$

where

$$f = \frac{1}{6}\frac{\Delta P}{L_0}\frac{d_p}{\rho U^2}\frac{\epsilon^3}{q^3} \tag{23}$$

$$= \frac{1}{30}\frac{\Delta P}{L}\frac{d_p}{\rho U^2}\epsilon^2\left(\frac{\epsilon}{1-\epsilon}\right)^{1.45} \tag{23a}$$

$$= \frac{C_D}{8}\left(\frac{U}{U_\infty}\right)^{-2}\frac{\epsilon^4}{y^2} \tag{23b}$$

where equation (23a) is restricted to void fractions below ~ 0.95. From equation (23b) the friction factor is seen to be proportional to C_D in regions where $U/U_\infty = \epsilon^2/y$, which is the case for pure

*A comparison between equations (12) and (17a) gives a relation between the cross-section factor and the viscous drag coefficient $C_V(=24)$ for a single sphere [24]: $\lim_{\epsilon\to 1} zd_p/m = 3 = C_V/8$.

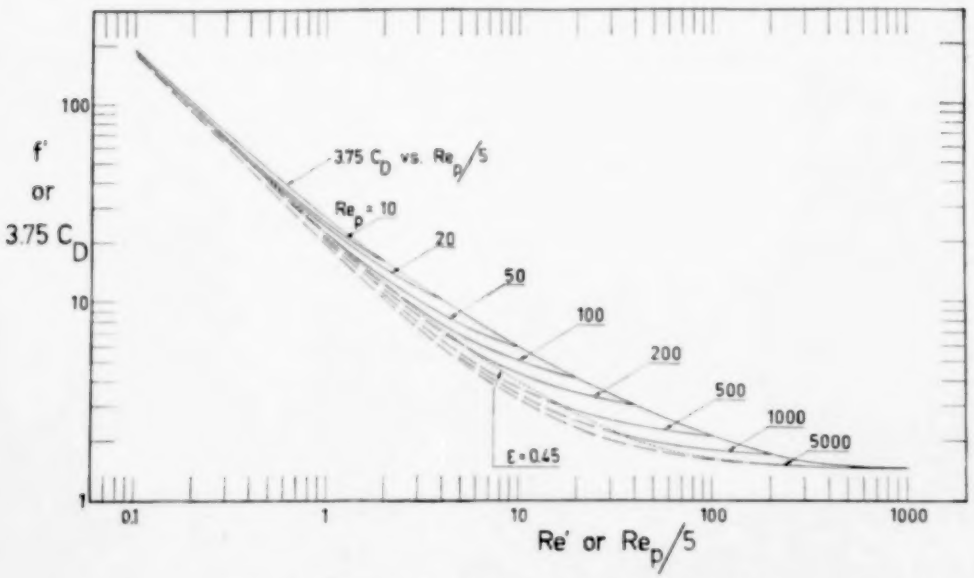

FIG. 9. The generalized friction factor vs. Reynolds number.

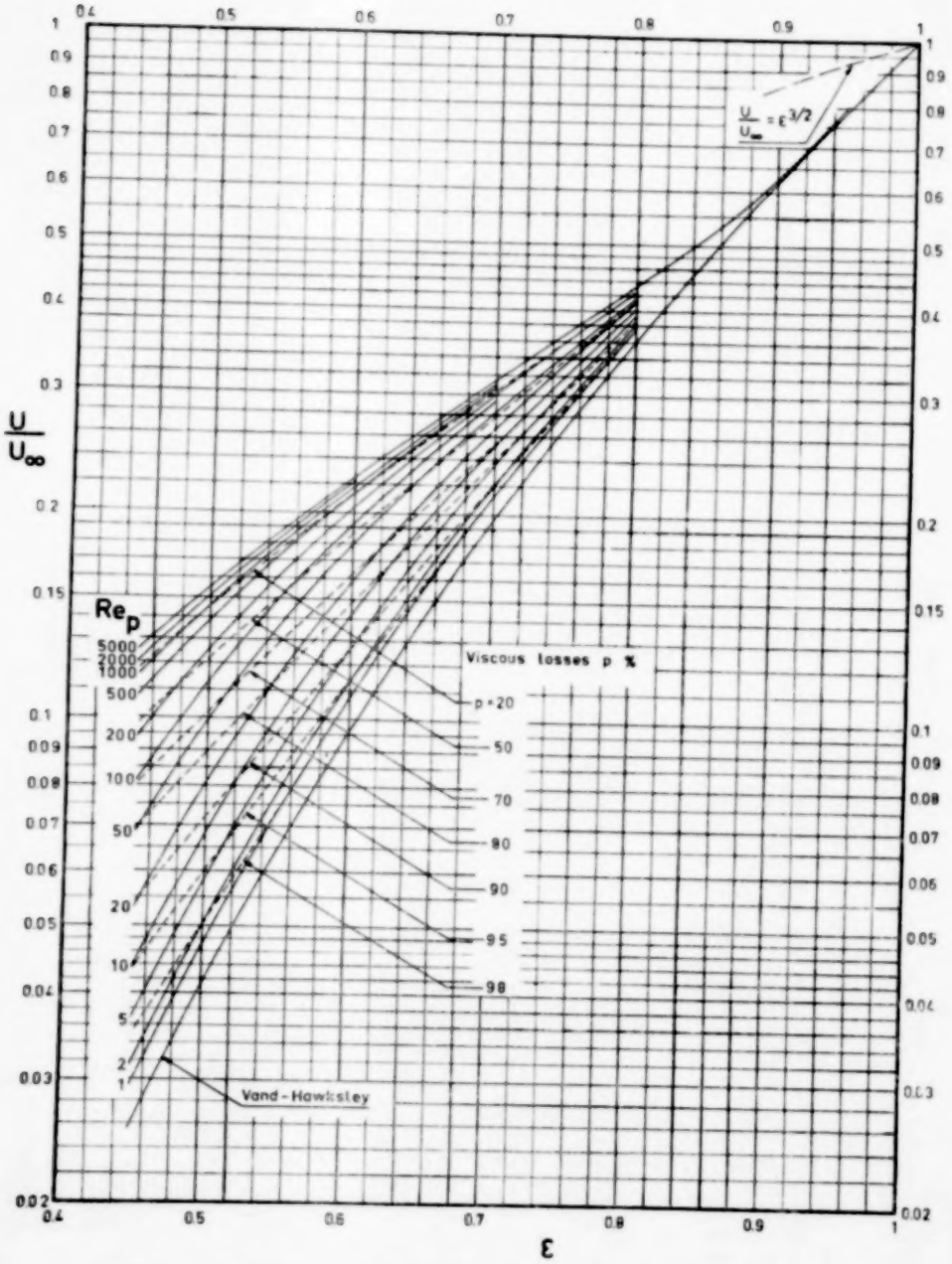

Fig. 10. The pressure drop equation presented in nomographic form.

VOL. 15 1961

viscous flow and, independently of Reynolds number, for $\epsilon > 0{\cdot}92$, cf. equation (28).

To eliminate certain constants we introduce

$$\mathrm{Re}' = \tfrac{3}{5}\,\mathrm{Re} \tag{24}$$

and

$$f' = 30 f \tag{25}$$

which leads to

$$f' = \frac{18}{\mathrm{Re}'} + \frac{15}{4} C_I \tag{26}$$

It ought to be pointed out that the right-hand sides of equations (24) and (25) include a factor 5 which is the empirical value of $8\,c''/C_I$, cf. equations (14) and (19). Equation (26) is reproduced in Fig. 9 for different values of Re_p.

Each friction factor curve is limited by two extremes the lower of which corresponds to the transition to a packed bed. In the Fig. the line corresponding to 45 per cent void fraction is drawn in order to give an idea of this lower limit. The upper extreme corresponds to $\mathrm{Re}' = \mathrm{Re}_p/5$ and at this extreme the friction factor curves end in the displaced standard drag coefficient curve for a single sphere, the displacement being dependent on the elimination of the constants mentioned above and on the different definitions of C_D and f.

Nomographic representation

The solution of equations (6) and (15) gives in each case the relationship between superficial velocity and void fraction. The calculations are tedious and the use of the friction factor diagram does not assist very much because of the complicated void fraction functions in both abscissa and ordinate. However, it is possible to solve the problem in a convenient way using the same

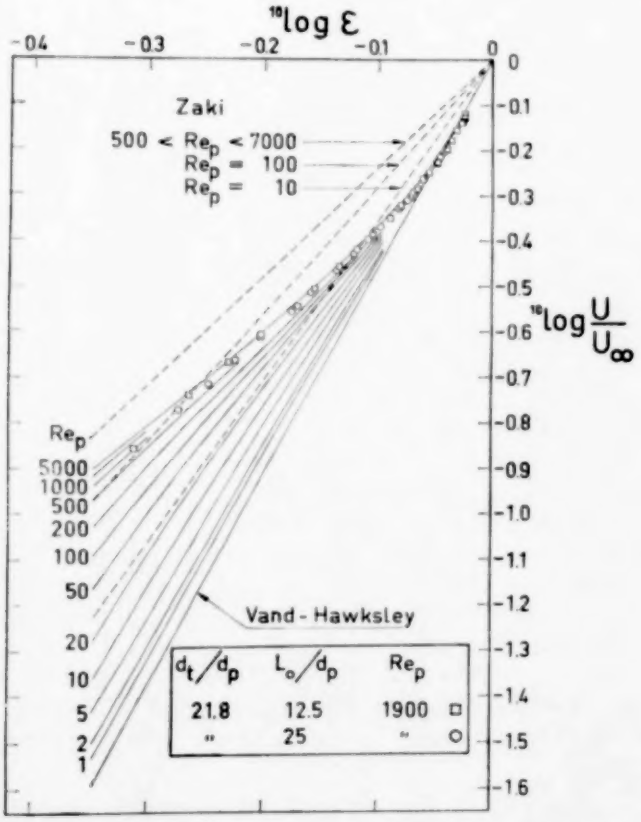

FIG. 11. The pressure drop equation compared to ZAKI's solution.

equations plus equation (12) written in the form

$$g(\rho_s - \rho) = 18\frac{\mu U_\infty}{d_p^2} + \frac{3}{4}C_I\frac{\rho U_\infty^2}{d_p} \qquad (12a)$$

The solution is given by equation (27):

$$\frac{U}{U_\infty} = \frac{1}{2\phi}\frac{\epsilon y}{q^3}\left\{\sqrt{\left[1 + \frac{4\epsilon q^3}{y^2}(\phi + \phi^2)\right]} - 1\right\} \qquad (27)$$

where $\phi = (C_D \mathrm{Re}_p/24) - 1$. This equation is reproduced in Fig. 10 which also shows lines of constant fraction viscous losses. The considerable difference between the Zaki-solution and equation (27) is demonstrated in Fig. 11.

There are different ways to remove the inconsistency of equation (27) for $\epsilon \gtrsim 0{\cdot}95$ at larger particle Reynolds numbers. For instance, neglecting viscous forces in equations (15) and (12a) and giving the tortuosity factor a value of one, we get the relationship $U/U_\infty = \epsilon^{3/2}$, which is also shown in Fig. 10. However, judging from the same Fig. it is more probable that U/U_∞ has the same void fraction dependence in the viscous and the inertial regions. Thus, again neglecting the viscous forces in the same equations and substituting for U in equation (15) from the relationship $U/U_\infty = \epsilon^2/y$, we get $q^3 = y^2/\epsilon$ or

$$q \approx \epsilon^{-2} \qquad (28)$$

which is valid for $\epsilon > 0{\cdot}92$. Although not experimentally proved, this relationship is recommended here.

In the region $0{\cdot}92 < \epsilon < 0{\cdot}94$ equations (20) and (28) result in the same value of the tortuosity factor. According to equation (28) this factor is not a function of m_s/m for $\epsilon > 0{\cdot}94$ and thus the channel model fails in this region which therefore ought to be regarded as a transition region between channel flow and free particle flow.

The reproduction of Reynolds number as a function of void fraction and particle Reynolds number clearly shows the great importance of choosing appropriate values of the two empirical constants in this study, viz. n and $c_i/c'' = C_I/8c'' = \lim_{\epsilon\to 1} \mathrm{Re}'/\mathrm{Re}_p$, cf. equations (14) and (24). Figure 12 thus shows the ratio

$$\frac{\mathrm{Re}'}{\mathrm{Re}_p} = \frac{1}{y\,\epsilon}\left(\frac{1-\epsilon}{\epsilon}\right)^{3n}\frac{U}{U_\infty} \qquad (29)$$

for $n = 0{\cdot}15$ and $c_i/c'' = 0{\cdot}2$. Without changing c_i/c'' but choosing $3n = 0{\cdot}432$ in accordance with the results from the large-scale experiments (Fig. 5a) the ratio $\mathrm{Re}'/\mathrm{Re}_p$ exceeds 0·2 for high void fractions (Fig. 12, separate curves). For $\epsilon > 0{\cdot}93$ this is equivalent to the abnormal behaviour of a decreasing Reynolds number at increasing fluid velocity. Thus a change of the tortuosity factor exponent to a lower value prescribes a larger $\lim_{\epsilon\to 1} \mathrm{Re}'/\mathrm{Re}_p$.

For laminar flow the following relationship can be deduced:

$$\frac{\mathrm{Re}'}{\mathrm{Re}_p} = \frac{\epsilon}{y^2}\left(\frac{1-\epsilon}{\epsilon}\right)^{3n} \qquad (29a)$$

and for very large Re_p (viscous losses being neglected) the corresponding expression is

$$\frac{\mathrm{Re}'}{\mathrm{Re}_p} = \frac{\epsilon^{1/2}}{y}\left(\frac{1-\epsilon}{\epsilon}\right)^{3n/2}\left(\frac{C_I}{8\,c''}\right)^{1/2} \qquad (29b)$$

Together with the condition that

$$\frac{\mathrm{Re}'}{\mathrm{Re}_p} \leqslant \lim_{\epsilon\to 1}\frac{\mathrm{Re}'}{\mathrm{Re}_p} \equiv \frac{C_I}{8\,c''} \qquad (30)$$

both equation (29a) and equation (29b) prescribe that

$$\frac{8\,c''}{C_I} \leqslant \frac{y^2}{\epsilon}\left(\frac{1-\epsilon}{\epsilon}\right)^{-3n} \qquad (31)$$

Thus, for a certain void fraction, ϵ_m, which depends on the value of n ($0{\cdot}925 < \epsilon_m < 0{\cdot}930$) the theoretical maximum of c''/c_i is given by

$$\left(\frac{c''}{c_i}\right)_{\max.} = \frac{y^2}{\epsilon_m}\left(\frac{1-\epsilon_m}{\epsilon_m}\right)^{-3n} \qquad (31a)$$

This relation is shown in Fig. 13*. In view of this Fig. it must be concluded that the values of n and c'' found in this investigation are satisfactory although a somewhat lower c'' would result in a smoother transition to free particle flow at unit void fraction (a lower c'' should, however, be avoided due to the experimental results).

*The direct physical meaning of the ratio c''/c_i is, according to equation (11), the tortuosity factor at 50 per cent void fraction raised to the third power.

VOL. 15 1961

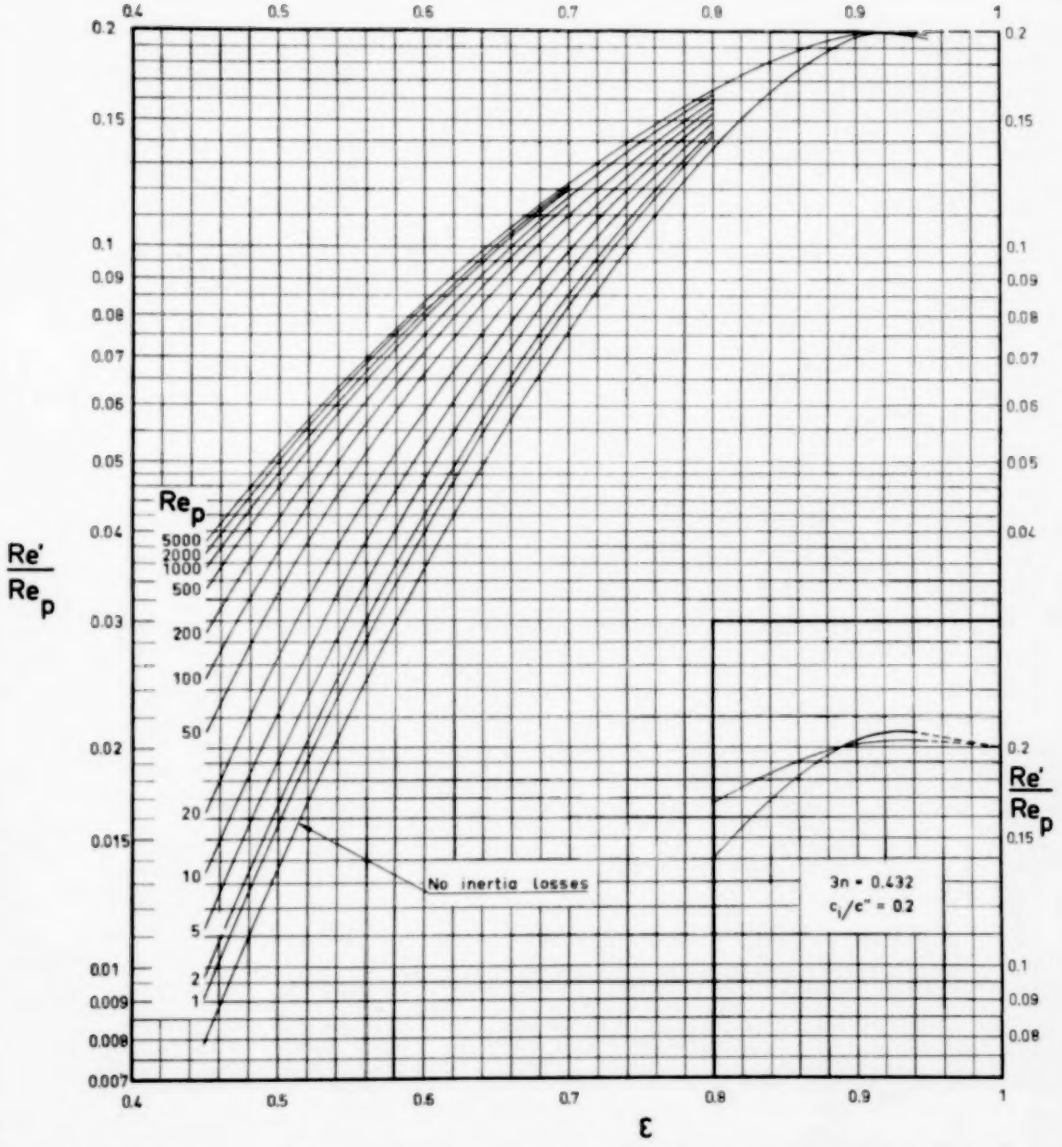

FIG. 12. The relationship between Reynolds number Re′, particle Reynolds number and void fraction. ($3n = 0{\cdot}45$, $c_i/c'' = 0{\cdot}2$).

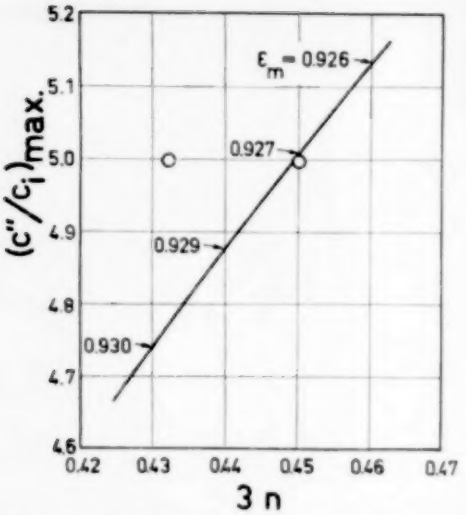

Fig. 13. The theoretical maximum value of c''/c_i vs. the tortuosity factor exponent. The values of c_i/c'' and $3n$ discussed in Fig. 12 are shown here as open circles.

Comparison with previously published data

Some published data are consistent with the pressure drop equation while others are not. Data from various sources are represented in Figs. 14 (a) and (b) which show $c_i q^3$ vs. m_s/m for different particle Reynolds numbers. Wilhelm and Kwauk's data [10] for Socony beads and glass beads are in rather good agreement with the equation as are two of the series by Lewis *et al.* [25]. The latter data show, however, a rather large spread because of the high sensitivity to experimental errors in the region of low particle Reynolds numbers. The data of Tesařík [26] show some disagreement, but this author reports a standard viscosity of 1 cP as do Wilhelm and Kwauk. Although Bandukwala's data [27] are in good agreement with the equation at very low Reynolds numbers (not shown here) his results deviate considerably in the region $5 < \mathrm{Re}_p < 73$ in the same way as one of Lewis' series. This divergence might be due to bubble formation or channeling, since the equation is very sensitive to deviations from ideal conditions. Non-uniformities were also reported by Bandukwala. However, in the present investigation, the fluidization of glass beads in liquids must be characterized as very smooth. Young's data [28] relate to the same Reynolds number range as those of Bandukwala but they are in good agreement with the equation. The difference might be due to differences in inlet conditions.

In experiments of this kind a wrong determination of the bed height has a most deleterious effect on the value of $c_i q^3$ calculated according to equation (8). In further studying this problem we rearrange equation (8):

$$c_i q^3 = \frac{3}{\mathrm{Re}_p}\left(\frac{U}{U_\infty}\right)^{-2}\left[\frac{C_D \mathrm{Re}_p}{24}\varepsilon^3 - \frac{U}{U_\infty}\varepsilon\, y\right] \qquad (8a)$$

Differentiating the logarithm of this equation with respect to ε (keeping U/U_∞ constant) and substituting $d\varepsilon$ according to the relation

$$d\varepsilon = (1-\varepsilon)\frac{dL}{L}$$

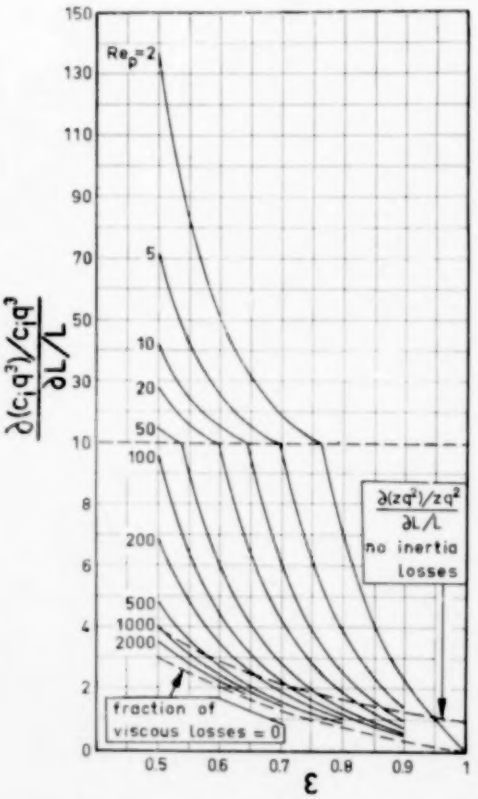

Fig. 15. The error arising from a wrong determination of bed height vs. void fraction, and for different particle Reynolds numbers, is shown.

VOL. 15 1961

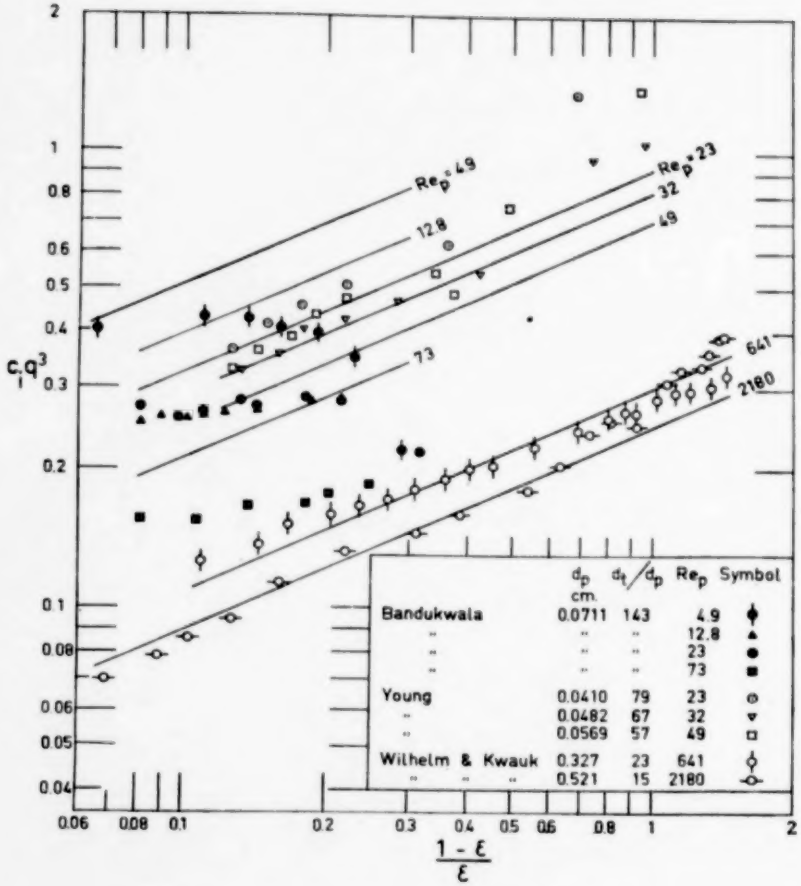

FIG. 14 (a). The factor $c_i q^3$ based on published liquid fluidization data compared with the author's equation.

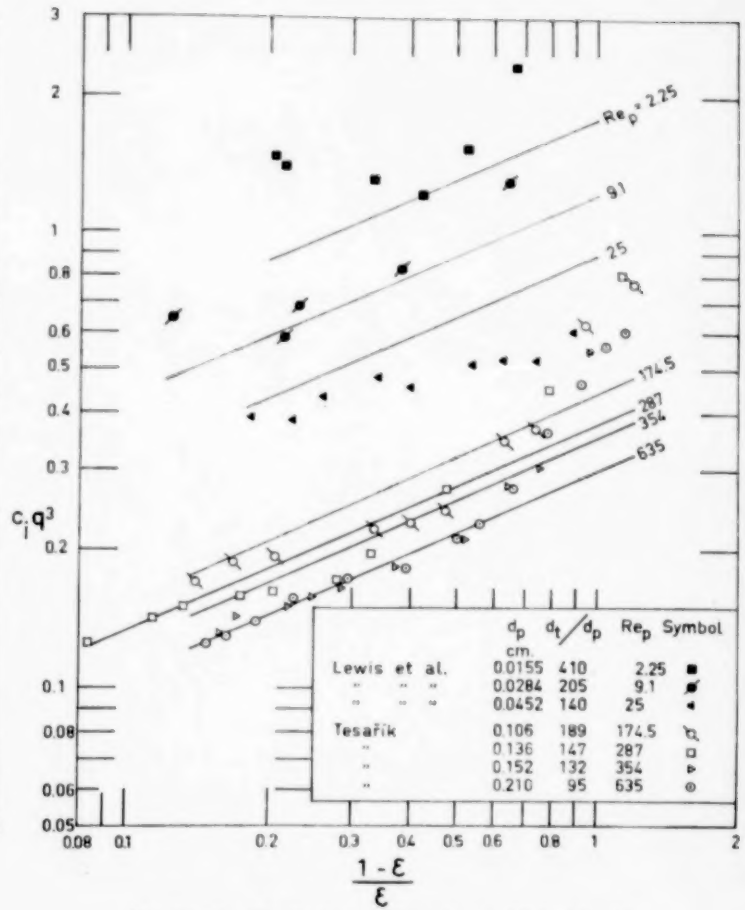

FIG. 14 (b). The factor c_i/q^3 based on published liquid fluidization data compared with the author's equation.

we finally get

$$\frac{\partial(c_f q^3)/c_f q^3}{\partial L/L} =$$

$$\frac{(C_D \mathrm{Re}_p/8)\epsilon^2 - (U/U_\infty)(y + \epsilon\, dy/d\epsilon)}{(C_D\, \mathrm{Re}_p/24)\,\epsilon^3 - (U/U_\infty)\,\epsilon\, y}(1-\epsilon) \quad (32)$$

This equation is illustrated in Fig. 15 for different values of particle Reynolds number. Obviously there is a great need for accurate experimentation especially in the transition region at low void fraction. The corresponding curve for

$$\frac{\partial(zq^2)/zq^2}{\partial L/L}$$

for low Reynolds numbers is also shown in Fig. 15.

Conditions of similarity

Employing equations (6) and (16) equation (17a) may be written in the form

$$\left[\frac{gm}{u^2}\frac{1-\epsilon}{q}\frac{\rho^s-\rho}{\rho}\right]_i = \left[\frac{1}{\mathrm{Re}} + g\,(\mathrm{Re}_p)\right]_i \quad (33)$$

where the index $i = 1, 2, 3, \ldots$ refers to different fluidized systems with specified physical properties. Since geometrical similarity between two systems m and n presupposes that ϵ_m equals ϵ_n and since the Reynolds number is uniquely determined by the void fraction and the particle Reynolds number (cf. Fig. 12), the right-hand sides of equation (33) are equal for the two systems if, and only if, the particle Reynolds numbers are also equal. Thus the particle Reynolds number is a criterion for the *possibility* of obtaining hydrodynamic and geometric similarity in ideal fluidization.

The left-hand sides of equation (33) by their nature are modified Froude numbers (and friction factors). Eliminating the velocity by multiplication with the Reynolds number raised to the second power and dropping the void fraction we get a "particle Kármán number":

$$K_p = \frac{g d_p^3}{\nu^2}\frac{\rho_s - \rho}{\rho} \quad (34)$$

which is a similarly criterion equivalent to the particle Reynolds number.

The outer dimensions of the fluidized bed give rise to additional geometric similarity conditions (d_t/d_p and L_0/d_p). These geometric factors as well as the densities of solid and fluid have a considerable effect upon the degree of non-ideal behaviour of the fluidized bed.

Conclusions

(1) The pressure drop equation presented here covers the void fraction region from the packed bed to the free fall of a single sphere.

(2) The tortuosity factor introduced in the pressure drop equation is a pure geometrical factor. It is determined by the relations $q = 1{\cdot}71\,(m_s/m)^{0{\cdot}15}$ for $0{\cdot}45 \leqslant \epsilon \leqslant 0{\cdot}94$ and $q \approx \epsilon^{-2}$ for $\epsilon > 0{\cdot}92$.

(3) The cross-section factor is best evaluated from the Vand-Hawksley equation or from $U/U_\infty = \epsilon^{4{\cdot}59}$.

(4) The wall effect in the viscous region can be approximated roughly by the Faxén correction factor.

(5) A simple graphical representation of the pressure drop equation is given.

(6) The consistency of the equation has been demonstrated for ideal fluidization of equally-sized spheres in the regions: $0{\cdot}003 \leqslant \mathrm{Re}_p \leqslant 2000$ and $0{\cdot}45 \leqslant \epsilon \leqslant 0{\cdot}95$.

(7) Any inconsistency of the equation due to non-uniform particle size or non-spherical particle shape has not been investigated.

(8) The equation is inconsistent for non-ideal fluidization; it is therefore a very sensitive tool for investigating deviations from ideal conditions.

Acknowledgements—The author wishes to express his sincere gratitude to the Head of the Division, Professor Dr. Otto Stelling, for his kind help and never-failing interest in this work. Thanks are also due to the Swedish Technical Research Council for financial assistance.

Notation

c', c'' = dimensionless factors defined in equations (10) and (11)
d_p = particle diameter
d_t = diameter of bed
F = average force acting on the particles per unit surface area
g = gravity
L = bed height
L_e = equivalent channel length

$L_0 = L(1 - \epsilon)$
m = hydraulic radius
m_s = solid phase radius
n = exponent in expression for tortuosity factor
ΔP = pressure drop
q = tortuosity factor
S = wetted surface per unit bed volume
U = superficial velocity
U_∞ = terminal velocity of freely falling particle
$u = Uq/\epsilon$ = actual average velocity in the bed

$$y = \exp \frac{2{\cdot}5(1 - \epsilon)}{1 - (39/64)(1 - \epsilon)} \sim \epsilon^{-2{\cdot}39}$$

z = cross-section factor
ϵ = void fraction
μ = viscosity
ν = kinematic viscosity
ρ = fluid density
ρ_s = solid density
C_D = standard drag coefficient for a single sphere
C_I = inertial drag coefficient for a single sphere
C_V = viscous drag coefficient for a single sphere
$\epsilon_i = C_I/8$
$f = F/\rho u^2$ = friction factor
$f' = 30f$

$$K_p = \frac{g d_p^{\,3}}{\nu^2} \frac{\rho_s - \rho}{\rho} = \text{particle Kármán number}$$

$$\mathrm{Re} = \frac{mu}{z\nu} = \text{Reynolds number}$$

$$\mathrm{Re}' = \tfrac{2}{3}\,\mathrm{Re}$$

$$\mathrm{Re}_p = \frac{d_p U_\infty}{\nu} = \text{particle Reynolds number}$$

$$\phi = \frac{C_I}{C_V}\,\mathrm{Re}_p$$

References

[1] Zaki W. N. *J. Imp. Coll. Chem. Engng. Soc.* 1953 **7** 119.
[2] Ergun S. *Chem. Engng. Progr.* 1952 **48** 89.
[3] Andersson K. E. B. *Trans. Roy. Inst. Teckn., Stockholm* 1959 no. 131.
[4] Blake F. C. *Trans. Amer. Inst. Chem. Engrs.* 1921–22 **14** 415.
[5] Carman P. C. *Flow of Gases through Porous Media.* Butterworths, London 1956.
[6] Scheidegger A. E. *The Physics of Flow through Porous Media.* University of Toronto Press 1957.
[7] Hodgman C. D. *Handbook of Chemistry and Physics* (39th Ed.) p. 2049. Chemical Rubber Publishing Co., Ohio.
[8] Reboux P. *Phénomènes de Fluidisation.* Association Française de Fluidisation, Paris 1954.
[9] Wadell H. *J. Franklin Inst.* 1934 **217** 459.
[10] Wilhelm R. H. and Kwauk M. *Chem. Engng. Progr.* 1948 **44** 201.
[11] Happel J. and Pfeffer R. *Amer. Inst. Chem. Engrs. J.* 1960 **6** 129.
[12] Hawksley P. G. W. *Some Aspects of Fluid Flow*, p. 114. Arnold Press, New York 1950.
[13] Vand V. *J. Phys. Coll. Chem.* 1948 **52** 277.
[14] Faxén H. Dissertation, Uppsala University 1921 ; *Ark. Mat., Astr. Fys.* 1922–23 **17** no. 27.
[15] Munroe H. S. *Trans. Amer. Inst. Min. Engrs.* 1888 **17** 637.
[16] Schlichting H. *Grenzschicht-Theorie.* Verlag G. Braun, Karlsruhe 1958.
[17] Kliachko L. S. *Heat Ventilation* (S.S.S.R.) 1934 (through Torobin L. B. and Gauvin W. H. *Canad. J. Chem. Engng.* 1959 **37** 129).
[18] Oseen C. W. *Ark. Mat., Astr. Fys.* 1910 **6** no. 29 ; 1913 **9** no. 16.
[19] Sparrow E. M. and Loeffler, Jr. A. L. *Amer. Inst. Chem. Engrs. J.* 1959 **5** 325.
[20] Emersleben O. *Phys. Z.* 1925 **26** 601 (corrected in Ref. 3).
[21] Sullivan R. R. *J. Appl. Phys.* 1942 **13** 725.
[22] Willey M. R. J. and Spangler M. B. *Bull. Amer. Assoc. Petr. Geol.* 1952 **36** 359.
[23] Willey M. R. J. and Gardner G. H. F. *World Oil* 1958 **146** no. 4 121.
[24] Becker H. A. *Canad. J. Chem. Engng.* 1959 **37** 85.
[25] Lewis W. K., Gilliland E. R. and Bauer W. C. *Industr. Engng. Chem.* 1949 **41** 1104.
[26] Tesařik I. *Rozpr. České. Akad. Věd, Řada TV* 1956 **66** 1 (English summary).
[27] Bandukwala A. K. M.S. Thesis University of Illinois 1956.
[28] Young R. J. *J. Appl. Chem.* 1952 **2** S55.

Chemical Engineering Science, 1961, Vol. 15, pp. 298 to 302. Pergamon Press Ltd., London. Printed in Great Britain.

Performance and design of hydrocyclones—I

General considerations

K. RIETEMA*

Koninklijke/Shell-Laboratorium, Amsterdam
(Shell Internationale Research Maatschappij)

(*Received* 28 *July* 1960)

Abstract—In a series of papers correlations are developed for the pressure drop and the separating power of hydrocyclones and rules for establishing the optimum design of hydrocyclones are derived.

In the first two parts general considerations are given and a pressure drop correlation is derived. It is obtained as the product of two independent functions, one of which describes the dependence on the Reynolds number based on inlet conditions, and the other the dependence on the shape of the cyclone.

Résumé—Dans une série d'articles l'auteur développe des systèmes de corrélations pour la chute de pression et le pouvoir de séparation d'hydrocyclones, ainsi que des règles pour calculer la forme optimale de ces appareils.

Dans les premières deux parties l'auteur développe des considérations générales et déduit une relation pour la chute de pression dans l'hydrocyclone. Elle s'obtient comme le produit de deux fonctions indépendantes, l'une desquelles décrit la dépendance de la chute de pression du nombre de Reynolds qui est déterminée par les conditions régnant dans l'arrivée, et l'autre sa dépendance de la forme du cyclone.

Zusammenfassung—In einigen aufeinanderfolgenden Artikeln werden Beziehungen für das Druckgefälle und das Trennungsvermögen von Hydrozyklonen, sowie Regeln für die Berechnung der optimalen Form solcher Zyklone ausgearbeitet.

In den ersten zwei Teilen werden einige allgemeine Betrachtungen über Hydrozyklone gegeben und wird eine Beziehung für das Druckgefälle im Hydrozyklon abgeleitet. Sie ist das Produkt zweier unabhängigen Funktionen, von denen eine die Abhängigkeit von der Reynolds-Zahl, deren Grösse von den im Einlass herrschenden Bedingungen bestimmt wird, die andere die Abhängigkeit von der Form des Zyklons beschreibt.

VOL. 15 1961

INTRODUCTION

THE HYDROCYCLONE was introduced after World War II by the Dutch State Mines as a new tool to separate dispersed solid material from a liquid of lower density.

Since then a large number of publications on this apparatus have appeared; only some of these, however, present quantitative data, while analytical studies are scarcer still.

Although the usefulness of hydrocyclones for the above-mentioned unit operation is widely recognized, no rules have as yet been published which permit of designing a cyclone for a specific separation problem.

The most outstanding articles on hydrocyclones are those of DAHLSTROM [1] and of KELSALL [2, 3]. DAHLSTROM gives correlations for the pressure drop and for the separating power of hydrocyclones. He investigated the influence of inlet and overflow nozzle diameters, but assumed that there is no interrelation between the dependences on these parameters. Besides, this author did not examine the influence of the Reynolds number.

KELSALL studied hydrocyclones of a geometrical shape which were entirely different from those of DAHLSTROM. He determined flow pattern, pressure drop and separating power, but gave no correlations for these quantities. His pressure

*Now Professor of Chemical Engineering at the Technical University of Eindhoven, Holland.

drop measurements would seem to be incorrect since he did not make any corrections for the pipe friction in the feed line to the cyclone.

During recent years an investigation has been carried out at the Koninklijke/Shell-Laboratorium, Amsterdam, to gain a better understanding of the performance of hydrocyclones and to establish correlations and rules on which to base the design of hydrocyclones for a given separation problem.

The results of this study are described in the present series of publications.

1. Phenomenology of the Hydrocyclone

A hydrocyclone is a tool to separate dispersed material from a liquid by means of centrifugal action. It consists of a cylindrical tube or shell, closed at the top by a flat plate and ending at the bottom in a cone with an opening at its apex (see Fig. 1). Fixed in the centre of the top plate is a cylindrical tube (vortex finder). The liquid or suspension to be separated is injected tangentially into the upper part of the cylindrical section, causing rotation of the liquid contained in the cyclone.

The solids to be separated can be of lower or of higher density than the continuous liquid phase. This article will deal only with cyclones for the separation of a solid material of a density higher than that of the continuous phase. In such cyclones the central outlet on the side of the inlet (called the overflow nozzle) discharges the clarified liquid (overflow), while the outlet at the apex discharges the concentrated solids (underflow).

The names "overflow" and "underflow" have come into use on account of the fact that the cyclone is mostly used in a vertical position (see Fig. 1), although this is not strictly necessary.

Operating a cyclone requires a certain pressure drop which increases with the throughput and further depends on the construction of the cyclone. Inside the cyclone there exists a pressure gradient. In nearly all practical cases a gas core develops; special measures have to be taken to prevent this. The absence of a gas core generally results in an increase of the total pressure drop at the same throughput and a lowering of the efficiency.

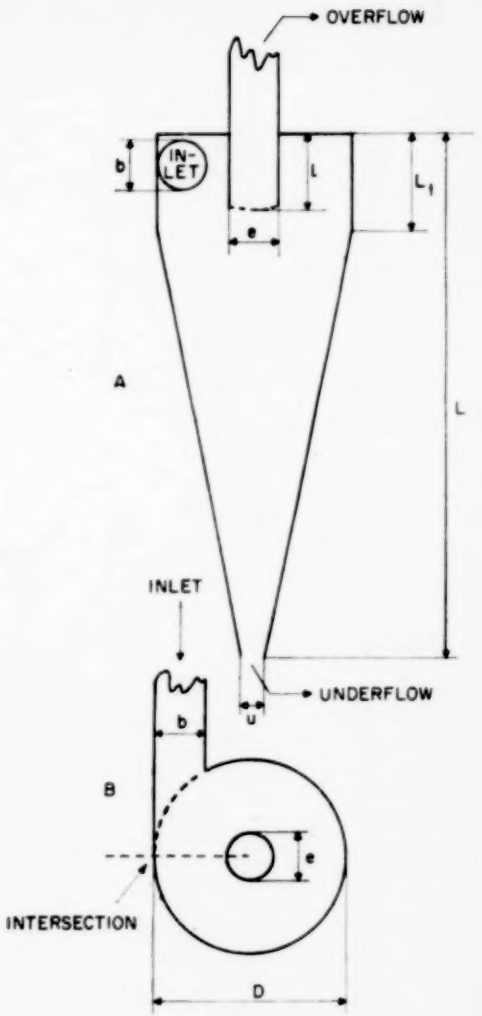

Fig. 1. Cross-sections of a hydrocyclone.

The underflow discharge is as a rule of the typical umbrella shape also occurring with centrifugal spray nozzles. When, however, the total pressure drop is not high enough or the solid concentration in the underflow is very high, this spray-type discharge changes into a jet-type or drop-type discharge.

2. Flow Pattern in the Cyclone

The flow pattern in a hydrocyclone has been determined experimentally by Kelsall [2]. It can be described by means of two plots. In the

first, the tangential velocity is given as a function of the radius r (Fig. 2); the second plot shows a

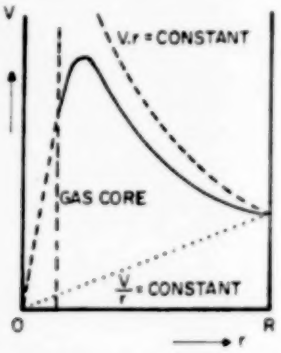

FIG. 2. Tangential velocity profile.

vertical cross-section of the cyclone in which the streamlines due to a combination of the axial and radial velocities are indicated (Fig. 3).

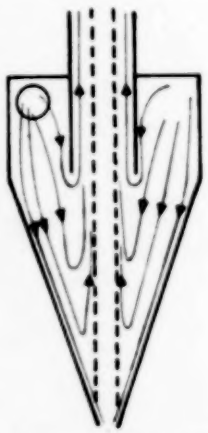

FIG. 3. Axial and radial flow pattern.

According to recent measurements made by BRADLEY and PULLING [4] there is a "stationary" layer below the vortex finder where the axial and radial velocities are zero. The existence of this layer had already been reported by FONTEIN [5]; it is, however, of no importance for the studies reported in the present series of articles.

The tangential velocity increases as the radius decreases because of the law of conservation of angular momentum. This means that the product of tangential velocity and radius tends to be a constant (dashed line, Fig. 2). However, owing to wall friction and internal friction caused by viscosity and turbulence this law is not strictly obeyed. If friction losses were predominant the tangential velocity would be proportional to the radius (dotted line, Fig. 2). In reality the tangential velocity profile is somewhere between these two limits.

Since separation requires high tangential velocities, the internal surface of the cyclone should be made as smooth as possible in order to decrease wall friction and turbulence.

In well-constructed cyclones the tangential velocity profile tends more towards obedience to the "constant V/r" law as the Reynolds number is higher.

In the central part of the rotating liquid under the vortex finder there is practically no radial velocity and, therefore, little or no radial transport of angular momentum. In this part, therefore, friction losses predominate, which results in a tangential velocity profile that tends to obey the "constant V/r" law.

In a theoretical derivation of the tangential velocity profile we started from the Navier–Stokes equations, which describe the hydrodynamic behaviour of fluids in motion. Generally these equations cannot be solved. With some special assumptions, however, they can sometimes be modified and then be solved for a particular case.

One of these modifications is that when the time average is taken, the turbulent fluctuations can be neglected, while the quadratic terms of these fluctuations can be represented by introducing a term ϵ, which is called the turbulent kinematic viscosity and which must be added to the ordinary kinematic fluid viscosity.

For so-called flat-box cyclones these derivations and the solutions have been published by KRAJENBRINK and RIETEMA [6]. The hydrocyclone can be treated along similar lines.

The equation of motion describing the tangential velocity profile is as follows:

$$U\frac{\partial V}{\partial r} + W\frac{\partial V}{\partial z} + \frac{UV}{r} = (\nu + \epsilon)\left(\frac{1}{r}\frac{\partial}{\partial r}\left(r\frac{\partial V}{\partial r}\right) + \frac{\partial^2 V}{\partial z^2} - \frac{V}{r^2}\right) \quad (1)$$

It is assumed that V does not depend on z, an assumption which is true not too close to the cyclone wall, as shown by the experiments of KELSALL [2] and TER LINDEN [7].

Now, V only depends on r, so that we can write, after some rearrangement

$$-\frac{U}{r}\frac{dVr}{dr}+(\nu+\epsilon)\left(\frac{d}{dr}\frac{1}{r}\frac{dVr}{dr}\right)=0. \qquad (2)$$

When introducing

$$\lambda=\frac{-U_0R^*}{\nu+\epsilon},\quad \phi=\frac{Vr}{V_0R} \text{ and } \sigma=\frac{r}{R}:$$

$$\lambda\frac{U}{U_0}\frac{1}{\sigma}\frac{d\phi}{d\sigma}+\left(\frac{d}{d\sigma}\frac{1}{\sigma}\frac{d\phi}{d\sigma}\right)=0. \qquad (3)$$

One boundary condition is given by $\phi = 1$ for $\sigma = 1$. When the cyclone operates with an air core (for which $\sigma = \sigma_1$) the other boundary condition follows from the consideration that at a free surface no shearing stresses should occur:

$$\frac{d(\phi/\sigma)}{d\sigma}=\frac{\phi}{\sigma^2} \text{ at } \sigma=\sigma_1.$$

Assuming, finally, that throughout the cyclone the radial velocity is constant ($U = U_0$), which assumption is also justified by the results obtained by KELSALL [2] and TER LINDEN [7], the solution becomes

$$\phi=C_2-C_1\exp(-\lambda\sigma)\left(\frac{\sigma}{\lambda}+\frac{1}{\lambda^2}\right),$$

where

$$C_1=\frac{\lambda^2}{-\exp(-\lambda)-\lambda\exp(-\lambda)+(\sigma_1^2/2)\lambda^2\exp(-\lambda\sigma_1)+\sigma_1\lambda\exp(-\lambda\sigma_1)+\exp(-\lambda\sigma_1)}$$

and

$$C_2=1+C_1\exp(-\lambda)\left(\frac{1}{\lambda}+\frac{1}{\lambda^2}\right).$$

ϕ has been calculated for $\sigma_1 = 0{\cdot}1$ and different values of λ and is given in Fig. 4, where $\phi/\sigma = V/V_0$ has been plotted against σ.

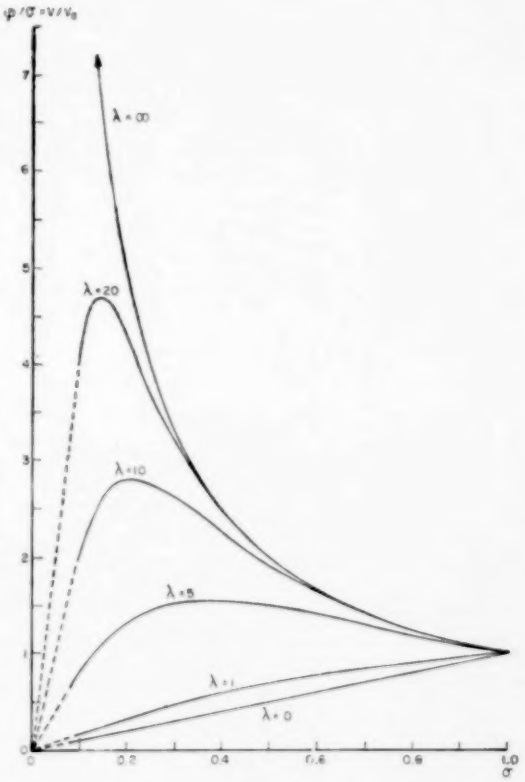

FIG. 4. Theoretically derived tangential velocity profiles in cyclones with an air core at $\sigma = 0{\cdot}1$ and for different values of λ.

From a comparison with the results obtained by KELSALL [2] it easily follows that in conical hydrocyclones λ has a value of at least 10. This result will be used in Part III [8] where the influence of turbulence on the separation will be considered.

*The radial velocity U_0 is directed against r and is therefore negative.

References

[1] Dahlstrom D. A. *Trans. Amer. Inst. Min. (Metall.) Engrs.* 1949 **184** 33.
[2] Kelsall D. F. *Trans. Inst. Chem. Engrs.* 1952 **30** 87.
[3] Kelsall D. F. *Chem. Engng. Sci.* 1953 **2** 254.
[4] Bradley D. and Pulling D. J. *Trans. Inst. Chem. Engrs.* 1959 **37** 34.
[5] Fontein F. J., Communication at Symposium on Cyclones, Utrecht, December 1958. To be published in *De Ingenieur (Utrecht)*.
[6] Rietema K. and Krajenbrink H. J. *Appl. Sci. Res.* 1958/59 **A 8** 177.
[7] Ter Linden A. J. *J. Proc. Inst. Mech. Engrs.* 1949 **160**.
[8] Rietema K. *Chem. Engng. Sci.* 1961 **14** 1.

VOL. 15 1961

Chemical Engineering Science, 1961, Vol. 15, pp. 303 to 309. Pergamon Press Ltd., London. Printed in Great Britain.

Performance and design of hydrocyclones—II

Pressure drop in the hydrocyclone

K. Rietema

Koninklijke/Shell-Laboratorium, Amsterdam
(Shell Internationale Research Maatschappij)

(*Received* 25 *July* 1960)

Introduction

As already mentioned in Part I the pressure drop is a very important operation characteristic of the hydrocyclone and reliable pressure drop correlations are essential when this tool is to be used for solving a specific separation problem.

It could be tried to calculate the pressure drop on the basis of the theoretical tangential velocity profiles derived in Part I by integration of the pressure gradient $dp/dr = \rho V^2/r$. This is impossible, however, because both the parameter λ and the diameter of the air core vary in an unknown way with the construction of the cyclone and with the inlet Reynolds number. These two factors strongly influence the tangential velocities obtained in the interior of the cyclone and, therefore, also the pressure drop.

It was concluded that accurate pressure drop correlations can only be obtained by an experimental investigation of the influence of the two factors mentioned.

1. Experiments

Experiments have been carried out with a cyclone of constant cone angle, 3 in. in diameter, whose length could be varied and whose inlet, overflow and underflow nozzles could be changed. For the construction of this cyclone see Fig. 1.

The influence of the viscosity and the Reynolds number was investigated with the aid of water and mixtures of water and glycerol as fluids. The overflow and underflow were freely received in an open vessel, so that a gas core could always develop.

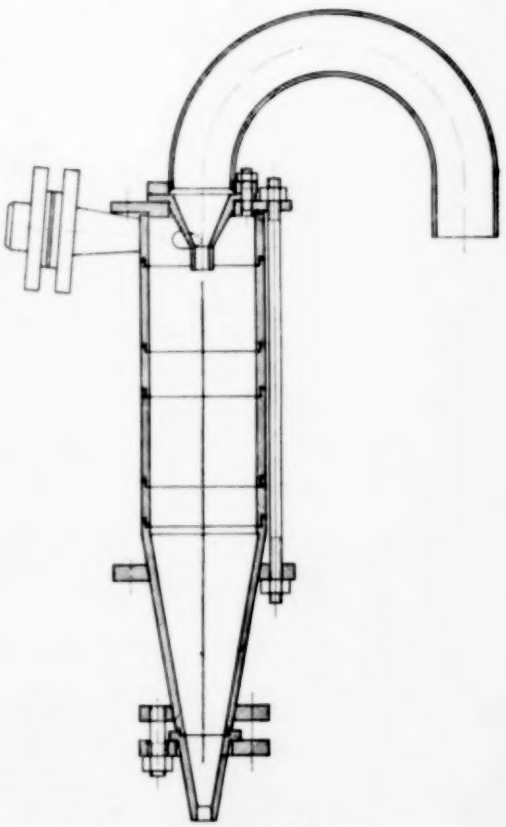

Fig. 1. Construction of the cyclone.

The results are presented in Figs. 2 and 3 and Tables 1 and 2.

A dimensional analysis shows that the total pressure drop expressed in numbers of inlet velocity heads can generally be indicated as

*Now Professor of Chemical Engineering at the Technical University of Eindhoven, Holland.

Table 1. *Cyclone pressure drop experiments*

Dependence on inlet Reynolds number

Cyclone diameter = 75 mm Cyclone length = 396 mm

Inlet diameter ***b*** (cm)	*Overflow diameter* ***e*** (cm)	*Underflow diameter* ***a*** (cm)	*Viscosity of water–glycerol* (cP)	*Density of water–glycerol* (g/cm³)	*Overflow rate* (ml/sec)	*Underflow rate* (ml/sec)	*Through-put* (ml/sec)	*Pressure drop* (atm)	*Static pressure drop* (atm)	*Inlet velocity head* (atm)	$F = \frac{(\Delta p)_s}{\frac{1}{2}\rho V_0^2}$	*Inlet Reynolds number*
1·0	1·0	1·0	1·0	1·0	290	330	620	1·8	1·49	0·31	4·8	78,000
					180	220	400	0·60	0·47	0·13	3·6	51,000
					97	160	257	0·20	0·146	0·053	2·8	32,000
—	—	0·7	—	—	487	150	637	2·15	1·82	0·327	5·6	81,000
					300	167	467	0·78	0·60	0·177	3·4	59,500
					155	77	232	0·20	0·156	0·044	3·6	29,600
—	—	0·5	—	—	580	42	622	2·40	2·08	0·315	6·6	79,300
					340	33	373	0·72	0·61	0·113	5·4	47,500
					193	31	224	0·22	0·179	0·041	4·4	28,500
—	—	—	5·0	1·10	440	60	500	0·97	0·75	0·223	3·4	14,000
					400	58	458	0·73	0·54	0·187	2·9	12,800
					318	47	365	0·37	0·25	0·119	2·1	10,230
					208	45	253	0·16	0·103	0·057	1·8	7100
—	—	—	25·0	1·19	510	94	614	0·72	0·355	0·365	1·0	3720
					402	94	496	0·50	0·26	0·237	1·1	3010
					276	85	361	0·30	0·17	0·126	1·3	2190
					222	77	299	0·20	0·114	0·0862	1·3	1810
					134	61	195	0·10	0·063	0·0366	1·7	1180
					108	56	164	0·07	0·044	0·0260	1·7	995
1·0	1·5	1·0	1·0	1·0	500	100	600	1·0	0·71	0·29	2·5	76,500
					205	87	292	0·20	0·13	0·069	1·9	37,200
					58	127	185	0·07	0·042	0·028	1·5	23,600
—	2·0	1·0	1·0	1·0	700	18	718	0·90	0·48	0·418	1·2	91,500
					390	30	420	0·29	0·15	0·143	1·1	53,500
					160	77	237	0·10	0·054	0·0455	1·2	30,200
—	—	—	5·0	1·10	700	52	752	0·92	0·41	0·505	0·82	21,100
					567	60	627	0·60	0·25	0·350	0·71	17,600
					392	85	477	0·33	0·13	0·203	0·64	13,400
					254	99	353	0·16	0·049	0·111	0·45	9900
—	—	—	25·0	1·19	490	140	630	0·55	0·17	0·383	0·44	3820
					244	238	482	0·34	0·12	0·224	0·54	2930
					220	238	458	0·30	0·10	0·203	0·49	2780
					125	230	355	0·19	0·068	0·122	0·56	2160
					—	232	232	0·10	0·048	0·052	0·92	1410

Table 1—(contd.)

Inlet diameter b (cm)	*Overflow diameter e* (cm)	*Underflow diameter u* (cm)	*Viscosity of water–glycerol* (cP)	*Density of water–glycerol* (g/cm³)	*Overflow rate* (ml/sec)	*Underflow rate* (ml/sec)	*Through-put* (ml/sec)	*Pressure drop* (atm)	*Static pressure drop* (atm)	*Inlet velocity head* (atm)	$(\Delta p)_s$ $F = \frac{1}{2}\rho V^2{}_0$	*Inlet Reynolds number*
2·0	1·0	1·0	1·0	1·0	320	390	710	0·76	0·75	0·0255	29	45,200
					220	290	510	0·35	0·34	0·0132	26	32,480
					125	200	325	0·125	0·12	0·00536	23	20,660
—	—	0·7	—	—	460	187	647	0·97	0·95	0·0212	45	41,200
					287	133	420	0·34	0·33	0·0089	48	26,780
					155	100	255	0·10	0·098	0·0033	30	16,220
—	—	0·5	—	—	537	83	617	0·97	0·95	0·0193	50	39,340
					350	58	408	0·35	0·35	0·0084	41	26,000
					220	47	267	0·12	0·118	0·036	33	17,000
—	—	—	10·0	1·15	673	157	830	0·85	0·82	0·0403	20	6080
					587	135	722	0·60	0·58	0·0304	19	5280
					480	110	590	0·32	0·31	0·0202	15	4320
					346	87	433	0·14	0·133	0·0110	12	3170
					134	80	214	0·07	0·068	0·0027	25	1570
—	—	—	27·0	1·19	475	158	633	0·44	0·42	0·0242	17	1780
					495	127	622	0·33	0·31	0·0233	13	1750
					380	103	483	0·20	0·19	0·0141	14	1350
					249	77	326	0·11	0·105	0·0064	16	915
—	1·5	1·0	1·0	1·0	500	165	665	0·40	0·39	0·0225	17	42,400
					340	140	480	0·16	0·15	0·0117	13	30,600
					200	137	337	0·07	0·066	0·0057	12	21,440
—	2·0	1·0	1·0	1·0	700	67	767	0·22	0·20	0·0289	6·7	48,800
					460	105	565	0·10	0·090	0·0162	5·6	36,000
					330	87	417	0·06	0·054	0·0088	6·1	26,560
—	—	—	10·0	1·15	693	150	843	0·15	0·12	0·0515	2·8	6180
					610	145	755	0·088	0·066	0·0333	2·0	5530
					420	159	579	0·060	0·047	0·0195	2·4	4240
—	—	—	27·0	1·19	442	217	659	0·070	0·053	0·0261	2·0	1850
					220	238	458	0·038	0·030	0·0126	2·4	1283
—	1·0	0·5	1·0	1·0	710	51	761	1·1	1·07	0·029	37	48,500
					930	98	1028	3·1	3·05	0·053	57	65,000
					1510	173	1683	8·1	7·96	0·144	55	107,000
—	2·0	1·0	—	—	3320	2·6	3323	5·1	4·57	0·56	8·2	212,000
					2180	5·7	2186	2·0	1·76	0·24	7·3	139,000
					1000	7·6	1008	0·8	0·74	0·059	12·5	69,000

Table 2. Cyclone pressure drop experiments at constant Reynolds number and without underflow
Cyclone diameter = 75 mm

Cyclone length (mm)	*Inlet diameter* (mm)	*Overflow diameter* (mm)	*b/c*	*Throughput* (ml/sec)	$(\Delta p)_t$ (atm)	$(\Delta p)_s$ (atm)	*F*	Re_{inlet}	F_{25000}	*n*	*γ*
218	25	10	2·5	480	0·64	0·64	132	24,500	133		
		15	1·67	518	0·26	0·26	43	26,500	42	2·8	22·4
		20	1·25	500	0·103	0·098	19	25,600	19		
		30	0·83	512	0·040	0·035	6·3	26,200	6·2		
	20	10	2·0	416	0·61	0·60	68	26,600	66		
		15	1·33	418	0·23	0·22	25	26,700	24	2·5	25·5
		20	1·0	400	0·096	0·089	11	25,600	11		
		30	0·67	402	0·050	0·043	5·3	25,700	5·2		
	15	10	1·5	304	0·43	0·42	28	25,900	28		
		15	1·0	310	0·19	0·18	12	26,400	11·5	2·3	22·8
		20	0·75	304	0·094	0·079	5·4	25,900	5·3		
		30	0·50	310	0·049	0·034	2·2	26,400	2·1		
	10	10	1·0	220	0·32	0·28	7·7	28,200	7·3		
		15	0·67	224	0·19	0·15	3·7	28,600	3·5	1·9	16·0
		20	0·50	216	0·12	0·08	2·1	27,600	2·0		
		30	0·33	220	0·070	0·034	0·93	28,200	0·88		
273	25	10	2·5	480	0·52	0·52	111	24,500	112		
		15	1·67	492	0·18	0·18	36	25,200	36	3·0	18·8
		20	1·25	486	0·065	0·061	12·5	24,900	12·5		
		30	0·83	510	0·043	0·038	7·1	26,100	6·9		
	20	10	2·0	376	0·47	0·47	66	24,000	67		
		15	1·33	400	0·16	0·16	20	25,600	19·5	2·8	20·2
		20	1·0	418	0·086	0·077	8·7	26,700	8·4		
		30	0·67	420	0·044	0·035	3·9	26,800	3·8		
	15	10	1·5	308	0·39	0·37	19	26,300	19		
		15	1·0	304	0·15	0·13	7·1	26,000	6·9	2·5	17·6
		20	0·75	304	0·066	0·048	2·6	26,000	2·6		
		30	0·50	292	0·040	0·023	1·4	24,900	1·4		
	10	10	1·0	216	0·25	0·22	5·8	27,600	5·6		
		15	0·67	218	0·14	0·10	2·6	27,900	2·5	2·0	13·6
		20	0·50	204	0·076	0·042	1·25	26,100	1·23		
		30	0·33	204	0·064	0·030	0·9	26,100	0·87		
396	25	10	2·5	502	0·47	0·47	90	25,700	89		
		15	1·67	514	0·17	0·17	28	26,300	28	3·0	17·3
		20	1·25	518	0·071	0·065	10·7	26,500	10·4		
		30	0·83	506	0·028	0·023	4·3	25,900	4·3		
	20	10	2·0	412	0·42	0·42	49	26,300	48		
		15	1·33	420	0·14	0·14	15	26,800	14·5	2·8	20·4
		20	1·0	410	0·058	0·050	6·5	26,200	6·3		
		30	0·67	400	0·032	0·024	3·0	25,600	2·9		
	15	10	1·5	318	0·31	0·29	16·3	27,100	15·6		
		15	1·0	310	0·11	0·10	5·9	26,400	5·7	2·5	18·5
		20	0·75	318	0·062	0·044	2·5	27,100	2·4		
		30	0·50	320	0·042	0·024	1·3	27,300	1·24		
	10	10	1·0	218	0·22	0·18	4·6	27,900	4·3		
		15	0·67	224	0·12	0·08	2·0	28,600	1·82	2·8	13·5
		20	0·50	202	0·075	0·042	1·3	25,800	1·25		
		30	0·33	212	0·058	0·022	0·61	27,100	0·59		

$$G = \frac{(\Delta p)_t}{\frac{1}{2}\rho V_0^2} = \text{function of } (b/D,\ e/D,\ u/D,$$

$$L_1/D, L_2/D,\ l/D,\ \mathrm{Re}_{\mathrm{inlet}},\ C,\ \alpha,\ gD/\tfrac{1}{2}V_0^2).$$

The first six parameters in this correlation determine the cyclone geometry. Like everywhere else in this study the Reynolds number has been related to the conditions at the inlet.

In normal practice the cyclone is always operated in such a way that the static pressure loss through the cyclone $(\Delta p)_s$ is high as compared with the static pressure head in the cyclone due to gravity: $\rho g (L_1 + L_2) \cos \alpha$. In that case any influence of α and $gD/\frac{1}{2}V_0^2$ cannot be expected.

On account of its complexity and considering the fact that it will depend also on the degree of thickening and on the underflow rate the influence of the concentration was not investigated. When no thickening occurs and the suspension still behaves as a Newtonian liquid (no plastic or pseudo-plastic properties), the influence of the concentration will be accounted for by using the average density of the feed suspension instead of the liquid density.

When thickening does occur, but the feed concentration is lower than 1 per cent by weight, generally the decrease in total pressure drop is smaller than the accuracy of the final pressure-drop correlation and can therefore be neglected.

The influence of l/D was not investigated either; it is thought to be of minor importance as long as l/D is not too high, as is the case for the cyclones normally used.

The influence of u/D was not investigated since in practical use the total underflow is obtained not by using a certain apex opening but by adjusting the pressure difference between overflow and underflow outlets. The important variable was thought to be the ratio O/q (as long as this ratio is not smaller than 0·7) which is used in the correlation.

So the pressure drop correlation sought reduces to

$$F = \frac{(\Delta p)_s}{\frac{1}{2}\rho V_0^2} =$$

$$= \text{function of } (\mathrm{Re}_{\mathrm{inlet}},\ b/D,\ e/D,\ L/D, O/q.$$

The total pressure drop $(\Delta p)_t$ necessary to operate a cyclone consists of three components:

1. The inlet velocity head $= \frac{1}{2}\rho V_0^2$, where ρ = liquid density and V_0 = inlet velocity. This is the dynamic pressure which a pump should produce to accelerate the feed liquid from the position of rest to the inlet velocity V_0.
2. The friction losses in the cyclone.
3. The centrifugal head. The tangential velocity causes a radial pressure gradient given by $dp/dr = \rho V^2/r$ which, integrated from the centre towards the cyclone radius R near the inlet, is called the centrifugal head

$$\left(= \int_0^R \frac{\rho V^2}{r}\, dr \right).$$

Components 2 and 3 together determine the static pressure loss $(\Delta p)_s$ of the cyclone, which is often expressed in numbers of inlet velocity heads and is then called the cyclone pressure loss factor $F = (\Delta p)_s / \frac{1}{2}\rho V_0^2 = G - 1$.

When the Reynolds number (related to the inlet) in the cyclone is increased from less than 1000 to more than 100,000 F first decreases, but $\mathrm{Re} > 5000$ increases again. Below this critical Reynolds number the friction loss (which, when expressed in numbers of inlet velocity heads, decreases as Re increases) is predominant. Above this critical Reynolds number the centrifugal head (which increases with Re, even when expressed in numbers of inlet velocity heads) is more important. This is clearly illustrated in Fig. 2 where for different types of cyclones F is plotted vs. the inlet Reynolds number.

The critical Reynolds number is not the same for all cyclones, but for general purpose cyclones it is never higher than 8000, whereas for actual separation cyclones should be operated at much higher Reynolds numbers.

In the range of practical application, therefore, the static pressure drop of a cyclone may be assumed to be determined by the centrifugal head only, which in its turn is determined by the tangential velocity profile. This velocity profile depends largely on the internal friction losses and only to a less extent also on wall

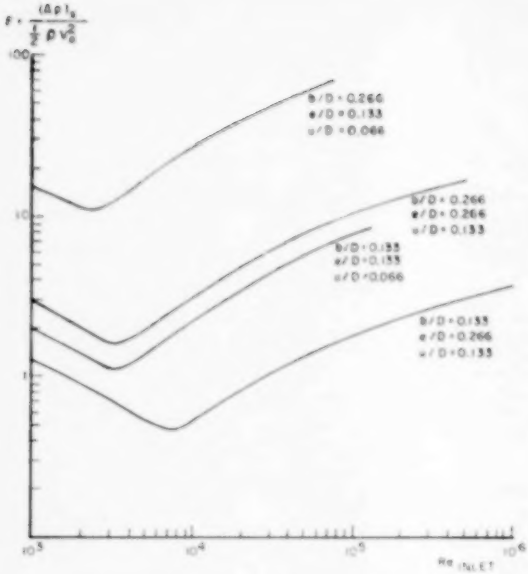

FIG. 2. Reynolds dependence of cyclone pressure drop.

friction or in such a way that an increase of wall friction decreases the tangential velocity and, in consequence, the static pressure drop.

Now one may argue that a large wall surface at a large radius has about the same influence as a small wall surface or a small radius; this leads to the conclusion that the cone angle of the cyclone is not important, but only the total length of the cyclone.

In this investigation this was assumed to be true and, therefore, the static pressure drop was correlated only with the sum of L_1 and L_2, an assumption which is thought to be justified for practical cyclones and for a correlation which does not pretend to a higher accuracy than 10 per cent.

2. Final Correlation

It proved possible to split the general correlation for F into a Reynolds dependence $f(\mathrm{Re})$ and a function describing the influence of the cyclone geometry at a constant Reynolds number, for which $\mathrm{Re} = 25{,}000$ was chosen. Thus:

$$\text{for } \mathrm{Re} > 8000 \qquad F = fF_{25{,}000},$$

where

$$F_{25{,}000} = \frac{(\Delta p)_s}{\frac{1}{2}\rho V_0^2} = \gamma \left(\frac{b}{e}\right)^n \left(\frac{D}{L}\right)^{0.7} \left(\frac{O}{q}\right)^{0.8}.$$

The functions n and γ are shown in Fig. 3 (b) and (c), the function f is shown in Fig. 3 (a).

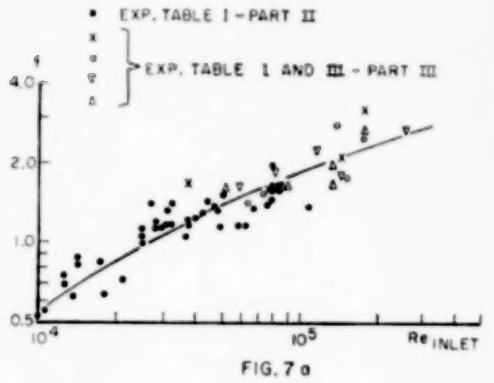

FIG. 7a

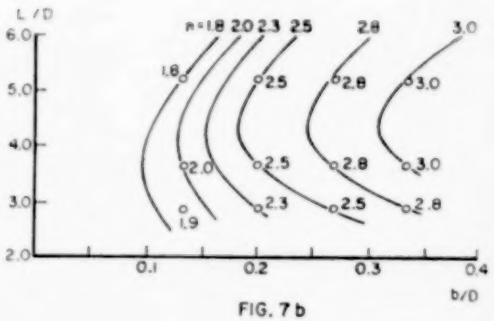

FIG. 7b

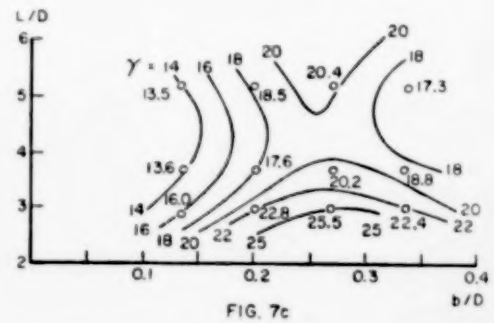

FIG. 7c

FIG. 3. (a, b and c). Value of the functions f, n and γ as occurring in the pressure drop correlation.

The mean deviation of the points in Fig. 3 (a) is 15 per cent. Therefore an accuracy of this order of magnitude can be expected for the correlation. In general this is sufficient for

VOL. 15 1961

practical application, the more so since a rough wall or some uneveness may lead to a deviation of the same order.

It should be remarked that this pressure drop correlation is valid only for cyclones operating with an air core and without any kind of device after the overflow outlet to recover pressure from the rotation still present in the overflow stream.

When no air core is present this has in general the effect of increasing the pressure drop by a factor of two.

Notation

a = diameter of air core in cyclone
b = diameter of cyclone inlet
C = concentration of solids in suspension
Cy_{50} = cyclone correlation number based on d_{50}
Cy_{80} = cyclone correlation number based on d_{80}
D = cyclone diameter
d_{20} = diameter of particles separated to 20 per cent
d_{50} = diameter of particles separated to 50 per cent
d_{80} = diameter of particles separated to 80 per cent
E = turbulent diffusion coefficient
e = diameter of overflow outlet
F = cyclone pressure loss factor $= (\Delta p)_s / \frac{1}{2} \rho V_0^2$
G = total pressure loss factor $= (\Delta p)_t / \frac{1}{2} \rho V_0^2$
g = gravitational acceleration
L = total length of cyclone from top plate to apex
L_1 = length of cylindrical part of cyclone
L_2 = length of conical part of cyclone
l = length of vortex finder
n = power factor occurring in pressure drop correlation
O = overflow rate of cyclone
p = static pressure in cyclone
$(\Delta p)_t$ = total pressure drop necessary to operate a cyclone
$(\Delta p)_s$ = static pressure drop from inlet to outlet
q = throughput of cyclone
R = radius of cyclone
$R_1 = R - \frac{1}{2}a - \frac{1}{2}b$
r = radial co-ordinate in cyclone
T = residence time of particle in cyclone
U = radial velocity of liquid
U_0 = radial velocity of liquid at radius of cyclone
U_p = radial velocity of particle relative to the liquid
u = diameter of underflow nozzle
V = tangential velocity in cyclone
V_0 = linear inlet velocity
W = axial velocity in cyclone
z = axial co-ordinate in cyclone
α = inclination of cyclone axis to the vertical
γ = factor occurring in pressure drop correlation
ϵ = turbulent kinematic viscosity
η = dynamic liquid viscosity
λ = dimensionless parameter describing the tangential velocity profile
ν = kinematic liquid viscosity
ρ = liquid density
$\Delta\rho$ = difference between density of solid and that of liquid
$\sigma = r/R$
$\sigma_1 = a/R$
ϕ = ratio of angular momentum at radius r to inlet angular momentum

Chemical Engineering Science, 1961, Vol. 15, pp. 310 to 319. Pergamon Press Ltd., London. Printed in Great Britain.

Performance and design of hydrocyclones—III

Separating power of the hydrocyclone

K. Rietema*

Koninklijke/Shell-Laboratorium, Amsterdam
(Shell Internationale Research Maatschappij)

(*Received* 28 *July* 1960)

Abstract—A new theory on the separation in hydrocyclones is developed on the basis of the dynamic behaviour of the particles to be separated. This theory leads to the derivation of a dimensionless cyclone separation number, which—as experiments have confirmed—is only dependent on the shape of the cyclone. With the aid of this number an optimum cyclone design can be found.

Literature data on hydrocyclones prove to be in good agreement with the results of this investigation.

Résumé—On expose une nouvelle théorie sur la séparation dans des hydrocyclones. Elle est basée sur le comportement dynamique des particules qui doivent être séparées. Cette théorie mène à un nombre de séparation sans dimensions pour le cyclone, qui—selon l'évidence expérimentale—dépend seulement de la forme du cyclone. A l'aide de ce nombre la forme optimale du cyclone peut être déterminée.

Il s'est trouvé que des données de la littérature sur les hydrocyclones s'accordent bien avec les résultats obtenus dans cette étude.

Zusammenfassung—Eine neue Theorie über die Trennung in Hydrozyklonen wird entwickelt, die auf das dynamische Verhalten der zu trennenden Teilchen basiert ist. Sie führt zur Ableitung einer dimensionslosen Zyklontrennungszahl. Versuche haben bestätigt, dass diese Zahl nur von der Form des Zyklons abhängig ist. Die optimale Form eines Zyklons lässt sich mit Hilfe dieser Zahl bestimmen.

Es stellt sich heraus, dass zwischen den Literaturdaten über Hydrozyklonen und den Ergebnissen dieser Arbeit gute Übereinstimmung besteht.

Introduction

Theories on the separation in cyclones have been developed by various investigators, e.g. Ter Linden [1], Tarján [2], de Gelder [3] and Bradley and Pulling [4]. They are based on the concept of the stability radius, at which centrifugal forces acting on the particle are balanced by the drag forces exerted by the radial flow.

According to these theories particles which have a stability radius smaller than the radius of the overflow nozzle are carried off through the overflow, while particles with stability radii larger than the overflow nozzle radius are discharged at the apex.

As will be clear, these theories assume that all particles will arrive at their stability radius in time, in other words, that equilibrium conditions prevail in the cyclone.

The theory developed in this paper, however, is a dynamic one and it assumes that particles with a stability radius smaller than the overflow nozzle radius may very well be separated towards the wall already before they have reached their stability radius.

Generally the separation efficiency is expressed in terms of the 50 per cent diameter, which is the diameter of a particle which has equal chances of being separated and of being entrained.

It will be shown that for well-designed cyclones

*Now Professor of Chemical Engineering at the Technical University of Eindhoven, Holland.

the relation between 50 per cent diameter, pressure drop, throughput and cyclone size is given by

$$Cy_{50} = \frac{d_{50}^2 \, \Delta\rho}{\eta} L \frac{(\Delta p)_i}{\rho q} = \text{constant.}$$

1. Derivation of Separation Formula

The separation in a hydrocyclone is due to the centrifugal forces generated by the tangential motion of the liquid. When the particles to be separated are of a density different from that of the dispersing liquid they acquire a radial velocity with respect to the liquid because of these centrifugal forces. When the particles are of a higher density, this radial velocity is directed outwards and when the centrifugal forces are strong enough the particles reach the cyclone wall on their way from the inlet downwards and are then separated.

A particle may not reach the wall:

(a) If the radial velocity of the liquid, which is directed inwards, is too large and thus causes it to be entrained towards the centre.
(b) If it enters the cyclone at too great a distance from the wall.
(c) If its residence time is too short.
(d) On account of turbulence, which causes eddy diffusion of the particles, to the effect that differences in concentration are evened out.

The idea underlying the derivation of the efficiency correlation was that for a certain cyclone there should be a relation between the static pressure drop and the separation achieved when expressed in terms of the 50 per cent separation diameter. This idea was inspired by the fact that the separation as well as the static pressure drop are determined by the centrifugal acceleration field in the cyclone.

The derivation is based on two assumptions:

(a) The turbulent eddy diffusion has a negligible effect on the separation.
(b) The Reynolds number as related to the particles separated is so low that Stokes' law for the free fall velocity applies.

The justification of these assumptions is given in the Appendix.

The formula will be derived for a conical cyclone as shown in Fig. 1.

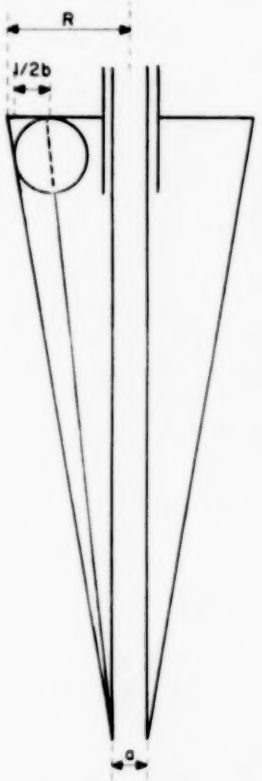

Fig. 1. Schematic separation zone in a hydrocyclone.

Suppose there is an imaginary screen coaxial with the conical cyclone wall which divides the cyclone inlet into two halves of equal cross-sectional area. Under the conditions indicated above it is now reasonable to assume that all particles having a diameter equal to the 50 per cent separation diameter and entering the cyclone through the inner half of the inlet leave the cyclone through the overflow nozzle and that particles with the same diameter entering through the outer half of the inlet leave the cyclone at the apex. A particle of the same diameter which is injected at the centre of the inlet will just be

separated. Such a particle will now be considered and followed on its path to the apex.

On injection into the cyclone its distance from the wall is $= \frac{1}{2}b$.

At the moment it reaches the apex its distance to the wall should be reduced to zero. The radial velocity of the particle then equals $(U - U_p)$.

From Stokes' law it follows that for a particle at a radius r in the cyclone

$$U_p = \frac{d_{50}^2 \, \Delta\rho}{18\eta} \frac{V^2}{r},$$

where V^2/r denotes the centrifugal acceleration.

During its residence time T the particle should cover, in a radial direction, a distance equal to the radius of the inlet centre minus the radius of the air core $= R - \frac{1}{2}b - \frac{1}{2}a$ (see Fig. 1). Therefore,

$$\int_0^T (U - U_p)\, dt = R - \tfrac{1}{2}b - \tfrac{1}{2}a = R_1, \text{ or}$$

$$\int_0^T U_p \, dt = \int_0^T U dt - R_1.$$

On the basis of the measurements of KELSALL [3] and TER LINDEN [1] it may be assumed that both the axial and the radial liquid velocities are constant in the separation zone.

Then, $$\int_0^T U dt = \int_0^T U \frac{dL}{W} = \frac{U}{W} L.$$

It now follows that

$$\frac{d_{50}^2 \, \Delta\rho}{18\eta} \int_0^T \frac{V^2}{r} \, dt = \frac{U}{W} L - R_1,$$

or

$$\frac{d_{50}^2 \, \Delta\rho}{18\eta} \int_{R-\frac{1}{2}b}^{\frac{1}{2}a} \frac{V^2}{r} \frac{dt}{dr} \, dr = \frac{U}{W} L - R_1.$$

In the above formula dt/dr expresses the reciprocal radial velocity of the particle. When it is assumed that the axial velocity of the particle under consideration is equal to that of the liquid and, therefore, is constant (see above) it follows that on an average the radial velocity of the particle must be constant also, since otherwi the particle would leave the separation zone very close to the wall (the shaded area in Fig. 1) and then it would not be separated.

On an average $$\frac{dr}{dt} \simeq \frac{W}{L} R_1 \text{ and}$$

$$\frac{dt}{dr} \simeq \frac{L}{W} \frac{1}{R_1}.$$

For a liquid cyclone operating with a gas core the static pressure drop is equal to the centrifugal head:

$$(\Delta p)_s = \int_{R-\frac{1}{2}b}^{\frac{1}{2}a} \frac{\rho V^2}{r} \, dr.$$

The separation formula can now be elaborated to

$$\frac{d_{50}^2 \Delta\rho}{18\eta} \frac{L}{W} \frac{1}{R_1} \frac{(\Delta p)_s}{\rho} = \frac{U}{W} L - R_1.$$

There will be a certain relation between the axial velocity and the inlet velocity

$$W = C_1 V_0 = C_1 \frac{4q}{\pi b^2}$$

$$\frac{d_{50}^2 \Delta\rho}{\eta} L \frac{(\Delta p)_s}{\rho q} = \frac{72 C_1}{\pi} \frac{R_1}{b^2} \left(\frac{U}{W} L - R_1 \right).$$

In this formula both members are dimensionless. The right-hand member contains only cyclone dimensions and velocity ratios. Therefore it might be expected that for a cyclone of a given shape it will be a constant. Then also the left-hand member must be a constant and seems to be a characteristic cyclone number.

For practical reasons this number is modified into the cyclone correlation number

$$Cy_{50} = \frac{d_{50}^2 \Delta\rho}{\eta} L \frac{(\Delta p)_t}{\rho q}.$$

A drawback of this modification is that now an extra influence of the inlet Reynolds number on Cy_{50} is introduced. For, the ratio

$$\frac{(\Delta p)_t}{(\Delta p)_s}$$

is $= 1 + 1/F$, where F is dependent on the inlet Reynolds number as discussed in Part II

VOL. 15 1961

[6]. It is clear, however, that when $F \gg 1$ the Reynolds number dependence of this ratio is negligible and it is fortunate that for efficient cyclones this is indeed the case.

2. Experiments

To determine the Cy_{50} number for all types of cyclones theoretically on the basis of the formula derived above it would be necessary to have available all data on velocity profiles in these cyclones. This was considered too difficult. An experimental investigation in which the Cy_{50} number was determined from the separation ability of the cyclones was thought to be more straightforward.

Therefore, experiments have been carried out to determine the Cy_{50} number for cyclones of different design and under different conditions. Most of these experiments were performed with a cyclone of 3 in. diameter whose length could be varied and whose inlet overflow and underflow nozzles could be changed (see Fig. 1 of Part II) [6]. As the suspension to be separated a mixture of quartz fines in water was used (see Tables 1, 2 and 3 below).

The underflow of the cyclone was freely discharged, while the overflow could leave the cyclone via a half-turn bend.

The overflow and underflow rates were measured at a certain pressure drop and samples were taken to determine the solid concentration and the particle size distribution in the two flows. The latter was measured by means of a sedimentation analysis. From these measurements the 50 per cent separation diameter d_{50} was determined for each experiment and thus the Cy_{50} number could be calculated. The 80 per cent and the 20 per cent separation diameters, defined in the same manner as d_{50}, were also determined.

The inaccuracy which might be expected in this procedure is about 5 per cent for the 50 per cent separation diameter. This means that the total error in Cy_{50} is about 10 per cent.

The dependence on the ratio L/D follows from Fig. 2. When L/D is increased the separation shifts to smaller particles in such a way that Cy_{50} remains constant. It is clear that if L/D is further increased a state will be reached where

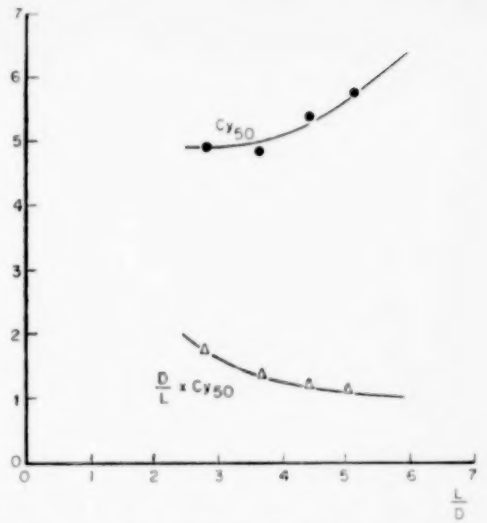

Fig. 2. Dependence of Cy_{50} and $(D/L)\,Cy_{50}$ on L/D for a cyclone with $b/D = 0{\cdot}20$ and $e/D = 0{\cdot}04$.

adding to the length of the cyclone merely means adding dead space, which does not improve the separation. The d_{50} obtained will then remain constant, which means that Cy_{50} will increase proportionally with L/D.

Therefore, when operating cyclones of constant diameter it is favourable to increase the ratio L/D, but not beyond $L/D = 5$, since on further raising this ratio $(D/L)\,Cy_{50}$ and hence d_{50} remain constant (see Fig. 2).

The influence of the pressure drop on Cy_{50} for a certain cyclone ($L/D \simeq 5$, $b/D = 0{\cdot}266$, $e/D = 0{\cdot}333$) is shown in Fig. 3, where the

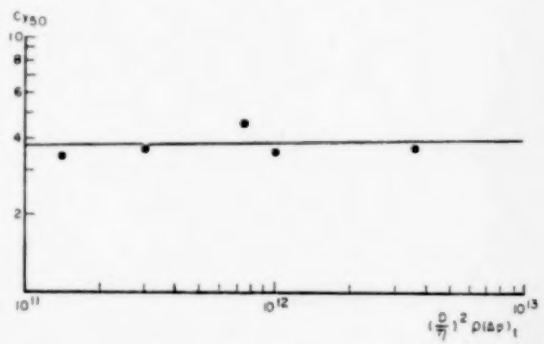

Fig. 3. Dependence of Cy_{50} on pressure drop for a cyclone with $L/D \simeq 5$, $b/D = 0{\cdot}266$ and $e = 0{\cdot}333$.

Table 2. Cyclone separation experiments
Influence of L/D

Cyclone diameter = 75 mm — Inlet diameter = 15 mm
Overflow diameter = 30 mm — Underflow diameter = 20 mm

Exp. No.	*Length of cyclone* (mm)	L/D	*Overflow* (g/sec)	*Solids in overflow* (g/sec)	*Underflow* (g/sec)	*Solids in underflow* (g/sec)	$(\Delta p)_t$ (atm)	*Temp.* (°C)	d_{50} (μ)	Cy_{50}
156	383	5·10	1910	19·9	245	25·9	2·38	17·8	9·5	5·8
157	327	4·35	1837	19·1	204	23·6	2·37	18·0	9·7	5·4
158	270	3·60	1780	15·7	180	24·5	2·41	18·0	9·8	4·8
159	212	2·83	1688	19·4	127	16·4	2·37	18·2	10·8	4·9

Table 3. Cyclone separation experiments
Influence of pressure drop

Cyclone diameter = 75 mm — Inlet diameter = 20 mm — Overflow diameter = 25 mm
Cyclone length = 396 mm — Underflow diameter = 15 mm

Exp. No.	*Overflow* (g/sec)	*Solids in overflow* (g/sec)	*Underflow* (g/sec)	*Solids in underflow* (g/sec)	$(\Delta p)_t$ (atm)	*Temp.* (°C)	*Liquid viscosity* (cP)	*Density difference* (g/cm³)	*System*	d_{50} (μ)	Re_{inlet}	$\left(\frac{D}{\eta}\right)^2 \rho (\Delta p)_t$	Cy_{50}
155	860	12·8	140	9·8	0·30	16·8	1·10	1·6	water–quartz	14·0	58,000	14×10^{10}	3·4
151	1290	19·0	190	18·0	0·73	14·0	1·17	1·6	—	11·5	80,500	30×10^{10}	3·5
152	1845	22·9	295	28·9	1·80	14·0	1·17	1·6	—	10·0	116,000	74×10^{10}	4·5
153	2430	26·0	313	45·1	2·45	14·0	1·17	1·6	—	8·5	149,000	100×10^{10}	3·5
200	2330	2·3	122	1·5	2·9	350	0·63	0·8	Slurry oil-catalyst	8·0	250,000	360×10^{10}	3·6

Exp. No.	*Inlet diameter b* (mm)	*Overflow diameter a* (mm)	*Underflow diameter c* (mm)	*Cyclone diameter D* (mm)	*Cyclone length L* (mm)	L/D	*Overflow* (g/sec)	*Solids in overflow* (g/sec)	*Underflow* (g/sec)	*Solids in underflow* (g/sec)	$(\Delta p)_t$ (atm)	*Temp.* (°C)	d_{50} (μ)	Cy_{50}
177	25	30	20	75	396	5·28	1910	19·9	245	25·9	2·38	17·8	9·5	5·8
176					327	4·35	1837	19·1	204	23·6	2·37	18·0	9·7	5·4
175					270	3·60	1780	15·7	180	24·5	2·41	18·0	9·8	4·8
174					212	2·83	1688	19·4	127	16·4	2·37	18·2	10·8	4·9
179	15				396	5·28	1910	19·9	245	25·9	2·38	17·8	9·5	5·8
141					327	4·35	1837	19·1	204	23·6	2·37	18·0	9·7	5·4
153					270	3·60	1780	15·7	180	24·5	2·41	18·0	9·8	4·8
154					212	2·83	1688	19·4	127	16·4	2·37	18·2	10·8	4·9
180	10				396	5·28	1910	19·9	245	25·9	2·38	17·8	9·5	5·8
145					327	4·35	1837	19·1	204	23·6	2·37	18·0	9·7	5·4
144					270	3·60	1780	15·7	180	24·5	2·41	18·0	9·8	4·8
182					212	2·83	1688	19·4	127	16·4	2·37	18·2	10·8	4·9
169	8				396	5·28	1910	19·9	245	25·9	2·38	17·8	9·5	5·8
148					327	4·35	1837	19·1	204	23·6	2·37	18·0	9·7	5·4
183					270	3·60	1780	15·7	180	24·5	2·41	18·0	9·8	4·8
184					212	2·83	1688	19·4	127	16·4	2·37	18·2	10·8	4·9
185	6				396	5·28	1910	19·9	245	25·9	2·38	17·8	9·5	5·8
186					327	4·35	1837	19·1	204	23·6	2·37	18·0	9·7	5·4
187					270	3·60	1780	15·7	180	24·5	2·41	18·0	9·8	4·8
188					212	2·83	1688	19·4	127	16·4	2·37	18·2	10·8	4·9
189	4				396	5·28	1910	19·9	245	25·9	2·38	17·8	9·5	5·8
190					327	4·35	1837	19·1	204	23·6	2·37	18·0	9·7	5·4
191					270	3·60	1780	15·7	180	24·5	2·41	18·0	9·8	4·8
192					212	2·83	1688	19·4	127	16·4	2·37	18·2	10·8	4·9

Table 1. *Cyclone separation experiments*

Influence of b/D and e/D

Cyclone diameter = 75 mm

Cyclone length = 370–430 mm

Overflow diameter e (mm)	*Underflow diameter* u (mm)	*Overflow* (g/sec)	*Solids in overflow* (g/sec)	*Underflow* (g/sec)	*Solids in underflow* (g/sec)	$(\Delta p)_t$ (atm)	$(\Delta p)_s$ (atm)	*Temp* (°C)	d_{20} (μ)	d_{50} (μ)	d_{80} (μ)	$\mathrm{Re}_{\mathrm{inlet}}$	$\left(\frac{D}{\eta}\right)^2 \rho\,(\Delta p)_t$	Cy_{50}	Cy_{80}	d_{80}/d_{20}
35	15	3320	48·2	237	29·8	1·93	1·67	18·4	8·0	12·0	32·0	173,000	$0{\cdot}98 \times 10^{12}$	4·8	30·0	4·0
25	15	2570	32·5	334	33·8	2·03	1·85	18·4	6·0	10·0	18·0	142,000	$1{\cdot}04 \times 10^{12}$	4·2	13·5	3·0
15	7	1580	16·9	153	13·5	2·33	2·27	18·0	6·0	12·0	20·0	83,500	$1{\cdot}17 \times 10^{12}$	12·0	33·0	3·3
8	5	550	6·3	228	8·6	2·67	2·54	17·4	6·0	9·5	20·0	37,000	$1{\cdot}30 \times 10^{12}$	19·0	84·0	3·3
35	20	2610	38·1	96	8·2	1·78	1·41	11·2	8·0	13·0	30·0	136,000	$0{\cdot}63 \times 10^{12}$	5·4	29·0	3·7
30	20	2270	26·1	406	31·3	2·05	1·69	20·0	5·0	9·0	16·0	171,000	$1{\cdot}14 \times 10^{12}$	3·8	12·0	3·2
25	15	2430	26·0	313	45·1	2·45	2·07	14·0	6·0	8·5	12·0	149,000	$1{\cdot}00 \times 10^{12}$	3·5	7·0	2·0
15	10	1150	13·6	324	11·6	2·05	1·94	11·2	5·0	9·5	16·0	74,500	$0{\cdot}72 \times 10^{12}$	6·5	18·0	3·2
10	5	830	8·9	143	9·4	2·48	2·43	20·0	6·0	10·0	20·0	62,000	$1{\cdot}36 \times 10^{12}$	17·0	68·0	3·2
35	20	2100	29·0	140	22·9	2·33	1·53	17·2	7·0	12·0	25·0	176,000	$1{\cdot}12 \times 10^{12}$	8·6	37·0	3·6
30	20	1725	22·3	309	13·2	1·91	1·25	11·2	5·0	13·0	17·0	136,000	$0{\cdot}67 \times 10^{12}$	7·7	13·5	3·4
20	12	1570	17·3	171	30·1	2·56	2·07	17·2	5·0	8·5	12·0	137,000	$1{\cdot}24 \times 10^{12}$	6·3	15·0	2·4
15	10	980	11·0	238	11·3	2·09	1·85	11·2	6·5	8·5	12·0	82,000	$0{\cdot}74 \times 10^{12}$	6·4	15·5	1·9
12	7	890	8·9	185	19·7	2·68	2·49	17·2	5·0	7·0	11·0	84,500	$1{\cdot}30 \times 10^{12}$	7·5	19·0	2·2
12	7	890	8·5	184	19·8	2·71	2·53	16·5	4·0	7·0	10·0	83,000	$1{\cdot}25 \times 10^{12}$	7·5	15·5	2·5
10	5	665	7·8	106	6·7	2·25	2·05	11·2	7·0	10·0	16·0	52,000	$0{\cdot}80 \times 10^{12}$	16·0	41·0	2·3
8	4	570	6·1	99	12·8	2·81	2·74	17·2	4·5	9·0	16·0	52,500	$1{\cdot}37 \times 10^{12}$	22·0	70·0	3·5
35	25	1170	15·5	169	17·2	2·18	0·73	18·0	6·0	12·0	20·0	162,000	$1{\cdot}10 \times 10^{12}$	13·0	36·0	3·3
20	15	780	5·4	217	15·3	1·94	1·13	15·2	6·0	8·0	11·0	100,000	$0{\cdot}85 \times 10^{12}$	7·0	13·0	1·8
10	5	580	4·6	74	12·3	2·46	2·12	18·0	5·0	6·0	8·0	78,500	$1{\cdot}23 \times 10^{12}$	8·7	15·5	1·6
8	4	435	3·45	73	9·5	2·43	2·22	18·0	3·5	5·0 5·5	8·0	61,000	$1{\cdot}23 \times 10^{12}$	8·6	20·0	2·3
6	4	260	1·80	115	6·65	2·36	2·28	18·0	3·0	4·5	8·0	47,500	$1{\cdot}18 \times 10^{12}$	8·5	24·0	2·5
25	15	800	9·5	59	13·2	2·31	0·85	17·8	6·5	9·0	13·0	129,000	$1{\cdot}15 \times 10^{12}$	13·0	27·0	2·0
12	7	569	3·65	78	9·1	2·71	1·88	17·4	4·5	5·5	9·0	96,000	$1{\cdot}33 \times 10^{12}$	8·0	21·0	2·0
6	4	238	1·35	102	5·65	2·60	2·37	17·8	2·5	4·0	7·0	51,000	$1{\cdot}31 \times 10^{12}$	8·0	25·0	2·8

Table 4. Cyclone separation experiments

KELSALL's and DAHLSTROM's experiments

Experiments	*Cyclone diameter* (mm)	*Cyclone length* (mm)	*Inlet diameter* (mm)	*Overflow diameter* (mm)	*System*	*Liquid viscosity* (cP)	*Density difference (inlet)* ($g.cm^{-3}$)	*Throughput* (g/sec)	*Reynolds number*	*Pressure loss factor F (calculated)*	$(\Delta p)_f$ *(calculated)* (atm)	d_{50} (μ)
KELSALL [7]												
Series 1 first exp.	75	228	16·0	6·4	water-plastic spheres	1	0·18	396	32,000	90·0	1·80	34
Series 2 first exp.	—	—	9·5	6·4		—	—	230	31,000	14·5	0·61	28
Series 3 first exp.	—	—	6·4	4·8		—	—	205	41,000	7·0	1·68	13·5
Series 4 first exp.	—	—	6·4	6·4		—	—	264	53,000	5·4	2·24	16
Series 5 first exp.	—	—	6·4	8·0		—	—	304	61,000	4·0	2·30	20
Series 6 first exp.	—	—	6·4	9·5		—	—	341	68,000	3·4	2·56	20
DAHLSTROM [8]												
DAHLSTROM's Fig. 9 (a)												
second point to the right	230	870	44·5	30·8	water-quartz fines	1·0	1·6	5800	167,000	10·0	0·79	16
third point to the right	—	—	38·0	30·8		—	—	5800	195,000	7·5	1·07	15
DAHLSTROM's Fig. 9 (b)												
left point	—	—	52·5	31·0		—	—	6840	100,000	50·0	2·5	13
right point	—	—	52·5	62·0		—	—	6840	100,000	7·5	0·42	21
DAHLSTROM's Fig. 9 (c)												
upper line	—	—	52·5	30·8		—	—	3480	85,000	13·5	0·19	25
lower line	—	—	22·2	30·8		—	—	4920	280,000	1·9	2·33	12·5

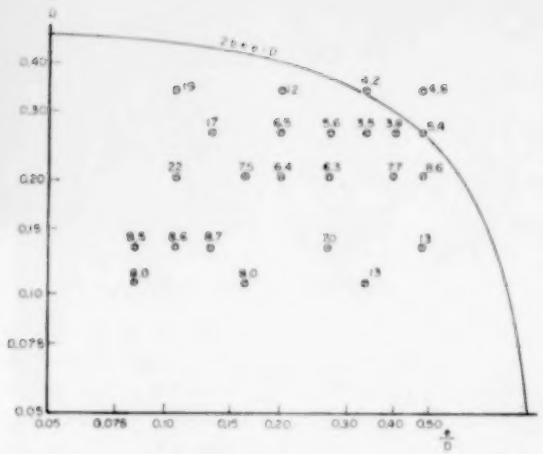

FIG. 4. Values of Cy_{50} for different inlet and outlet diameters with $D = 75$ mm and $L = 390$ mm.

pressure drop is measured by the dimensionless parameter.

$$\frac{\rho D^2 (\Delta p)_t}{\eta^2}.$$

There seems to be a slight increase of Cy_{50} with this parameter, which, however, falls within the above-mentioned range of error.

The influence of b/D and e/D has been investigated at a constant value of $(D^2/\eta^2)\,\rho\,(\Delta p)_t$. The results are presented in Fig. 4, where the value of Cy_{50} is given for different combinations of b/D and e/D (at constant L/D). In this and the following graphs also a curve is shown which is determined by $D = 2b + e$ and which can be expected to be the limit which should not be exceeded, since otherwise the incoming stream would collide with the wall of the vortex finder and then generate severe turbulence. Outside this curve $D = 2b + e$ the Cy number is therefore expected to increase.

3. Discussion

It is interesting to compare our results with those of other investigators, viz. Kelsall [7] and Dahlstrom [8] (see Table 4). Kelsall carried out experiments with plastic spheres of a density of 1·18 g/cm³ in water. The cyclone he used was also a 3 in. cyclone, but of a shorter length ($L/D = 3$). Since the pressure drop was determined across the combined cyclone and feed line, the latter showing an appreciable friction resistance, this pressure drop could not be relied on. Therefore, the pressure drop which had to be used for the cyclone correlation number was calculated by means of the correlation mentioned in Part II [6].

Dahlstrom's experiments were made with a quartz–water suspension in a 9-in. cyclone.

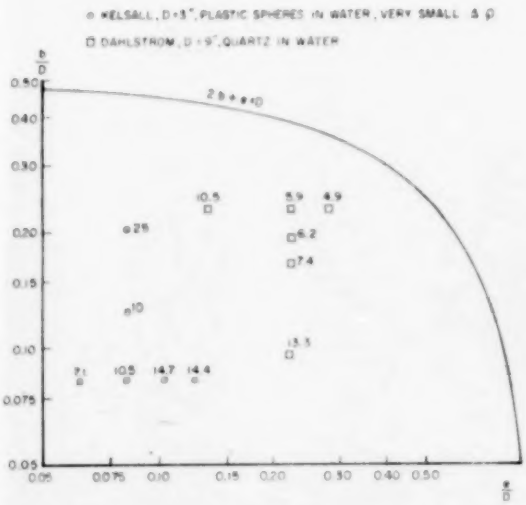

FIG. 5. Cyclone experiments of Kelsall and Dahlstrom.

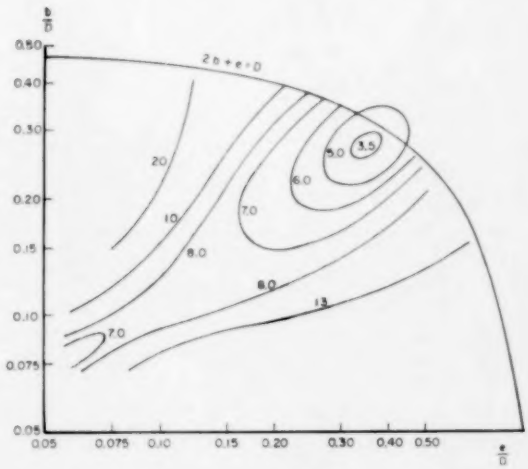

FIG. 6. Contours of constant Cy_{50} for $L/D = 5$.

	Cy_{50}	Cy_{50} corrected for $\frac{L}{D} \simeq 5$
	22·0	25·0
	8·6	10·0
	6·2	7·1
	9·1	10·5
	12·7	14·7
	12·5	14·4
	5·4	6·2
	6·3	7·4
	9·2	10·5
	4·2	4·9
	5·1	5·9
	11·3	13·3

Since DAHLSTROM did not mention the pressure drop in these experiments, it has also been calculated with the aid of the above-mentioned correlation. For the DAHLSTROM cyclone L/D was 3·8.

To compare the experiments of KELSALL and DAHLSTROM with our experiments, the Cy_{50} numbers derived from the former were increased by 15 per cent in order to account for the difference in L/D ratio (see Fig. 2). The results are given in Fig. 5.

It is clear that the results shown in Figs. 4 and 5 agree quite well. This is the more satisfactory as now different cyclone diameters, different viscosities and different density differences are covered by the over-all picture. This increases the reliability of the final result given in Fig. 6 where contours of constant Cy_{50} are drawn (for $L/D = 5$). When a cyclone number Cy_{80} is based on the 80 per cent separation diameter d_{80} in the same way as C_{50} was based on d_{50}, a similar plot of Cy_{80} vs. b/D and e/D can be drawn (see Fig. 7).

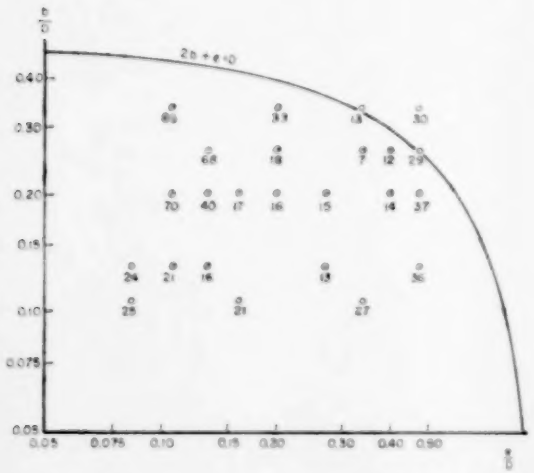

FIG. 7. Cy_{80} number as a function of b/D and e/D.

When returning now to the theoretical formula derived in Part I, the following can be concluded:

Assuming $U/W = R/L$, which means that the vortex flow in the cyclone downwards runs parallel to the wall, the value of $Cy_{50} = 3{\cdot}50$ for the optimal cyclone points to a value of $C_1 = W/V_0 = 1/6$ which is reasonable well in accordance with the experiments of KELSALL and TER LINDEN.

The optimum design of cyclones for separation can be based on Cy_{80} or Cy_{50}. These numbers should be as small as possible, since

d_{80} and d_{50} should be as small as possible
$(\Delta p)_t$ should be as small as possible
q should be as large as possible.

It is a favourable circumstance that Cy_{50} is practically independent of the pressure drop parameter $(\rho D^2/\eta^2)\ (\Delta p)_t$ (see Fig. 3), since this makes it possible to indicate a minimum value for Cy_{50} which is independent of further conditions and, therefore, leads to an optimum design of the cyclone. It is assumed that the same holds true for Cy_{80}.

So far nothing has been said about the length of the vortex finder, l, although this too is of some importance. If it is too short, there may be a short-circuiting flow from the inlet to the overflow; if it is too long, the wall friction will be unduly high, especially since at the location of the vortex finder the tangential velocities are very high.

The influence of l/D has not been investigated systematically. There are indications, however,

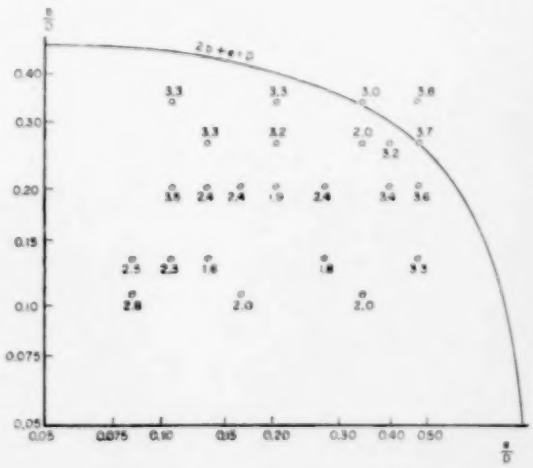

FIG. 8. Classification (expressed as the ratio d_{80}/d_{20}) as a function of b/D and e/D.

that the optimum ratio is 0·4. This ratio is not very critical. It can therefore be concluded that for optimum separation

$$\frac{L}{D} = 5\,\frac{b}{D} = 0{\cdot}28\,\frac{e}{D} = 0{\cdot}34\,\frac{l}{D} = 0{\cdot}4.$$

For classification the optimum design is different. Here the optimum design is found if d_{80}/d_{20} is as close to unity as possible. In Fig. 8 this ratio has been plotted against b/D and e/D, again for $L/D = 5$, from which it follows that now b/D and e/D should both be 0·14.

There are indications, e.g. from KELSALL's experiments, that for optimum classification the ratio L/D should be smaller and $\simeq 2{\cdot}5$.

Therefore, for optimum classification the best estimate of the cyclone dimensions is considered to be

$$\frac{L}{D} = 2{\cdot}5\,\frac{b}{D} = 0{\cdot}14\,\frac{e}{D} = 0{\cdot}14\,\frac{l}{D} = 0{\cdot}4.$$

APPENDIX

The Validity of Stokes' Law

Since in the characteristic cyclone number only the 50 per cent diameter occurs, it is sufficient to show that the Reynolds number related to a particle of that diameter is sufficiently low.

The settling velocity (related to the liquid) of such a particle =

$$\frac{\frac{1}{2}b}{\text{residence time}} = \frac{1}{2}b\,\frac{q}{\text{volume of cyclone}} = \frac{6qb}{\pi D^2 L},$$

The Reynolds number related to

$$d_{50} = \frac{d_{50}}{\nu}\,\frac{6qb}{\pi D^2 L} = \frac{3}{2}\,\frac{\rho V_0 d_{50}}{\eta}\,\frac{b^3}{D^2 L}.$$

From $Cy_{50} = \dfrac{{d_{50}}^2 \Delta\rho}{\eta}\,L\,\dfrac{(\Delta p)_l}{\rho q}$ it follows that

$$\mathrm{Re}_{\text{inlet}} = \frac{b\rho V_0}{\eta} = \frac{1}{Cy_{50}}\,\frac{{d_{50}}^2\Delta\rho}{\eta^2}\,\frac{4L}{\pi b}\,\frac{1}{2}\,{V_0}^2\,G$$

$$= \frac{1}{Cy_{50}}\left(\frac{3}{2}\,\frac{d_{50}\,\rho V_0}{\eta}\,\frac{b^3}{D^2 L}\right)^2 \frac{\Delta\rho}{\rho}\,\frac{8}{9}\,\frac{L^3 D^4}{\pi b^7}\,G$$

$$= \frac{1}{Cy_{50}}\,\{\text{Reynolds } d_{50}\}^2\,\frac{\Delta\rho}{\rho}\,\frac{8}{9\pi}\,\frac{L^3 D^4}{b^7}\,G$$

$$(\text{Reynolds } d_{50}) = \sqrt{\left(Cy_{50}\,\frac{\mathrm{Re}_{\text{inlet}}}{G}\,\frac{\rho}{\Delta\rho}\,\frac{9\pi}{8}\,\frac{b^7}{L^3 D^4}\right)}.$$

For a cyclone of optimum efficiency (see Section 5) this becomes

$$(\text{Reynolds } d_{50}) = \sqrt{\left(\frac{\mathrm{Re}_{\text{inlet}}}{G}\,\frac{\rho}{\Delta\rho}\right)} \times 2{\cdot}05 \times 10^{-3}.$$

For $\Delta\rho = \rho$ and $\mathrm{Re}_{\text{inlet}} = 50{,}000$ $(G = 5{\cdot}0)$, $\mathrm{Re}\text{–}d_{50} = 0{\cdot}2$

$= 400{,}000$ $(G = 10)$, $= 0{\cdot}4$.

Even when $\Delta\rho = \rho/10$, which is an extreme case,

at $\mathrm{Re}_{\text{inlet}} = 50{,}000$, $Re\text{–}d_{50} = 0{\cdot}7$

and at $\mathrm{Re}_{\text{inlet}} = 400{,}000$, $Re\text{–}d_{50} = 1{\cdot}4$.

At these $\mathrm{Re}\text{–}d_{50}$ values the deviation from Stokes' law is still less than 5 per cent so that in general it can be concluded that application of Stokes' law is justified.

The influence of eddy diffusion

Particles suspended in a fluid subject to a turbulent motion are scattered by the turbulence, the effect of which can be described by an eddy diffusion coefficient which is equal to or smaller than the diffusion of the fluid particles itself.

Measurements on eddy diffusion in a cyclone are, however, unknown in the literature; moreover, it is very difficult, if not impossible, to calculate the influence of such a diffusion on the separation.

If it is assumed, however, that the eddy diffusion is equal to the eddy viscosity, an assumption which is generally accepted, it is possible to evaluate its influence from the tangential velocity profiles.

In Part I [6] the tangential velocity profile in conical cyclones was derived theoretically and correlated with the parameter $\lambda = U_0 R/(\nu + \epsilon) \approx U_0 R/\epsilon$.

By comparison with experimental results as obtained by KELSALL [5] and by TER LINDEN [1] in normal conical cyclones λ proves to have a value of at least 10.

Assuming that the eddy diffusivity $E = \epsilon$ it follows that $E = \epsilon < U_0 R/10$.

If we now consider particles of the same density as the surrounding liquid and on which, therefore, no centrifugal force is acting, we find a change in concentration with the radial distance as shown in Fig. 9.

At the inlet the concentration is uniform over the whole width of the inlet and zero outside the inlet.

Near the apex a more even concentration distribution is obtained as shown by the continuous curve which is given by the solution of the differential equation

$$\frac{\partial C}{\partial t} = E\,\frac{\partial^2 C}{\partial x^2},$$

where the inlet concentration distribution is the boundary condition at $t = 0$ and at $t = \infty$ the concentration is constant from $x = 0$ to $x = R$, while $\partial C/\partial x = 0$ for $x = 0$ and $x = R$.

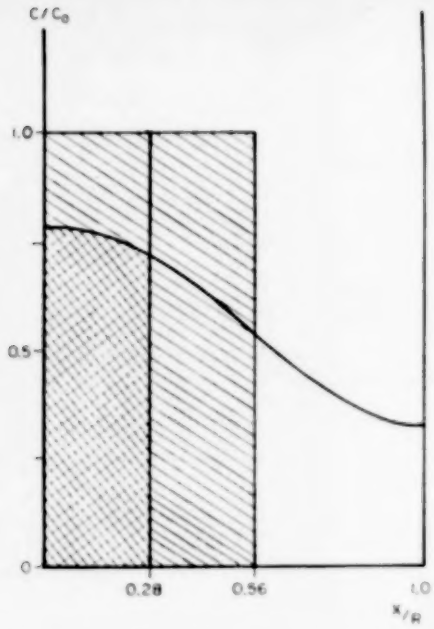

FIG. 9. Influence of eddy diffusion on particle concentration when $\tau = 0{\cdot}1$.

The mathematical solution runs

$$\frac{C}{C_0} = \frac{b}{R} + \frac{1}{\Pi}\sum_{n=1}^{\infty}\frac{1}{n}\exp\left[-(\Pi n)^2\tau\right]\left\{\sin \Pi n\left(\frac{b+x}{R}\right) + \sin \Pi n\left(\frac{b-x}{R}\right)\right\},$$

where $\tau = Et/R^2$ and C_0 the concentration at the inlet at $t = 0$.

The time t is the time in which the particles travel from the inlet to the apex:

$$t = \frac{L}{W} = \frac{R}{U_0}.$$

Remembering that

$$E < \frac{U_0 R}{10} \text{ it follows that}$$

$$\tau < \frac{U_0 R}{10}\frac{R}{U_0}\frac{1}{R^2} = \frac{1}{10}.$$

The curve indicated in Fig. 9 is for $b/R = 0{\cdot}56$ and $\tau = 1/10$.

Since in many cases λ will prove to be higher than 10 (at high Reynolds numbers a value of $\lambda = 20$ or 30 does not seem unreasonable) means this that the influence of eddy diffusion will be even smaller than indicated in Fig. 9.

Further, in actual operation the influence of diffusion is also decreased by the following effect:

Particles which are separated and have reached the wall are taken up in the boundary layer in which there is practically no turbulence and no eddy diffusion. Hence these particles will never leave this boundary layer any more. This effect, therefore, makes up for the loss caused by diffusion at the inside of the separation zone.

Altogether it will be clear now that diffusion of this magnitude only slightly affects the total amount of particles which are not further removed from the wall than a distance $= \frac{1}{2}b$. If there is still a small decrease of this amount this will only affect the calculation of the d_{50}-particle in such a way that the actually obtained d_{50}-particle is shifted to a somewhat larger size.

NOTATIONS

a = diameter of air core in cyclone
b = diameter of cyclone inlet
C = concentration of solids in suspension
Cy_{50} = cyclone correlation number based on d_{50}
Cy_{80} = cyclone correlation number based on d_{80}
D = cyclone diameter
d_{20} = diameter of particles separated to 20 per cent
d_{50} = diameter of particles separated to 50 per cent
d_{80} = diameter of particles separated to 80 per cent
E = turbulent diffusion coefficient
c = diameter of overflow outlet
F = cyclone pressure loss factor $= (\Delta p)_s/\frac{1}{2}\rho V_0^2$
G = total pressure loss factor $= (\Delta p)_t/\frac{1}{2}\rho V_0^2$
g = gravitational acceleration
L = total length of cyclone from top plate to apex
L_1 = length of cylindrical part of cyclone
L_2 = length of conical part of cyclone
l = length of vortex finder
n = power factor occurring in pressure drop correlation
O = overflow rate of cyclone
p = static pressure in cyclone
$(\Delta p)_t$ = total pressure drop necessary to operate a cyclone
$(\Delta p)_s$ = static pressure drop from inlet to outlet
q = throughput of cyclone
R = radius of cyclone
$R_1 = R - \frac{1}{2}a - \frac{1}{2}b$
r = radial co-ordinate in cyclone
T = residence time of particle in cyclone
U = radial velocity of liquid
U_0 = radial velocity of liquid at radius of cyclone
U_p = radial velocity of particle relative to the liquid
u = diameter of underflow nozzle
V = tangential velocity in cyclone
V_0 = linear inlet velocity
W = axial velocity in cyclone
z = axial co-ordinate in cyclone
α = inclination of cyclone axis to the vertical
γ = factor occurring in pressure drop correlation

VOL. 15 1961

ϵ = turbulent kinematic viscosity
η = dynamic liquid viscosity
λ = dimensionless parameter describing the tangential velocity profile
ν = kinematic liquid viscosity
ρ = liquid density
$\Delta\rho$ = difference between density of solid and that of liquid
$\sigma = r/R$
$\sigma_1 = a/R$
ϕ = ratio of angular momentum at radius r to inlet angular momentum

References

[1] Ter Linden A. J. *Proc. Inst. Mech. Engrs.* 1949 **160**.

[2] Tarjan G. *Acta. Tech. Acad. Sci. Hungar.* 1953 **7** 389.

[3] Gelder de A. L. *Symp. Scaling-up Chem. Plant. Proc.* 1957 Institute of Chemical Engineers.

[4] Bradley D. and Pulling D. J. *Trans. Inst. Chem. Engrs.* 1959 **37** 34.

[5] Kelsall D. F. *Trans. Inst. Chem. Engrs.* 1952 **30** 87.

[6] Rietema K. *Chem. Engng. Sci.* (Parts I and II of this series), (this issue).

[7] Kelsall D. F. *Chem. Engng. Sci.* 1953 **2** 254.

[8] Dahlstrom D. A. *Trans. Amer. Inst. Min. (Metall.) Engrs.* 1949 **184** 33.

Chemical Engineering Science, 1961, Vol. 15, pp. 320 to 325. Pergamon Press Ltd., London. Printed in Great Britain.

Performance and design of hydrocyclones—IV

Design of hydrocyclones

K. Rietema*

Koninklijke/Shell-Laboratorium, Amsterdam
(Shell Internationale Research Maatschappij)

Abstract—This is the fourth part of a series of papers on hydrocyclones. In Part I general considerations were presented, in Part II a pressure drop correlation was given, while in Part III a cyclone separation number was derived whose value was determined experimentally. An optimal cyclone shape was indicated.

In this part rules are given that enable hydrocyclones to be designed for any separation problem in which the size of the particles to be separated is known. Constructional details and items to be observed in designing a cyclone or cyclone battery are discussed.

Finally the design method is illustrated by an example.

Résumé—Le présent article est la quatrième partie d'une série traitant d'hydrocyclones. La première partie traite des considérations générales et la deuxième partie traite de la corrélation entre la chute de pression et le pouvoir de séparation; dans la troisième l'auteur déduit un nombre de séparation pour le cyclone, dont la valeur a été déterminée expérimentalement, et indique la forme optimale du cyclone.

Cet article donne de simples règles permettant de calculer et de projeter un hydrocyclone pour tout problème de séparation, pourvu que les dimensions des particules soient connues.

Des détails importants qui doivent être observés dans la construction d'un cyclone ou d'une installation de cyclones sont discutés.

Finalement la méthode de construction est illustrée à l'aide d'un exemple.

Zusammenfassung—Dies ist der letzte einer Folge von Artikeln über Hydrozyklonen. Im 1. Teil wurden allgemeine Betrachtungen angestellt, im 2. Teil wurde eine Beziehung für das Druckgefälle ausgearbeitet, im 3. Teil eine Zyklontrennungszahl, deren Wert sich durch Versuche ermitteln liess. Eine optimale Form des Zyklons wurde angegeben.

In diezem 4. Teil werden einfache Regeln angegeben, mit denen es möglich ist, für jedes Trennungsproblem, wobei die Grösse der zu trennenden Teilchen bekannt ist, einen Hydrozyklon zu entwerfen. Wichtige Einzelheiten, die bei Entwurf und Bau eines Zyklons oder einer Zyklonanlage zu berücksichtigen sind, werden besprochen.

Zum Schluss wird die Anwendung der Berechnungsmethode an einem Beispiel gezeigt.

Introduction

The performance of a hydrocyclone used for the separation of a given solids–liquid system is determined by its throughput. This means that at a certain throughput both the pressure drop and the separation obtained are fixed.

If a better separation is required, i.e. if finer particles must be separated and discharged with the underflow, this goal can be attained by increasing the throughput, which, however, means that also the total pressure drop will increase. If this is not allowed the only possibility is to take a cyclone of another design or a smaller one. In order to be able to handle the same throughput a larger number of cyclones must then be run in parallel.

In the following we will only consider cyclones of optimum design, as discussed in Part III [1] of this series, which is fixed by the following relations between the cyclone dimensions:

see Fig. 1

$$L/D \simeq 5$$
$$b/D = 0{\cdot}28$$
$$e/D = 0{\cdot}34$$
$$l/D \simeq 0{\cdot}4$$

*Now Professor of Chemical Engineering at the Technical University of Eindhoven, Holland.

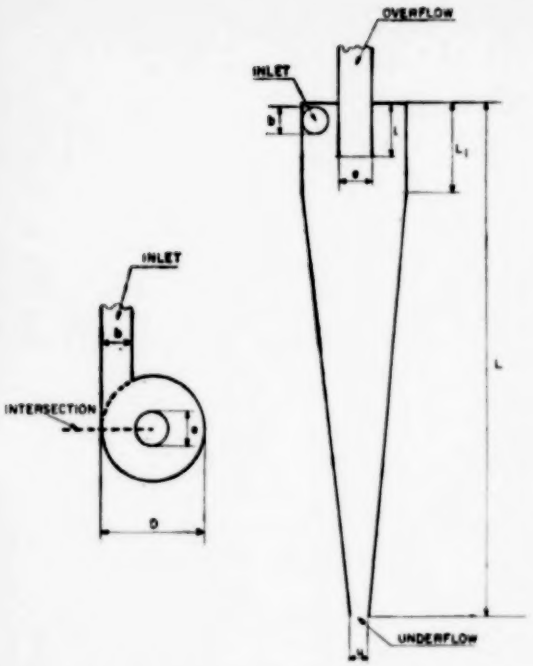

FIG. 1. Cross-section of a hydrocyclone.

For cyclones of this design the cyclone separation number

$$Cy_{50} = \frac{d_{50}^2\,\Delta\rho}{\eta}\,\frac{L\,(\Delta p)_t}{\rho q} = 3{\cdot}5,$$

while the total pressure drop, expressed in numbers of inlet velocity heads, depends on the inlet Reynolds number as indicated in Fig. 2 (see also Part II) [2].

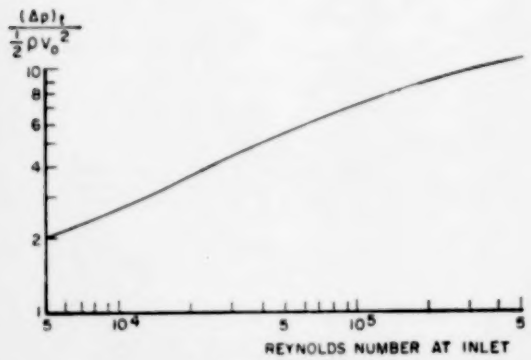

FIG. 2. Relation between pressure drop and inlet Reynolds number of recommended hydrocyclone of a gas core is present.

Both correlations hold in the case of purely Newtonian liquids if the solids concentration in the feed is not higher than 2 per cent by volume and if operation is such that a gas core can develop in the centre of the hydrocyclone.

1. Calculation of Hydrocyclones

For the design of a hydrocyclone battery the following factors must be known:

(a) The available pressure drop.
(b) The total throughput desired.
(c) The desired 50 per cent separation diameter.
(d) The physical properties of the system to be separated.

For each cyclone of the hydrocyclone battery the Reynolds number at the inlet can be calculated:

$$\mathrm{Re}_{\mathrm{inlet}} = \frac{b\rho V_0}{\eta} = \frac{4\rho q}{\pi b \eta}.$$

From Cy_{50} it follows that $\rho q = \dfrac{d_{50}^2\,\Delta\rho}{\eta}\,\dfrac{L(\Delta p)_t}{Cy_{50}}$.

Hence, $\mathrm{Re}_{\mathrm{inlet}} = \dfrac{4}{\pi}\,\dfrac{L}{b}\,\dfrac{1}{Cy_{50}}\,\dfrac{d_{50}^2\,\Delta\rho}{\eta}\,\dfrac{(\Delta p)_t}{\eta}$.

For cyclones of optimum design it follows that

$$\mathrm{Re}_{\mathrm{inlet}} = 6{\cdot}5\,\frac{d_{50}^2\,\Delta\rho}{\eta}\,\frac{(\Delta p)_t}{\eta}.$$

This means that the inlet Reynolds number can be calculated from the total available pressure drop, the desired 50 per cent separation diameter and the physical properties of the system to be separated.

The corresponding value of the pressure-drop factor $G = (\Delta p)_t/\frac{1}{2}\rho V_0^2$ can now be read from Fig. 2; hence, V_0 can be calculated, after which the inlet diameter b and, consequently, the cyclone diameter D, follow from the value of $\mathrm{Re}_{\mathrm{inlet}}$ already known.

The quantities required are more rapidly obtained with the aid of Fig. 3.

Here two newly-derived dimensionless numbers are related to

$$\frac{\mathrm{Re}_{\mathrm{inlet}}}{6{\cdot}5} = \frac{d_{50}^2\,\Delta\rho}{\eta}\,\frac{(\Delta p)_t}{\eta}.$$

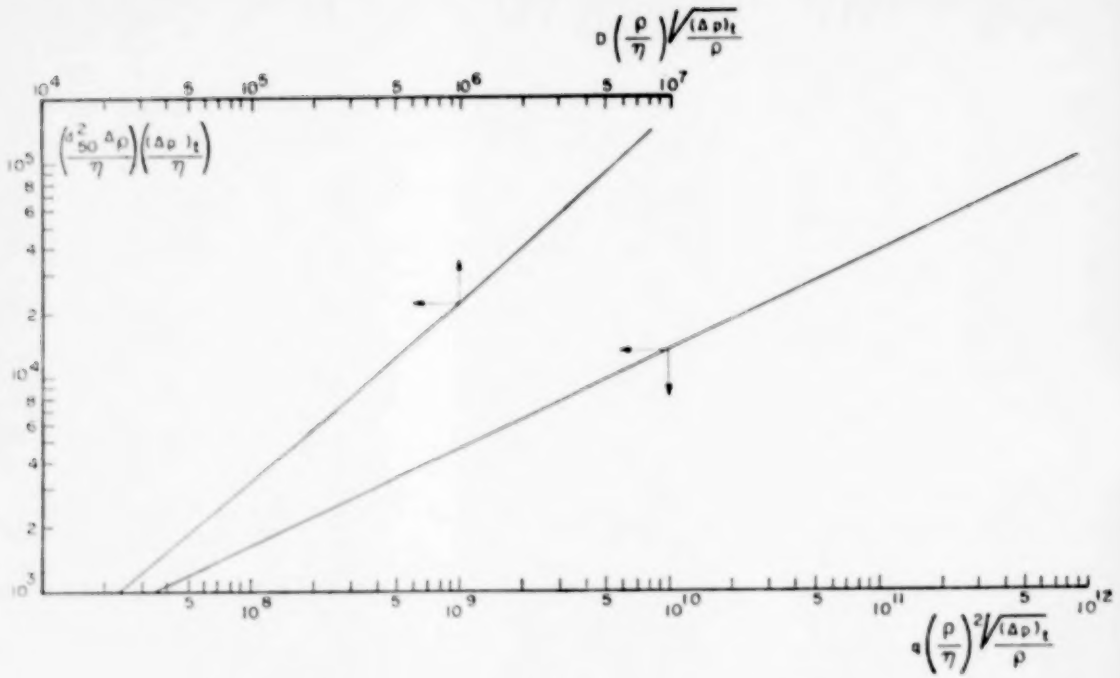

FIG. 3. Hydrocyclone correlations between separation characteristics, cyclone diameter and cyclone throughput if a gas core is present.

These two numbers are derived as follows:

$$\frac{D}{b} \times \mathrm{Re}_{\mathrm{inlet}} \times \sqrt{\frac{G}{2}} = D\,\frac{\rho}{\eta}\sqrt{\frac{(\Delta p)_t}{\rho}}$$

and

$$\frac{\pi}{4}(\mathrm{Re}_{\mathrm{inlet}})^2 \times \sqrt{\frac{G}{2}} = q\left(\frac{\rho}{\eta}\right)^2\sqrt{\frac{(\Delta p)_t}{\rho}}.$$

The relation between these two numbers and the inlet Reynolds number can be calculated from the relation between G and $\mathrm{Re}_{\mathrm{inlet}}$ (taking into account that for cyclones of optimum design $b/D = 0{\cdot}28$).

Their values can be read from Fig. 3 when

$$\frac{d_{50}^2\,\Delta\rho}{\eta}\,\frac{(\Delta p)_t}{\eta}$$

has been calculated.

Next, diameter D and throughput q of each cyclone can be calculated.

If the total desired throughput amounts to Q, the number, n, of cyclones which must be run in parallel to handle this throughput follows from

$$n = Q/q.$$

2. Determination of the Desired 50 per cent Separation Diameter

The separation curve of a hydrocyclone is given in Fig. 4, where the particle size is expressed in 50 per cent separation diameter and S means the percentage of solids separated.

If the particle size distribution of the cyclone feed is known and is equal to $g\,(d_p)$, for a certain d_{50} the percentage of solids not separated by the cyclone can be calculated by means of

$$\text{(percentage solids not separated)} = \frac{\int_0^\infty (100 - S)\,g\,(d_p)\,d\,d_p}{\int_0^\infty g\,(d_p)\,d\,d_p}.$$

VOL. 15 1961

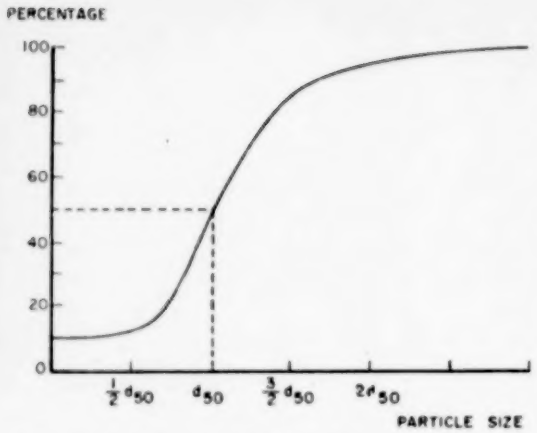

FIG. 4. Percentage of solids of particle size states separated in cyclone (as determined experimentally for 10 per cent underflow).

If this percentage is determined for several values of d_{50}, by interpolation the d_{50} can be found on which the design of the cyclone battery has to be based in order to separate the desired percentage of total solids.

3. Important Points in the Construction

In order to guarantee a good separation the following constructional details must be adhered to:

1. The inlet should be perfectly tangential to the cyclone body, which means that the intersection of the inlet pipe and the inside of the cyclone should just reach the point where the radius of the cyclone which is perpendicular to the inlet axis intersects the cyclone body (see Fig. 1b). There should be no hole or any other kind of uneveness at this point.

2. The inside of the cyclone and the inlet pipe should be perfectly smooth in order to reduce turbulence and erosion as much as possible.

3. The wall thickness of the vortex finder should not exceed 1/10 of its internal diameter.

4. In the case of a multi-hydrocyclone, where several cyclones have one common feed line, the separate inlet pipes should have at least a length of four times their diameter.

When from a constructional point of view rectangular inlets are preferable, there is no objection to this, provided the above rules are followed and the cross-section of the rectangular inlet pipe has the same surface area as that of the circular pipe, which would follow from the calculation.

5. In order to prevent as much as possible erosion, which is strongest at the intersection of inlet and cyclone body and at the apex, it is recommended to use very hard materials for the construction.

4. Example of a Separation Problem

Problem

In a refinery a hot oil stream flowing from a heating unit contained fine solid particles at an average concentration of approximately 0·1 per cent by weight. This solid content had to be reduced to less than 0·02 per cent by weight. Since large quantities of oil were involved from which very fine particles had to be removed at high temperatures installation of a hydrocyclone battery seemed an attractive solution. The more so because the oil stream flowed from the unit at a pressure of several atmospheres. Relevant physical data were:

(a) Hydrocarbon phase

temperature	240°C
density (240°C)	760 kg/m³
viscosity (240°C)	0·7 cP (0·7 × 10^{-3} kg/m sec)

(b) Solid phase

density (oil wetted)	1800 kg/m³
range of particle sizes	1–50 μ
particle size distribution:	See Fig. 5

(c) Available pressure 5–7 atm abs.

Design of the cyclone unit

(a) *Calculation of data.* The calculation will proceed as indicated in Section 1. First a separation diameter d_{50} must be chosen. It appears from Fig. 5 that all particles larger than approximately 5 μ must be separated. To ensure good separation a value of 4 μ is chosen for d_{50}. The available pressure drop across the cyclone unit is taken as 4 atm. It follows that the value of the dimensionless group:

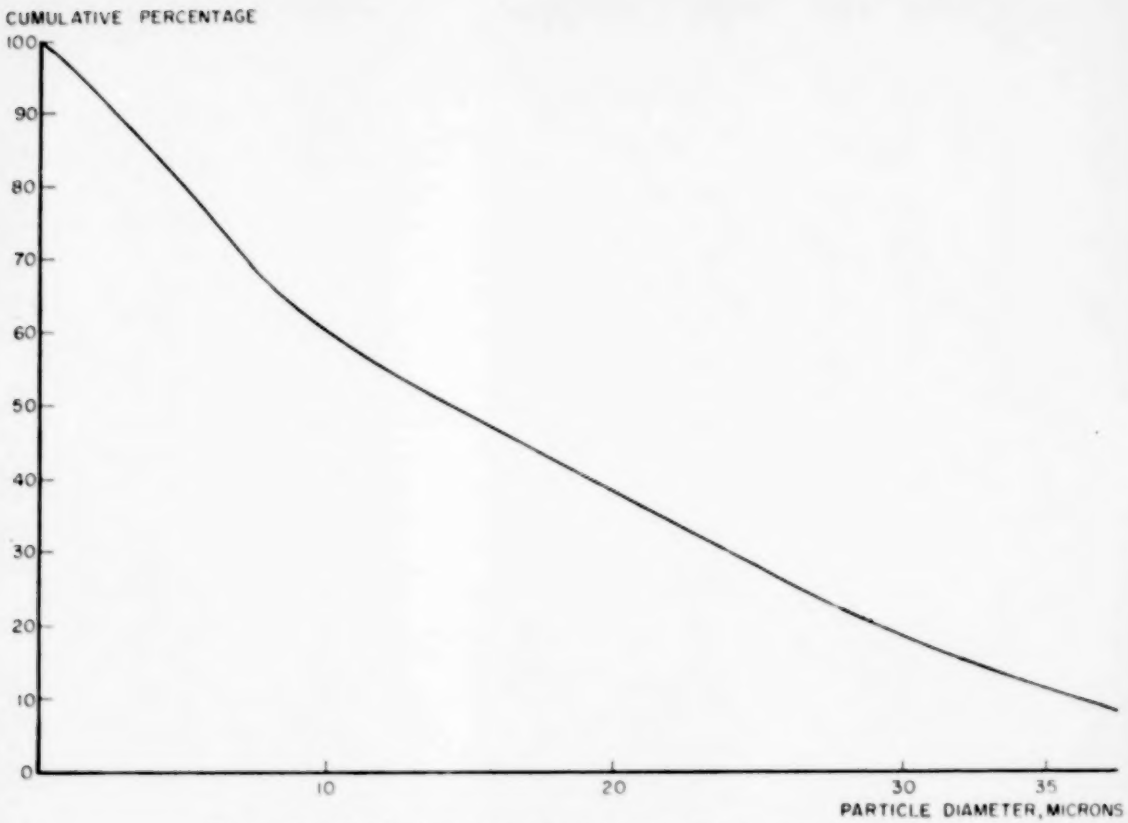

Fig. 5. Size distribution of solids in the feed of a hydrocyclone battery.

$$\frac{d_{50}^2\,\Delta\rho\,\Delta p}{\eta^2} = 1{\cdot}3 \times 10^4,$$

and thus from Fig. 3

$$D\,\rho/\eta\,\sqrt{\frac{\Delta p}{\rho}} = 5{\cdot}6 \times 10^5,$$

$$q\,(\rho/\eta)^2\,\sqrt{\frac{\Delta p}{\rho}} = 10^{10},$$

from which D (cyclone diameter) 22·5 mm

and q (throughput of a single cyclone)

$0{\cdot}37 \times 10^{-3}$ m^3/sec,

which is equivalent to 24 tons/day.

Because all geometrical ratios for the hydrocyclone are fixed (see Introduction and Fig. 1) it follows that:

inlet diameter	$b = 0{\cdot}28 \times D = 6{\cdot}3$ mm
overflow diameter	$e = 0{\cdot}34 \times D = 7{\cdot}6$ mm
cyclone length	$L = 5 \times D = 113$ mm

For handling 1000 tons/day of oil 1000/24 = 42 cyclones in parallel are required.

(b) *Lay-out of cyclone unit.* For reasons of operational flexibility the cyclones were assembled in six units of nine cyclones in parallel each. The hot oil also contained some dissolved gases, which will partly be flashed off during the drop in pressure in the cyclone. Thus special measures for ensuring formation of a gas core in the cyclones were not considered necessary.

Because the concentration of solids in the feed was rather low the underflow rate of the cyclones could be restricted to a value less than normal. By choosing a small underflow diameter it was set at 3 to 5 per cent by volume of the feed flow rate.

VOL. 15 1961

(c) *Performance of the cyclone unit.* The performance of the unit was closely followed during a period of several hundred hours. Even when the solids concentration in the feed occasionally was as high as three times the average value, separation was quite satisfactory. Analysis of the overflow regularly showed solids contents between 0·02 and 0·01 per cent by weight. No serious operational difficulties were encountered under normal operating conditions.

Notation

b = inlet diameter
Cy_{50} = characteristic cyclone number
d_p = particle diameter
d_{50} = diameter of particles which are separated for 50 per cent
D = cyclone diameter
e = overflow diameter
G = ratio of total pressure loss and inlet velocity head
l = vortex finder length
L = length of cyclone from top plate to apex
L_1 = length of cyclindrical part of cyclone body
n = total number of cyclones which are run in parallel
$(\Delta p)_t$ = total pressure loss necessary to operate the cyclone
q = throughput of one cyclone
Q = throughput of a cyclone battery
S = percentage of solids of uniform particle size separated in cyclone
u = underflow diameter
V_0 = linear inlet velocity
η = liquid viscosity
ρ = liquid density
$\Delta\rho$ = difference in density between solid and liquid

References

[1] Rietema K. *Chem. Engng. Sci.* (Part III of this series), (this issue).
[2] Rietema K. *Chem. Engng. Sci.* (Part I and II of this series), (this issue).

Chemical Engineering Science, 1961, Vol. 15, pp. 326 to 331. Pergamon Press Ltd., London. Printed in Great Britain.

Letters to the Editors

The influence of heat generation on the catalyst effectiveness factor

(*Received* 28 *July* 1960 ; *and in revised form* 19 *September* 1960)

IN THE DESIGN of chemical reactors and in experimental kinetic studies involving porous catalyst pellets it is sometimes important to allow for the effect of diffusional resistance inside the pellet. When the pellets are sufficiently large, when the specific rate is great, or when the diffusion through the pores is slow, the concentration of a reactant inside the catalyst may be appreciably smaller than that in the surrounding fluid. As a result the reaction rate may be smaller than it could be if diffusion were very easy. The ratio of the rates is called the " effectiveness factor," first used by THIELE [1] in 1939.

Following THIELE most mathematical developments of equations for the effectiveness factor have been based on the assumption that the interior of the catalyst pellet is everywhere at the same temperature as the fluid outside even though the concentrations of reactants are reduced by diffusional resistance. This is despite the fact that the heat of reaction is absorbed or released inside the pellet and has to be conducted in or out. The assumption of negligible heat effect has usually been accepted because of the dense structure of most catalyst supports and the case of heat flow through the solid. However, PRATER [2] has pointed out that a significant temperature difference may exist between the interior and the surface of a pellet of a commercial platinum–alumina reforming catalyst. For the dehydrogenation of *cyclo*hexane at 400 °C and 25 atm he estimates that the centre temperature is about 53°C cooler than the surrounding fluid. Quite evidently such differences may affect the internal reaction rate. The effectiveness factor must therefore depend on thermal resistance and heat of reaction parameters in addition to the diffusion parameters. The object of this communication is to show that a simple extension can be made to THIELE's [1] well-known result to allow for heat effects when the temperature difference across the pellet is small but not negligible.

Consider a first-order, irreversible chemical reaction occurring inside a porous homogeneous sphere. Because the structure of a catalyst pellet is much more conducive to heat transfer than to mass transfer it is assumed that all of the mass-transfer resistance is in the interior of the sphere whereas thermal resistance exists both in the surrounding fluid and within the pellet. The steady-state material and energy balances lead do the boundary value problem :

$$d^2\bar{c}/d\phi^2 = (k/k_0)\,\bar{c} \tag{1}$$

$$d^2\theta/d\phi^2 = -(k/k_0)\,\bar{c} \tag{2}$$

$$\bar{c}(\Phi) = \Phi \tag{3a}$$

$$\bar{c}'(0) = 0 \tag{3b}$$

$$(\mathrm{Nu}\,\Phi - 1)\,\theta(\Phi) + \Phi\cdot\theta'(\Phi) = 0 \tag{3c}$$

$$\theta'(0) = 0 \tag{3d}$$

where $k = k(T)$. The dimensionless variables are defined by

$$\phi = r\sqrt{k_0/D} \tag{4a}$$

$$\bar{c} = (c/c_0)\,r\sqrt{(k_0/D)} \tag{4b}$$

$$\theta = \frac{T - T_0}{(D\,Q\,c_0/\lambda)}\,r\sqrt{(k_0/D)} \tag{4c}$$

and the dimensionless parameters are

$$\Phi = r_0\sqrt{(k_0/D)} \tag{5a}$$

$$\mathrm{Nu} = \frac{h\sqrt{(D/k_0)}}{\lambda} \tag{5b}$$

$$\epsilon = DEQ\,c_0/\lambda\,RT_0^2 \tag{5c}$$

This problem was solved by a perturbation technique using the dimensionless heat effect parameter, ϵ, to form the perturbation series

$$\bar{c} = \bar{c}_0(\phi) + \epsilon\,\bar{c}_1(\phi) + \epsilon^2\,\bar{c}_2(\phi) + \ldots \tag{6}$$

$$\theta = \theta_0(\phi) + \epsilon\,\theta_1(\phi) + \epsilon^2\,\theta_2(\phi) + \ldots . \tag{7}$$

The dimensionless ratio of reaction rate constants is represented by the series

$$\frac{k}{k_0} = \exp\left[-\frac{E}{R}\left(\frac{1}{T} - \frac{1}{T_0}\right)\right] \approx 1 + \epsilon\,\theta_0\,\phi^{-1} + \epsilon^2(\theta_1\,\phi^{-1} + \theta_0^2\,\phi^{-2}) + \ldots \tag{8}$$

An infinite set of differential equations and a sufficient set of expanded boundary conditions result when (6), (7) and (8) are substituted into (1), (2) and (3), and the coefficients of successive powers of ϵ are separately equated to zero. Solutions have been obtained for the zero-th and first-order perturbation functions, $c_0(\phi)$, $c_1(\phi)$, $\theta_0(\phi)$, and $\theta_1(\phi)$.

The result is used to find the effectiveness factor, defined as the ratio of the rate of conversion in the pellet to that expected if the concentration of reactant *and* the temperature were everywhere equal to the values of the same quantities in the surrounding fluid.

$$\eta = \frac{D\, 4\pi r_0^2 c'(r_0)}{\frac{4}{3}\pi r_0^3 k_0 c_0} = 3\,\Phi^{-3}\left[-\bar{c}(\Phi) + \Phi\,\bar{c}'(\Phi)\right].$$

$$= \eta_0 + \epsilon\,\eta_1 + \ldots . \qquad (9)$$

The zero-th perturbation η_0, is the result obtained by THIELE [1],

$$\eta_0 = 3\,\Phi^{-2}(\Phi \coth \Phi - 1) \qquad (10)$$

to which must be added the correction term proportional to the first perturbation function,

$$\eta_1 = \frac{3}{\sinh^2 \Phi}\left[\frac{M}{2}\left(\frac{\sinh 2\Phi}{2\Phi} - 1\right) - \frac{3}{4}\frac{\Phi\, V(\Phi)}{\sinh \Phi}\right] \qquad (11)$$

where

$$M = 1 + \frac{\Phi \coth \Phi - 1}{\mathrm{Nu}\ \Phi} \qquad (12)$$

and

$$V(\Phi) = \sum_{n=1}^{\infty} \frac{3^{2n} - 1}{(2n+1)(2n+1)!}\,\Phi^{2n} \qquad (13)$$

A few values of η_1 are listed in Table 1, where they are seen to depend on the dimensionless particle size parameter, $\Phi = r_0\sqrt{(k_0/D)}$, and on the surface thermal resistance parameter, $\mathrm{Nu} = (h/\lambda)\sqrt{(D/k_0)}$. The maxima in the curves depend on the fact that small particles have nearly uniform temperatures while the reaction is confined to the surface layers of the larger ones, making the thermal resistance of the interior inconsequential.

Since ϵ is positive for exothermic reactions addition of the correction term to THIELE's isothermal result may make the effectiveness factor exceed unity, at least for a finite range of the particle size parameter. This results of course from the reaction-rate constant being greater than its value at the surrounding fluid temperature, even though the reactant concentration is smaller.

Table 1. *Values of Effectiveness Factor First Perturbation Function*

Dimensionless radius of particle (Φ)	*First perturbation function* (η_1)			
	Nu = 1	Nu = 3	Nu = 10	Nu = ∞
0·1	0·0339	0·0117	0·00392	0·000594
0·2	0·0685	0·0244	0·00894	0·00233
0·4	0·139	0·0532	0·0231	0·0102
0·6	0·208	0·0838	0·0403	0·0217
0·8	0·272	0·114	0·0594	0·0358
1·0	0·328	0·143	0·0786	0·0509
2·0	0·463	0·225	0·142	0·106
4·0	0·379	0·192	0·126	0·0983
6·0	0·281	0·143	0·0936	0·0742

For small values of Φ, (9) is approximated by

$$\eta \approx 1 - \frac{\Phi^2}{15} + \epsilon\left(\frac{\Phi^2}{3} + \frac{\Phi}{3\,\mathrm{Nu}}\right) \qquad (14)$$

which, for positive ϵ, gives

$$\eta_{\max.} \approx 1 + \frac{5}{12}(\epsilon/\mathrm{Nu})^2 \qquad (15)$$

and

$$\Phi_{\mathrm{opt.}} \approx 5\,\epsilon/2\,\mathrm{Nu} \qquad (16)$$

Fig. 1 shows how the effectiveness is altered by the heat effects.

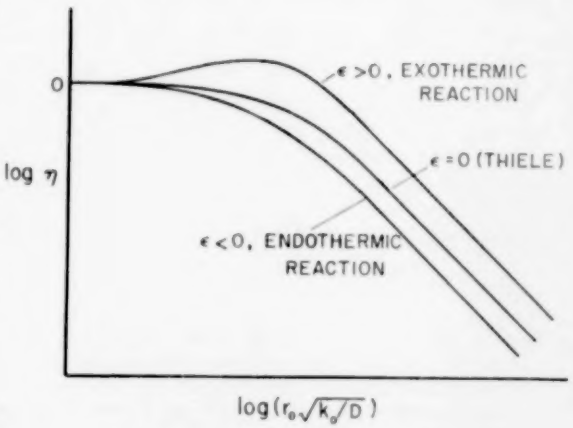

FIG. 1. Effect of heat of reaction on catalyst effectivenes factor, η.

As a numerical example the vapour phase catalytic hydration of ethylene oxide is considered. This reaction with spherical particles of polystyrene–sulphonic acid ion exchange resin used as catalysts was studied at the University of Delaware by METZNER and EHRREICH [3]. Their Run 43d was made at the following conditions: temperature, 160 °C; total pressure, 80 p.s.i.a.; resin diameter, 0·78 mm; water: EtO molal ratio, 10 : 1; N_{Re}, 100. Because of the large excess of water the reaction is assumed to be first order with respect to ethylene oxide. For these conditions, $\Phi = 3{\cdot}0$, $\mathrm{Nu} = 0{\cdot}5$, and $\epsilon = 0{\cdot}04$. These values lead to $\eta_1 = 0{\cdot}60$ and to $\eta = 0{\cdot}70$.

When the temperature difference across the pellet is not small, as in PRATER's example, the perturbation solution is not applicable. Further work is being done here to treat cases of this type.

University of Delaware, Newark, Delaware. U.S.A.

J. D. TINKLER
R. L. PIGFORD

NOMENCLATURE

c, c_0 = concentrations of reactant at any radial distance and at the pellet surface, respectively g mole/cm³

$\bar{c}$ = dimensionless concentration function $(c/c_0)\, r\, \sqrt{(k_0/D)}$

D = diffusion coefficient of reactant in pellet cm²/sec

E = activation energy for reaction cal/g mole

h = heat transfer coefficient at pellet surface cal/sec cm² °C

k, k_0 = first-order reaction rate constant at any temperature and at surrounding fluid temperature, respectively sec⁻¹

N_{Re} = modified Reynolds number for use in packed-bed calculations

Nu = Nusselt modulus $(h/\lambda)\, \sqrt{(D/k_0)}$

Q = heat of reaction, positive for exothermic reaction cal/g mole

r = radial distance from pellet centre cm

r_0 = radius of pellet cm

R = gas constant cal/g mole °K

T, T_0 = absolute temperature in pellet and in surrounding fluid, respectively °K

ϵ = dimensionless heat effect parameter $D\, E\, Q\, c_0/\lambda\, R\, T_0^2$

θ = dimensionless temperature of a point in pellet $\dfrac{r\,(\sqrt{(k_0/D)})\,\lambda(T - T_0)}{D\, Q\, c_0}$

λ = thermal conductivity of pellet cal/sec cm °C

η = effectiveness factor

ϕ = dimensionless distance from pellet centre $r\, \sqrt{(k_0/D)}$

Φ = dimensionless pellet radius $r_0\, \sqrt{(k_0/D)}$

VOL. 15 1961

REFERENCES

[1] THIELE E. W. *Industr. Engng. Chem.* 1939 **31** 916.

[2] PRATER C. O. *Chem. Engng. Sci.* 1958 **8** 284.

[3] METZNER A. B. and EHRREICH J. E. *Amer. Inst. Chem. Engrs. J.* 1959 **5** 496.

Bemerkung zu der Arbeit: "An analysis of chemical reactor stability and control*"

(*Received* 31 *March* 1961)

Bei der Untersuchung der Stabilität eines Rührkessels stiessen R. ARIS und N. R. AMUNDSON auf Schwierigkeiten bei einer physikalisch-anschaulichen Interpretation des zweiten Stabilitätskriteriums (vergl. auch *Chem. Engng. Sci.* 1961 **14** 251). Sie kann jedoch wie folgt gegeben werden:

Die Material- und die Wärmebilanz, die das dynamische Verhalten eines kontinuierlich durchströmten Rührkessels beschreiben, in welchem eine exotherme Reaktion abläuft, lauten:

$$V\frac{dx}{dt} = q\,(x_0 - x) - VR \qquad (1)$$

$$Vc\,\rho\frac{dT}{dt} = qc\,\rho\,(T_0 - T) - VU^* - (\Delta H)\,VR \qquad (2)$$

Die einzelnen Terme der Gleichungen haben folgende Bedeutung:

$V\frac{dx}{dt}$ – Zeitliche Aenderung der im Volumen V befindlichen Masse X

$q\,(x_0 - x)$ – Differenz zwischen Massenzufluss und Massenabfluss pro Zeiteinheit

$-VR$ – In der Zeiteinheit durch Reaktion verbrauchte Masse des Stoffes X im Volumen V

$Vc\rho\frac{dT}{dt}$ – Zeitliche Aenderung der im Volumen V gespeicherten Wärmemenge

$q\,c\rho\,(T_0 - T)$ – Differenz des Wärmeinhaltes von Zu- und Abfluss pro Zeiteinheit

$-VU^*$ – In der Zeiteinheit durch Kühlung aus dem Volumen V abgeführte Wärmemenge

$-(\Delta H)\,VR$ – In der Zeiteinheit durch Reaktion im Volumen V erzeugte Wärmemenge

Mit den Substitutionen

$$\tau = \frac{q\cdot t}{V};\quad \xi = \frac{x}{x_0};\quad \eta = \frac{c\,\rho\,T}{(\Delta H)\,x_0};\quad P = \frac{VR}{qx_0};$$

$$U = \frac{VU^*}{qx_0\,(\Delta H)}$$

lassen sich die beiden Bilanzen in folgender vereinfachter Form schreiben

$$\dot{\xi} = 1 - \xi - P\,(\xi, \eta) = \overline{P\,(\xi, \eta)} \qquad (3)$$

$$\dot{\eta} = \eta - \eta_0 - P\,(\xi, \eta) - U\,(\eta) = \overline{Q\,(\xi, \eta)} \qquad (4)$$

Die beiden Gleichungen enthalten auf ihren rechten Seiten stark nicht lineare Terme. Zur Stabilitätsunter-

*ARIS R. und AMUNDSON N. R. *Chem. Engng. Sci.* 1958 **7** 121.

suchung des Systems in einem vorgegebenen Betriebspunkt (η_s, ξ_s) genügt es aber bekanntlich, die für diesen Punkt linearisierte Form der Differentialgleichungen (3) und (4) zu betrachten. Sie lauten

$$\frac{d}{dt}(\xi - \xi_s) = (\overline{P_\xi})_s(\xi - \xi_s) + (\overline{P_\eta})_s(\eta - \eta_s) \qquad (5)$$

$$\frac{d}{dt}(\eta - \eta_s) = (\overline{Q_\xi})_s(\xi - \xi_s) + (\overline{Q_\eta})_s(\eta - \eta_s) \qquad (6)$$

wobei $(\overline{P_\xi})_s = \left(\frac{\partial \overline{P}}{\partial \xi}\right)_s$, entwickelt an der Stelle ξ_s, η_s usw . . . Setzt man

$$\eta - \eta_s = y$$

und löst das Gleichungssystem nach y auf, so erhält man

$$\ddot{y} - \{(\overline{P_\xi})_s + (\overline{Q_\eta})_s\}\dot{y} + \\ + \{(\overline{P_\xi})_s \cdot (\overline{Q_\eta})_s - (\overline{Q_\xi})_s(\overline{P_\eta})_s\}\, y = 0 \qquad (7)$$

Bei Stabilität müssen die beiden Bedingungen

$$(\overline{P_\xi})_s \cdot (\overline{Q_\eta})_s - (\overline{Q_\xi})_s(\overline{P_\eta})_s > 0 \qquad (8)$$

$$(\overline{P_\xi})_s + (\overline{Q_\eta})_s < 0 \qquad (9)$$

erfüllt sein. Unter Berücksichtigung von Gleichung (3) und (4) lauten diese in etwas anderer Form

$$(1 + P_\xi) \cdot (1 + U_\eta) > - P_\eta \qquad (8a)$$

$$2 + P_\xi + U_\eta > - P_\eta \qquad (9a)$$

Eine physikalisch-anschauliche Interpretation der Gleichung (8a) gelingt bekanntlich in einfacher Weise anhand eines Diagrammes, in welchem unter Voraussetzung des Verschwindens der zeitlichen Ableitungen in den Gleichungen (1) und (2), die durch Reaktion entstehende und durch das Kühlsystem sowie den abfliessenden Produktstrom abgeführten Wärmemengen über der Temperatur aufgetragen sind (Abb.1). Die Bedingung (8a) besagt, dass im Schittpunkt beider Kurven die Wärmeabführung stärker mit der Temperatur zunehmen muss als die Reaktionswärme ; mit anderen Worten, die Kurve der abgeführten Wärme muss steiler verlaufen als diejenige der entstehenden Reaktionswärme. In Anlehnung an die Terminologie anderer Fachgebiete soll diese Bedingung als Stabilitätskriterium für monotone oder statische Stabilität bezeichnet werden, da für ihre physikalische Deutung das Verschwinden der zeitlichen Ableitungen vorausgesetzt werden kann.

Die anschauliche Erklärung des zweiten Stabilitätskriteriums stiess bisher auf Schwierigkeiten, obwohl bereits in der Regelungstechnik Fragen dieser Art grundsätzlich geklärt sind [1], und eine Übertragung der Ergebnisse auf das vorliegende Problem leicht möglich ist. Das zweite Stabilitätskriterium stellt die Bedingung für sogenannte oszillatorische oder dynamische Stabilität dar.

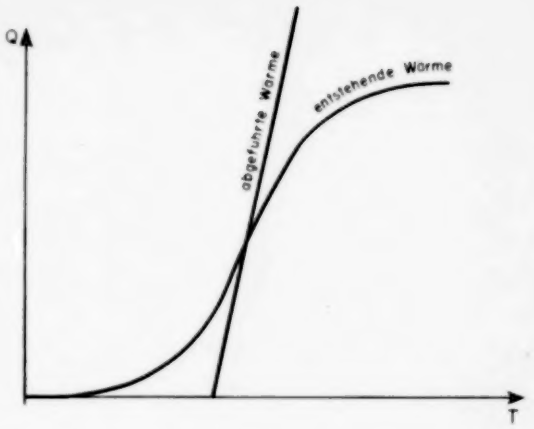

FIG. 1

Zur Untersuchung der Stabilität eines Systems kann nämlich der stationäre Zustand, der für die Ableitung des ersten Stabilitätskriteriums allein notwendig ist, nicht ausreichen. Vielmehr muss man stets von dem gekoppelten System linearisierter Differentialgleichungen (Gleichung 5 und Gleichung 6) ausgehen, das erwiesenermassen streng für die Ableitung der Stabilitätsbedingungen gilt. Die Form der Differentialgleichungen zeigt, dass man den Rührkessel anschaulich als ein System mit zwei Speichern, einem Wärmespeicher und einem Massespeicher, betrachten kann. Die Kopplung der beiden Differentialgleichungen besagt, dass diese beiden Speicher miteinander in Austausch stehen. Das dynamische Zusammenspiel der beiden Speicher kann daher unter gewissen Voraussetzungen zu Schwingungen in der Konzentration und der Temperatur führen, die zweifellos, trotz statischer Stabilität, je nach den Zahlenwerten der Koeffizienten in den Differentialgleichungen ungedämpft sein können.

Qualitativ lässt sich dieses Zusammenspiel folgendermassen beschreiben (vergl. Abb. 2): Es werde eine Reaktion n-ter Ordnung vorausgesetzt, wobei $n \geqslant 1$ ist. Die Temperatur des Rührkessels sei nun durch eine plötzliche Störung etwas höher als dem Arbeitspunkt (η_s, ξ_s) entspricht. Wegen der hierdurch hervorgerufenen höheren Reaktionsgeschwindigkeit wird pro Zeiteinheit mehr Stoffmenge x verbraucht und gleichzeitig mehr Wärme frei. Die Temperatur kann daher trotz verstärkter Wärmeabführung zunächst noch weiter anwachsen, bis zu dem Zeitpunkt, wo der Einfluss der kleiner werdenden Konzentration auf die Reaktionsgeschwindigkeit den Einfluss der anwachsenden Temperatur gerade aufhebt. Der Wärmespeicher hat sich auf Kosten des Massespeichers über den Wert angefüllt, der dem Arbeitspunkt entspricht.

Von nun an kann aber die entstehende Wärme die abgeführte Wärmemenge nicht mehr ausgleichen. Die Temperatur fällt wieder und – unterstützt durch die zu

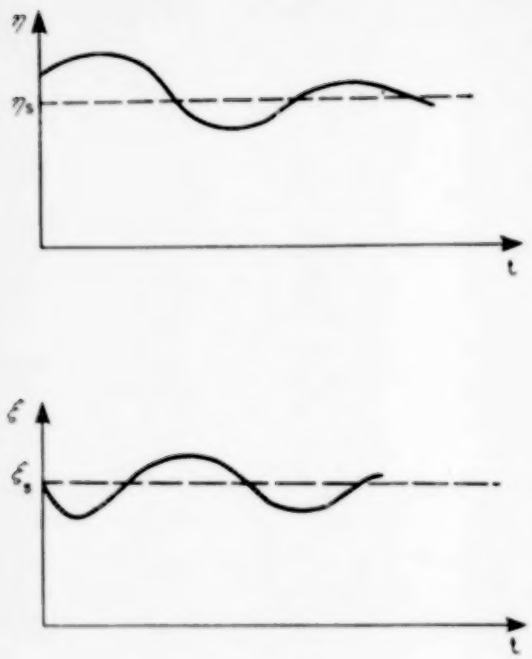

Fig. 2.

niedrige Konzentration – sinkt die Reaktionsgeschwindigkeit unter ihren Sollwert im Arbeitspunkt. Dadurch wächst die Konzentration über ihren Sollwert hinaus, während die Temperatur unter den Sollwert fällt. Der Massespeicher ist nun im Begriff sich auf Kosten des Wärmespeichers aufzufüllen. Durch die grösser werdende Konzentration steigt aber die Reaktionsgeschwindigkeit wieder an, damit ergibt sich eine höhere Wärmeentwicklung, und die durch die verminderte Wärmeabführung wachsende Temperatur unterstützt ihrerseits das weitere Anwachsen der Reaktionsgeschwindigkeit, so dass das Spiel von neuem beginnt. Auf diese Weise können sich also, je nach den Bedingungen, allein durch das dynamische Zusammenspiel beider Speicher, gedämpfte oder ungedämpfte Schwingungen ergeben. Die zweite Stabilitätsbedingung begrenzt nun die Grösse der Koeffizienten der Differentialgleichungen auf Werte, bei denen oszillatorische Stabilität herrscht.

Um zu untersuchen, unter welchen Bedingungen bei monotoner Stabilität oszillatorische Instabilität vorliegt, sollen die Stabilitätskriterien in den ursprünglichen Grössen geschrieben werden. Der einfacheren Gleichungen wegen sei dabei vorausgesetzt, dass die abgeführte Wärmemenge linear mit der Temperatur ansteigt. Wenn T' die Temperatur des Kühlsystems ist, gilt dann

$$U^* = U'(T - T')$$

Ausserdem sei eine Reaktion 1. Ordnung angenommen, also

$$R = k_0 e^{-\frac{E}{RT}}$$

Die beiden Stabilitätskriterien lauten dann in den ursprünglichen Variablen

$$\left(1 + \frac{Vk_0}{q} e^{-\frac{E}{RT_s}}\right)\left(1 + \frac{VU'}{c\,\rho\,q}\right) > -\frac{k_0 V(\Delta H) x_0 E}{q c\,\rho\,RT_s^2} \frac{e^{-\frac{E}{RT_s}}}{1 + \frac{Vk_0}{q} e^{-E/RT_s}} \tag{8b}$$

$$2 + \frac{Vk_0}{q} e^{-\frac{E}{RT_s}} + \frac{VU'}{c\,\rho\,q} > -\frac{k_0 V(\Delta H) x_0 E}{q c\,\rho\,RT_s^2} \frac{e^{-\frac{E}{RT_s}}}{1 + \frac{Vk_0}{q} e^{-E/RT_s}} \tag{9b}$$

Für den Fall einer adiabatischen Betriebsweise des Rührkessels ($U' = 0$) vereinfachen sich diese Beziehungen zu

$$1 + \frac{Vk_0}{q} e^{-\frac{E}{RT_s}} > -\frac{k_0 V(\Delta H) x_0 E}{c\,\rho\,q\,RT_s^2} \frac{e^{-\frac{E}{RT_s}}}{1 + \frac{Vk_0}{q} e^{-E/RT_s}} \tag{10a}$$

$$2 + \frac{Vk_0}{q} e^{-\frac{E}{RT_s}} > -\frac{k_0 V(\Delta H) x_0 E}{c\,\rho\,q\,RT_s^2} \frac{e^{-\frac{E}{RT_s}}}{1 + \frac{Vk_0}{q} e^{-E/RT_s}} \tag{10b}$$

In diesem Grenzfall herrscht also bei statischer Stabilität stets auch dynamische Stabilität.

Dynamische Instabilität kann bei statischer Stabilität nur dann auftreten, wenn die folgende Ungleichung erfüllt ist

$$(1 + P_\xi)\cdot(1 + U_\eta) > 2 + P_\xi + U_\eta \tag{11}$$

Diese Beziehung lässt sich vereinfachen zu

$$U_\eta P_\xi > 1 \tag{12}$$

Für eine Reaktion 1. Ordnung ergibt sich mit den ursprünglichen Variablen

$$\frac{VU' k_0 V}{c\,\rho\,q} e^{-\frac{E}{RT_s}} > 1 \tag{13}$$

Substituiert man

$$\frac{V}{q} = \Theta; \qquad k_0 e^{-\frac{E}{RT_s}} = k_1; \qquad VU' = k_w F$$

wobei F die gesamte Wärmeübertragungsfläche und k_w

VOL. 15 1961

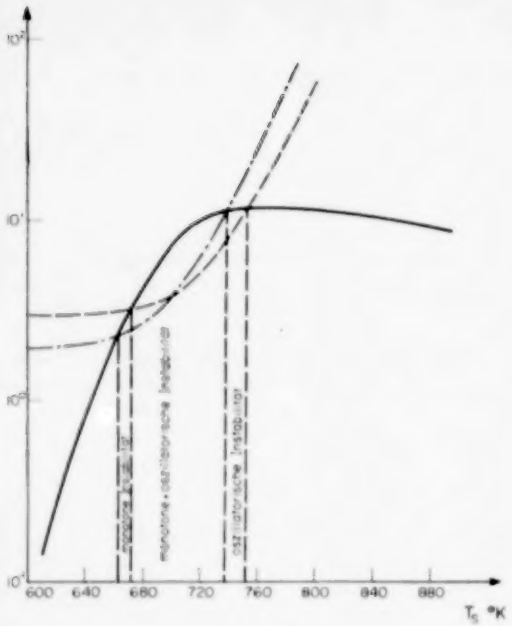

FIG. 3.

——— $-\alpha \cdot \beta e^{-\frac{E}{RT_s}} \dfrac{1}{1+\alpha e^{-ER/T_s}}$

– – – $2+\alpha e^{-\frac{E}{RT_s}}+U'\dfrac{V}{c\rho q}$

— · — $\left(1+\alpha e^{-\frac{E}{RT_s}}\right)\cdot\left(1+U'\dfrac{V}{c\rho q}\right)$

die Wärmedurchgangszahl darstellt, so ergibt sich die einfache Beziehung

$$\Theta k_1 > \frac{qc\rho}{k_w F} \tag{15}$$

In Abbildung 3 sind für die Werte

$$\frac{VU'}{c\rho q} = 1\,; \qquad E = 4{\cdot}5 \text{ k cal}\,; \qquad \alpha = \frac{k_0 V}{q} = 10^{14}\,;$$

$$\beta = \frac{(\Delta H)x_0 E}{c\rho R} = 7{\cdot}5 \times 10^6$$

die linken und rechten Seiten der Ungleichungen (8a) und (9a) logarithmisch über der Temperatur aufgetragen. Man erkennt, dass in diesem speziellen Fall ein Temperaturbereich ($738° \leqslant T \leqslant 753°$) besteht, für den trotz monotoner Stabilität oszillatorische Instabilität herrscht. Dieser Bereich wächst mit U', der Steigung der Wärmeabführungsgeraden, was entsprechend den früheren Überlegungen leicht einzusehen ist.

Eine qualitative Betrachtung lässt vermuten, dass im Falle oszillatorischer Instabilität und monotoner Stabilität wegen der Nichtlinearität des Systems, die Schwingungen nicht dauernd aufklingen, sondern auf eine Amplitude bestimmter Grösse begrenzt werden. In der x–T–Phasenebene müsste sich diese Eigenschaft des Systems in einem stabilen Grenzzyklus wiederspiegeln, der dauernd durchlaufen wird.

Institut für chemische Technologie der technischen Hochschule Darmstadt.

E. D. GILLES
H. HOFMANN

REFERENCE

[1] OPPELT, W. *Kleines Handbuch technischer Regelvorgänge*, Verlag Chemie.

Chemical Engineering Science, 1961, Vol. 15, pp. 332 to 333. Pergamon Press Ltd., London. Printed in Great Britain.

Book Reviews

A. S. Foust, L. A. Wenzel, C. W. Clump, L. Maus and L. B. Andersen: **Principles of Unit Operations.** John Wiley, New York, 1960. 578 pp. 120s.

Inevitably this book will be compared with "Unit Operations," published by Wiley ten years ago.* It has the same large format, detailed diagrams beautifully executed in the same style, and generally gives the impression of repeating the same formula which proved so successful in the earlier work. However, its treatment of the subject matter is quite different. Since Brown appeared there has been an increasing emphasis on principles in chemical engineering education. In this book, what is termed the unified approach is attempted. The unit operations are classified into two main groups, stagewise operations and rate operations. Since the principles of rate operations are considered separately from the application, the text is divided into three parts.

Part I of 76 pages deals with stage operations, the individual mass transfer operations such as distillation, solvent extraction etc. being fused together. One chapter for example, is wholly concerned with equilibrium phase relationships; another with counter-current multistage operations; and so on. There is little reference to actual equipment except for an introductory chapter and a few photographs to add relief.

Part II of 134 pages, covers the theoretical aspects of rate operations. Momentum, heat and mass transfer are developed in parallel, first in relation to molecular transport, then for the turbulent regime.

Part III, the major part, occupying the remainder of the book, is concerned with those unit operations which can be said to depend on rate of transfer. In spite of its arrangement, this part has a rather more conventional look, and the practical aspects are most excellently illustrated.

Clearly, two concepts have been allowed to dominate the book, namely the idea of an equilibrium stage and the similarity between heat, mass and momentum transfer. Thus fluid mechanics is mostly regarded as momentum transfer, steady flow in a pipe being a case of transfer with internal momentum generation. The energy principle for a fluid can hardly be fitted into this scheme and so is postponed to Part III, the part dealing with applications. Filtration, sedimentation and fluidization are classed as momentum transfer; the characterization of particulate solids is thereby relegated to an appendix; and size reduction is omitted altogether.

Individual sections within each chapter are, on the whole, carefully written but can be criticised again on the grounds of emphasis and arrangement. In particular, in Part II, there is too much stress on the oversimplified mean free path treatment of molecular transport in gases. Then follows a sudden switch to non-Newtonian fluids. Furthermore, some of the references seem erudite rather than serious recommendations for supplementary reading.

Opinion will certainly be divided on whether unit operations should be broken down and constrained within such a rigid framework as that employed here. Instead of providing the student with the adaptable approach demanded by the ever increasing tempo of technological change, there is the danger of engendering the very inflexibility the authors wish to avoid. It is indeed unfortunate that this book, which undoubtedly represents an important publishing venture in the chemical engineering field, cannot be unreservedly recommended, and seems unlikely to gain the wide acceptance accorded to the earlier book of Brown.

J. C. Lee

*G. G. Brown: Unit Operations. John Wiley, New York 1950.

R. Byron Bird, Warren E. Stewart and Edwin N. Lightfoot: **Transport Phenomena.** John Wiley, New York, London. 1960, 780 pp. $13·75.

This is probably the most important textbook on chemical engineering to appear in many years. The subjects of momentum, energy and mass transfer, which the book is about, are of basic importance in chemical engineering, and competence in the analytical treatment of these phenomena is one criterion of a good engineer. The book is timely, because there is currently a great enthusiasm for the analytical approach, and a helpful text has been wanting.

The core of the book is the presentation of generalized equations of continuity, of motion and of energy for isothermal, non-isothermal and multicomponent systems involving transport in arbitrary continua. Most of the 780 pages are devoted to worked problems, and the student learns by the problem or "case" method. Momentum, energy and mass transfer are given seven chapters each (plus one on radiation) and the text may be used in teaching these subjects in order. Alternatively, seven sub-sections (molecular transport, transport in laminar flow or in solids, etc.) may be followed in sequence with applications to all three transport phenomena. The level of mathematics is fairly advanced by standards of undergraduate instruction in the United States, many illustrative examples involving Bessel functions, partial differential equations, Laplace transforms and tensor analysis. The material based on ordinary differential equations, however, provides an adequate text for a course requiring less advanced

preparation in mathematics. The numerous questions for discussion and the unsolved problems at the end of each chapter are excellent.

Since the book is on analysis, the worked examples, which constitute most of it, are selected from those problems which *can* be solved, rather than from those which *need* to be solved. One deals with the laminar flow of a liquid over an inclined plate with viscosity a stated function of *position*. One deals with the oscillations of a damped manometer. Five pages are devoted to the problem of an adiabatic packed catalytic reactor, with the assumption that heat release is linear in temperature, without relation to the extent of completion of the chemical reaction. Turbulent flow and transport between phases, perhaps because they are less subject to analysis, are allotted less space than transport in laminar and stagnant systems. In very few instances are the analytical results compared with experimental data.

In a sense this is a dangerous book, for it is so well done that it will probably accelerate the trend towards emphasis on analysis in chemical engineering curricula. The danger stems from the current situation in engineering education, and is in no way attributable to the authors. Process design and conception generally are difficult to teach, but analysis is of no use until there is something to analyse. If perspective is lost through enthusiasm for scientific and mathematical analyses, the engineer will be less effective in industry. The book poses a challenge for someone to produce an equally good text dealing with the *engineering* aspects of chemical engineering.

T. K. Sherwood

SELECTION OF CURRENT PAPERS OF INTEREST TO CHEMICAL ENGINEERS

E. H. Binns, K. H. Squire and L. J. Wood: The distribution of phenol between toluene and water and between aqueous solutions of sodium phenate. *Trans. Faraday Soc.* 1960 **56** 1770–1775.

P. N. Snowden and J. C. R. Turner: The concentration dependence of the Soret effect (i.e. thermal diffusion) (See also *Trans. Faraday Soc.* 1960 **56** 1409). *Trans. Faraday Soc.* 1960 **56** 1812–1819.

M. Blank and F. J. W. Roughton: The permeability of monolayers to carbon dioxide. *Trans. Faraday Soc.* 1960 **56** 1832–1841.

F. I. Musk and E. D. Totman: Multicomponent distillation calculations (by computer) where the feed-plate location and number of theoretical plates are unspecified. *J. Appl. Chem.* 1960 **10** 477–483.

D. W. Jordan: Method for calculating boundary value problems in heat conduction for the cylindrical cavity and the half space, by means of convolution integrals. *Brit. J. Appl. Phys.* 1961 **12** 14–19.

VOL. 15 1961

A. Witkowski: The theory of the distillation column. *J. Phys. Chem.* 1960 **12** 1822–1825.

L. G. Longsworth: The mutual diffusion of light and heavy water. *J. Phys. Chem.* 1960 **12** 1914–1917.

P. A. E. Crosse, D. H. Lucas and W. L. Snowsill: Instrument for recording the dust nuisance emitted by chimneys. *J. Sci. Instrum.* 1961 **38** 12–17.

J. Scanlan and J. R. Dunn: Automatic apparatus for measurement of the rate of absorption or evolution of gas. *J. Sci. Instrum.* 1961 **38** 28–30.

R. Aris: On the dispersion of a solute in a pulsating gas flow through a tube (see also *Proc. Roy. Soc.* 1956 **A235** 67 1959 **A252** 538) *Proc. Roy. Soc.* 1960 **A259** 370–376.

W. J. Rouleau: Pressure surges in pipelines carrying viscous liquids. *J. Basic. Engng* 1960 **82** 912–920.

T. W. van der Lingen: A jet pump design theory. *J. Basic. Engng.* 1960 **82** 947–960.

De F. P. Rudd and B. Widom: Critical solution phenomena in two-component liquid systems. The system water–ethylene glycol–mono-*iso*butyl ether. *J. Chem. Phys.* 1960 **33** 1816–1819.

K. S. Krishnan and R. Sundaram: Radiative transfer of energy in the core of a heated tube. *Nature* (*Lond.*) 1960 **188** 483–484.

A. H. Doveton and K. C. W. Pedder: The simulation of a large chemical plant (for the manufacture of hydrogen peroxide) on an electronic analogue computer. *Trans. Soc. Instrum. Tech.* 1960 **12** 180–188.

J. B. Brackenridge: Transverse oscillations of a liquid jet—I. *J. Acoust. Soc. Amer.* 1960 **32** 1237–1242.

H. J. Naake, K. Tamm, P. Dammig and H. W. Helberg: Formation of air bubbles in air saturated water at reduced pressure and their indication by an acoustical messuring procedure. *Acustica* 1958 **8** 142–152.

H. J. Naake, K. Tamm, P. Dammig and H. W. Helberg: Observation of the formation and growth of bubbles in water containing air, by optical methods. *Acustica* 1958 **8** 193–196.

S. Nagata and I. Yamaguchi: Mass transfer and chemical reaction in liquid–liquid agitation systems. *Mem. Fac. Engng. Kyoto Univ.* 1960 **22** 249–276.

E. Ruckenstein: On the mechanism of turbulent mass transfer in the immediate vicinity of a wall. (See also *Chem. Engng. Sci.* 1958 **7** 265). *Rev. Phys.* (*Bucharest*) 1959 **4** 397–407.

W. Eguchi, M. Harada and S. Nagata: Effect of liquid-and gas-mixing on the rate of mass transfer between two phases in cross channel flow. *Mem. Fac. Engng. Kyoto Univ.* 1960 **22** 326–342.

S. Bretsznajder, L. Lesniewicz and I. Moscicka: Determination of the mass transfer coefficient in undefined hydrodynamical conditions. *Bull. Acad. polon. sci. III.* 1959 **7** 559–563.

S. Bretsznajder and W. Pasiuk: Influence of pulsation on the absorption of gases into liquids. *Bull. Acad. polon. sci., III.* 1959 **7** 591–593.

SELECTION OF CURRENT SOVIET PAPERS OF INTEREST TO CHEMICAL ENGINEERS*

M. S. Vitukhnovskaya and E. A. Belyanskaya: On application of regenerators for regeneration of spent sulphuric acid. *Zh. prikl. Khim.* 1960 **33** 2427–2434.

D. Ya. Evdokov: Oxidation of arsenic compounds by atmospheric oxygen on active charcoal in the presence of nitrogen oxides and nitric acid. *Zh. prikl. Khim.* 1960 **33** 2435–2439.

M. I. Kurochkina and P. G. Romankov: Kinetics of the process of desorption from porous adsorbents in the regime of internal diffusion. *Zh. prikl. Khim.* 1960 **33** 2497–2506.

A. A. Noskov and N. V. Ozerova: Plate efficiencies of sieve trays in rectification columns. *Zh. prikl. Khim.* 1960 **33** 2506–2511.

I. M. Artyukov: On scaling-up of reaction equipment in some processes of heterogeneous conversion of hydrocarbons. *Zh. prikl. Khim.* 1960 **33** 2512–2520.

N. I. Drozdov, L. I. Kisarova and G. I. Sidelnikova: Absorption of acetone in water in foam apparatus. *Zh. prikl. Khim.* 1960 **33** 2609–2612.

M. I. Kurochkina and P. G. Romankov: Kinetics of the process of desorption from porous adsorbent in a suspended bed. *Zh. prikl. Khim.* **33** 2657–2664.

V. N. Lepilin, N. B. Rashkovskaya and P. G. Romankov: Some adsorption and desorption problems in suspended adsorbent beds. *Zh. prikl. Khim.* 1960 **33** 2664–2671.

S. K. Ogodornikov, V. B. Kogan and M. S. Nemtsov: Liquid–vapour equilibrium in binary systems formed by methanol and various hydrocarbons. *Zh. prikl. Khim.* 1960 **33** 2685–2693.

V. Yu. Aristovich, N. V. Lutugina, Yu. I. Malenko and A. G. Morachevski: Investigation of vapour–liquid equilibrium and of rectification of the ternary system water – formic acid – acetic acid. *Zh. prikl. Khim.* 1960 **33** 2693–2698.

M. I. Shakhparonov, S. L. Leichuk, K. M. Korchemskaya, M. E. Martinova, I. I. Baburina and R. D. Voronina: Investigation of vapour pressure and density in binary systems methyldichlorosilane – triethylchlorosilane and silicochloroform – benzene. *Zh. prikl. Khim.* 1960 **33** 2699–2703.

Y. N. Garber and G. G. Rabikhina: Vapour–liquid equilibrium in the system isomeric cresols – ethyl benzoate. *Zh. prikl. Khim.* 1960 **33** 2782–2783.

R. P. Kirsanova and S. Sh. Bik: Vapour–liquid equilibrium in the system allyl alcohol – *iso*propanol at atmospheric pressure. *Zh. prikl. Khim.* 1960 **33** 2784–2786.

M. P. Susarev and R. V. Dizlova: Vapour–liquid equilibrium in the systen *cyclo*hexane – *cyclo*hexanol – *cyclo*hexanon. *Zh. prikl. Khim.* 1960 **33** 2786–2788.

L. D. Berman: On calculation of processes of heat and mass transfer in cross-current. *Zh. prikl. Khim.* 1960 **33** 2789–2791

A. G. Kasatkin, S. Z. Kagan and V. G. Trukhanov: Empircial equations for equilbrium distribution in systems liquid–liquid. *Khim. Prom.* 1960 (6) 488–492.

N. A. Malefeev, V. A. Malyusov and N. M. Zhavoronkov: Study of the process of azeotropic distillation of the system styrene – ethylbenzene. *Khim. Prom.* 1960 (6) 492–496.

S. M. Karpacheva, E. P. Rodionov and G. M. Popova: Comparison of effectiveness of extraction of pulsed columns using continuous aqueous and organic phases. *Khim. Prom.* 1960 (6) 496–499.

G. D. Efremova and G. A. Sorina: Phase and volume relationships in the system ethylene–butane. *Khim. Prom.* 1960 (6) 503–510.

*To assist readers, translations of any article appearing in the above list can be obtained at a reasonable charge. All orders should be addressed to the Administrative Secretary of the Pergamon Instititute at either Headington Hill Hall, Oxford or 122 East 55th Street, New York 22 whichever is more convenient.

B. A. Chertkov: Coefficients of mass transfer in the absorption of SO_2 in multistage absorbers. *Khim. Prom.* 1960 (7) 559–562.

K. S. Koltsov and A. M. Planovski: Influence of concentration and of physico-chemical properties of components in the rectification process on the mass transfer coefficient. *Khim. Prom.* 1960 (7) 573-577.

F. I. Murashkevich: Calculation and application of a turbulent washer. *Khim. Prom.* 1960 (7) 577–587.

V. V. Aronovich: Automatic control of the operation of impeller pumps. *Khim. Prom.* 1960 (7) 587–591.

N. A. Kochergin, V. M. Olevski and V. V. Dilman: Investigation of the operation of perforated plates in distillation. *Khim. Prom.* 1960 (7) 591–595.

N. A. Smirnova and A. G. Morachevski: Vapour–liquid equilibrium and miscibility of components in the system propyl acetate–water. *Zh. fiz. Khim.* 1960 **34** 2546–2553.

A. P. Zinoveeva: Transient dynamic characteristic of some types of chemical reactors. *Khim. Tekh. Topl. Masel.* 1960 **5** (12) 1–10.

A. A. Kondratev: Calculation of minimum reflux when feeding the column with crude below its boiling point or superheated. (Example of rectification of multicomponent mixtures). *Khim. Tekh. Topl. Masel* 1960 **5** (12) 47–49.

A. S. Predvoditelev: Rates of chemical reactions in turbulent flow. (Fundamental statements of theory). *Inzh. Fiz. Zh.* 1960 **3** (11) 3–10.

G. D. Rabinivich: Heat transfer in a bed of dispersed material. *Inzh. Fiz. Zh.* 1960 **3** (11) 18–25.

M. F. Kazanski and P. P. Lutsik: The effect of type of bond of adsorbed moisture on the kinetics of the hydrothermal field of a polycapillary-porous colloidal solid during drying. *Inzh. Fiz. Zh.* 1960 **3** (11) 26–33.

L. V. Gorelik: Forces arising during non-stationary filtration. *Inzh. Fiz. Zh.* 1960 **3** (11).

G. V. Tsiklauri and V. V. Usanov: Heat transfer in a pipe at high speeds. *Inzh. Fiz. Zh.* 1960 **3** (11) 48–51.

V. K. Grmolin: Intensification of convectional heat transfer in a pipe by spiral flow of constant pitch length. *Inz. Fiz. Zh.* 1960 **3** (11) 52–57.

V. V. Shorokhod: Viscosity of certain two-phase mixtures. *Inzh. Fiz. Zh.* 1960 **3** (11) 69–71.

T. L. Perelman: Distribution of temperature in a cylinder with internal heat generation and cooling by a turbulent liquid stream. *Inzh. Fiz. Zh.* 1960 **3** (11) 72–76.

N. I. Kopylov: Investigation of the viscosity of certain liquids over a wide temperature range. *Inzh. Fiz. Zh.* 1960 **3** (11) 97–101.

G. T. Levit and Yu. A. Zeigarnik: Increase in economy of milling of coal in a hammer mill with a centrifugal separator. *Teploenergetika* 1960 **7** (11) 26–32.

A. P. Tretyakov and Cheng Hua-Ding: Effect of ultrasonics on the intensification of heat transfer. *Teploenergetika* 1960 **7** (11) 64–66.

I. V. Dubrovin: Influence of the temperature factor on heat transfer. *Teploenergetika* 1960 **7** (11) 69–74.

V. M. Kapinos: Solution of problems in stationary heat conduction by taking into account the dependance of conductivity on temperature. *Teploenergetika* 1960 **7** (11) 74–79.

D. T. Karpukhovich: Choice of the optimum diameter of the vortex chamber in a centrifugal sprayer. *Teploenergetika* 1960 **7** (11) 79–81.

V. V. Konsetov: Experimental investigation into heat transfer in condensation of steam in horizontal and slightly inclined pipes. *Teploenergetika* 1960 **7** (12) 67–71.

VOL. 15 1961

ERRATA

T. Sitaramayya and G. S. Laddha: Hold up in packed liquid–liquid extraction columns. *Chem. Engng. Sci.* 1961 **13** 267.

The last equation of the paper should read

$$\left[\frac{V_d}{x} + \frac{V_c}{1-x}\right]\left[\frac{a}{\epsilon^3 g}\frac{\rho_c}{\Delta\rho}\right]^{1/2} = 0{\cdot}683\,(1-x)$$

It is regretted that the title section for Volume 13, supplied with Vol. 13 No. 4, contained an erroneous list of contents; the latter has now been reprinted and is enclosed with this issue.